UNIVERSITY OF TRENTO
Italy
International PhD Program in Biomolecular Sciences
Centre for Integrative Biology
XXVIII Cycle

MOLECULAR MECHANISMS AND INSIGHTS INTO THE NAMPT INHIBITOR (FK866) RESISTANCE IN CANCERS

Tutor: Dr. **ALESSANDRO PROVENZANI**
Advisor: Dr. **VITO GIUSEPPE D'AGOSTINO**
Centre for Integrative Biology, CIBIO
Laboratory of Genomic Screening

Ph.D. Thesis of
NATTHAKAN THONGON
Centre for Integrative Biology, CIBIO
Laboratory of Genomic Screening

Academic year 2015-2016

ABSTRACT

Nicotinamide phosphoribosyltransferase (NAMPT), the rate-limiting enzyme in NAD+ biosynthesis from nicotinamide, is one of the major factors regulating cell metabolism and NAMPT is considered a promising target for treating cancer. The NAMPT inhibitor (FK866) has exhibited anticancer activity in several preclinical models by depleting NAD+ and ATP levels. Recently, we showed that FK866 induced translation arrest through the activation of 5'AMP-activated protein kinase (AMPK), inhibition of mTOR/4EBP1 signaling, and phosphorylation of EIF2a in leukemia cells. Cancer drug resistance continues to be a major challenge in medical oncology. Deregulated cellular metabolism is linked to such cell resistance. Indeed, both components of the glycolytic and mitochondrial pathways are involved in altered metabolism conferring chemoresistance in several cancers. In this study, we developed FK866-resistant models in T-lymphoblastic leukemia (CCRF-CEM) and breast cancer (MDA-MB231) cell lines to investigate the molecular mechanism of pharmacoresistance to NAMPT inhibitor (FK866). Our resistant cells were not inhibited at the translational level by FK866 and the drug-induced metabolic adaptations of the resistant cells conferred an advantage to counteract FK866 toxicity. We reveal a molecular mechanism by which FK866 resistant CCRF-CEM cells utilize alternative sources for NAD production to fuel cell metabolism, and metabolic reprogramming was associated to the drug resistance. Importantly, the FK866-induced metabolic alteration was overcome by the co-administration of FK866 with compounds targeting metabolism, thereby rendering a synergistic outcome and restoring cell susceptibility towards FK866. We highlighted a molecular target that favors acquiring of resistance in leukemia and breast cancer cells. In conclusion, targeting metabolic alterations associated with drug resistance to FK866 may open up unexplored opportunities for the development of new therapeutic strategies as a combinatorial treatment for cancer.

.

ORIGINAL AUTHORSHIP

Declaration

I Natthakan Thongon confirm that this is my own work and the use of all material from other sources has been properly and fully acknowledged.

ABBREVIATIONS

2DG	2-Deoxyglucose
4EBP1	Eukaryotic translation initiation factor 4E-Binding Protein 1
ADP	adenosine diphosphate
AKT	RAC-alpha serine/threonine-protein kinase
AML	Acute Myeloid Leukemia
AMP	Adenosine Mono Phosphate
AMPK	AMP-activated Protein Kinase
ATP	Adenosine TriPhosphate
B-CLL	B-cell Chronic Lymphocytic Leukemia
BAD	BCL2-antagonist of cell death
BCL-2	B-Cell Lymphoma 2
CoQ	Coenzyme Q
CoQH	ubisemiquinone
COX	cytochrome C oxidase
EIF2a	Eukaryotic translation Initiation Factor 2 alpha
EIF4E	Eukaryotic translation Initiation Factor 4E
EMT	Epithelial-Mesenchymal Transition
eNAMPT	extracellular form of NAMPT
iNAMPT	intracellular form of NAMPT
ER	Endoplasmic Reticulum
FAD	Flavin Adenine Dinucleotide
FADH2	Flavin Adenine Dinucleotide dihyrdrate
FOXM1	Forkhead box protein 1
G-6-P	glucose-6-phosphate
HIF1	Hypoxia-Inducible Factor 1
HK	Hexokinase
IDO	Indoleamine-2,3,-Dioxigenase
LAT1	L-type amino acid transporter
LDHA	Lactate Dehydrogenase isoform A
LKB1	Liver Kinase B1
MCL1	Myeloid Cell Leukemia 1
MDR	MultiDrug Resistance
mRNA	messenger Ribonucleid Acid
mtDNA	mitochondria DNA

ABBREVIATIONS

mTORC1	Mammalian target of rapamycin complex 1
mTORC2	Mammalian target of rapamycin complex 2
MYC	v-myc avian myelocytomatosis viral oncogene homolog
NA	Nicotinic Acid
NAD+	Nicotinamide Adenine Dinucleotide
NADH	Nicotinamide Adenine Dinucleotide Hydrate
NAM	Nicotinamide
NAMPT	Nicotinamide PhosphoribosylTransferase
NAPRT	Nicotinic Acid PhosphoribosylTransferase
NMN	Nicotinamide MonoNucleotide
NMNAT	Nicotinamide/Nicotinic acid MonoNucleotide AdenylylTransferase
NR	Nicotinamide Riboside
NRK	Nicotinamide Riboside Kinase
OXPHOS	Oxidative phosphorylation
PARP	Poly (ADP-Ribose) Polymerase
PBEF	Pre B-cell colony Enhancing Factor
PDK1	Pyruvate dehydrogenase kinase 1
PEP	Phosphoenolpyruvate
PFK-1	Phosphofructokinase-1
PFKFB	6-phosphofruto-2-kinase/fructose-2,6-bisphosphatase
PGI	Phosphoglucose isomerase
PI	Propidium Iodide
PI3K	PhosphoInositide-3-Kinase
PK	Pyruvate kinase
PPP	Ppentose phosphate pathway
QPRT	Quinolinic acid phosphoribosyltransferase
ROS	Reactive Oxygen Species
RT-PCR	Reverse Transcription Polymerase Chain Reaction
S6K1	ribosomal S6 kinase
SIRT	Sirtuin
T-ALL	T-cell Acute Lymphoblastic Leukemia
TCA	TriCarboxylic Acid
TDO	Tryptophan-2,3,-DiOxigenase
TP53	Tumor Protein p53
TSC2	Tuberous Sclerosis Complex-2
UPR	Unfolded Protein Response
VDAC	voltage-dependent anion channel

CONTENTS

FIGURE INDEX

TABLE INDEX

FIRST PROJECT

MOLECULAR MECHANISM OF PHARMACORESISTANCE TO THE NAMPT INHIBITOR (FK866) IN CANCERS

INTRODUCTION

Hallmarks of cancer

Uncontrolled cell division and acquired aberrant function of normal cells have been associated with vital causes of cancer development [1]. The factors that gradually transforms a normal cell into a precancerous or premalignant stage then ultimately becomes a cancer cell, have been described as the "Hallmarks of Cancer" [1,2]. Reprogramming of energy metabolism is one of the significant hallmarks contributing to cancer. Adaptations of cellular metabolism pathways is frequent in cancer rather more than in normal tissue (**Figure 1**) [2]. Enhanced aerobic glycolysis, reduction of oxidative phosphorylation (OXPHOS) function and increased generation of biosynthetic intermediate substances to meet the metabolic demands are frequently found in cancer to maintain cell growth and proliferation [3,4].

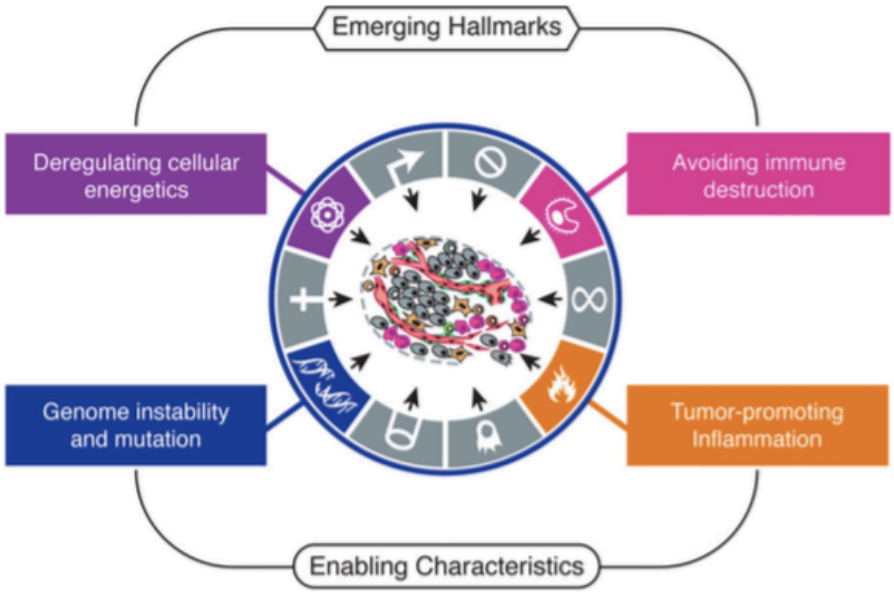

Figure 1 Emerging Hallmarks of cancer
The capability to modify or reprogram cellular metabolism to support cancer proliferation reflecting the deregulation of cellular energy is one of a significant hallmarks of cancer. Metabolic alterations have been considered as a part of oncogenesis and tumor progression [2].

Metabolism of cancer

Metabolic reprogramming in cancer cells are commonly revealed by dysregulation of metabolic enzymes or oncogenic signaling [3]. As illustrated in **Figure 2**, phosphatidylinositol 3−kinase (PI3K)-AKT and mammalian target of rapamycin (mTOR) are canonical oncogenic signaling pathways which directly regulate the core carbon metabolism in the cells [5]. Several metabolic enzymes, including hexokinase 2 (HK2), lactate dehydrogenase A (LDHA) and pyruvate dehydrogenase kinase 1 (PDK1), are well-known transcriptional targets of *MYC* and hypoxia-inducible factor-1 (*HIF-1*), oncogenic transcription factors [6]. Tumor cells have aberrant activation of mTOR [7] that induces anabolic growth by nucleotide, protein, and lipid synthesis. Loss of tumor suppressor like *p53* or activation of oncogenes such as *MYC* further promotes anabolism through the transcriptional regulation of metabolic genes [6].

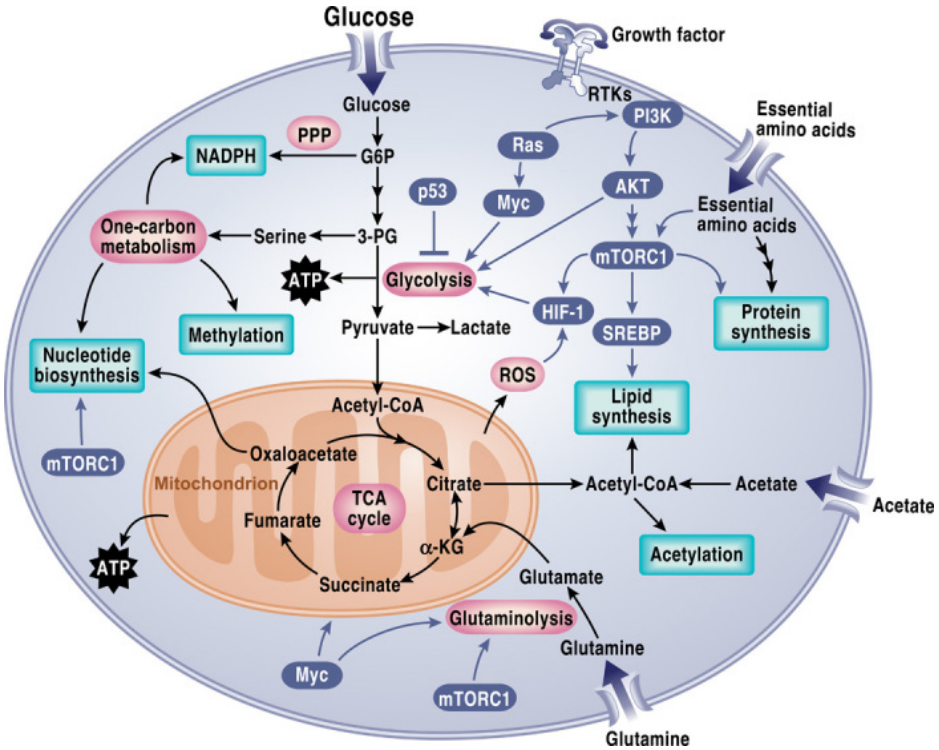

Figure 2 Overview of core metabolic pathways and metabolic enzymes involved in cancer metabolism.
This figure illustrates various aspects of energy metabolism regulation, including glycolysis, TCA cycle, pentose phosphate pathway (PPP), glutaminolysis, fatty acid biosynthesis pathway, PI3K/mTOR, AMPK signaling cascade and apoptosis pathways. Three transcription factors, *HIF-1, c-MYC* and *p53* are key regulators of cancer metabolism in many cell lines [6].

Metabolic difference between differentiated cells (normal) and proliferating cells (Cancer)

Aberrant biochemical features and the abnormal metabolism of glucose have been found to be common and revealed consequences of oncogenic signaling and adaptation in cancer cells [8]. Glucose has been well described as a main source of energy and an initiated carbon source for various anabolic pathways in mammalian cells [9]. Glycolysis-derived pyruvate predominantly occurs in the normal cells or quiescent cells whereas the conspicuous alteration in glucose metabolism by strongly increased glucose uptake and glycolysis yielding intermediate glycolytic metabolites has been found in most of cancer cells [9]. In the presence of sufficient oxygen, most pyruvate can be converted to lactate through LDH enzyme and this metabolic phenomenon referring to aerobic glycolysis was first described by Otto Warburg, a German scientist in 1930 which has been later known as the "Warburg effect" (**Figure 3**) [10].

The Warburg effect in cancer

Warburg experiment was primarily described and focused on glycolysis demonstrating a reversed Pasteur effect (the inhibition of fermentation by O_2) in all of the investigated cancer cells at that moment [9,10]. Cancer cells produce lactic acid from glucose even under non-hypoxic conditions. Thus, they determined that under aerobic conditions, tumor tissues metabolite approximately ten-fold more glucose to lactate in a given time than normal tissues [10,11]. Metabolic switch from OXPHOS towards aerobic glycolysis (Warburg effect) is now a well-established link between cancer and peculiar glucose metabolism. Indeed, glycolysis dependent metabolism to generate ATP as a primary source for cellular energy has been consistently observed in most cancer from different tissue origins [12,13], suggesting that the metabolic alteration commonly occurs in cancers. Several factors have been suggested as potential mechanism leading to increase glycolysis in cancer cells and thus contribute to the Warburg effect including *(i) mitochondrial defects, (ii) hypoxic environment in cancer, (iii) oncogenic signaling induced cancer and alteration of metabolic enzymes* [12].

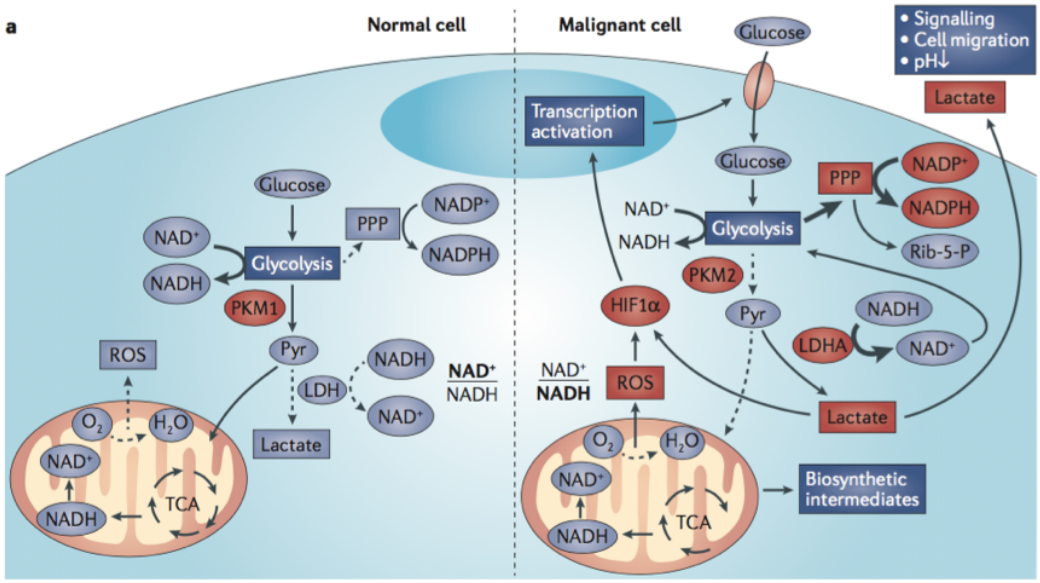

Figure 3 The Warburg effect

Schematic representation of the metabolic differences between a normal cell and a malignant cell. In normal cells, pyruvate is generated through glycolysis pathway in cytosol and then it is transported into mitochondria and further metabolized via TCA cycle. In cancer cells, a high rate of glycolysis and increased of glycolytic enzyme are observed. Glucose is metabolized to pyruvate and the production of lactate occurs even in the presence of oxygen condition [14].

(i) Mitochondria respiration damage

Dysfunction or damage of mitochondria by mutation is contributed to an enhance of glycolysis [12]. Mitochondria DNA (mtDNA) has high mutation rate in several cancers such as in leukemia [15] colon cancer [16] and prostate cancer [17]. For instant, mutation of mtDNA strongly induces malfunction of OXPHOS and affects the cellular respiratory. Moreover, low capacity of histone protection, and impairment of DNA repair were found in mtDNA mutation [12]. Since, glycolysis in the cytosol and OXPHOS in mitochondria are two major metabolic pathways responsible for ATP generation from molecules of glucose. To this regard, malfunction of the mitochondrial respiratory chain or mitochondria damage possibly potentiate the cancer cells to rely more and become addicted to glycolytic metabolism for ATP production. Despite, OXPHOS generates ATP much more efficient (36 ATP per a molecule of glucose) than by glycolysis (only 2 ATP) but a small loss of mitochondria function is strongly influent cellular respiration. Therefore, increased glycolytic activity is extensively required to sustain the energy balance especially in cancer cells [18].

(ii) Hypoxia

When oxygen is limited or in a hypoxic condition, cancer cells might be forced to rely more on glycolytic pathway instead of mitochondria respiration to generate ATP [16]. Hypoxia is highly-present in human malignancies, especially has frequently been found in solid tumor tissue due to the penetration of oxygen becomes limited when the tumor mass reaches certain size [19]. Moreover, solid tumors display less well-oxygenated in respect to normal tissues from the same origins which they arose [20]. Under such conditions, OXPHOS may not proceed normally and hampers this metabolic pathway by hypoxia resulting in cell death due to the very low level of oxygen as well as an insufficient of cellular ATP levels [21]. Consequently, increase of glycolysis may reflect to cellular adaptation to oxygen insufficient condition. Hypoxia inducible factor 1 (HIF-1) regulates cellular response to hypoxia leading to the activation of genes associated to glucose uptake, apoptosis, and metastasis [19]. In normal cells, hypoxia plays a role in translation inhibition either through mTOR pathway activation or regulation of EIF2a. The activation of AMPK or PERK in response to metabolic alteration by hypoxia is HIF-independent [22]. AY87-2243 is presented as an inhibitor of HIF-1 activity and of HIF-1a stability and now this compound has been entering into Phase I clinical trial [13]. However, validation of HIF-1 as druggable anticancer target is still pending.

(iii) Oncogenic signals and alteration of metabolic enzymes

The Warburg effect has been interconnected with activation of certain oncogenes, such as *MYC*, *Ras*, and *Akt*. Loss of tumor suppressor genes results in the deregulated conversion of glucose to lactate [23]. In cancer, genetic deregulation of *MYC* expression and loss of checkpoint components, such as P53, permitted MYC to drive malignant transformation [24]. A decrease of phosphoglucomutase (PGM) by p53 exhibited a decrease in glycolysis. However, enhanced glycolytic flux has been reported in some *p53* mutant cancer [25,26]. *GLUT1* and *GLUT4* genes are regulated by *p53* [27]. Inhibition of *H-Ras* by trans-farnesylthiosalicylic acid results in inhibition of glycolysis by decreasing *HIF-1a* regulated genes such vascular endothelial growth factor and *GLUT1*, inhibiting glycolytic enzymes such as PFKFB4 and PFKFB3 and leading to cell death in human glioblastoma U87 cells [28]. The signaling through the insulin receptor

activates PI3K/Akt inducing glucose uptake and glycolysis [29]. Recently, Yu and colleagues found that the proviral insertion in murine lymphomas 2 (*PIM2*) oncogene promotes PKM2-dependent glycolysis and reduces mitochondrial respiration in HEPG2 and HEK293 cell lines [30]. Alterations of metabolic enzymes has been considered as a cause of metabolic changes in cancer [31]. Increase of HK2 expression in cancer led to an elevate of glycolysis [32]. Fumarate hydratase (FH) and succinate dehydrogenase (SDH) are two important enzymes which play fundamental roles in ATP production in mitochondria [33]. Mutant of SDH subunit leads to an accumulation of succinate in cytosol where it inhibits prolyhydroxylase (PHD). Stabilization and activation of HIF-1a are regulated by PHD [33]. A tumor suppressor gene *N-Myc* downstream regulated gene 2 (*NDRG2*) inhibits cancer growth, metastasis and cell invasion. NDRG2 was found to regulate also glucose transporters and glycolytic enzymes such as GLUT1, HK2, PKM2 and LDH [34]. In addition, increased ROS generation and intrinsic oxidative stress may lead to suppression of ROS-sensitive enzymes involved in TCA cycle enzymes, therefore increased ROS generation spontaneously forces cells to increase glycolysis in order to maintain cellular energy level [12].

NAD metabolism and NAMPT enzyme activity

NAD

In addition to enzymes such as HK2 or LDH that play important roles in aerobic glycolysis, nicotinamide adenine dinucleotide (NAD) is also a fundamental cofactor for the redox reactions in the metabolic pathways, especially in cancer [35]. NAD is used as a substrate for several families of enzymes including poly ADP-ribose polymerases (PARPs) and sirtuins, that involved in numerous biological functions including cell survival and death [36]. The mammalian NAD+ dependent protein deacetylase SIRT1, and systemic NAD+ biosynthesis mediated by nicotinamide phosphoribosyltransferase (NAMPT) are two critical components comprising in NAD regulation [35]. SIRT1 displays its function as a key mediator controlling metabolism in various types of tissues, while NAMPT-mediated NAD biosynthesis regulates circadian-oscillatory of NAD+ production [36]. NAD can be synthesized through two metabolic pathways which are the *de novo* pathway starting from amino acids or in salvage pathways by recycling

nicotinamide (NAM) back to NAD [35,37]. As illustrated in **Figure 4**, NAD synthesis in mammalian cell comprises of multiple steps and the first rate-limiting step of the *de novo* pathway is catalyzed by TDOs (mainly in the liver) or IDOs through *de novo* pathway starting from tryptophan. L-tryptophan is converted to nicotinic acid mononucleotide (NAMN). Nicotinic acid (NA) enters the *de novo* pathway and is phosphoribosylated to NAMN by nicotinic acid phosphoribosyl transferase (NAPRT). Then the conversion of NAMN to nicotinic acid adenine dinucleotide (NAAD) is performed by nicotinamide/nicotinic acid mononucleotide adenylyl-transferases 1-3 (NMNAT1-3) enzyme. At the final stage, NAAD is amidated by NAD synthase (NADS) to generate NAD.

For the NAD salvage pathway, NAM is another important NAD precursor and a product of deacetylation and ADP-ribosylation reactions which are catalyzed by several NAD-dependent enzymes including SIRTs, PARPs, and MARTs as well as some ADP-ribosylcyclases enzyme such as CD38 [38]. The key enzyme NAMPT has been considered as the rate-limiting step enzyme in the NAD salvage pathway. NAMPT catalyzes the formation of nicotinamide mononucleotide (NMN) from NAM and PRPP. NMN is then converted into NAD by NMNAT1-3. Moreover, NR enters to cell via nucleoside transporter then NR is re-phosphorylated to NMN by nicotinamide riboside kinases (NRK1) [37]. Recently, Ratajczak and colleagues demonstrated a crucial role of NRK1 which is necessity for the use of exogenous NR and also NMN for NAD biosynthesis. However, the NRK1 function is dispensable from NAM in regulation of NAD production [39].

Sirtuins are a family of protein deacetylases and adenosine diphosphate (ADP)-ribosyltransferases. NAD is required for sirtuin function. Among sirtuin protein family, SIRT1 plays important roles in regulation of many cellular functions. Fatty acid metabolism, cell proliferation, and glucose homeostasis are associated by SIRT regulation [36,40]. As illustrated in **Figure 5**, SIRT1 prevents cell from the oxidative stress by deacetylation of substrates such as P53 and FOXO1 transcriptional factors [40]. In addition, *SIRT1* is overexpressed in many primary solid tumors and especially hematopoietic malignant cells [41] and serves as a key physiological downstream effector for *NAMPT* in regulating cell metabolism, differentiation and circadian clock [40,41].

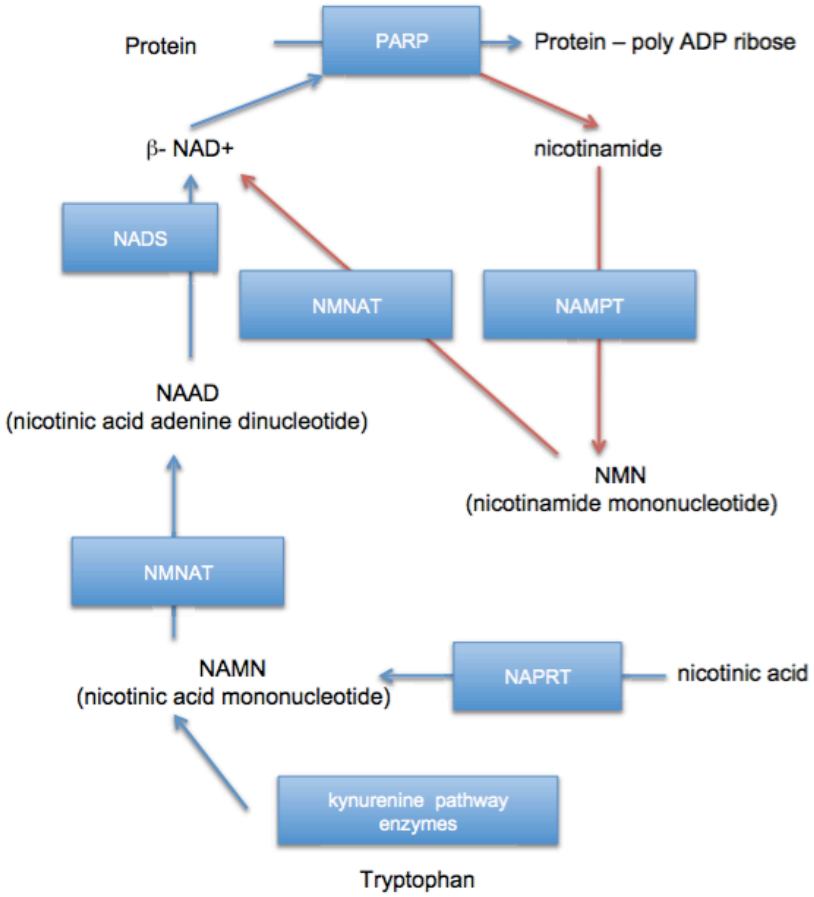

Figure 4 Schematic of mammalian NAD metabolism
NAD can be synthesized through two metabolic pathways. NAD is produced either in a *de novo* pathway from Tryptophan or in salvage pathways by recycling substrate such as nicotinamide back to NAD. By-product of the PARSylation of proteins PARP reactions is performed by utilized β-NAD as a substrate to generate NAM. β-NAD is largely provided in high-active PARPs cells by the salvage pathway [37].

NAMPT/PBEF/visfatin

Preiss and Handler firstly described the NAMPT enzyme activity in 1957 [42]. Based on the enzymatic activity reflecting different pathological functions, NAMPT, PBEF, and visfatin, these three different nomenclatures have been given to this NAMPT protein. Later, NAMPT was approved and has been used as the official name for both gene and protein [35]. Human NAMPT protein consists 491 aminoacids and the molecular weight of NAMPT is approximately 55 kDa [42]. Both intracellular and extracellular forms of NAMPT has been found to be expressed in mammal [35,43] and to avoid misunderstanding, eNAMPT and iNAMPT are used as terms referring to the extracellular and intracellular forms of

NAMPT, respectively. eNAMPT has been found in human [44] and mouse circulation [45] which appears to be modified post translationally and is secreted possibly by hepatocytes and fully differentiated adipocytes [35]. iNAMPT has been definitely established as an NAD biosynthetic enzyme [45] while eNAMPT functions as a growth factor [35,38]. As describe in the review [46], iNAMPT overexpressed has been demonstrated in variety of human malignant tumors. For example, high expression of iNAMPT results in an increase of cellular stromal cell-derived factor-1 (SDF1) level in colon cancer [47], promotes gastric cancer progression [48] and also correlates with greater aggressive malignant lymphoma [49]. Levels of iNAMPT reflects to a worse prognosis in many cancer cells such as endometrial adenocarcinoma [50] and prostate cancer [41]. Interestingly, several reports demonstrated that overexpression of iNAMPT confers resistance to chemotherapeutic agents such as doxorubicin [51], etoposide [41], and fluorouracil [48].

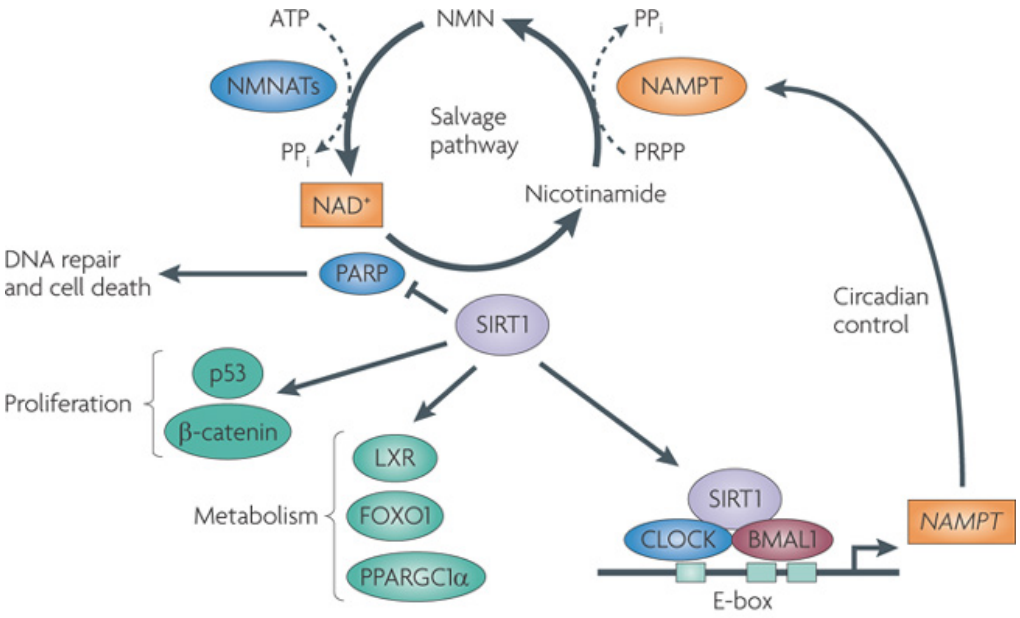

Figure 5 Circadian regulation of the NAD salvage pathway
NAMPT is a rate-limiting enzyme in mammalian NAD+ biosynthesis from NAM. NAMPT catalyses the transfer of PRPP to NAM to produce NMN, then NMN is further converted to NAD+ by nicotinamide mononucleotide adenylyltransferases (NMNATs; there are three *NMNAT* genes 1-3). The activity of SIRT1 and PARPs are determined by the oscillations in NAMPT levels and variations of NAD+ levels. SIRT1 can also deacetylate and regulate proteins involved in cellular metabolism and cell proliferation. [40].

Systemic NAD synthesis is mediated by eNAMPT which its level is not only critical for normal β-cell function but also associates to macrophage survival during ER stress through activation of IL6 secretion and stat3 [52]. In this regard, eNAMPT exerts function independently of NAD synthesis with low catalytic activity under normal condition. However, overexpression and high-secretion of eNAMPT have been described as causes of cardiac hypertrophy in murine cardiomyocytes [46,53] and in advance stage of hepatocellular carcinoma [54].

As illustrated in **Figure 6**, physiological levels of cellular NAD and NAM recycling are regulated by NAMPT activity. SIRT1, 6, 7 and PARP-1 are NAD-dependent enzymes which are found to be expressed in nucleus while SIRT1 and SIRT2 are expressed in the cytoplasm, and SIRT3, 4, 5 are expressed in mitochondria [35]. The ectoenzyme CD38 produces cyclic adenosine diphosphate ribose (cADPR) which regulates intracellular Ca2+ signaling. CD38 is broadly expressed as a transmembrane protein which catalyzes the breakdown of NAD and NADP to generate cADPR [55]. It has been reported that *NAMPT* expression is regulated by the circadian CLOCK and BMAL1 transcription factors which form complex with SIRT1 in the nucleus [38,56]. A feedback loop involving NAMPT/NAD+ and SIRT1/CLOCK:BMAL1 complex has been described by inhibition of NAMPT that activates clock gene *Per2.* However, transcription factor CLOCK can also bind to NAMPT and up-regulates *NAMPT* expression [56,57]. Nevertheless, NAMPT could be stimulated by other stimuli such as the mechanical stress and pro-inflammatory cytokines including TNF-a, IL-1 and IFN [58]. Interestingly, NAMPT is secreted from different cell types and is probably released from damaged cells together with ATP and PRPP. Extracellular production of NMN potentially occurs from the conversion of NAM and NMN. NMN enters to the cell, possibly after conversion to NR by the ectocellular enzymes CD38 and CD73 [38].

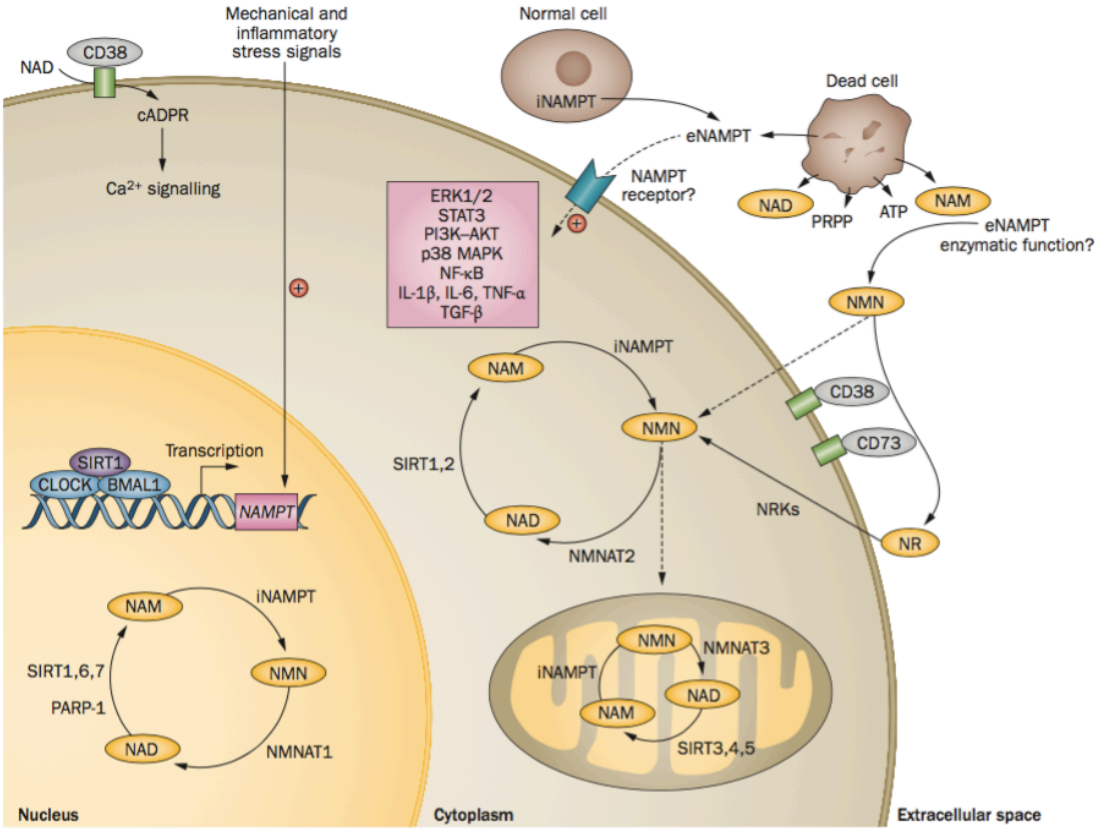

Figure 6 Physiological actions of NAMPT

Two forms of NAMPT have been found in mammalian cells. Intracellular form of NAMPT or iNAMPT is ubiquitously expressed whereas extracellular form of NAMPT or eNAMPT is positively secreted from adipose tissue and expressed with higher enzymatic activity in respect to iNAMPT. Nicotinamide ribose (NR) is another key of NAD intermediate which can be produced from extracellular NMN by CD73. NR enters to cell via nucleoside transporter then NR is rephosphorylated to NMN by NRK1. Then, NMN is further converted to NAD by NMNAT1-3 [35,38].

TRYPTOPHAN

Mammalian NAD biosynthesis can be synthesized via *de novo* synthesis pathway starting from tryptophan (Trp) [38,55]. As illustrated in **Figure 7**, multistep reactions are required for NAD production. The *de novo* pathway is comprised into two parts; the first part has been called as the kynurenine pathway (KP) which involves metabolic conversion of tryptophan to α-amino-β-carboxymuconate-ε-semialdehyde (ACMS), thereby produces picolinic acid at the final step before entering TCA cycle via acetyl-CoA. Metabolic conversion of ACMS to NAD is the second part of the *de novo* pathway of NAD synthesis [59]. The initial step of the KP is mainly regulated by two key enzymes which are indoleamine 2,3-dioxygenase 1 (IDO-1) and tryptophan 2,3-dioxygenase (TDO) [60]. TDO

metabolites tryptophan to kynurenine, which is then converted to either kynurenic acid (KYNA) by kynurenine aminotransferase (KAT) or 3-hydroxykynurenine by kynurenine monooxygenase (KMO). Kynureninase (KYNU) metabolites 3-hydroxykynurenine to 3-hydroxyanthranilic acid which then further converts to acetyl CoA. Non-enzymatically transformed to quinolinic acid is the final step producing the precursor for NAD+ synthesis [59–61].

IDO-1 is broadly expressed in most tissues and is involved in the metabolism of Tryptophan [60] while *TDO* is constitutively expressed in liver and brain [59]. In addition, IDO1 responses are found to be mediated by downstream stress response pathways including GCN2 and mTORC1 which are important regulators activated under insufficient of amino acids [60,62]. In 2013, Wu wei and colleagues reported that lack of tryptophan caused by the over-activation of IDO induced an accumulation of uncharged tryptophan transfer RNA (Trp-tRNA). Silencing *IDO* by shRNA exerts antitumor efficiency in murine lung cancer model [63]. Depletion of tryptophan resulted in the blockade of activated T-cells at the G1 phase preventing lymphocyte proliferation [64]. In addition, phosphorylation of EIF2α mediated by GCN2 concurrently inhibits protein synthesis and arrests cell growth [62,65]. 3-hydroxyanthranilic acid and quinolinic acid can induce apoptosis by exerting cytotoxic properties on T-cells [66]. Quinolinic acid phosphoribosyltransferase (QPRT) is an enzyme in *"de novo"* NAD synthesis pathway which is responsible for the conversion of quinolinic acid an important NAD precursor to NAD+ [67,68]. QPRT was associated with malignancy and elevated expression level of QPRT increase resistance to oxidative stress induced by radiochemotherapy in glioma cells, conferring a poor prognosis [68].

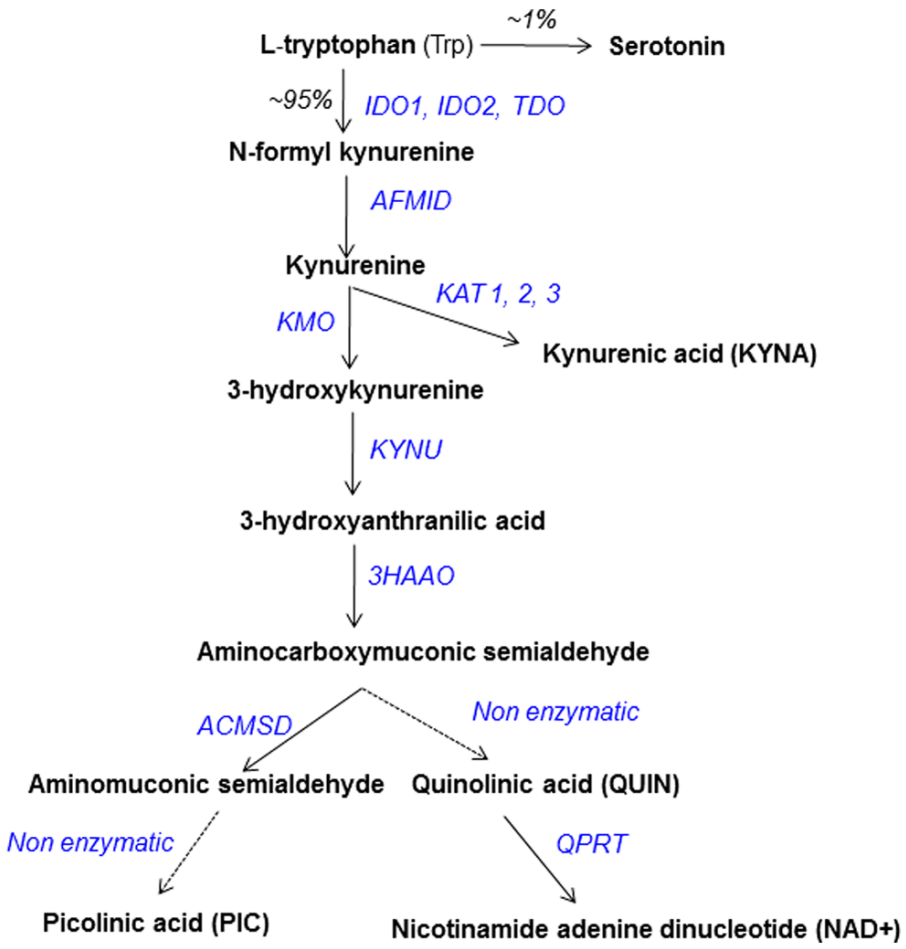

Figure 7 Simplified diagram of NAD *de novo* pathway from tryptophan [59].

NAMPT INHIBITORS

Inhibitors of NAMPT have been considered as promising cancer drugs and some of them are currently in clinical trials such as FK866, CHS-828 and the CHS-828 prodrug EB1627/GMX1777 [69]. NAMPT belongs to a dimeric class of type II phosphoribosyltransferase enzyme [45,69]. Indeed, NAMPT is mostly present as a dimer in cells and is profoundly affected by histidine autophosphorylation at residue His247. Interestingly, the crystal structures of the complexes with either NMN or FK866/APO866 (N-[4-(1-benzoyl-4-piperidinyl)butyl]-3-(3-pyridinyl)-2E-propenamide) (**Figure 8**) was shown to directly compete with NAM and acted as a competitive substrate binding to the catalytic pocket [70] deliberating the anticancer effect of FK866. Depletion of intracellular NAD content and thereby markedly replenishing ATP levels have been denoted as pharmacological signatures of NAMPT inhibitors contributing cell death in particular of FK866 [69,71].

FK866 is a specific, competitive, and potent inhibitor of NAMPT that displays cytotoxicity in a broad panel of cancer cell lines [38,49,69]. Informatively, FK866 potentiated cell death inducing apoptosis in HepG2 (human liver carcinoma cells) and caused gradual NAD+ depletion through specific inhibition of NAPRT but it did not directly inhibit mitochondrial respiratory activity [72]. Anti-tumor activity of FK866 has been found to prevent and abrogate tumor growth both in *vivo* and in *vitro* [23,73]. Interestingly, FK866 displayed toxicity to human AML, lymphoblastic lymphoma, and leukemia but there was no report regarding to the significant toxicity to the animals [74]. Assessment of FK866 has been suggested for the potential prevention of plaque vulnerability due to it reduced CXCL1 production associated neutrophil infiltration in atherosclerotic mice [75]. FK866 induced the delayed energy stress in hepatocarcinoma cells, by triggering the activation of AMPKα and downregulation of mTOR signaling resulting in cancer cell death [76]. FK866 strongly induced AMPK activation and inhibits of protein translation via EIF2a-dependent pathway in leukemia and EIF2a was highlighted as an early response to energy stress induced by FK866 [71]. To date, FK866 has successfully passed phase I and II clinical trials as single-agent therapies for several different cancers. The recommended phase II dose of FK866 is 0.126 mg/m^2/h given as a continuous 96h infusion every 28 days [77]. Unfortunately, recent results of FK866 have not been promising due to its constantly exposes side effect induced thrombocytopenia [73]. CHS-828 (**Figure 8**), a pyridyl cyanoguanidine, is another small molecule inhibitor of NAMPT displaying cytotoxicity in many cell lines including breast, lung, fibroblasts and endothelial cancer cells [78]. In 2010, Olesen and coworkers revealed that APO866/FK866, CHS-828 and TP201565 shared the same binding site in the active site of NAMPT enzyme [69]. A prodrug EB1627/GMX1777 is currently also in phase I trials. CHS-828 has completed phase I of clinical trial with a dose of 420mg of CHS-828 administered every 3 weeks is recommended for treatment [79]. Adverse effects of CHS-828 and GMX1777 such as hematuria, leucopenia and thrombocytopenia were also notable during clinical trial [79]. As NAMPT is essential for the replenishment of the intracellular NAD and ATP, thus targeting NAMPT activity may serve as a potential therapeutic strategy for treating leukemia and human solid tumors.

Specially, combining FK866 to other drugs targeting metabolism may enhance therapeutic efficacy of NAMPT inhibitors particularly in hematopoietic cancer.

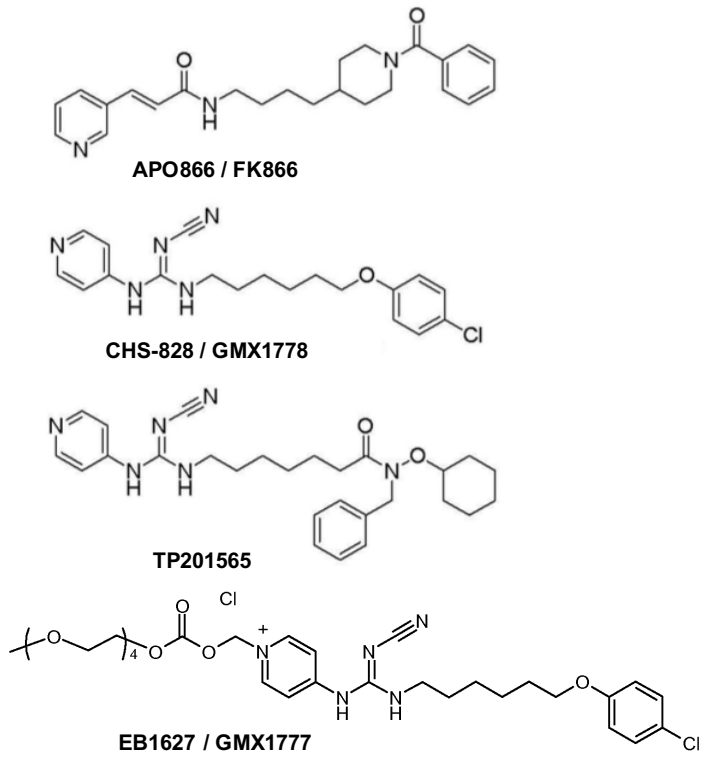

Figure 8 Chemical structures of NAMPT inhibitors
FK866 (APO866), CHS-828, and TP201565. FK866, CHS-828, and GMX1777 are chemically distinct whereas TP201565 is an synthetic analogue of CHS-828 [69].

Glutamine pathway and Asparagine synthetase

Beside glucose metabolism, glutamine (Gln) is a major nutrient consumed in cancer cells and it is the most abundant free amino acid in the body [80]. Glutamine pathway has also been interested as a potent target of cancer therapy and its transport rate is higher in cancer in respect to normal cells [81,82]. Glutamine belongs to a group of conditionally essential amino acid. In particular, under stress condition the dependency of growing cancer cells on glutamine is observed in intestinal mucosa cells [83]. In fact, glutamine can be considered as a non-essential amino acid due to, it can be synthesized by the metabolism of other amino acids during recycling and scavenging of ammonia in muscle and other organs [83]. The maintenance of high levels of glutamine in the blood provides a source of carbon and nitrogen to support biosynthesis and cellular homeostasis. Glutamine is transported into cells mainly through L-type amino acid transporter

(LAT1, a heterodimer of *SLC1A5* and *SLC3A)* a similar channel where facilitated tryptophan transportation [84,85]. High levels of L-glutamine evades the need for L-glutamine uptake influencing the activation of mTOR. Thus, L-glutamine level predominantly modulates mTOR activation, protein translation and autophagy to maintain growth and proliferation of mammalian cells [83,84]. mTOR itself regulates glutamine metabolism by cell-type specific mechanisms, either by inhibiting expression of mitochondrial SIRT4, or relieving repression of glutamate dehydrogenase (GLUD) [85]. Glutamine input associates to overall support of amino acid pools of the cell under stress response. GCN2 or aminoacid-sensing kinases (encoded by *EFF2AK4*) are activated during amino acid deprivation or amino acid starvation conditions [83,86]. Glutamine deprivation leads to uncharged tRNAs, or to a depletion of downstream products such as asparagine. GCN2 can be bound and activated by uncharged tRNAs, subsequently phosphorylates EIF2a and enhances *ATF4* and *ATF5* expression [83,87,88]. Moreover, oncogenic insults such as *MYC* was found to upregulate glutamine transporters and induced the expression of kidney-type glutaminase (GLS) at both mRNA and protein levels [83,85].

The Asparagine synthetase (ASNS) is an enzyme catalyzes conversion of L-aspartate and L-glutamine into L-asparagine and L-glutamate. It is an ATP dependent conversion reaction (**Figure 9**) [80,87]. L-asparaginase was synthesized by *Escherichia coli* at constant rates under anaerobic conditions [89]. Bacteria L-Asparaginase (L-Asp) has been approved from FDA and applied for ALL cells treatment. ALL cells express very low level of asparagine synthetase enzyme [90]. Up-regulation of *ASNS* expression can be caused by the activation of GCN2-EIF2a-ATF4 signaling pathway. Increased of *ASNS* might be one of metabolic response coordinating solid tumor adaptation to nutrient deprivation and/or hypoxia [87]. However, the high-glutaminase activity of l-asparaginase from *Acinetobacter glutaminasificans* showed non-specificity towards cancer cells [81,89]. Depletion of glutamine largely increases toxicity that is greater than its anticancer activity resulting in a low therapeutic index of L-Asparaginase. Moreover, leukemic cells have found to become resistant to the treatment [91]. L-Asparaginase therapy is often limited by toxic side effects [80]. Therefore, another L-Asparaginase from *Erwinia chrysanthemi* (ErA) was engineered with

the design of mutants diminished the ability to hydrolyze L-glutamine and in order to reduce the glutaminase activity, which is holding promise as a novel L-Asparaginase with fewer side effects for hematopoietic cancer therapy [81].

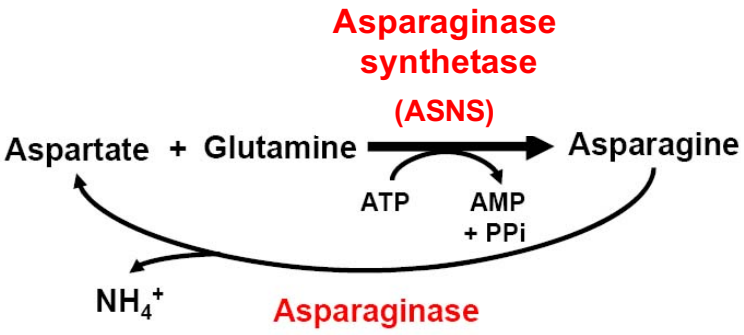

Figure 9 The biosynthetic reaction catalyzed by ASNS
The Asparagine synthetase (ASNS) is an enzyme catalyzes the conversion of L-aspartate and L-glutamine into L-asparagine and L-glutamate [80].

Drug resistance

Chemotherapy is the common approach to cancer treatment, however, drug resistance and the distant metastasis remain unresolved clinical problems [92]. Many cases of drug resistance have been revealed in clinical observations such as patients with breast cancer developed resistance to adriamycin, doxorubicin and docetaxel [93,94], ibrutinib resistance in chronic lymphocytic leukemia (CLL) [95], Imatinib resistance in chronic myeloid leukemia (CML) [96], Bromodomain and extraterminal domain (BET) inhibitors are promising epigenetic drug for acute myeloid leukemia (AML) treatment, but the resistance to BET inhibitors in leukemia stem cells population becomes a major limitation of these drugs [97], PARP inhibitors resistance in breast cancer [98]. In 2015, the drug-resistance profile in multiple-relapsed ALL was examined from 154 pediatric ALL samples demonstrating high incidence of patient becomes resistant to those common therapeutic agents. ALL were more drug resistant to dexamethasone (>1.5 times), L-asparaginase (5 times), etoposide (2.6 times), vincristine (3.1 times) e.g [99]. The resistance to a standard chemotherapy of T-ALL, L-asparaginase has been found to link to *ASNS* expression which can be silenced through methylation [100].

Although extensive studies for understating drug resistance and the mechanism of chemoresistance have been carried out but many questions remain undiscovered. Due to aforementioned NAD metabolism, NAMPT expression correlates with cancer malignancy. NAD+ dependent network governed self-renewal and radiation resistance in glioblastoma through NAMPT-E2F2-differentiation axis 101. However, the link between tumor metabolism and drug resistance in particular to a NAMPT inhibitor (FK866) has not been intensively investigated yet. Therefore, the aim of thesis was to elucidate the molecular mechanism of pharmacoresistance to a NAMPT inhibitor (FK866) and metabolic alteration associated drug resistance as well as identify therapeutic targets that could contribute to overcome the cancer resistance or improve the therapeutic outcome in T-lymphoblastic and breast cancer cells. Targeting lactate dehydrogenase has been widely interested for cancer therapy. High level of LDH is correlated with poor prognosis in many cancers [102,103] and caused of drug resistance in breast cancer [104]. Lactate dehydrogenase (LDH) is composed of two major subunits, LDHA (muscle, M) and LDHB (heart, H). LDH is a tetrameric enzyme that are encoded by two separate genes, *LDHA* and *LDHB*, respectively [105] (Figure 10A). This enzyme function as a catalytic enzyme to convert pyruvate into lactate coupled with an oxidation of NADH to NAD+ [106]. Under hypoxic condition, *HIF-1* was found to activate LDH and coordinately increased the conversion pyruvate to lactate [23]. Human *LDHA* or *hLDH5* is highly expressed in many cancer cells as the result of hypoxic condition as well as mutation of mitochondria genes [107]. *LDHA* not only accelerates cancer cell proliferation by regulating ATP production, but also plays a role in NAD+ regeneration driven glycolysis [23]. An increased expression of forkhead box protein 1 (FOXM1) upregulated *hLDHA* expression coordinately with increased LDH activity, lactate production, and glucose utilization in pancreatic cancer [108]. As illustrated in Figure 10B, in normal cells, glucose is metabolized into pyruvate then enters to TCA by acetyl Co-A under normoxia. While under hypoxic condition, OXPHOS remains inactive and LDH catalyzes the conversion of pyruvate together with oxidation of NADH to NAD+ to produce lactate [107]. Tumor cells have developed the ability to function in more acidic microenvironment than normal cells, thus elevated levels of *hLDH5* causes higher lactate production, which also triggers an increase in extracellular acidosis, resulting in a low pH allowing tumor invasion

and metastasis (Figure 10B) [107,109]. On the other hand, the silencing of *hLDHA* expression by shRNA displayed a reduction in the ability of tumors to proliferate under hypoxic conditions, markedly delayed tumor formation and stimulated mitochondrial respiration [23,103]. A few selective hLDHA inhibitors have been developed, GSK2837808A (GSK) recently showed potent NADH-competitive to hLDH5 exhibiting inhibitory activity in the nanomolar range in hepatocarcinoma cells [110,111]. MicroRNAs (miRNAs) can play as oncogenes or tumor suppressors, accordingly to the differential expression in diverse cancers. Recently, miR-383 has been reported to regulate *LDHA* expression in which the direct binding of miR-383 to its 3'-untranslated region (3'UTR) suppressed *LDHA* mRNA expression affecting glycolysis in ovarian cancer cells [112]. As well as, miR-34a, miR-34c, miR-369-3p, miR-374a, and miR-4524a/b were reported as target *LDHA* regulating glycolysis in colorectal cancer cells [113]. Thus, targeting LDH may progressively support the development of new strategies to treat metabolic cancers.

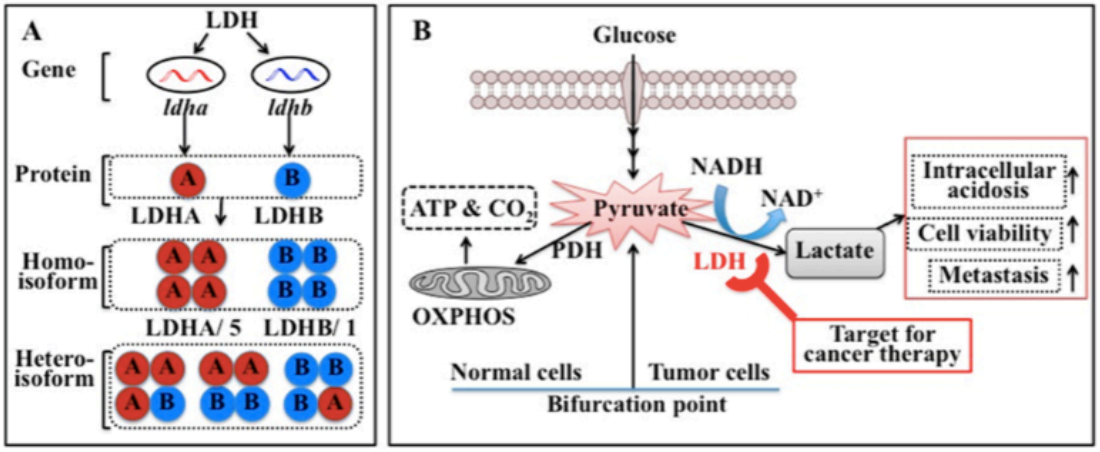

Figure 10 Schematic representation of LDH

A. LDH isoforms in human**, B** metabolic pathway in normal and cancer cells [107]**.**

Oxidative phosphorylation

Multiple step flow of electrons through mitochondrial respiratory chain has been known as oxidative phosphorylation (OXPHOS). As illustrated in **Figure 11**, OXPHOS comprises five multisubunit protein complexes (I-V) and two electron carriers localized on the inner mitochondrial membrane which are Coenzyme Q and cytochrome c [114]. Critical complexes of electrontransport chain and other protein subunits have been documented and known by their enzymatic reactions

including complex I (NADH-ubiquinone oxidoreductase), complex II (succinate-ubiquinone oxidoreductase), ubiquinone (CoQ), ubisemiquinone (CoQH), ubiquinol (CoQH2), complex III (ubiquinol-cytochrome c oxidase reductase), complex IV (cytochrome c oxidase or COX), and inorganic phosphate (Pi) [114].

Coordinated transport of electrons and protons resulted in the production of ATP has been considered as the main function of this system. Intermediary metabolism of protein, carbohydrate, and fat are used to generate NADH and $FADH_2$ and then continuously donate electrons to complex I and complex II, respectively. Electrons pass sequentially to ubiquinone in order to form ubisemiquinone and ubiquinol. Transferred electrons to complex III and cytochrome c and then move to complex IV. A molecule of water can be generated by the donation of an electron to oxygen during this process. Energy transformation is liberated by the flow of electrons which is used by complexes I, III and IV for protons pump. Moreover, complex V plays a role in regulation of proton gradient to generate the mitochondrial membrane potential for ATP synthesis. ATP can be produced from cytosolic ADP and Pi [18,114].

Glycolytic enzymes

Aerobic glycolysis is one of the well-defined metabolic phenotype of cancer via transcriptional upregulation of glycolytic enzymes [10]. As illustrated in **Figure 12**, glucose is converted to fructose-1,6-bisphosphate by two molecules of ATP and then sequential reactions of glucose is catalysed by specific enzymes in each step including hexokinase (HK), phosphoglucose isomerase (PGI), and phosphofructokinase (PFK) in the first phase of glycolysis. Apart from LDH, HK2 also plays a role in the regulation of the mitochondria-initiated apoptotic events inducing cell death [32]. HK2 is directly regulated by *HIF* and considered as a *HIF-1* target gene product [115]. Increased expression of HK2 contributing to an elevated glycolysis was observed in most of immortalized and malignant cells[26]. Moreover, activity of mitochondrial hexokinase somehow regulates and is required for the growth factor-induced cell survival [3,116]. Transactivation of HK2 by the cooperation of *HIF-1* with *c-Myc* is occurred under hypoxia condition [115].

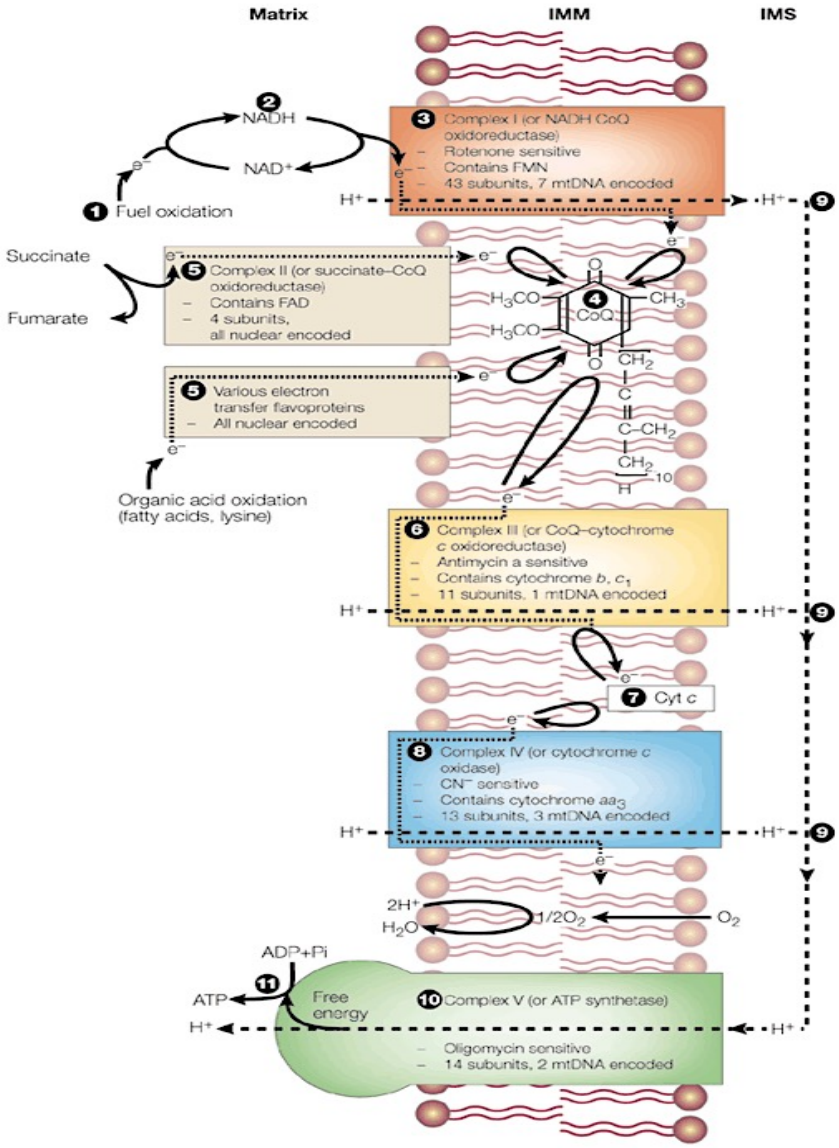

Figure 11 OXPHOS system in mammalian mitochondria [114].

Phosphofructokinase-1 (PFK1) is a catalyses enzyme in the committed steps of the glycolytic pathway by converting fructose-6-phosphate to fructose-1,6-bisphosphate, using ATP as the energy source [12]. PFKFB enzyme can be activated through phosphorylation at serine 462 of AMPK during hypoxia [117]. Moreover, inhibition of PFK by lactate reveals an important mechanism of the feedback inhibition in glycolysis [118]. Pyruvate kinase (PK) is a key enzyme in final step of glycolysis which it catalyzes the irreversible phosphoryl group and transfers from PEP to adenosine ADP, yielding pyruvate and ATP [12]. PKM2 is predominantly expressed in tumor cells and it has been used as a marker of intestinal inflammation [119]. Nuclear translocation of PKM2 leads the cooperation

with HIF-1 and concurrently triggers transactivated genes and further enhances glycolysis [120]. Tumors frequently appear to enhance glycolysis and suppressed OXPHOS [6]. Therefore, evaluation of glycolytic enzyme activity and OXPHOS function are important for understanding metabolic reprogramming in the cancer drug resistance in particular to FK866 resistance.

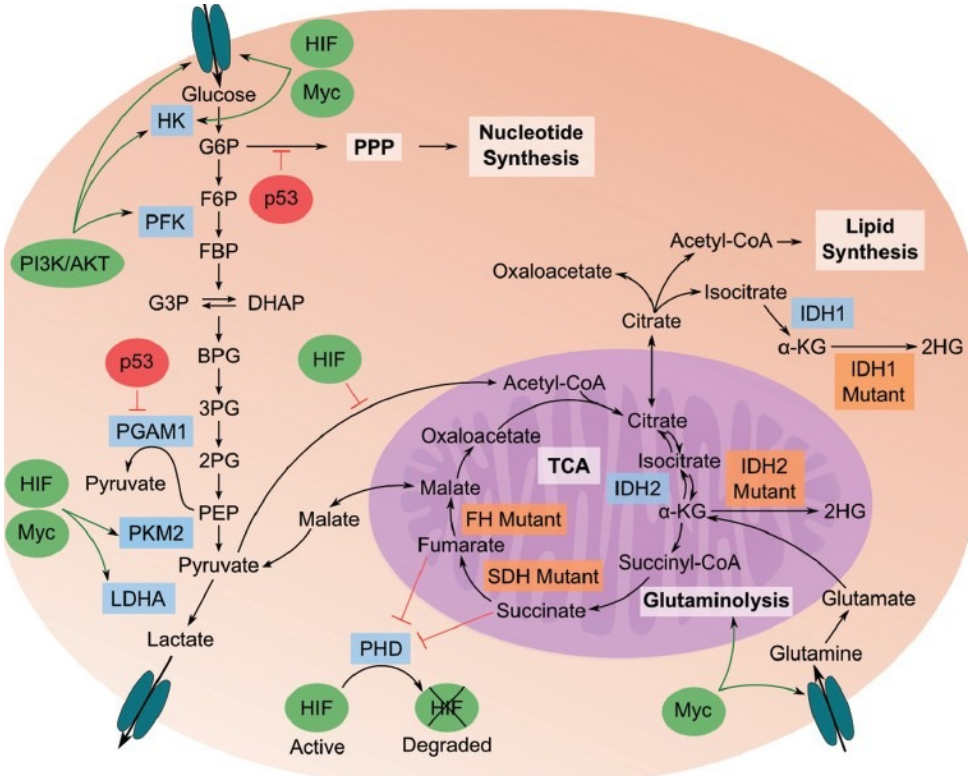

Figure 12 Glycolysis and TCA cycle in tumors
Glycolysis breaks down glucose into pyruvate, which is then converted to lactate. Pyruvate fuels either the production of lactate or it can be used to replenish the TCA cycle [13,121].

Signal transduction in cancers

Signaling transduction is responsible to maintain cell growth advantage in cancer as well as drug-resistant cancer. Canonical oncogenic signaling pathways, such as phosphatidylinositol 3−kinase (PI3K)-AKT/Protein Kinase B (PKB) and mammalian target of rapamycin (mTOR), these two signaling pathways have been consider as major players which directly regulate the core carbon metabolism resulting in the larger nutrient uptake supporting cell proliferation [122]. PI3K has also profound effects on tumor metabolism by providing strong growth and survival signal for cancer [123]. Therefore, we investigated the relevance of

drug resistance to MTOR/AMPK pathway activation and protein translation control.

MTOR

Signal transduction in mammalian cancers frequently involves the association or constitutive activation of receptor tyrosine kinases (RTKs) which are serine/threonine kinase including phosphatidylinositol 3-kinase (PI3K)/AKT kinase cascade [124,125], the protein kinase C (PKC) family [126], and the mitogen-activated protein kinase (MAPK)/Ras signaling cascades [127]. mTOR has been known as FRAP, RAFT1, and RAP1. mTOR is a Ser/Thr kinase that functions as a master switch between anabolic and catabolic metabolism in cancer [124]. It plays roles in the regulation of cell proliferation, metabolism and also apoptotic cells death, which is mainly dictated by cellular context and downstream targets including *p53*, B-cell lymphoma (*BCL2*), BCL2-antagonist of cell death (*BAD*), and *c-MYC* [128].

mTOR comprises two biochemically and functionally distinct complexes which are mTORC1 and mTORC2 [124]. As illustrated in **Figure 13**, mTORC1 includes regulatory-associated protein of mTOR or Raptor. Raptor acts as a scaffold protein to recruit downstream substrates of mTOR, which are eukaryotic translation initiation factor 4e-binding protein 1 (4EBP1) and ribosomal S6 kinase (S6K1). 4EBP1 and S6K1 are generally attributed to mTORC1-dependent protein translation control [5,124]. mTORC1 displays as a complex of mTOR, Raptor, PRAS40, mLST8 and Deptor while mTORC2 complex contains Rictor, mSIN1, mLST8 and Protor1. mLST8 binds to the mTOR kinase domain in both complexes, where mLST8 seems to be important for the complex assembly. Deptor acts as an inhibitor of both complexes mTOR1 and mTOR2 [57]. Dependent-phosphorylation at T2446/S2448 of mTOR is mediated by PI3K/Akt [125]. In addition, *CyclinD1*, *HIF1a*, and *MYC*, which in turn promoted cell cycle progression, cell growth and angiogenesis are controlled by mTORC1 [5]. In contrast, mTORC2 contains the rapamycin-insensitive companion of mTOR or Rictor subunit but Rictor is neither sensitive to nutrients nor inhibition of rapamycin [5,124]. mTOR2 has been documented to participate in cell survival and actin cytoskeleton rearrangements [125].

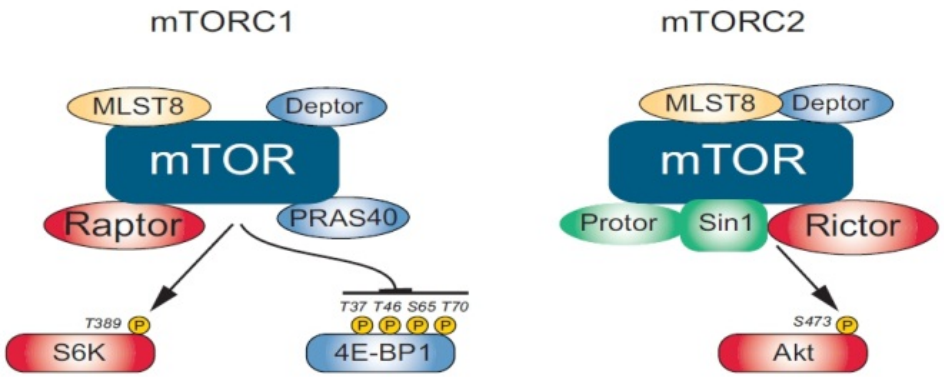

Figure 13 Composition of mTORC1 and mTORC2 [57].

The PI3K/AKT/mTOR signaling pathway

Regulation of the PI3K/AKT/mTOR pathway can be resulted from both exogenous or endogenous activation such as an exogenous activation by Ras which has been reported in a broad variety of solid tumors [129]. On the other hand, endogenous activation of PI3K/AKT/mTOR pathway could be triggered from either PTEN loss function or gene mutation/amplification [7]. Activation of various receptor tyrosine kinase (RTK) leads to auto-phosphorylation of intracellular component of these receptors. In particular, phosphorylation of PI3K subunits (p85 is a regulatory subunit and p110 is a catalytic subunit) by RTK can induce the allosteric activation of PI3K (**Figure 14**). Moreover, PI3K can also be indirectly activated by Ras [7]. Activation by Ras is mostly restricted to gastrointestinal malignancies whereas RTK activation has been widely reported in hematological and also solid tumors [7,130]. Reduction or loss of *PTEN* expression incidentally triggers PI3K signaling, thereby coordinating to oncogenesis in some human cancer [124,131]. Thus, PTEN has also been identified as a negative regulator of PI3K signaling contributing to the regulation of cell growth, proliferation, metabolism and also the survival of cancer [131]. Akt-mediated phosphorylation of TSC2 on S939/S981 directly inhibits the TSC1/TSC2 complex, thereby relieving inhibition of Rheb and activating mTORC1 [125]. TSC2 regulates mTOR1 by acts as a central receiver of inputs to stimulate mTOR1. Thus it was evident that cells which lack of TSC2 function still profound mTOR suppression due to the following AMPK activation [132].

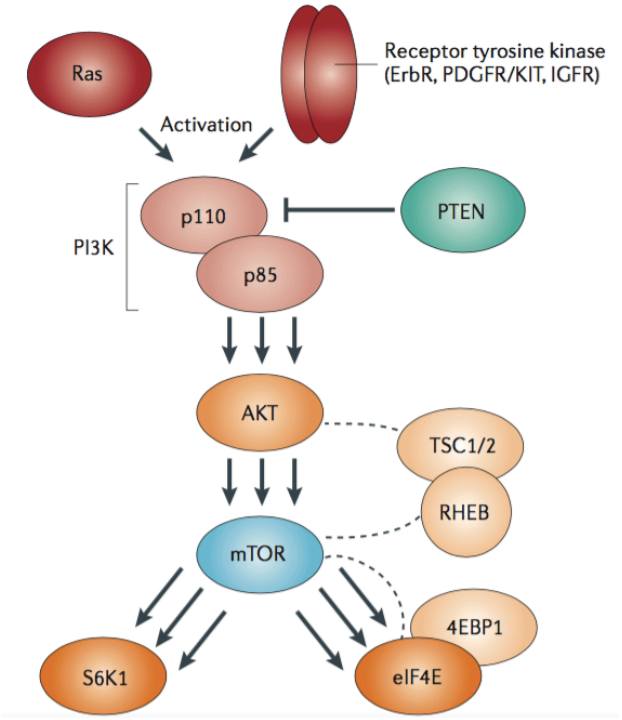

Figure 14 PI3K/AKT/mTOR Signaling pathways
Dysregulation of the PI3K/AKT/mTOR pathway can result from exogenous or endogenous activation. MTOR is activated by Rheb, resulting in modulation of protein synthesis by phosphorylating S6K1 and 4EBP1. Phosphorylation of 4EBP1 by MTOR signaling resulting in dissociation of MTOR from eIF4E [7,130].

Regulation of AMPK

AMPK has been well-defined as a central metabolic sensor in mammalian cells and it plays roles in regulation of many cellular energy supplies including lipid, cholesterol, and glucose metabolism [133]. An essential role of AMPK in balancing glycolysis and mitochondrial metabolism has been reported in T-ALL cells[134]. Mechanistically, AMPK is directly phosphorylated on T172 by LKB1 leading to activation of AMPK. LKB1-AMPK signaling pathway has a dominant role in regulation of glucose metabolism especially in metabolic tissues such as muscle, liver, and adipose tissues [5,135]. AMPK composes of hetero-trimer subunits which are a catalytic subunit (AMPKα) and two regulatory subunits (AMKPβ and AMPKγ). Hypoxia induction and nutrient deprivation are two important factors that activate AMPK thereby impact to intracellular ATP and AMP levels. A decline of ATP level concomitants an increase in intracellular AMP in AMPK activated cells [135]. mTOR is controlled by LKB1-AMPK activation [130,136]. AMPK can also be activated by two known AMPK activators which are CaMKK and TAK1. AMPK

activates mTOR by phosphorylation of raptor on S722/792. Activation of AMPK by energy stress further phosphorylates Raptor and induces the binding of raptor to 14-3-3 subsequently inhibits of mTORC1 activity [125,136]. In addition, inhibition of mTORC1 can be mediated by both AMPK and the signaling from GSK3β. The phosphorylation of TSC1/2 complex further exerts the positive regulation of TSC2 towards Rheb, thereby abrogates its simulative activity towards mTORC1 pathway (**Figure 15**) [125]. AMPK associates with inhibition of fatty acid and cholesterol synthesis by phosphorylating certain metabolic enzymes such as acetyl-CoA carboxylase 1 (ACC1) and HMg-CoA reductase (HMgCR) [133]. Nevertheless, AMPK has been found to regulate glycolysis though the modulation of phosphorylated PFK2 at Ser466 leads to an increases the levels of Fru-2,6-P2 thereby enhancing glycolytic flux [137]. Hypoxia directly activates AMPK which further inhibits mTORC1 in two ways by through Raptor inhibition and direct negative phosphorylation of TSC2 [125].

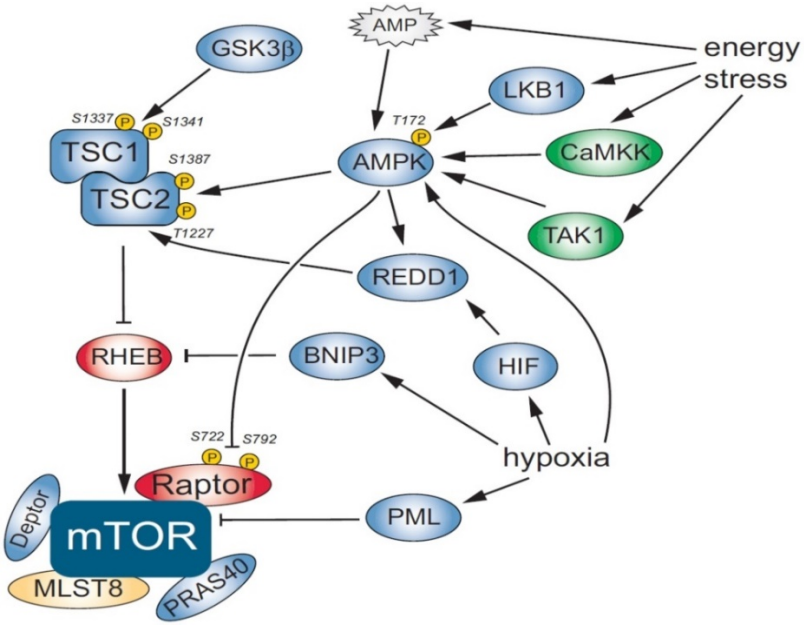

Figure 15 LKB1-AMPK signaling pathway
Schematic representation of the Liver Kinase B1(LKB1) dependent regulation of growth. Metabolism and mitochondrial homeostasis are regulated through AMPK and mTOR signaling pathways. Activation of LKB1/AMPK/mTOR pathway can be induced by energy stress [125].

Protein translation control

Control of mRNA translation plays an important role in several cellular processes including cell growth, proliferation, and differentiation[138,139]. Signaling by the PI3K/AKT/mTOR pathway mediates mRNA translation through modulation of S6K1 and 4EBP1 which are two distinct downstream signaling pathways (**Figure 13** and **14**) [5,135]. S6K1 and 4EBP1 control specific subsets of mRNA translation. 4EBP1 is a small protein which inhibits the initiation of protein translation by associating with eIF4E which is one of mRNA cap-binding subunit of eIF4F complex as illustrated in **Figure 16**. A review by Mamane *et al.,* has been well summarized the interaction of mTOR with translation proteins [5]. Under growth factor-deprivation such as lack of nutrients and hormone, unphosphorylated 4EBP1 binds tightly to eIF4E leading to inhibition the initiation of protein translation in normal cells. While in the presence of stimuli from several factors such as nutrients, hormones, growth factors, mitogens, cytokines and G-protein-coupled agonists response, induce the dissociation of eIF4E from mTOR complex (**Figure 16**) [5]. There are a number of protein subunits involved in cap translation such as eIF3, eIF4A (an ATP-dependent RNA helicase), eIF4B, eIF4E, and eIF4G (a large scaffolding protein). However, phosphorylation and activation of S6K1 further phosphorylates eIF4B at S422 then promotes its association with eIF3 [7]. Phosphorylation of 4EBP1 occurs at multiple sites and proceeds in a hierarchical manner (first at Thr37 and Thr46, then Thr70 and last at Ser65) [140]. In generally, under growth factor induction free eIF4E from the dissociation of mTOR can bind eIF4G, eIF4A, and eIF4B to form the multi-subunit of eIF4F complex. This complex facilitates cap-dependent protein translation [138–140] and induces translation of 5′-UTR (the 5′-untranslated terminal regions) [136]. On the other hand, treatment with rapamycin (a potent mTOR inhibitor) has been found to impact many events such as dephosphorylation of 4EBP1, increases in eIF4E binding, no forming of eIF4F multi-subunit complex and concomitant with impairment of 5′−UTRs translation initiation which is crucial for cell cycle transition from G1-to-S phase [7,138,139].

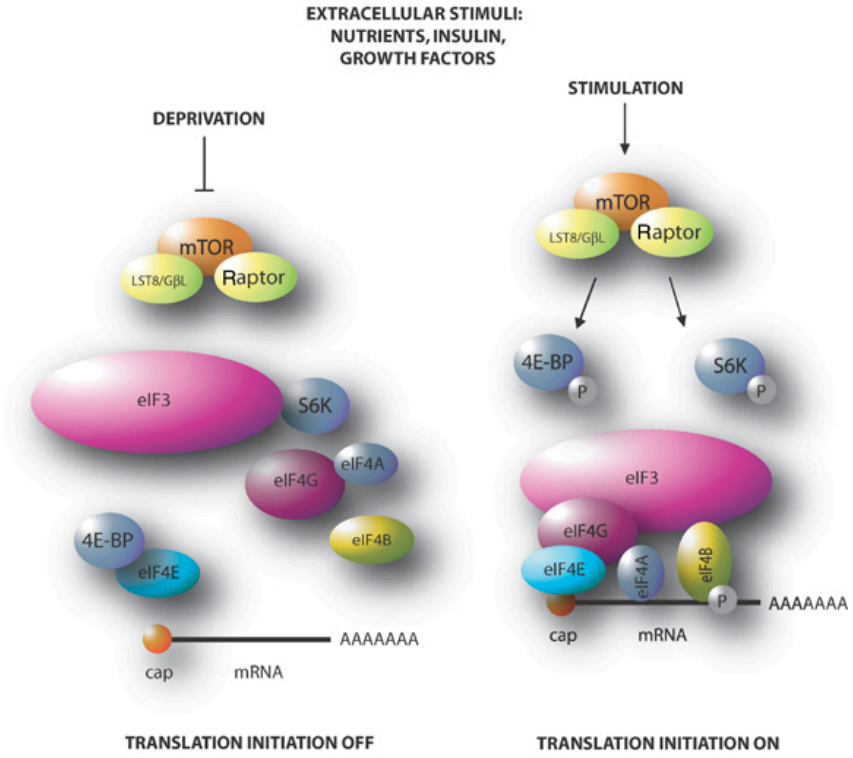

Figure 16 Activation of translation initiation by mTOR
Regulation of Cap-Dependent Translation Initiation by 4EBP1. In general, mTOR phosphorylates 4EBPs and S6Ks which are two downstream targets of mTOR pathway. In condition with no extracellular stimuli, S6K1 associates with eIF3, and 4EBP1 associates with eIF4E. Growth factors, nutrients as well as insulin signaling, recruit the mTOR complex in order to phosphorylate S6K1 and 4EBP1. Phosphorylated 4EBP1 by mTOR results in dissociation of 4EBP1 from eIF4E and dissociation S6K1 from eIF3. S6K1 further phosphorylates eIF4B at S422 contributing to the association of eIF4B with eIF3 subunit. These multiple interactions enhance cap-dependent translation [5].

CHOP activation

Endoplasmic reticulum (ER) stress has a profound impact to unfolded and malfolded client proteins leading to cell death in pathophysiological conditions [141]. Cell frequently adapt to ER stress by activating an integrated signal transduction pathway called the unfolded protein response (UPR) [142]. UPR is generally involved by 3 signaling pathways emanating from ER including IRE (inositol-requiring protein 1), PERK (PKR-like ER kinase), and ATF6 (activating transcription factor 6). All of them are integral ER membrane proteins [141,142]. The C/EBP homologous protein or CHOP is a transcription factor that is induced by ER stress. Phosphorylates EIF2a by PERK decreases EIF2a activity paradoxically activates *ATF4* mRNA expression (**Figure 17**) [86]. *GADD34* or *CHOP* is a direct target gene of ATF4. Phosphorylation of EIF2a by general

control non-depressible 2 (GCN2) inhibits global protein synthesis and blocks cap-dependent translation [87]. It has been reported that multiple basic-region leucine zipper (bZIP) transcriptional regulators, including ATF4, ATF3, and ATF2, work in concert to mediate activation of *CHOP* expression during nutrient limitation. But there are different mechanisms of CHOP regulation during amino acid starvation and ER stress [86,141]. Briefly, in response to ER stress, EIF2a is phosphorylated by PERK and induces *ATF4* expression whereas during nutrient limitation or amino acid deprivation, the uncharged tRNA binds to GCN2 and activates GCN2. Activation of GCN2 kinase sequentially induces expression of *ATF4, ATF3* and *CHOP* [86,87,141]. In addition, ER stress activates IRE1 by dissociation of IRE1 from BiP then the activated IRE1 further induces splicing of XBP1 which is a transcription factor regulated downstream target genes such as ER chaperones [143].

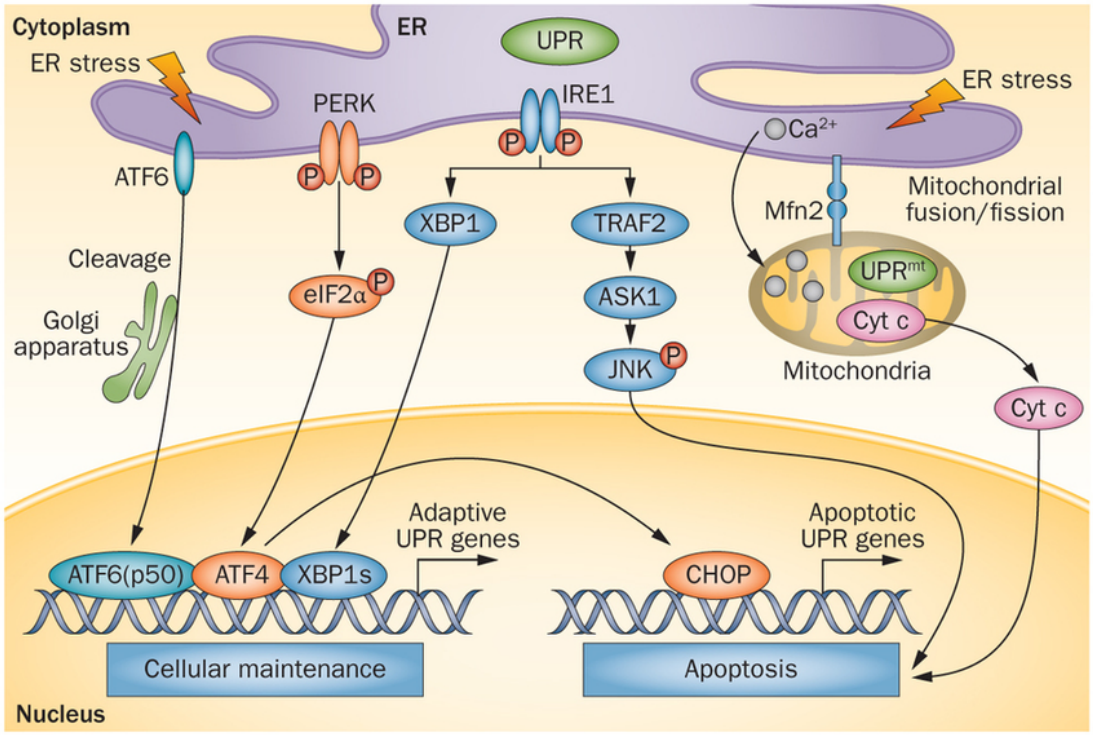

Figure 17 Mammalian UPR and CHOP activation pathways
The UPR encompasses signaling pathways which is triggered by the activation of ER stress transducers including IRE1, ATF6, and PERK. These transcription factors mainly upregulate the adaptive UPR pathway and normalize ER function via the ATF6, PERK–EIF2α–ATF4 or IRE1–XBP1 pathways. The adaptive UPR pathway fails to rescue the cells, and the apoptotic UPR pathway under long term stress condition [141].

MATERIAL AND METHODS

Chemicals and Reagents

Cell culture media were obtained from Invitrogen (Carlsbad, CA). Fetal bovine serum (FBS), L-glutamine, and penicillin-streptomycin were obtained from Lonza. All other chemicals and reagents used in this study were purchased from the following sources: FK866 (sc-205325;santa cruz), CHS-828 (200484-11-3) from Cayman chemical, JPH203 (a LAT-1 inhibitor) and L-asparaginase were kindly gifted from Dr. Jean-Francois Peyron [144], 2-Deoxyglucose (D3875;sigma), Oligomycin A (S1478;Selleckchem), MTT assay (M5655;Sigma), Ozblue cell viability kit (OZbiosciences), NAD/NADH Assay (G9071;Promega), Cell-tite Glo (G7570;promega), and GSK2837808A (GSK;Trocris).

Cell culture and development of NAMPT resistant cell models

Human T-cell acute lymphoblastic leukemia (CCRF-CEM) cells were purchased from the Interlab Cell line Collection bank (ICLC HTL01002) and human breast adenocarcinomar (MDA-MB231) cells were obtained from our in-house tissue culture cell bank (original source was ATCC). CCRF-CEM were grown in RPMI 1640 supplemented with 10% FBS, 2mM L-glutamine, and 100 U/ml penicillin-streptomycin. MDA-MB231 cells were grown in DMEM supplemented with 10% FBS, 2mM L-glutamine, and 100 U/ml penicillin-streptomycin. All lines were cultured at 37°C in a humidified atmosphere of 5%CO2. NAMPT resistant CCRF-CEM and MDA-MB231 models were gradually developed by increasing the concentration of FK866 up to 500nM of FK866. Cell viability was determined by exclusion of 0.2% trypan blue and MTT assay (Sigma). The FK866 resistant sublines were always maintained as static suspension in RPMI 1640 medium or DMEM medium supplemented with 10%FBS, 2mM L-glutamine, 100 U/ml penicillin-streptomycin and with 100nM FK866. A final concentration of the resistance subline selected for all experiments was a 100nM FK866 Resistant sublines.

Transfection, plasmids and siRNA

Transient transfection, pcDNA-PBP and NAMPT1 plasmids were kindly provided from Dr. Alessio Nencioni (Genova). Plasmids were transiently overexpressed in MDA MB231 cells using lipofectamin 3000 (Thermoscientific). *LDHA* siRNA (sc43893) and control siRNA-A (sc37007) were purchased from santacruz. Down regulation of *LDHA*, siRNAs targeting human *LDHA* were transfected via interferin transfection reagent (Polyplus) to transiently knock-down the *LDHA* expression in MDA PA and MDA RES cells which were detected by immunoblotting against LDH antibody.

In vitro cell viability and drug combination assays

Cell viability was measured by the colorimetric methyl-thiazolyltetrazolum (MTT) assay (sigma), XTT proliferation kit (sigma), Ozblue cell viability kit (OZbiosciences) and cytotoxicity assay based on LDH levels. Release of LDH from damaged cells is measured by suppling lactate using LDH kit (Pierce LDH cytotoxicity Assay; PG202275), NAD+ and iodonitro tetrazolium violet (INT) a tetrazolium salt as substrates. A red formazan product is proportional to the number of lysed cells which indicates dead cells. Dose response was calculated, plotted as a non-linear regression curve and EC50 values determined using Prism 5 (GraphPad software Inc). Percentage of cell inhibition was subjected for drug combination analysis as described as Combination index (CI) according to the Chou-Tala-lay [145]. Measure of synergism is given as CI where CI<1, CI=1, and CI>1 indicate drug synergism, additivity, and antagonism, respectively.

Flow cytometric cell cycle analysis

CEM cells were treated with Mock, GSK 10μM and GSK 20μM. Forty-eight hours after treatment they were resuspended in 1500 ml and lyzed with 0.5% Triton X for 15 min. Thereafter, they were then incubated with the DNA-staining chemical propidium iodide (PI) (FITC/Annnexin V Apoptosis detection kit; BD Pharmingen) for DNA content-based assessment of cell-cycle distribution for 10 min. Cell cycle analysis was performed using flow cytometric. Cell starvation was prepared in medium without FBS for overnight and treatment with 100ng/ml Nocoldazole for 24h were used as positive controls. Percentage of G1 phase, S phase, and G2 phase were analyzed using FACS.

Determination of NAD+-NADH and ATP levels

Intracellular NAD+-NADH levels were determined by luciferin-luciferase-based assay. Cells were treated with FK866 for 48h or other indicated treatments, harvested. Aliquots containing equal number of cells were processed using the NAD/NADH Assay (G9071;Promega) following the standard protocol. Intracellular ATP level was assessed using Cell titer-Glo Luminescent readout (G755A;Promega). NAD+-NADH and ATP values were measured by multilabel plate reader (Tecan infinite M200) and normalized to total amount of protein of cell lysates (Bradford Reagent, Sigma).

Immunoblotting Analysis

Cells were treated with FK866 or indicated treatments for 48h and at the end of the treatment periods, cells were harvested, lysed in RIPA buffer. Equal amount of cell extracts (20 µg of total proteins) were diluted in Laemmli sample solution (6X), resolved on SDS-PAGE gels, transferred to PVDF membranes and probed overnight at 4°C using the following primary antibodies including 4EBP1 (sc-6936), p-4EBP1(Ser65/Thr70; sc-12884), EIF4E (sc-9976), p-EIF4E Ser209 (sc-12885), MTOR (sc-8319), NAMPT(sc-130058), LDHA (sc-137243) from Santa Cruz; EIF2S1 (ab26197), p-EIF2S1 Ser51 (ab32157), and p-MTOR Ser 2448 (ab1093) from Abcam; AMPKα (2603), p-AMPKα Thr 172 (2531), and CHOP (2895) and anti-β-actin antibody (s3700) from Cell Signaling. Appropriated secondary antibodies (Santa cruz) were used to detect interested protein using a ECL select western blotting detection reagent (RPN2235; GE healthcare). Immunoblotting for β-actin was performed to verify equivalent amounts of loaded protein. Densitometric analysis of immunoreactive bands was analyzed using ImageJ software (NIH, USA).

Amino acid depletion experiment

The experiment was performed in amino acid depletion mixture composing Eagle's Balance salt solution, (E3024; Sigma) to normal 10% FBS in RPMI medium supplemented with 2mM L-glutamine (ratio 80:20). CEM Cells were treated with indicated treatments for 24h, lysed in RIPA lysis buffer and then equal amounts of proteins were separated by SDS–PAGE. Immunoblotting

against CHOP expression was detected and anti-β-actin antibody was used as a protein loading control.

Enzymatic activities, oxygen consumption, and ATP concentration

CCRF-CEM and MDA MB231 cells were incubated (or not) with FK866 for 48h. Cells were homogenized as described in [146]. The supernatants were immediately used for the assays of enzymatic activities. The simultaneous measurement of the enzymatic activities was performed by using the coupled fluorometric assay. The enzymes' activity of NAD biosynthesis pathway was referred to the protein concentration determined [146]. *(This experiment was conducted in collaboration with Prof. Nadia Raffaelli (University of Politecnica Delle Marche, Ancora, Italy).*

Oxygen consumption was measured at 25°C in a closed chamber (1.7 ml capacity) using a thermostatically controlled oxygraph apparatus equipped with amperometric electrode (Microrespiration, Unisense A/S, Århus, Denmark) as previously described [147]. ATP concentration was measured in a luminometer (Lumi-Scint, Bioscan) by the luciferin/luciferase chemiluminescent method as previously described [147]. In both cases, 5 mM pyruvate +2,5 mM malate or 20 mM succinate were used as respiring substrates to assess the activity of the pathway formed by Complexes I, III and IV and the pathway composed by Complex II, III and IV, respectively. *(This experiment was conducted in collaboration with Dr. Silvia Ravera, Istituto Giannina Gaslini, Genova, Italy).*

Mitochondria ATP measurement

CCRF-CEM parental and CCRF-CEM FK866 resistant subclones were directly treated with control (PBS), oligomycin A (10 µg/ml; Sigma), sodium iodoacetate (100 µM; Sigma) or both. Following a 1-hour incubation at 37°C, 25 µL of luciferine (150 µg/ml, Promega) was added to each well for a final volume of 125 µL. Plates were then analyzed (1sec measurement/well) for luminescence with a Berthold Technologies Luminoscan (in our model, emitted light start to decrease after 1min). By comparing the different conditions, percentages of glycolytic and mitochondrial ATP produced by CCRF-CEM-luc cells were determined as described in [148]. *(This experiment was conducted in collaboration with Dr. Jean-Francois Peyron, Ruxandra Moschoi and Johanna Chiche, U1065/C3M, Nice, France)*

Quantitative Real-time PCR

Total RNA was extracted using RNA extraction kit and contaminant DNA was removed by RNase-Free DNase kit (ZYMO research). cDNA synthesis was carried out with RevertAid RT kit (K1622;Themoscientific). Quantitative real-time PCR analyses were performed with triplicate using KAPA SYBR FAST Universal qPCR Kit on a CFX96-Real time PCR Detection system (BioRad). Primers's sequences are provided in **Appendix Table 3** and expression level are analyzed relative to *18S* or *GAPDH* as housekeeping genes.

Data management and statistical analysis

Data analysis was performed using Microsoft excel 2016 and plotted by GraphPad Prism 6 (Graphpad software Inc., San Diego, CA). Data are represented as the Mean with SD or SEM. Statistical analysis was performed by one-way analysis of variance (ANOVA) with Bonferroni's corrected t-test for post-hoc pair wise comparison and Student's t-test. ***$p<0.001$, **$p<0.01$, and *$p<0.05$ were considered statistically significant.

RESULTS

In 2015, our group published a research article ***"EIF2a-dependent translational arrest protects leukemia cells from the energetic stress induced by NAMPT inhibition"*** *in BMC Cancer Journal* [71]*. This publication reflects my personal contribution to the work, and provides background for my thesis study regarding to pharmacological effect of NAMPT inhibitor (FK866) in leukemia.*

In this article, we showed that FK866 induces a translational arrest in leukemia cells through inhibition of MTOR/4EBP1 signaling and of the initiation factors EIF4E and EIF2a. Specifically, treatment with FK866 is shown to induce AMPK activation, together with EIF2a phosphorylation, is responsible for the inhibition of protein synthesis. Notably, such an effect was also observed in patients' derived primary leukemia cells including T-cell Acute Lymphoblastic Leukemia. We concluded that tumors exhibiting an impaired LBK1-AMPK-EIF2a response may be especially susceptible to NAMPT inhibitors in particular in leukemia [71]*.*

*A hard copy of this article is enclosed in appendix (****page 128****). In this work we provided new insights into the molecular mechanism of NAMPT inhibition in leukemia cells. However, the mechanism of FK866 resistance in cancer has not been widely investigated. We aimed to investigate how cancer cells can escape from FK866 toxic insult. All presented results in this thesis body are unpublished data. For clarify, I myself performed and have been involved in all experiments except enzymatic activity assay which I was involved in sample preparation, thereby biochemical analysis was kindly conducted by the collaboration of Dr. Silvia Ravera (Istituto Giannina Gaslini, Genova, Italy) and Prof. Nadia Raffaelli (University of Politecnica Delle Marche, Ancora, Italy).*

Emergence of drug resistance in cancer cells is a major impediment of chemotherapy and metabolic alteration has been frequently perceived in cancer cells of various tissues. **Thus, the aim of my thesis was to investigate the molecular mechanism of pharmacoresistance to FK866 and metabolic alterations associated with drug resistance in cancer cell lines.**

Development of NAMPT inhibitor (FK866) resistant models

FK866 CCRF-CEM resistant cells were developed in our laboratory to investigate the molecular mechanism beneath the insurgence of pharmacoresistance to the NAMPT inhibitor. In-house CCRF-CEM parental cells (CEM PA) were gradually exposed into an initial dose of 0.1nM FK866 and cultured those surviving daughter cells with increasing doses until they acquired resistant to final concentration of 500nM FK866 as described in Chara Zucal's thesis [149]. We generated three populations of FK866 resistant cells which were resistant to FK866 at 10, 40 and 100nM, respectively. Cell viability test was performed in all FK866 resistant CCRF-CEM (CEM RES) along with FK866 administration for 48 and 72h. Unlikeness of FK866 resistant subclones (CEM RES 10, 40 and 100) were discriminated by differential resistance to FK866, while CEM RES 100 cells showed fully drug resistance (**Figure 18A** and **B**). Afterward, CEM RES 100nM subclone (referred as **CEM RES** in my thesis) was selected as a model for this study. CEM RES cells eventually gained the ability to proliferate during drug exposure for 4 days of treatment with 500nM FK866 (**Figure 18C**) [149]. CHS-828 or GMX1778 is an another known NAMPT inhibitor was tested in CEM cells. Potential anti-proliferative effects of CHS-828 was observed only in CEM parental cells (**CEM PA**) while CEM RES cells were not sensitive to the drug (**Figure 18D**) assuming that we accomplished generating a NAMPT-dependent CEM resistant model.

Characterization of NAMPT-dependent CEM resistant model

To address the pharmacological effect of FK866, NAD and ATP levels in CEM cells were measured. Cells were treated with 5nM FK866 for 48h. As shown in **Figure 19A** and **19B**, FK866 significantly decreased both NAD and ATP levels in CEM PA (***$p<0.001$). Therefore, inhibition of NAMPT by FK866 significantly impacted NAD and ATP levels. In collaboration with Prof. Nadia Raffaelli (University of Politecnica Delle Marche, Ancona, Italy), we managed to evaluate enzymatic levels of NAMPT. NAMPT enzymatic activity was decreased in CEM RES cells in respect to CEM PA while FK866 treatment did not affect to NAMPT activity (**Figure 19C**). In parallel, we evaluated *NAMPT* mRNA levels in both CEM PA and CEM RES cells. A significant decrease in *NAMPT* mRNA level (**$p<0.01$) was observed in CEM RES cells in comparison with CEM PA cells whereas, there

was no alteration in *NAMPT* mRNA levels along with FK866 administration in both parental and resistance (**Figure 19D**). Development of drug resistance to NAMPT inhibitors commonly depends on gene mutation [150]. However, we did not observe any mutations in *NAMPT* coding region neither in our CRM resistant nor CEM parental cells.

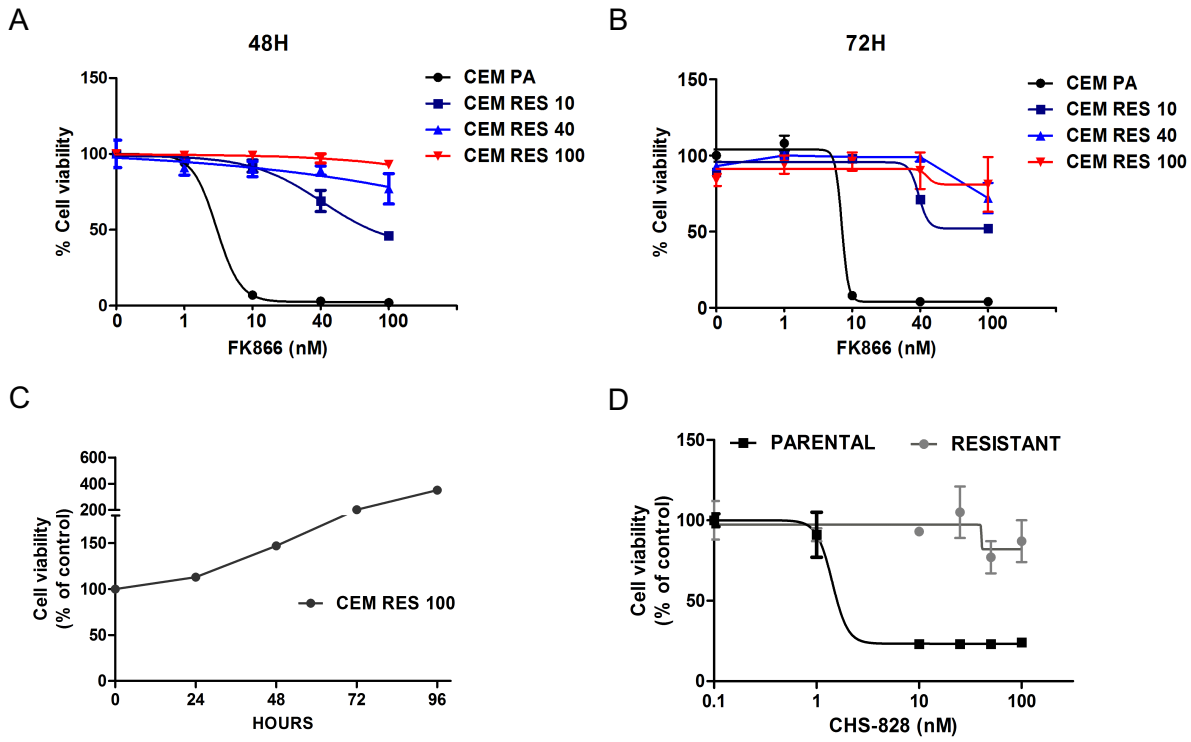

Figure 18 Insensitivity of NAMPT-dependent CCRF-CEM resistant cell lines to FK866

A and **B**, Effect of NAMPT inhibitor (FK866) in a panel of different CEM RES subclones including CEM RES resistance to FK866 at 10, 40, and 100nM indicated as CEM RES 10, 40, and 100, respectively. Cells were treated with FK866 for 48h and 72h. **C**, Four-day FK866 survival curve of CEM RES 100 cells are shown. **D**, Effect of a NAMPT inhibitor (CHS-828) on CEM PA and CEM RES cell lines. Cells were treated with CHS-828 for 48h. Cell viability was conducted by MTT assay. Values are normalized to untreated cells (Mock). Mean with SD of three independent experiments with technical triplicates were plotted.

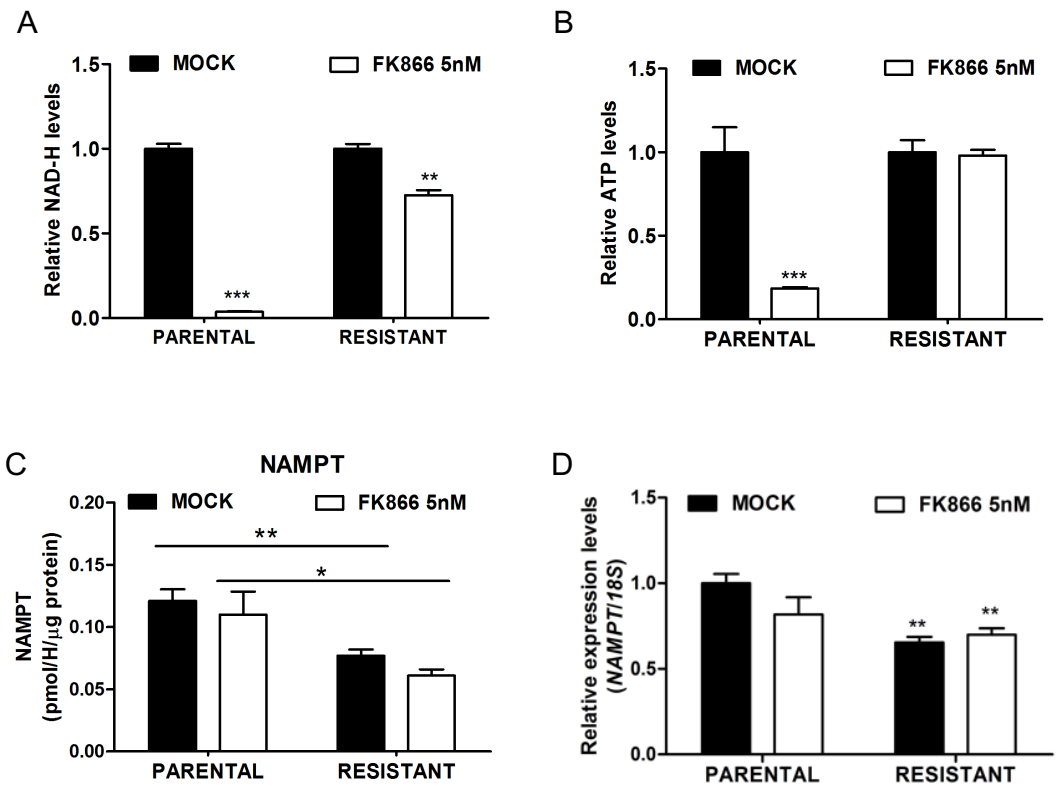

Figure 19 FK866 significantly decreases NAD and ATP levels in CEM cells.
A, Total NAD-NADH level was measured in CEM PA and CEM RES cells after 48h treatment with mock control (DMSO 0,01%) and 5nM FK866. **B**, Intracellular ATP levels were measured in CEM PA and CEM RES cells after 48h treatment with Mock, and 5nM FK866 for 48h. **C**, NAMPT enzymatic activity, Cells were treated with Mock and 5nM FK866 for 48h then NAMPT enzymatic level was measured. **D**, Quantitative RT-PCR targeting *NAMPT* was analyzed in CEM cells treated with mock and 5nM FK866 for 48h, *18S* expression was served as a housekeeping genes. Relative values are normalized to Mock. Data is represented as Mean with SD of three biological experiments with technical triplicates (***, $p<0.001$).

Translation control was not inhibited during FK866 treatment in CEM RES cells

Recently, our group demonstrated that FK866 induces a translational arrest in leukemia cells through inhibition of MTOR/4EBP1 signaling and of the initiation factors EIF4E and EIF2a. Specifically, treatment with FK866 is shown to induce AMPK activation, concomitant with EIF2a phosphorylation, is responsible for the inhibition of protein synthesis [71]. We asked whether translation regulation still functions when cells become resistant to FK866. To address this point, both CEM PA and CEM RES cells were treated with FK866 for 48h, phosphorylation of AMPK, mTOR1, 4EBP1, and EIF2a were evaluated by western blot analysis. In

CEM PA, phosphorylation of AMPK induced by FK866 was significantly increased subsequently inhibited mTOR/4EBP1 signaling, and increased the phosphorylation of EIF2a (**Figure 20A**). In contrast, the drug treatment did not activate AMPK and no alteration of protein translation mediated neither by phosphorylation of 4EBP1 nor phosphorylation of EIF2a were observed in the CEM RES cells reactivated by FK866 (**Figure 20C**). This supports the fact that these cells acquired detoxifying mechanism to pharmacological NAMPT inhibition.

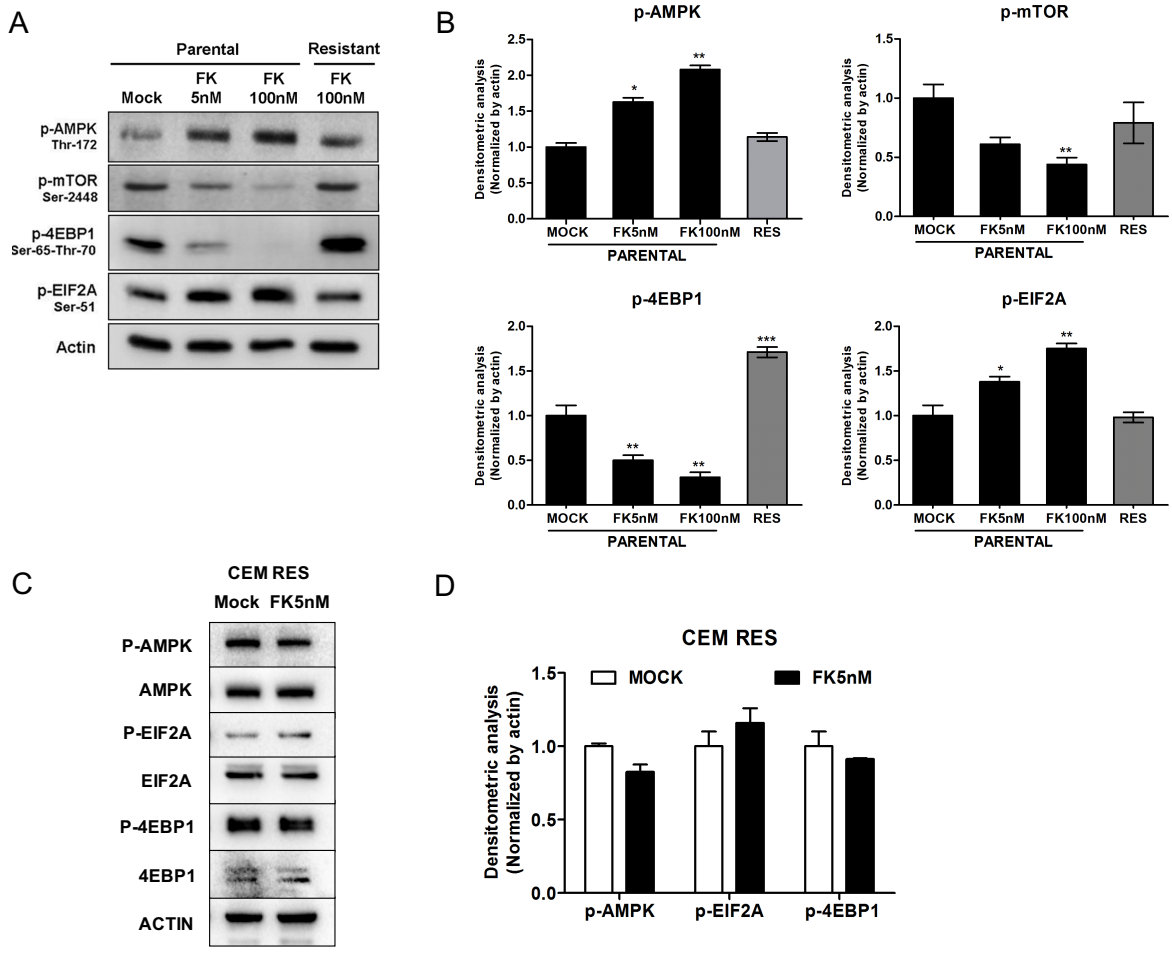

Figure 20 Signaling cascades controlling protein translation in CEM RES cells. **A**, CEM PA and CEM RES cells were treated with DMSO (Mock), and indicated concentrations of FK866 for 48h. **C**, CEM RES cells were treated with DMSO (Mock) and 5nM FK866 for 48h. Levels of p-AMPK (Thr-172), p-mTOR1 (Ser-2448), p-4EBP1 (Ser-65 and Thr-70), and p-EIF2a (Ser-51) and β-actin were detected by immunoblotting and a representative blotting from 3 biological experiments is shown. **B and D**, Densitometric analysis was conducted by Image J software. Protein expression was normalized by β-actin and relative expression level was plotted by Mean with SEM from 3 biological experiments (**p<0.001 compared to Mock).

Metabolic alteration in FK866 CEM RES

Drug resistance in cancer cells is recognized as the primary cause of failure of chemotherapeutic treatment in most human cancers. Development of cell resistance may be accompanied by deregulation of cellular metabolism. Given the low level of NAD/NADH in resistant cells (**Figure 18A**) we reasoned that oxidative metabolism could be impaired. To investigate drug adaptation in the resistant cells and to establish a potential correlation between CEM resistance and metabolic reprogramming, in collaboration with Dr. Jean-Francois Peyron (INSERM, Nice, France) we obtained the ATP output as a percentage of mitochondrial ATP and glycolytic ATP. Higher ATP production rates from glycolysis was found in CEM RES which was approximately 70% whereas in CEM PA was about 50-55% (**Figure 21A**). We hypothesized that metabolic adaptation in the resistant cells relies on glycolysis rather than OXPHOS. To address this issue, sample of CEM PA and CEM RES cells in different degree of resistance including CEM RES at 10nM, 40nM and 100nM of FK866 were subjected for biochemical analysis evaluating some critical markers reflecting metabolic functions and enzymes involved in glycolysis. In collaboration with Dr. Silvia Ravera (Istituto Gaslini, Genova, Italy) we managed to analyze oxygen consumption rate, and level of ATP synthesis in CEM PA and RES cells. ATP synthesis by Fo-F1 ATP synthase and the oxygen consumption rate (OCR) were reduced in fully resistant cells at 100nM as shown in **Figure 21B** and **21C**. Both pathways, made by complexes I, III and IV and complexes II, III and IV, were less functioning as shown by enzymatic activity evaluation in the presence of pyruvate/malate or succinate, respectively. Parental and resistant cells show a coupled OXPHOS as the P/O rate was within standard values.

As aerobic glycolysis is important for survival and proliferation of cancer cells, we speculated that CEM RES cell metabolism relies more on glycolysis, and to address this metabolic rewiring we investigated markers reflecting glycolysis pathway including glucose consumption and lactate production. Indeed, the decrease of OXPHOS activity accompanied with an increase of glucose consumption and lactate production were clearly observed in fully resistant CEM RES cells to 100nM FK866 (**Figure 22A** and **22B**). To confirm an enhanced glycolysis dependency, we further evaluated the activity of key glycolytic

enzymes including HK, PFK, PK, and LDH. All enzyme activities were significantly boosted in fully resistant cells ($p<0.001$), showing an enhancement in aerobic glycolysis in respect to parental cells (**Figure 22C**). These data suggested that the activation of aerobic glycolysis compensates the decrease of activity of the oxidative phosphorylation chain in the resistance.

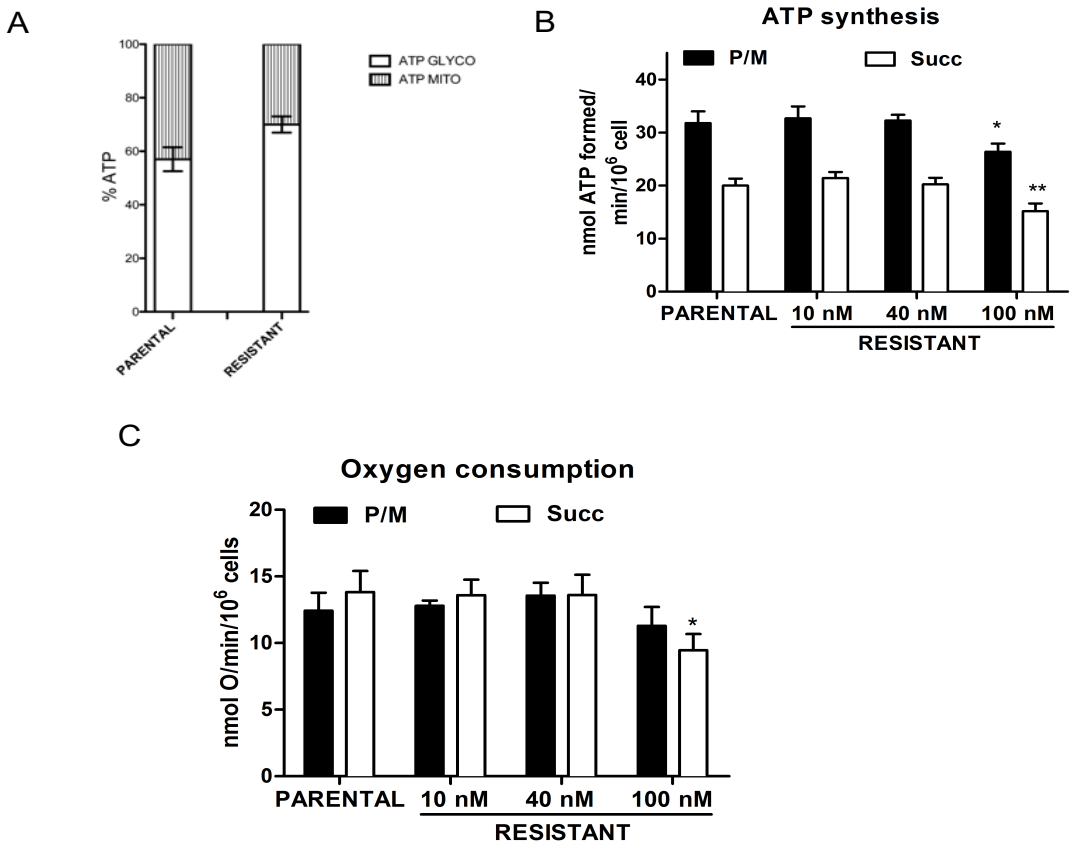

Figure 21 A decrease in mitochondria function in CEM RES cells

A, Percentage of ATP generated by Mitochondria and glycolysis in CEM PA and CEM RES cells, Data are plotted as percentage of ATP generated by mitochondria and glycolysis from two biological experiments with technical triplicate. **B**, ATP synthesis in CEM PA and CEM RES cells. **C**, Oxygen consumption in CEM PA and CEM RES cells. Values are represented as Mean with SD. of three independent experiments with technical triplicates. (***, $p<0.001$).

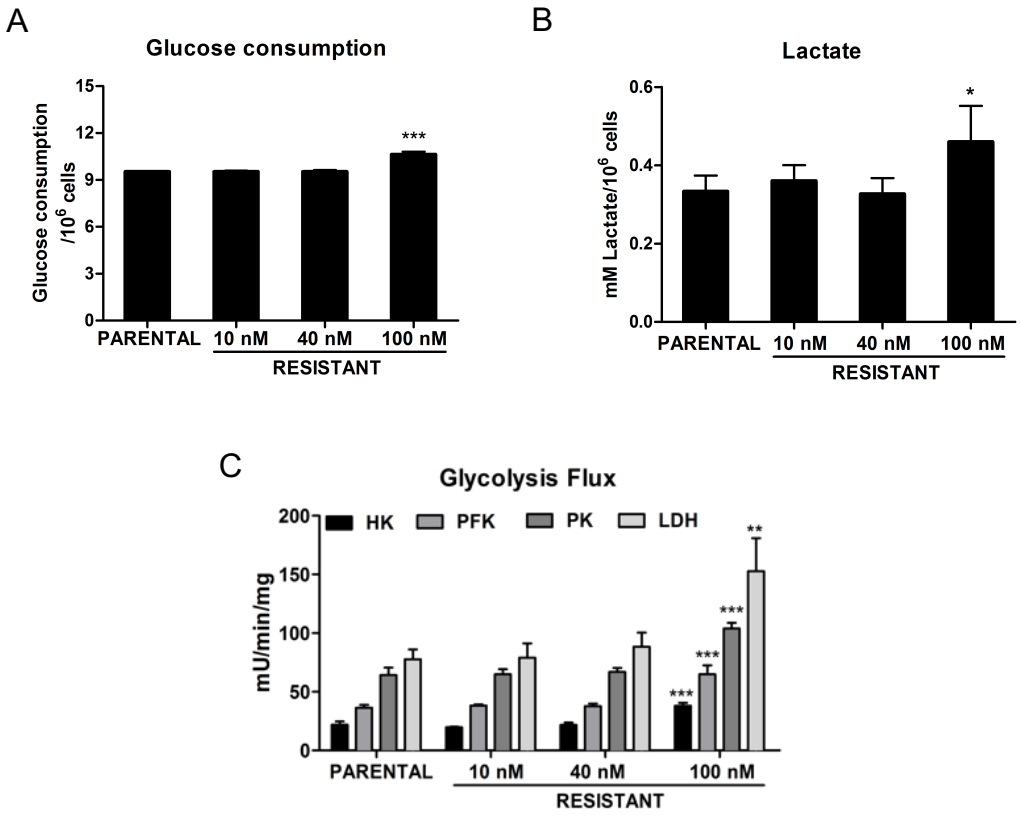

Figure 22 CEM RES cells display an enhanced glycolysis dependency.
CEM PA and CEM RES of 10nM, 40nM, and 100nM FK866 cells were subjected for the following analysis; **A**, glucose consumption, **B**, lactate production, and **C**, key glycolysis enzymatic activity including HK, PFK, PK, and LDH. The following parameters are determined as described in material and methods. Data is conducted and plotted as Mean with SD. from three biological experiments with technical triplicates (***p<0.001).

Therefore, induced FK866 resistance enhances glycolysis flux in CEM RES cells. We next analyzed mRNA expression of key enzymes involved in glycolysis (*HK2* and *LDHA*) and several genes associated with mitochondria oxidative phosphorylation (*ND1, ND2, ND3, ND3, NDL4, COX3*, and *ATP8*). A key glycolysis' enzyme, *LDHA* mRNA expression was slightly increased in the CEM RES in respect to CEM PA whereas *HK2* remained stable (**Figure 23A**). Inversely, a dramatic decrease in the mRNA level of all candidate mitochondrial genes were significantly detected in CEM RES cells (**Figure 23B**) providing a strong support that the resistant cells required less mitochondria function for their metabolic reprogramming. Nonetheless, we further investigated if resistant cells become addicted to and rely on glycolysis. Supporting data were obtained from test of two well-known metabolic inhibitors including 2-deoxyglucose (2DG) and

oligomycin A, well characterized inhibitors of glucose metabolism and mitochondria ATP synthase, respectively. We observed that CEM RES cells were more sensitive to 2DG treatment than parental cells (**Figure 24A**) while no differential sensitivity was observed between CEM PA and CEM RES cells during oligomycin A administration (**Figure 24B**). At 48h of treatment, EC50 of 2DG in CEM RES was 0.92 µM (R^2=0.967) whereas EC50 of 2DG in CEM PA was 2.11 µM (R^2=0.972). Therefore, the use of those inhibitors strongly distinguishes glucose addiction of CEM RES cells from CEM PA cells.

Taken together, CEM RES model primarily relies on aerobic glycolysis, consistent with the features of Warburg phenotypes, which can be tracked by decreased mitochondrial ATP generation, enhanced glycolytic rate, increased glucose consumption and concomitant with increased in lactate output.

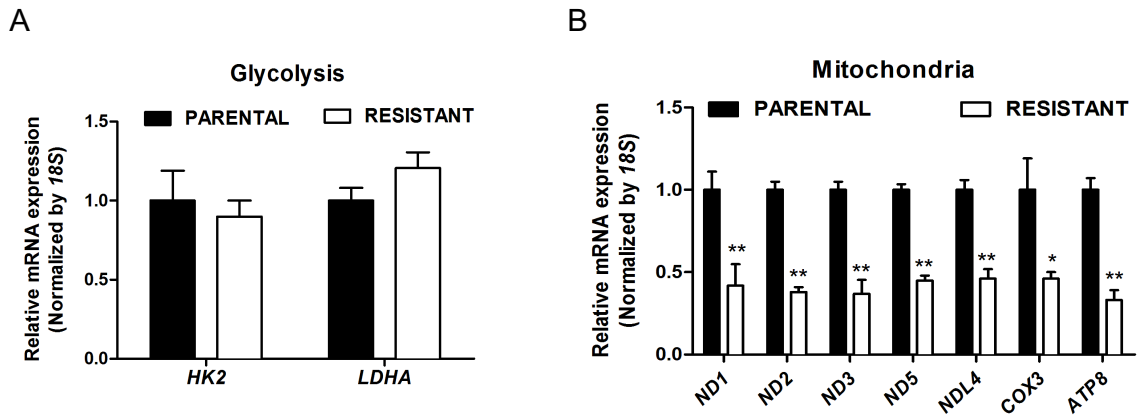

Figure 23 Down-regulation of genes involved in mitochondria function in CEM RES cells

A, Quantitative RT-PCR of CEM PA and CEM RES samples were performed to evaluate a panel of genes that encode glycolysis enzymes including *HK2* and *LDHA*. **B**, genes involved in mitochondria function including *ND1, ND2, ND3, ND3, NDL4, COX3*, and *ATP8* were analyzed. Level of *18S* mRNA expression was used to normalized the gene expression. Data is represented as Mean with SD of three biological experiments with technical triplicates (**p<0.01).

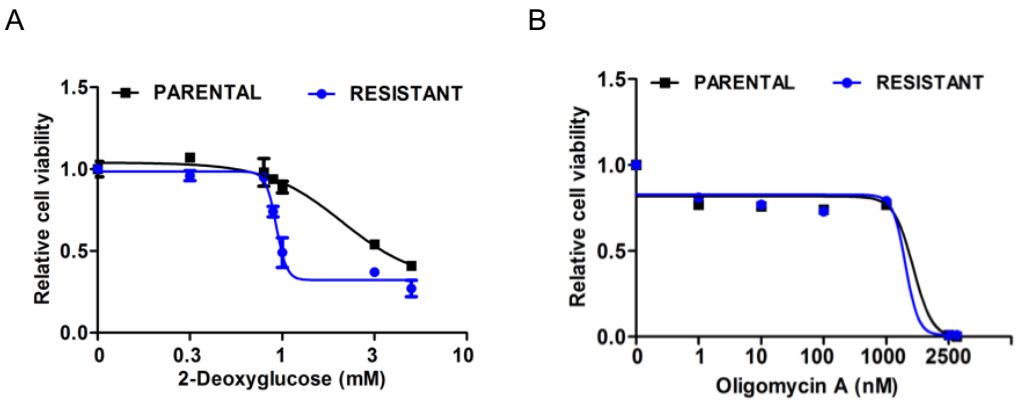

Figure 24 CEM RES cells are more vulnerable to glucose deprivation.
A, CEM RES cells are sensitive to glycolysis inhibitor (2-deoxyglucose). CEM PA and CEM RES cells were grown in the presence of various concentration of 2DG as indicated for 48h. **B**, An inhibitor of mitochondria ATP synthase has no impact on cell viability. CEM PA and CEM RES cells were treated with various concentration of oligomycin A for 48h. Cell viability was assessed by ozblue cell viability kit as describe in material and method. A representative viability curve from two independent experiments with technical triplicates is shown. Relative values of Mean with SD are normalized to untreated cells (Mock).

Utilization of Tryptophan; an alternative pathway for NAD production in CEM RES

As shown in **Figure 19A**, the reversion of NAD production in the resistant cells along with FK866 treatment was not caused by the mutations of the NAMPT enzyme, therefore cancer cells have developed different mechanism to acquire FK866 pharmacoresistance. Given the restoration of NAD levels, we hypothesized that other mechanisms of NAD production are actively working in CEM RES cells. An alternative pathway to produce NAD than the NAMPT-dependent pathway, is through the *"de novo"* pathway starting from Tryptophan [151]. Tryptophan is transported within the cells by the L-type amino acid transporter 1 (LAT1) and then metabolized to kynurenine and, through a number of reactions, to generate NAD [144]. In particular quinolinic acid phosphoribosyltransferase (QPRT), QPRT is an enzyme in "*de novo*" NAD synthesis pathway. We next validated several enzymes involved in NAD synthesis pathway in CEM cells. To investigate whether CEM RES cells activate an alternative NAD biosynthesis disregarding of NAMPT-dependent pathway. NADS activity was increased in CEM RES in respect to CEM PA whereas NMN activity was shown to be decreased in CEM RES. FK866 inhibits NMN activity in dose dependent manner

(**Supplementary Figure 1**). It was difficult to draw the correlation of all enzymatic activities in one direction. However, among of those investigated enzymes only QPRT activity was increased during FK866 treatment in the resistant cells (**Figure 25A**). This point attributes to the NAD biosynthetic pathway and a following question arises if CEM resistant cells obtain NAD from the *de novo* pathway to compensate the diminished NAD synthesis by NAMPT inhibitor. To test this hypothesis, mRNA expression level of *QPRT* was also investigated, treatment with FK866 did not affect *QPRT* mRNA expression levels in resistant cells, while its level decreased in parental cells (**Figure 25B**).

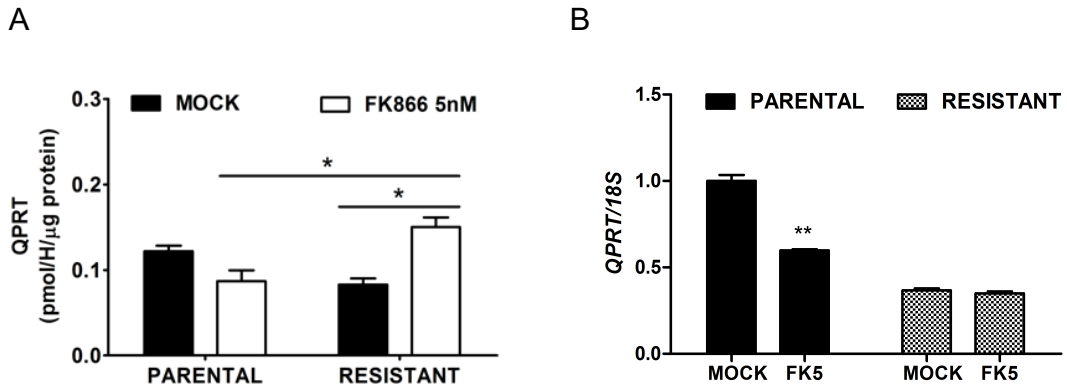

Figure 25 FK866 potentiates QRPT enzymatic activity in CEM RES cells.
CEM PA and CEM RES cells were treated with DMSO (Mock) and 5nM FK866 for 48h. **A**, QPRT enzymatic activity was measured in CEM cells. **B**, Relative mRNA expression level of *QRPT* normalized by *18S* is shown. Data was conducted and represented as Mean with SD. from two biological experiments with technical triplicates. (**p<0.05)

Metabolite of tryptophan is necessary for the synthesis of essential cellular cofactor NAD and nicotinic acid. Tryptophan is transported into the cells via LAT1 transporter [152]. LAT1 is over-expressed in murine lymphoma cells [144]. Recently, laboratory of Dr. Jean-Francois Peyron reported that overexpressed LAT1 in T-ALL/T-LL cancer cells reflects a cancer addiction towards increased nutrients uptake for mTOR1 and Akt activation and reprogrammed metabolism [144]. Importantly, they showed that JPH203, a potent LAT1 selective inhibitor decreased leukemic cell viability and proliferation. JPH203 also interfered with constitutive activation of mTORC1 and Akt, induced CHOP activation and showed the highest synergy with rapamycin induced-proliferation arrest and apoptosis. Interestingly, JPH203 was non-toxic to normal murine thymocyte and human peripheral blood lymphocyte [144].

Collaboration with Dr. Jean Francois Peyron group brought me an opportunity to do my research internship at INSERM institute, in Nice, France. ***My research focus during my period aboard was aimed to investigate the involvement of LAT1 to the mechanism of pharmacoresistance to FK866.***

Effect of a selective LAT1 inhibitor JPH203 was determined in CEM PA and CEM RES cells. Cells were treated with various concentrations of JPH203 (0.1 to 100 μM) for 72h. Interestingly, results showed that resistant cells were more sensitive to the drug as evident by the low IC50 than the parental one (**Figure 26A**). EC50 of JPH203 at 72h in CEM PA was 5.23 μM (R^2=0.90) and in CEM RES 2.76 μM (R^2=0.80). To understand more a role of LAT1 in resistant cells contributing cell viability, drug combination between FK866 and JPH203 was conducted. Combination of 4x4 concentrations of FK866 (0, 1, 3, and 5nM) and JPH203 (0, 1, 5, and 10 μM) were tested in CEM cells. Seventy-two hours of treatments, cell viability was estimated by XTT proliferation assay (**Figure 26B** and **26C**) and together with percentage of live and dead cells detecting by FACS analysis of DAPI staining (**Figure 27** and **28**). Percentage of cell inhibition was subjected for drug combination analysis as evaluated by combination index (**CI**). Drug combination was analyzed by Compusyn software [145]. Additive effects of drug combination between JPH203 and FK866 was shown at low doses of FK866 in CEM PA cells and appeared an antagonistic effect at higher concentrations. Interestingly, synergistic effect of JPH203 and FK866 (at 5μM of JPH203 with 1μM of FK866) was found to improve toxicity in CEM RES cells as evident by a low combination index (CI=0.65) (**Figure 29**) suggesting the synergistic effect of FK866 and JPH203. Higher efficacy of JPH203 appeared in the resistant rather than parental cells in both individual and also drug combination treatment.

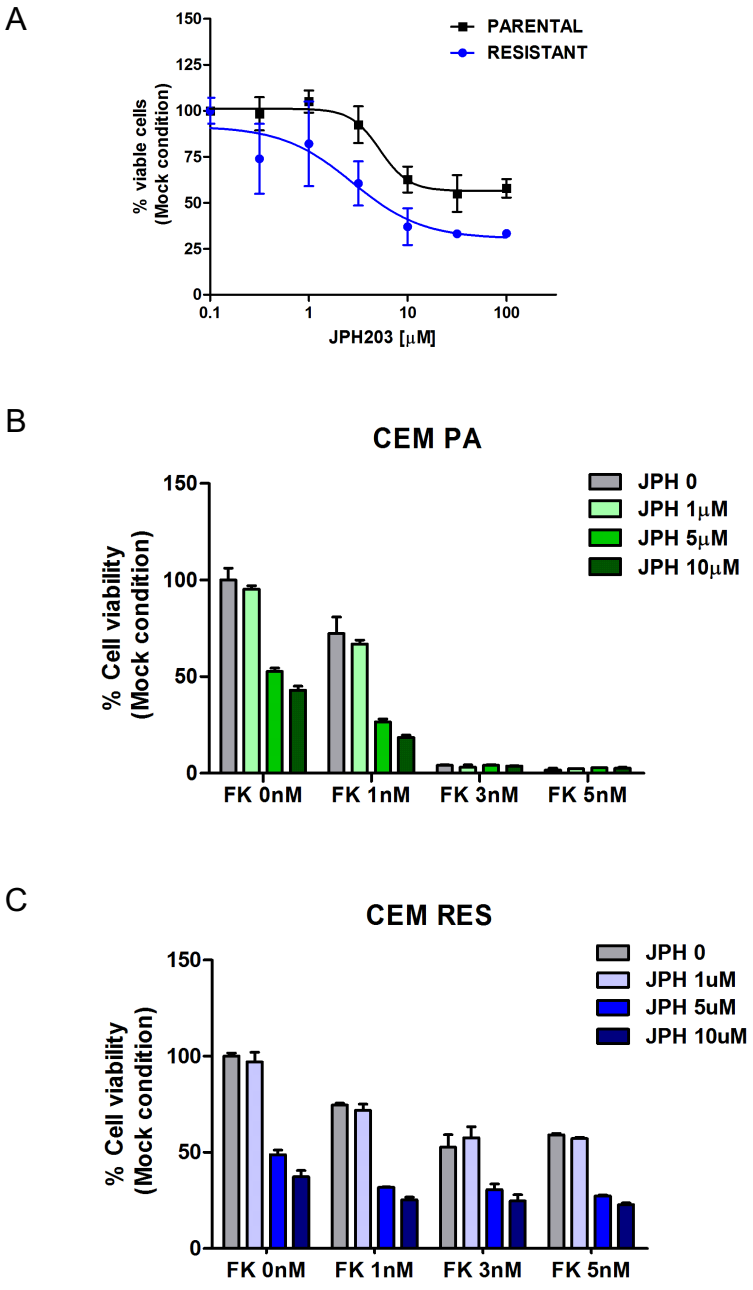

Figure 26 Effect of JPH203 a selective LAT1 inhibitor in CEM cell viability
A, CEM RES is more sensitive to JPH203. Cells were treated with JPH203 for 72h. **B** and **C**, drug combination of FK866 and JPH203 was conducted with 4x4 concentrations of FK866 (0, 1, 3, and 5nM) and JPH203 (0, 1, 5, and 10μM) for 48h in CEM PA and CEM RES cells, respectively. Cell viability was conducted by XTT assay. Data is represented Mean with SD of three biological experiments with technical triplicates.

A

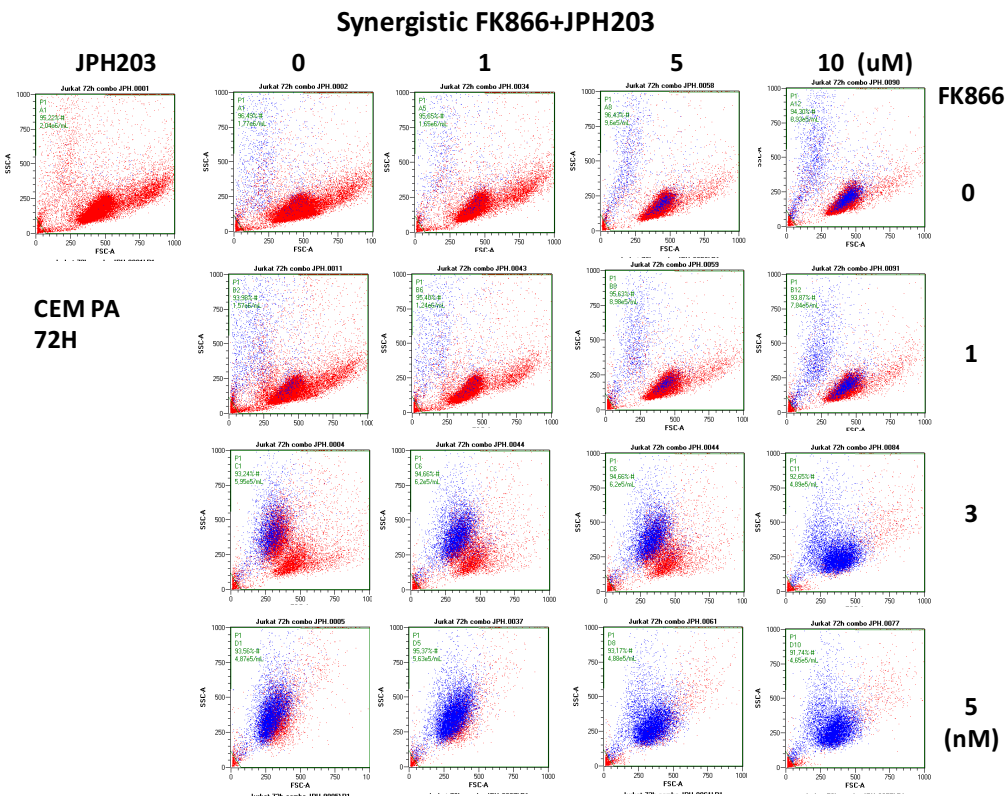

B

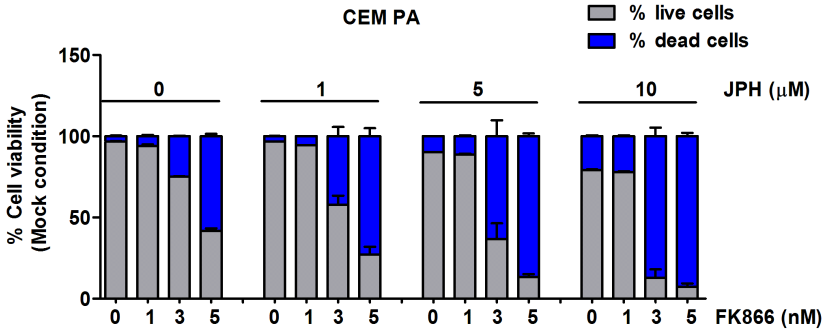

Figure 27 Drug combination of FK866 and JPH203 in CEM PA cells

CEM PA cells were treated with 4x4 concentrations of FK866 (0, 1, 3, and 5nM) and JPH203 (0, 1, 5, and 10μM) drug combination for 72h. **A**, Flow cytometry analysis of DAPI staining for live cells following drug combination was evaluated. **B**, A representative experiment from three biological experiments evaluating percentage of live and dead cells obtained from flow cytometry analysis were plotted as Mean with SD.

A

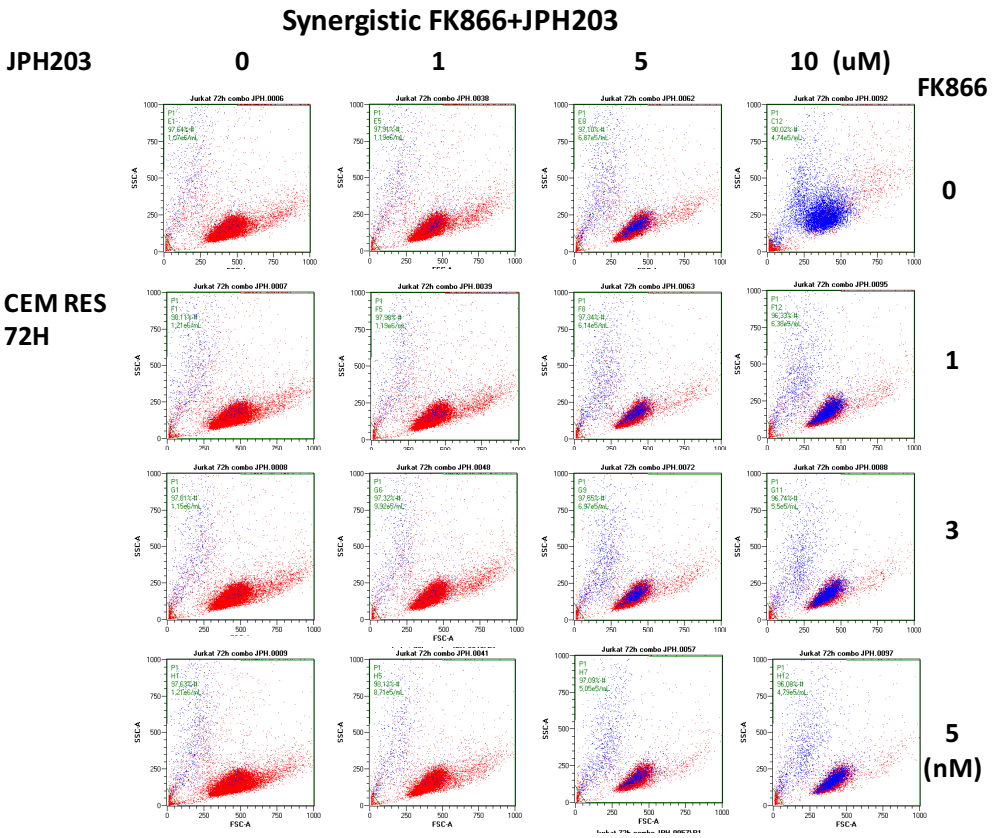

B

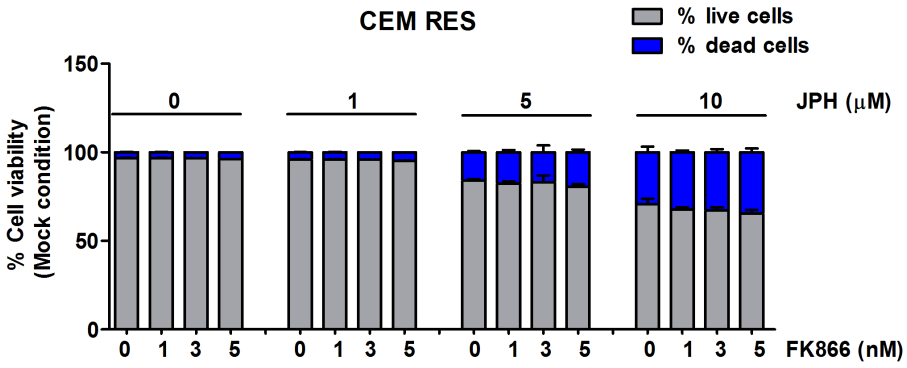

Figure 28 Drug combination of FK866 and JPH203 in CEM RES cells

CEM RES cells were treated with 4x4 concentrations of FK866 (0, 1, 3, and 5nM) and JPH203 (0, 1, 5, and 10μM) drug combination for 72h. **A**, Flow cytometry analysis of DAPI staining for live cells following drug combination was evaluated. **B**, A representative experiment from three biological experiments evaluating percentage of live and dead cells obtained from flow cytometry analysis were plotted as Mean with SD.

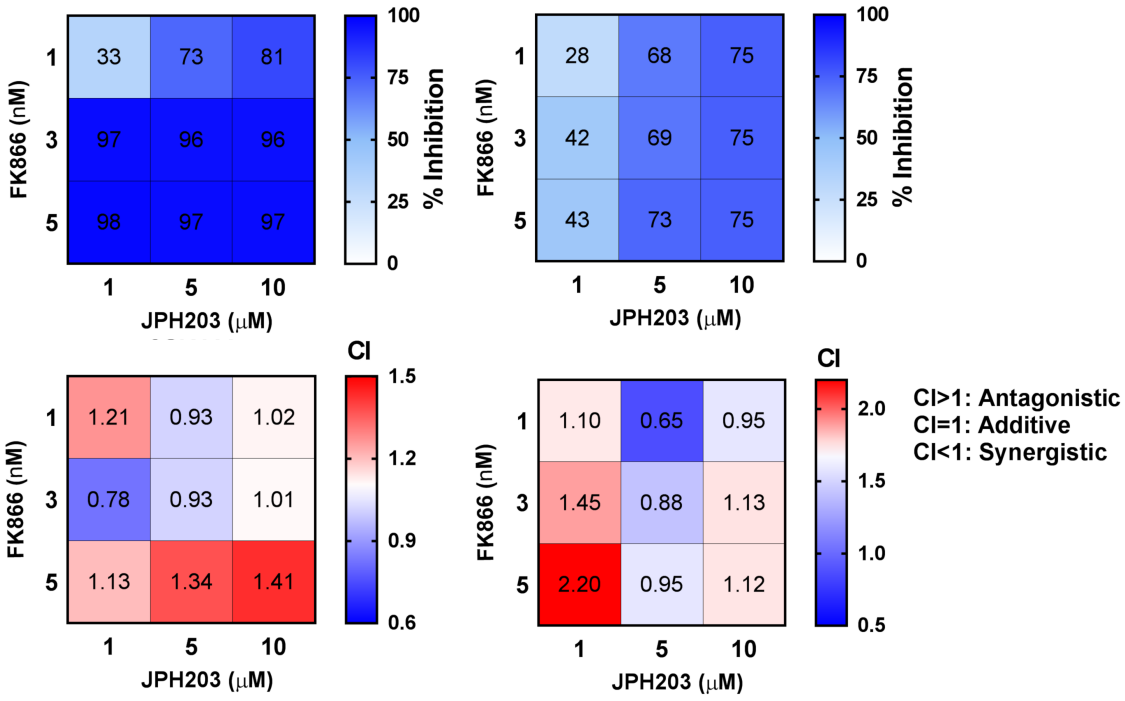

Figure 29 Drug combination screens identify synergistic effect of FK866 and JPH203 in CEM cells

Drug combination of FK866 and JPH203 was conducted with 4x4 concentrations of FK866 (0, 1, 3, and 5nM) and JPH203 (0, 1, 5, and 10μM). Cell viability was estimated after 72h of drug treatment by XTT assay and percentage of cell inhibition was subjected for combination index (CI) analysis. CI scores for a drug synergy screen was calculated by Compusyn software. (CI<1 indicates synergistic effect, CI=1 indicates additive effect, CI>1 indicates antagonistic effect). Each CI score represents data from two biological experiments with technical triplicates per condition.

Expression of ABC transporters prevents drug accumulation in the resistant cells by improving drug efflux [153]. Due to the limitation of instrument, I could not perform an amino acid uptake experiment. Alternatively, we investigated expression levels of LAT1 in parental and resistant cells. *LAT1* (*SLC7A5*) and CD98 (*SLC3A2*) constitute a heterodimeric transmembrane protein complex that catalyzes amino acid transport [154]. The mRNA expression of genes encoded *LAT1* including *SLC7A5* (a light chain of LAT1) and *SLC3A2* (a heavy chain) using qRT-PCR, and CD98 staining by FACS analysis were conducted. There was no difference in LAT1 encoded (*SLC7A5*) and (*SLC3A2*) mRNA expression between CEM RES and CEM PA cells (**Figure 30**). We assumed that expression levels of LAT1 might not be directly involved in the establishment of phamacoresistance to FK866. However, supporting evidence from JPH203

experiment indicated that blocking amino acid transportation through inhibition of LAT1 impacted cell viability, ATP and NAD levels in the resistant cells.

A

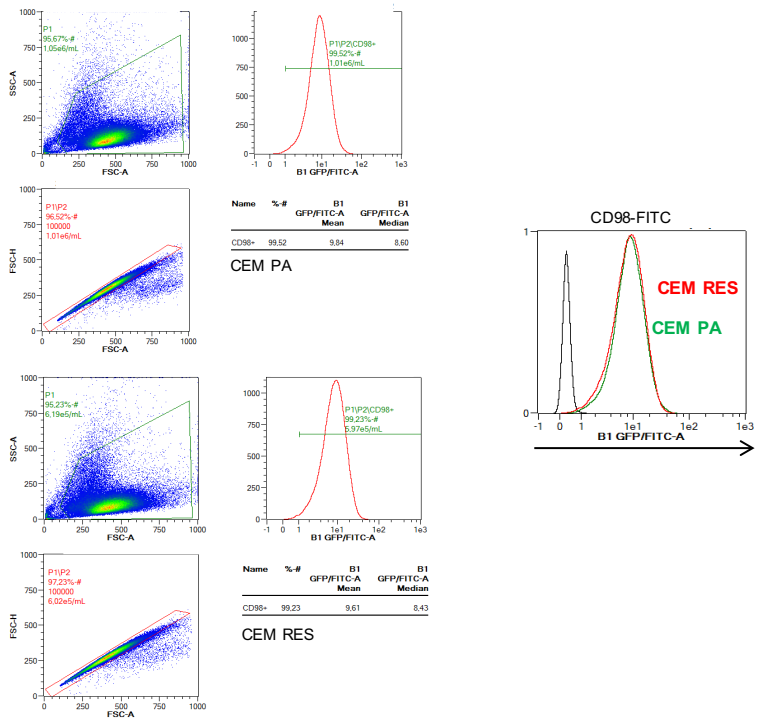

B

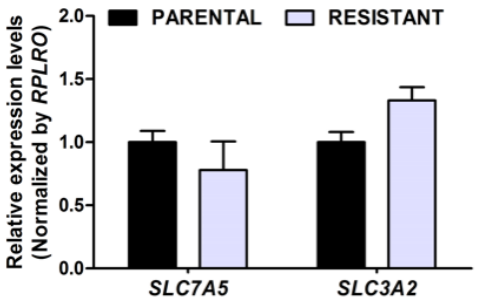

Figure 30 Characterization of LAT1 expression in CEM cells

A, CEM PA and CEM RES cells were stained with a FITC-labeled CD98 (LAT1) antibody and then were analyzed for LAT1 expression by flow cytometry. A representative data from two biological experiment was shown. **B**, Quantitative RT-PCR was performed in CEM PA and CEM RES cells targeting *SLC7A5* (a light chain of LAT1) and *SLC3A2* (a heavy chain of LAT1). Ribosomal protein (*RPLRO*) was used as a housekeeping gene. Data was conducted and represented as Mean with SD. from three biological experiments with technical triplicates.

Amino acids are obligatory for cellular functions and survival as they are recognized as important precursors for protein synthesis [155]. Some of these amino acids can be synthesized in mammalian cells from a variety of metabolic precursors (non-essential) and others need to be obtained from extracellular sources due to the absence of metabolic pathway for their synthesis *de novo* (essential) [155]. Thus, amino acid deprivation experiment was performed to address the roles of amino acids with regard to the acquiring for resistance. CHOP activation was chosen as a marker indicating cell death. We found that with conditional defects in cell viability induced CHOP activation appeared when CEM RES cells were cultured in amino acid deprivation (AA depletion) as well as supplemented with non-essential amino acid (AANE) (**Figure 31A**). Interestingly, an attenuated induction of CHOP was also noted in medium contained essential amino acids (AAE) suggesting a crucial role of AAE which was preferentially required for resistant cell survival.

L-tryptophan (Trp) is one of eight essential amino acids that cannot be synthesized in the human body and it is critical in a number of metabolic functions [156]. Earlier we hypothesized that *"de novo"* NAD synthesis pathway starting from L-tryptophan may serve as an alternative pathway of NAD production responsible for resistant cell survival during energetic stress. Thus, L-tryptophan was the first candidate to investigate this hypothesis. We focused our attention on the resistant model. Informatively, we attempted to clarify the hypothesis by performing numerous related experiments, the following experiments were conducted under a diluted amino acid free medium (see material and method). Firstly, supplemented with L-tryptophan (Trp) or Tryptophan together with a complete AAE solution (Trp+AAE) were introduced into treatment conditions. Immunoblotting of CHOP expression was detected 24h after treatment in CEM RES cells. As expected, FK866 did not affect CHOP activation due to those cells are resistant to FK866, unlikely a single JPH203 treatment and drug combination of FK866 and JPH203 significantly stimulated CHOP activation (**Figure 31B**). Importantly, a remarkable result was observed in tryptophan supplementation which we could appreciate significant suppression of CHOP activation in combined FK866 and JPH203 treatment indicating the rescues effect of tryptophan responsible for resistant cell survival during energetic stress

induction. Secondly, we further analyzed *CHOP* mRNA expression along with those indicated treatments in CEM RES cells. A relative increase in *CHOP* mRNA expression was induced by JPH203, and co-treatment of FK866 and JPH203 (**Figure 31C**). Accordingly, treatment with single JPH203 and the co-treatment activated the ATF4/CHOP pathway that was inhibited by tryptophan complementation. Thirdly, we investigated whether the presence of tryptophan could prevent the resistant cell death from the stress conditions induced by treatment. The addition of tryptophan potentiated the rescues of cell viability from combined JPH203+FK866 treatment (**Figure 32A**). Finally, we evaluated two important parameters including ATP and NAD+ levels in treated CEM RES cells. As expected, treatment with JPH203 and combined of the two drugs caused a dramatic drop in ATP and NADH levels in CEM RES cells. But those ATP and NADH levels were significantly elevated by tryptophan supplementation (**Figure 32B and 32C**) indicating the dependency of resistant cells on tryptophan metabolism for the production of these key metabolic molecules.

Taken all together, these data indicate that the development of FK866 resistance, by decreasing the production of NAD/NADH via NAMPT down-regulation is leading to the upregulation of alternative mechanism of NAD+ synthesis via tryptophan/QPRT pathway. CEM resistant cells utilized tryptophan as an alternative source to sustain NAD biosynthesis and to fuel cell metabolism during stress conditions.

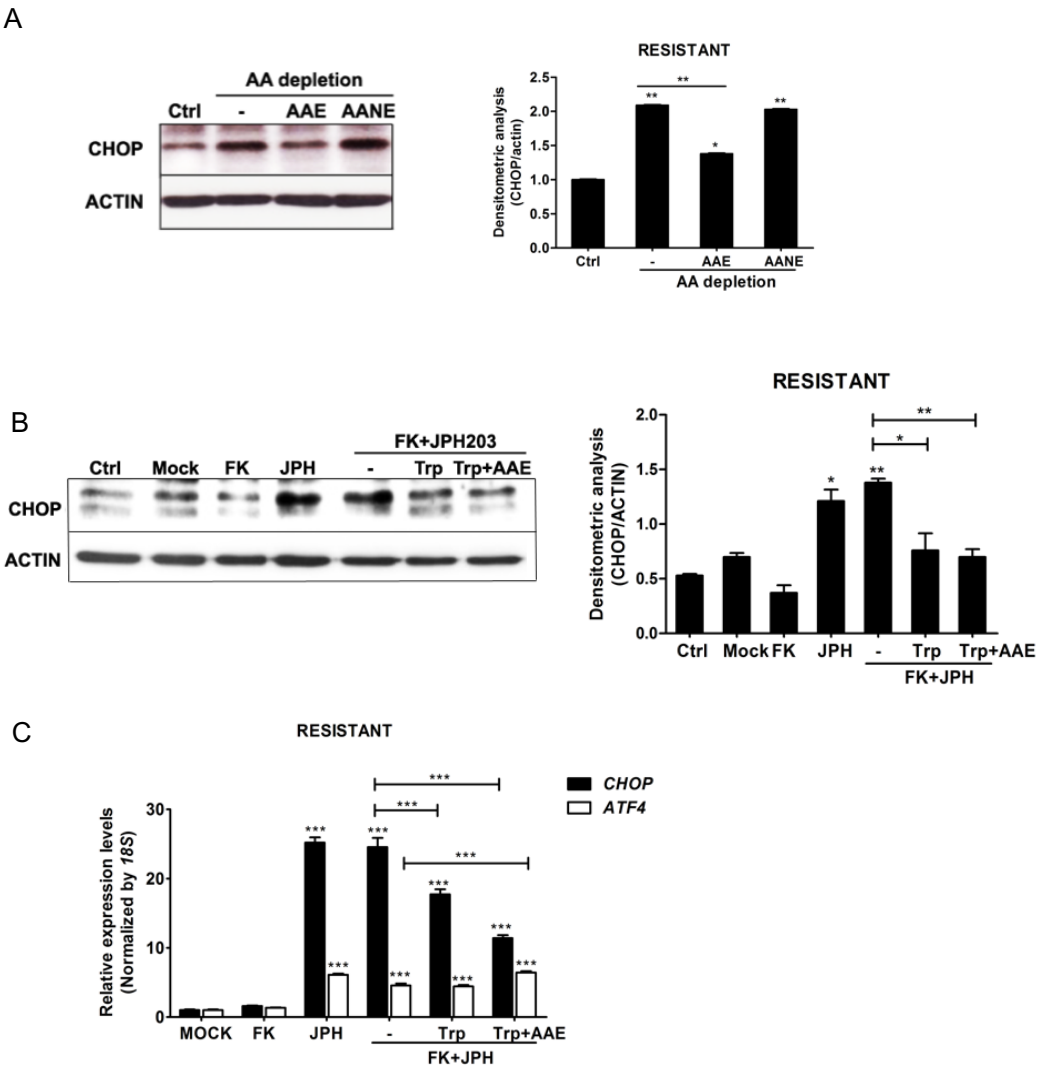

Figure 31 Tryptophan prevents CEM RES cell death under energetic stress.
A, CEM RES cells were incubated in different conditions of medium including normal RPMI medium (Ctrl), amino acid depletion medium (AA depletion) supplemented with essential amino acid (AAE) or non-essential amino acid (AANE) for 24h. Immunobloting analysis of CHOP was performed from whole cell lysate, β-ACTIN was used as a protein loading control. A representative blot from three biological experiments is shown. Densitometry analysis of CHOP was normalized by β-ACTIN. **B**, CEM RES cells were incubated in normal RPMI medium (Ctrl) and following treatments was prepared in AA depletion medium including DMSO (Mock), 5nM FK866, 10μM JPH203, combination treatment of FK866 and JPH203 in the presence of 0.5mM Tryptophan (Trp) or Trp and AAE (Trp+AAE) for 24h. Immunoblotting analysis of CHOP was performed from whole cell lysate, β-ACTIN was used as a protein loading control. **C**, CEM RES cells were treated with the different conditions as indicated above in **Figure 31B**. Quantitative RT-PCR of *CHOP* mRNA expression was conducted in CEM RES cells. *18S* was used as a housekeeping gene. Data is represented as Mean with SD. from three independent experiments with technical triplicates (***,p<0.001).

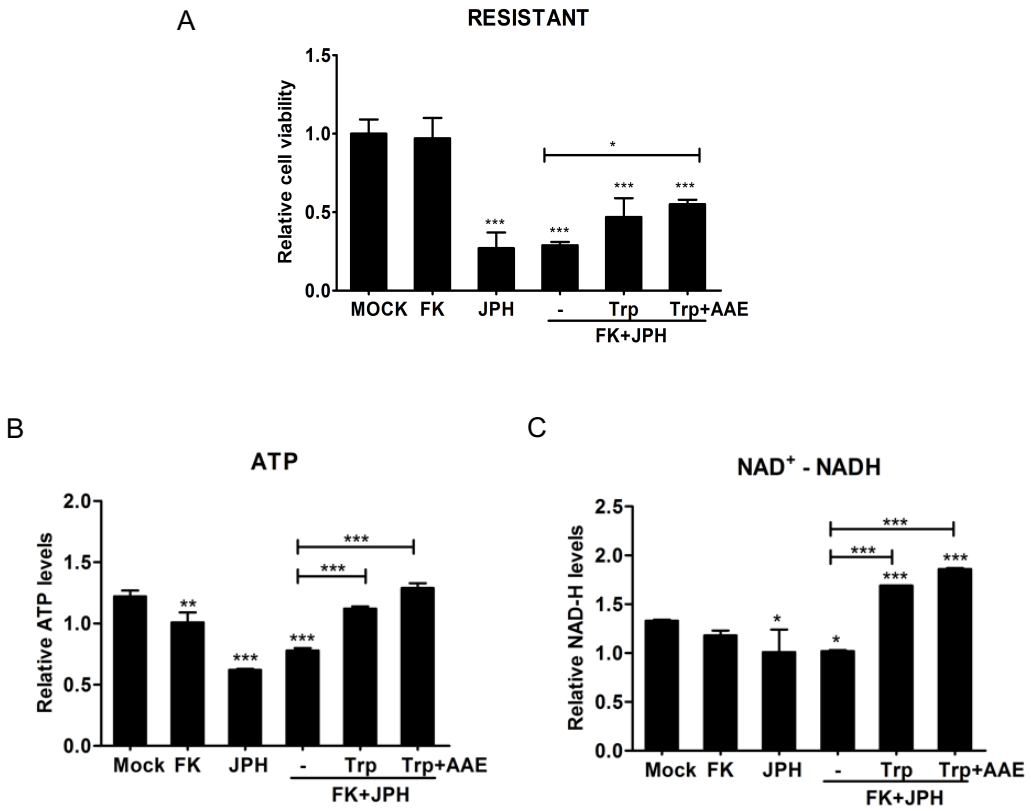

Figure 32 Utilization of tryptophan as an alternative source to rescue cell survival and sustain ATP and NAD production in the resistance during stress conditions. CEM RES cells were treated with DMSO (Mock), 5nM FK866, 10μM JPH203, cotreatment of FK866 and JPH203 with and without supplementation of 0.5mM L-tryptophan (Trp) or Trp and essential amino acid (Trp+AAE) for 24h. **A**, Cell viability was analyzed by XTT proliferation kit. **B**, Intracellular ATP levels were measured in CEM resistant cells after 24h treatment using Cell-titer glo kit. **C**, Total NAD-NADH levels were measured in CEM resistant cells after 24h treatment. Values are normalized to Mock condition. Relative value of Mean with SD from three biological experiments with technical triplicates was plotted. (***, $p<0.001$).

Characterization of L-Asparaginase response

Asparaginase is widely used in chemotherapeutic regimens for the treatment of acute lymphoblastic leukemia (ALL) and has led to a substantial improvement in cure rates, especially in children [157]. To provide another example of an amino acid interference impacted metabolism of the resistance, we evaluated whether the resistant cells are also more sensitive to L-glutamine depletion than parental cells. We initially started evaluating L-Asparaginase (L-Asp) efficacy, exploiting its ability specifically to degrade L-glutamine [158,159]. Indeed, CEM RES cells exhibited higher sensitivity toward L-Asp treatment than parental cells (**Figure 33A**) as indicated by IC50 which was 1.04 U/ml (R^2=0.97) and 0.50 U/ml

(R^2=0.97) in CEM PA and CEM RES cells at 48h, respectively. Furthermore, drug combinations of FK866 and L-Asp was performed in CEM cells. Combined treatment of FK866 and L-Asp impeded cell viability in both CEM PA (**Figure 33B**) and CEM RES cells (**Figure 33C**). Strong synergistic effect was obtained in the resistance as indicated by low CI score CI=0.26, CI=0.22, and CI=0.21 at low concentration of L-Asp (0.1U/ml L-Asp) with 1nM, 3nM, and 5nM of FK866, respectively (**Figure 34**). These results implicate the fundamental role of amino acid that generally attributes to cancer cell growth. Enzymatic activity of Asp is deamidatation of asparagine to aspartic acid and ammonia, but it also deamidates glutamine to glutamic acid and ammonia [160]. To investigate the contribution of L-glutamine (Gln) to cell survival. We performed experiments under amino acid free medium to exclude the possibility that retained Gln in the medium would interfere the system inducing cancer cell growth. CEM PA and CEM RES cells were treated with 1U/ml L-Asp in the presence and absence of Gln for 48h. Supplementation of Gln showed a modest but reproducible trend toward elevated cell viability in particular the resistant cell which revealed a higher response to Gln than that of CEM PA cells (**Figure 35A**). We asked whether the presence of Gln would selectively contribute to an impediment of CHOP activation in the resistant cells. CEM RES cells were treated with indicated treatment. Activation of CHOP protein and *CHOP* mRNA expression were intensely pronounced in replenishment of L-glutamine in resistant cells in particular along with L-Asp treatment (**Figure 35B** and **Figure 36A**). Supplementation of Gln functioned as a guardian to prevent the activation of *CHOP* mRNA expression (**Figure 36A**). Gln blocked the activation of CHOP during co-administration of the two drugs,. There was significant different in *ATF4* and *ANS1* mRNA expression during drug administration (**Figure 36A**). We next expendably examined if Gln could restore ATP and NAD levels during L-Asp or drug cotreatment. Depletion of ATP and NAD was found in 48h after L-Asp treatment in MDA RES cells (**Figure 36B** and **36C**). A well-defined impact of Gln in generating ATP and NADH production was observed in all treatment conditions suggesting that Gln results in broad defects in resistant cell mortality and declining in ATP and NAD production. Taken together these results indicate that FK866 resistant cells are relying on the presence of glutamine in the medium to

complement the reduction of endogenous NAD and, notably, the increased addiction to glutamine causes increased sensitivity to L-Asp.

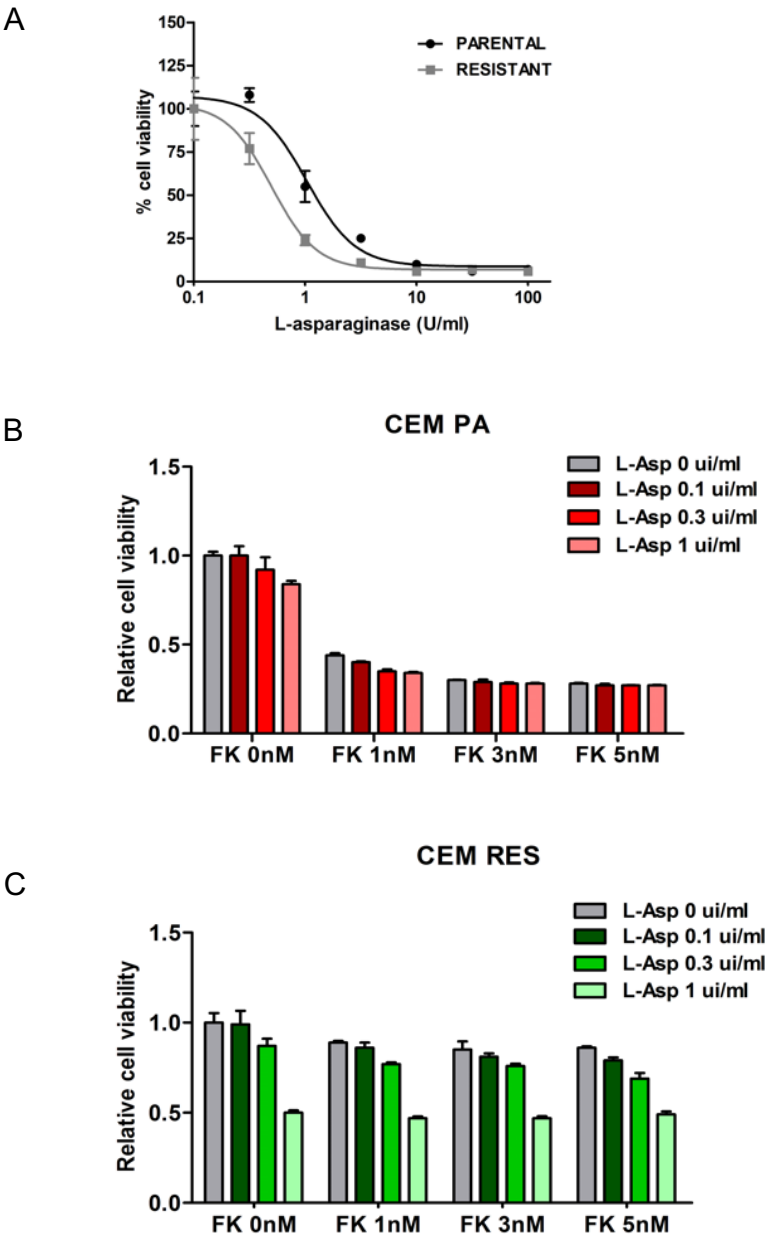

Figure 33 Effect of L-Asparaginase induced cell death in CEM cells
A, CEM cells were treated with various concentrations of L-Asparaginase (U/ml) for 48h. Cell viability was analyzed using XTT proliferation assay. **B**, Drug combination of FK866 (0, 1, 3, and 5nM) and L-Asp (0, 0.1, 0.3, and 1 U/ml) was performed in CEM PA cells for 48h. **C**, Drug combination of FK866 (0, 1, 3, and 5nM) and L-Asp (0, 0.1, 0.3, and 1 U/ml) was performed in CEM RES cells for 48h. Relative cell viability was measured and calculated from XTT proliferation assay. Data was plotted as relative of Mean with SD. of three biological experiments with technical triplicates.

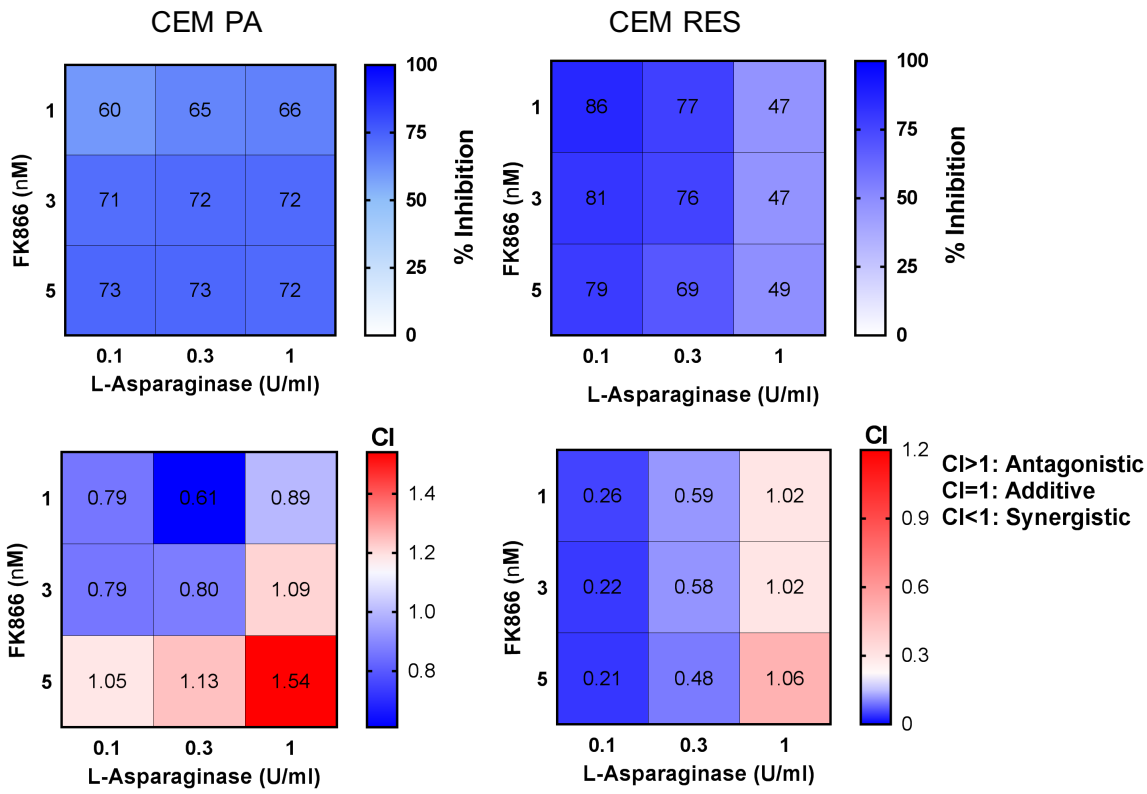

Figure 34 Drug combination screens of FK866 and L-Asparaginase in CEM cells
Drug combination of FK866 and L-Asp was conducted with 4x4 concentrations of FK866 (0, 1, 3, and 5nM) and L-Asp (0, 0.1, 0.3, and 1 U/ml). Cell viability was measured after 48h of drug treatment by XTT proliferation assay. and percentage of cell death was subjected for combination index (CI) analysis. CI scores for a drug synergy screen was calculated by Compusyn software. (CI<1 indicates synergistic, CI=1 indicates additive effect, CI>1 indicates antagonistic effect). CI score from a representative experiment of two biological experiments with technical triplicates per condition is shown.

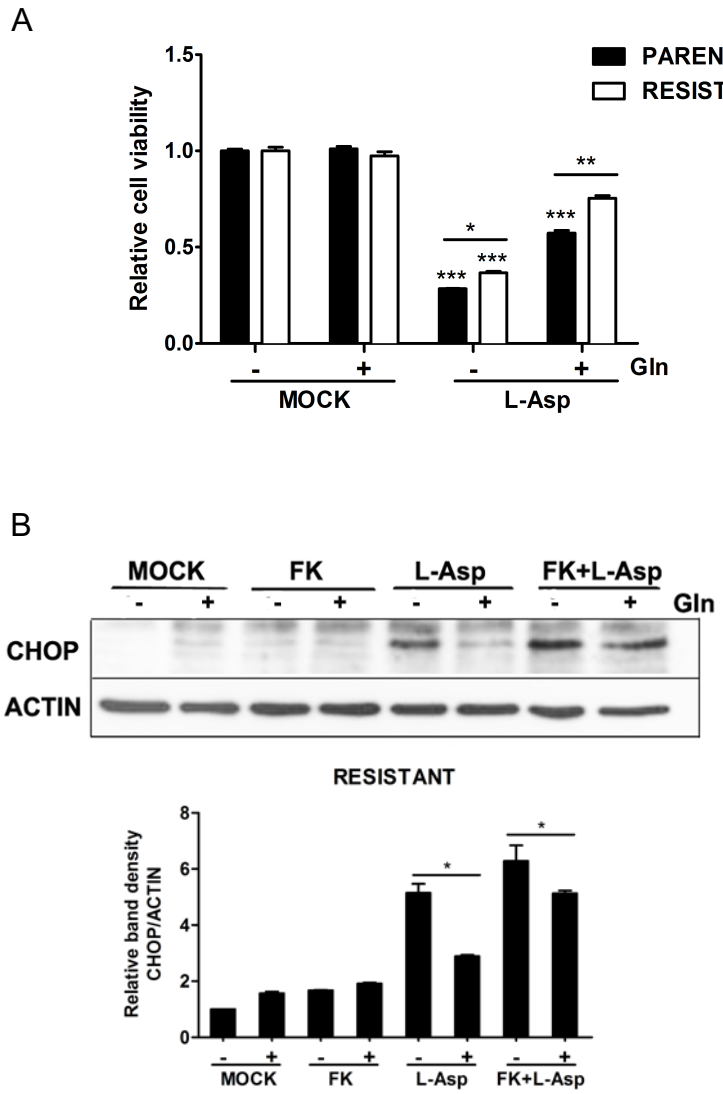

Figure 35 L-glutamine prevents cell death during energetic stress.
A, CEM PA and CEM RES cells were treated with 1U/ml L-Asp in the presence or absence of 2mM L-glutamine (Gln) supplementation for 48h. Cell viability was analyzed using XTT proliferation assay. **B**, CEM RES cells was treated with 5nM FK866, 1U/ml L-Asp, co-treatment with FK866 and L-Asp in the presence or absence 2mM Gln for 48h. CHOP protein level was verified by western blot analysis, β-ACTIN was used as a protein loading control. A representative of immunoblotting is shown and densitometric analysis of relative CHOP level was analyzed and normalized by β-ACTIN. Relative data of Mean with SD from three biological experiments with technical triplicates was represented. (***p<0.001).

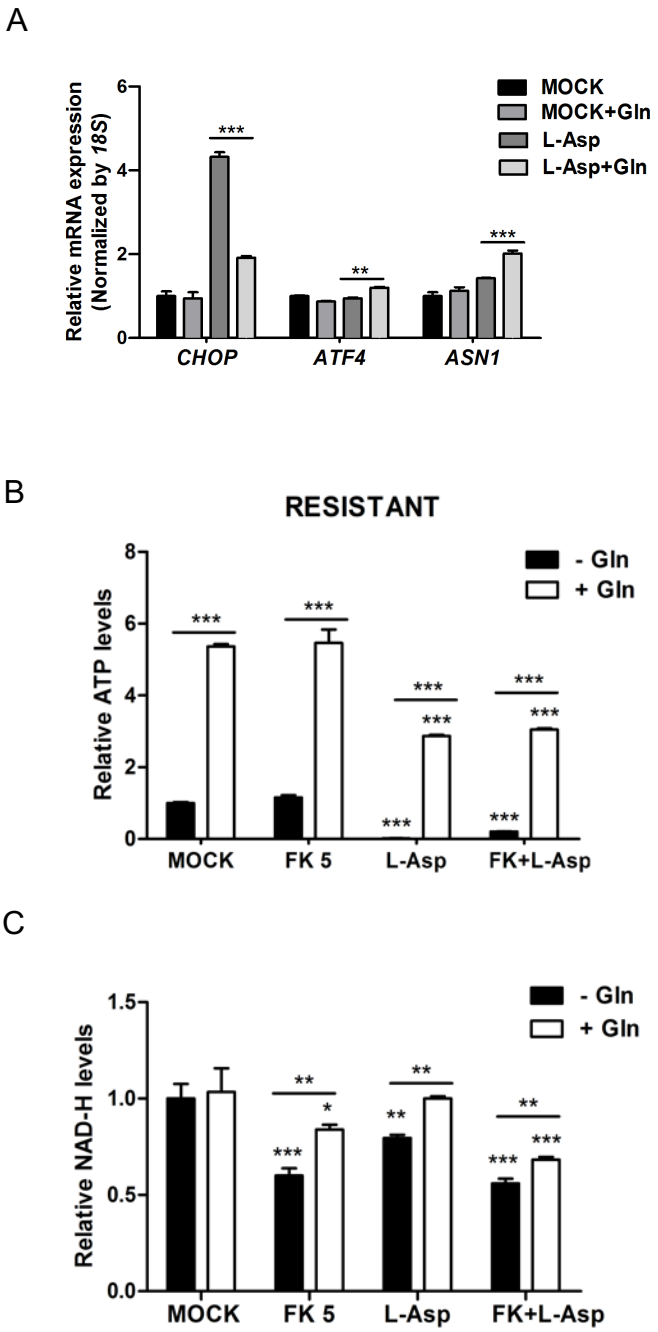

Figure 36 L-Glutamine exhibits rescues effect on ATP and NAD production during stress condition in CEM RES cells.

A, CEM RES cells were exposed to 5nM FK866, 1U/ml L-Asp, cotreatment with FK866 and L-Asp in the presence or absence 2mM Gln for 48h. *CHOP*, *ATF4*, and *ASN1* mRNA expression were verified by RT-PCR, *18S* was used as a house keeping gene. **B**, CEM RES cells were treated for the indicated treatments for 48h, and ATP levels were quantified by Cell Titer-glo assay. **C**, CEM RES cells were treated for the indicated treatments for 48h, and were then subjected for NAD measurement. Relative data with SD was conducted from three biological experiments with technical triplicates. (***p<0.001).

Development of a comparative NAMPT inhibitor resistant model in MDA-MB231 cell line.

To investigate the degree of generality of the identified resistant mechanism, we developed another strain of FK866 resistant cells derived from triple negative breast cancer MDA MB231 cell line, that is particularly sensitive to FK866 exposure [37]. We determined comparative mechanism of action of FK866 as depletion of NAD, likely through inhibition of NAMPT in MDA-MB231 parental cells (MDA PA) and MDA-MB231 FK866 resistant cells (MDA RES). MDA PA cells were sensitive to FK866 treatment (**Figure 37A**). We obtained a complete MDA RES model in which the resistance was resistant to FK866 treatment at indicated times (**Figure 37B**). To determine whether developed MDA RES cells are NAMPT-dependent resistance, MDA RES cells were tested to another NAMPT inhibitor (CHS-828) for 48h. Similar result with CEM RES cells was observed, CHS-828 strongly induced MDA PA cell death whereas it did not affected MDA RES cell viability (**Figure 37C**). Thus, we accomplished development of the NAMPT-dependent resistance MDA model that was clearly indicated by insensitivity to both FK866 and CHS-828 treatment. FK866 dramatically decreased ATP and NADH levels in MDA PA cells (**Figure 38A** and **38B**) but no change in ATP levels along with FK866 re-stimulation was obtained in MDA RES (**Figure 38A**). We noted that restoration of NAD levels was also found when MDA RES cells re-exposed to FK866 treatment corroborating with the previous observation in a CEM RES cell model (**Figure 19A**). However, the resistance to NAMPT could be caused by some mutation in NAMPT [157]. Additionally, we sequenced the *NAMPT* gene in the resistant and the parental cell lines. Apparently, no mutation of *NAMPT* genes were present in our CEM RES and MDA RES models.

Protein translation markers were investigated in comparison between MDA PA and MDA RES. Insensitivity to FK866 treatment in MDA RES was also evidence by the continuous activation of the translation machinery that was not affected by the stress response mediated by EIF2a, AMPK or by 4EBP1 phosphorylation (**Figure 39**). These results suggested the loss of protein translation inhibition in the MDA resistance as well as observed in CEM RES cells.

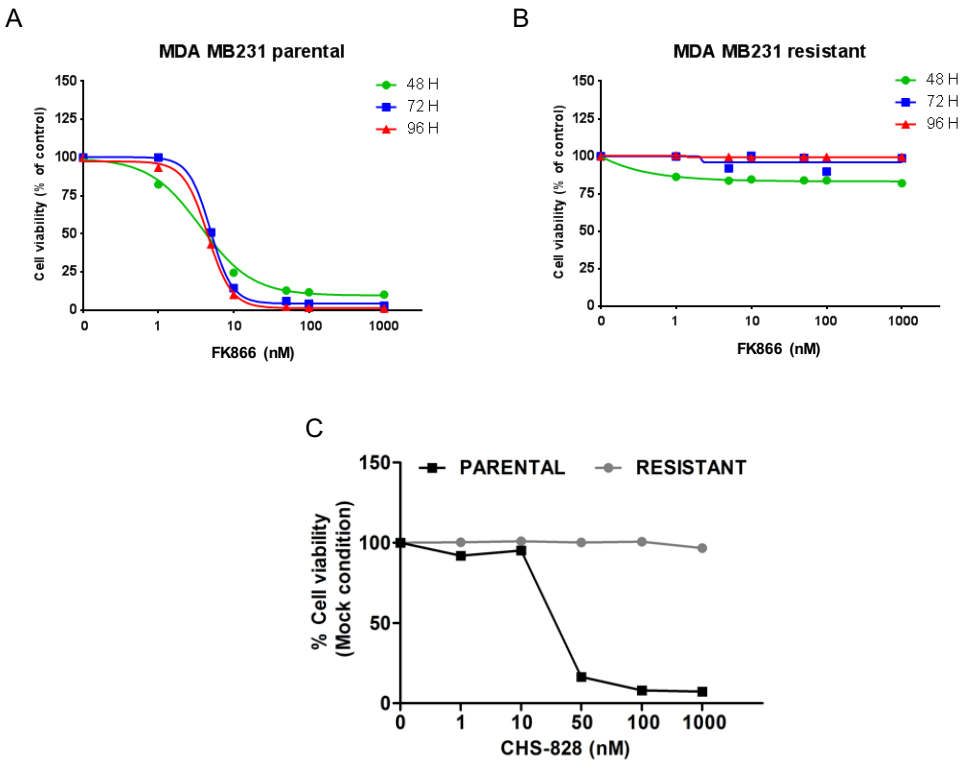

Figure 37 Characterization of NAMPT dependent-FK866 resistant MDA cells
A, Does-response sensitization to a NAMPT inhibitor (FK866) in MDA PA cells. Cells were exposed to various concentration of FK866 as indicated time points. Percentage of cell viability was analyzed by MTT assay. **B**, MDA RES cells were also exposed to FK866 as indicated times, then cell viability was determined by MTT assay. **C**, MDA PA and MDA RES cells were expose to another NAMPT inhibitor (CHS-828) for 48h. Cell viability was analyzed by MTT assay. Relative value of Mean with SD compared to mock control was plotted. A representative data from two biological experiment with technical triplicates is presented.

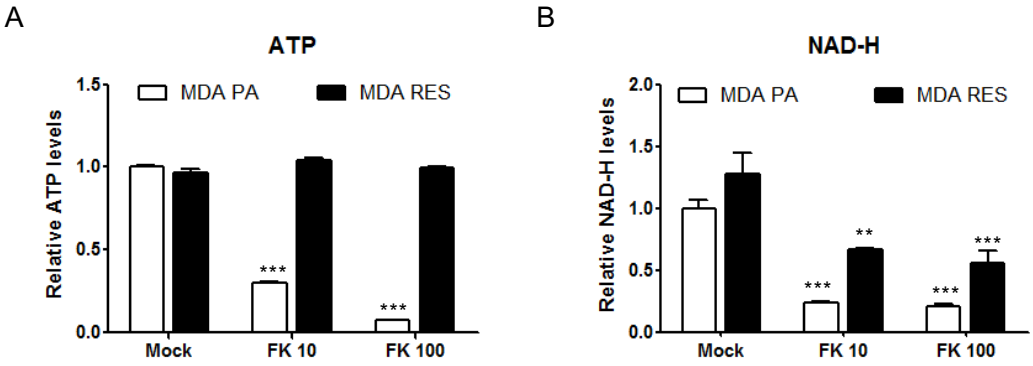

Figure 38 Evaluation of ATP and NAD levels in MDA cells
A, ATP levels was measured in MDA PA and MDA RES cells 48h after treatment with DMSO (Mock), 10 and 100nM FK866. **B**, Total NAD levels were measured in MDA PA and MDA RES cells 48h after treatment with DMSO (Mock), 10 and 100nM FK866. Data was represented as relative of Mean with SD conducted from three biological experiment with technical triplicates. (***p<0.001)

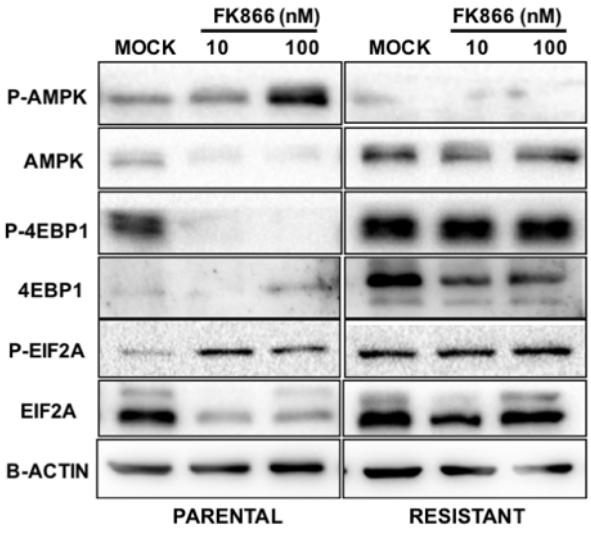

Figure 39 Protein translation control is not inhibited in MDA RES cells
Immunoblotting analysis of whole protein extract from MDA PA and MDA RES cells after 48h treatment with DMSO (Mock), 10 and 100nM FK866 was performed. A representative of immunoblotting from three biological experiments expressed levels of p-AMPK (Thr-172), p-mTOR1 (Ser-2448), p-4EBP1 (Ser-65 and Thr-70), p-EIF2a (Ser-51) and total form of those were shown. β-ACTIN was used as a protein loading control.

MDA RES cells share a number of common characteristic similar to those of CEM RES cells including insensitivity to NAMPT inhibitors (FK866 and CHS-828), no effect on ATP and an elevated NAD levels during FK866 treatment, no protein translation inhibition, and down-regulation of *NAMPT* mRNA expression in the resistant cells in respect to MDA PA cells (**Figure 40**). Although many similar phenotypes of the CEM resistance was observed in MDA RES cells, but a number of dissimilarities were found at the mRNA expression levels. FK866 treatment strongly decreased the expression levels of the enzymes involved in the *de novo* pathway for the synthesis of NAD such as *QPRT, IDO* and *KYNE* and of *NAMPT* itself (**Figure 40**). However, in this case we speculated that the alternative pathway may be not going through the *de novo* pathway since the enzymes involved are not overexpressed in respect to the parental cells. To address this question we evaluated the effect of amino acid deprivation in MDA RES. First, the LAT1 inhibitor JPH203 was tested in both parental and resistant cells to reproduce circumstances occurring in the cells during amino acid deprivation, tryptophan included. Indeed, MDA RES cells did not show differential sensitivity to JPH203 administration in respect to MDA PA cells (**Figure 41A**). Second, another amino acid deprivation was addressed in MDA cells using

L-Asparaginase treatment. Consistent with JPH203 treatment, drug sensitivity of MDA RES displayed no difference in sensitivity neither to JPH203 nor to L-Asp treatment (**Figure 41A** and **41B**) pointing out to a distinct mechanism governing cell metabolism between MDA RES and CEM RES cells.

We next investigated whether MDA resistance cells showed metabolic shift towards glycolysis. We first determined both glycolytic and mitochondrial pathways which may be involved in altered metabolism linked to mechanism of chemoresistance in MDA RES cells by testing with well-known metabolic inhibitors. No difference in drug sensitivity among MDA PA and MDA RES cells was detected neither with 2DG nor oligomycin treatments (**Figure 41C** and **41D**) supporting the idea that no specific dependency in metabolic reprogramming takes place in MDA RES cells. We further explored more the expression levels of glycolytic and mitochondria involved genes in MDA PA and MDA RES cells. Accordingly, the pattern of expression level of metabolic genes as the mitochondrial genes *COX3* and *ATP8* was unchanged or *ND* was shown much less affected (**Figure 42A**) compared to CEM RES cells (**Figure 23A**). To our surprise, *LDHA* was up-regulated in MDA RES whereas *HK2* was downregulated in MDA RES cells (**Figure 42A**). We next investigated the effect of FK866 on *LDHA* level, FK866 was no significantly affected in *LDHA* mRNA levels in the resistant cells (data not shown). Consistently, we found a significant increase in LDH release toxicity test toward FK866 treatment only in MDA PA but not in MDA RES cells (**Figure 42B**) as coherent with mRNA levels. Notably, MDA RES cells were not responding to glucose inhibitor treatment, suggesting a dynamic and differential ways of producing and sustaining NAD that may cause addiction in different cell lines.

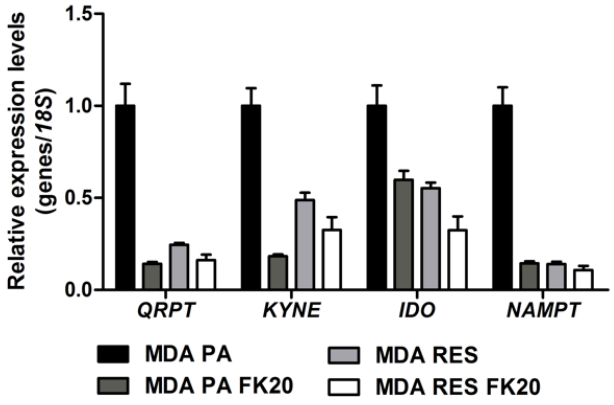

Figure 40 Down-regulation of *de novo* NAD synthesis target genes in MDA RES cells

MDA PA and MDA RES cells were treated with 20nM FK866 for 48h. Quantitative RT-PCR targeting *de novo* NAD synthesis genes including *QRPT*, *KYNE, IDO*, and salvage pathway *NAMPT* was analyzed. Data was represented as Mean with SD of two biological experiments with technical triplicates. *18S* was served as a housekeeping gene.

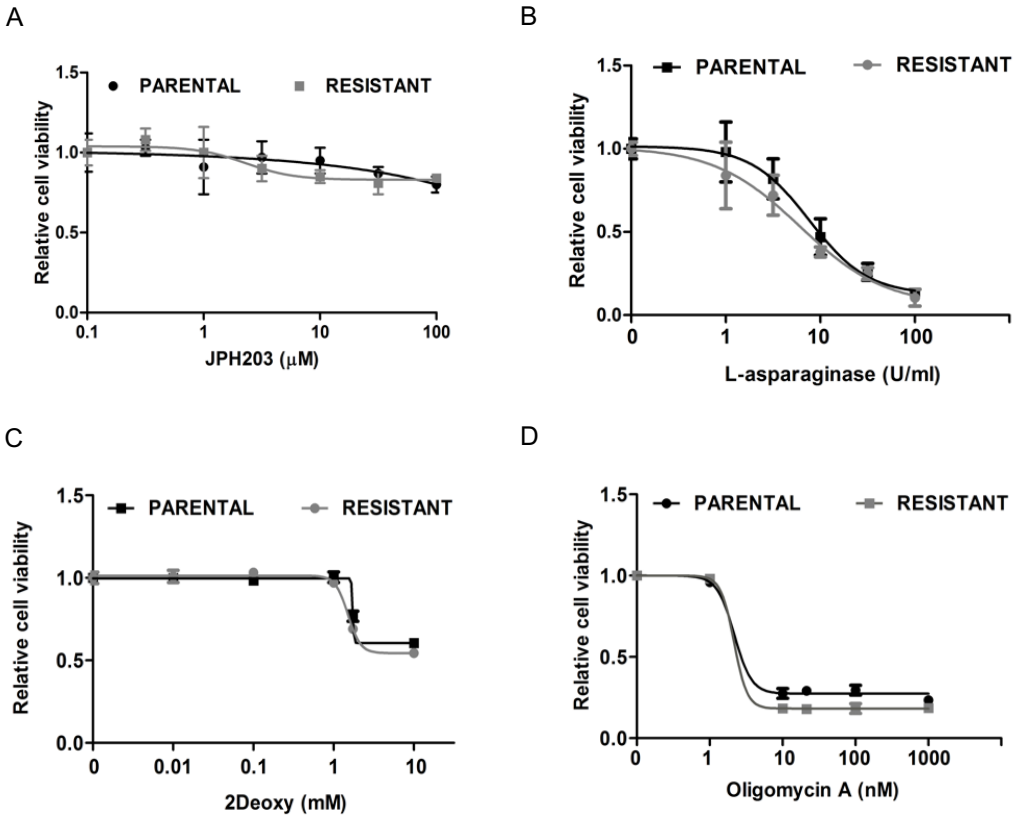

Figure 41 Drug sensitivity test in MDA MB231 cells

MDA PA and MDA RES cells were treated with various concentration of JPH203 (**A**), L-Asparaginase (**B**), 2DG (**C**), and oligomycin (**D**). Forty-eight hours after treatment, relative cell viability was analyzed using ozblue cell viability kit compared to mock (DMSO). Data was represented as relative of Mean with SD of three biological experiments with technical triplicates.

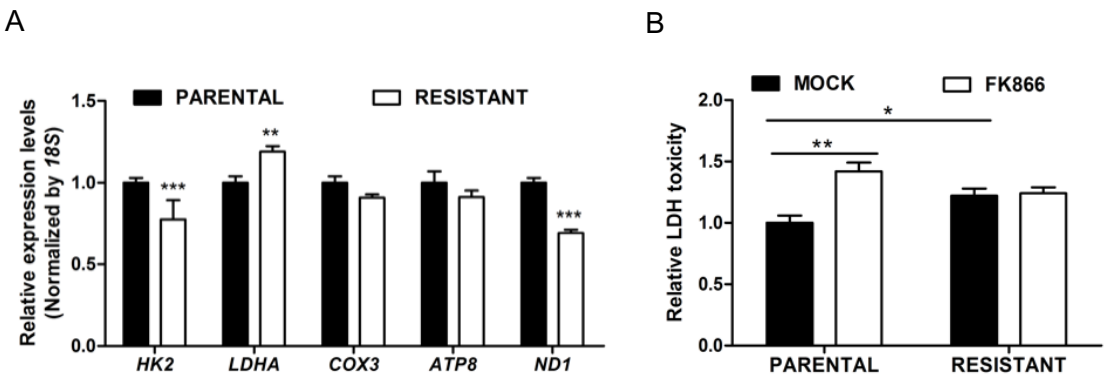

Figure 42 Expression levels of genes involved in glycolytic and OXPHOS
A, Quantitative RT-PCR targeting glycolytic genes (*HK2, LDHA*) and mitochondria genes (*COX3, ATP8, ND1*) were analyzed in MDA cells. *18S* was served as a housekeeping gene. **B**, FK866 exhibited toxicity in MDA PA cells. Cytotoxicity test was performed by LDH cytotoxicity kit measuring a release of LDH from damaged cells. Data was represented as relative of Mean with SD conducted from three biological experiments with technical triplicates.

Genetic evidences deciphering the mechanism of FK866 pharmacoresistance

NAMPT

By characterization of the resistance, we descriptively obtained many significant comparative data of the parental and resistance. To this regard, the simplest but hardest question then arises as to how cells acquire pharmacoresistance to FK866? Since, significant down regulation of *NAMPT* mRNA and enzymatic activity levels were commonly observed in both CEM RES and MDA RES cells in respect to the parental cells, we first reasoned that a relevance of this depletion in NAMPT level in the resistant cells. We sought to examine whether the acquired resistance is primarily caused by the genetic ablation of *NAMPT*. We created a robust over expression of *NAMPT* in MDA cells (**Figure 43A**). Cell viability, ATP, and NAD levels were experimentally analyzed. Overexpressed of *NAMPT* displayed functional effect in which it increased ATP and NADH levels in the resistant cells (**Figure 43C** and **D**). However, transient over-expressed *NAMPT* failed to reestablish or restore sensitivity toward FK866 treatment in MDA RES cells (**Figure 43B-D**).

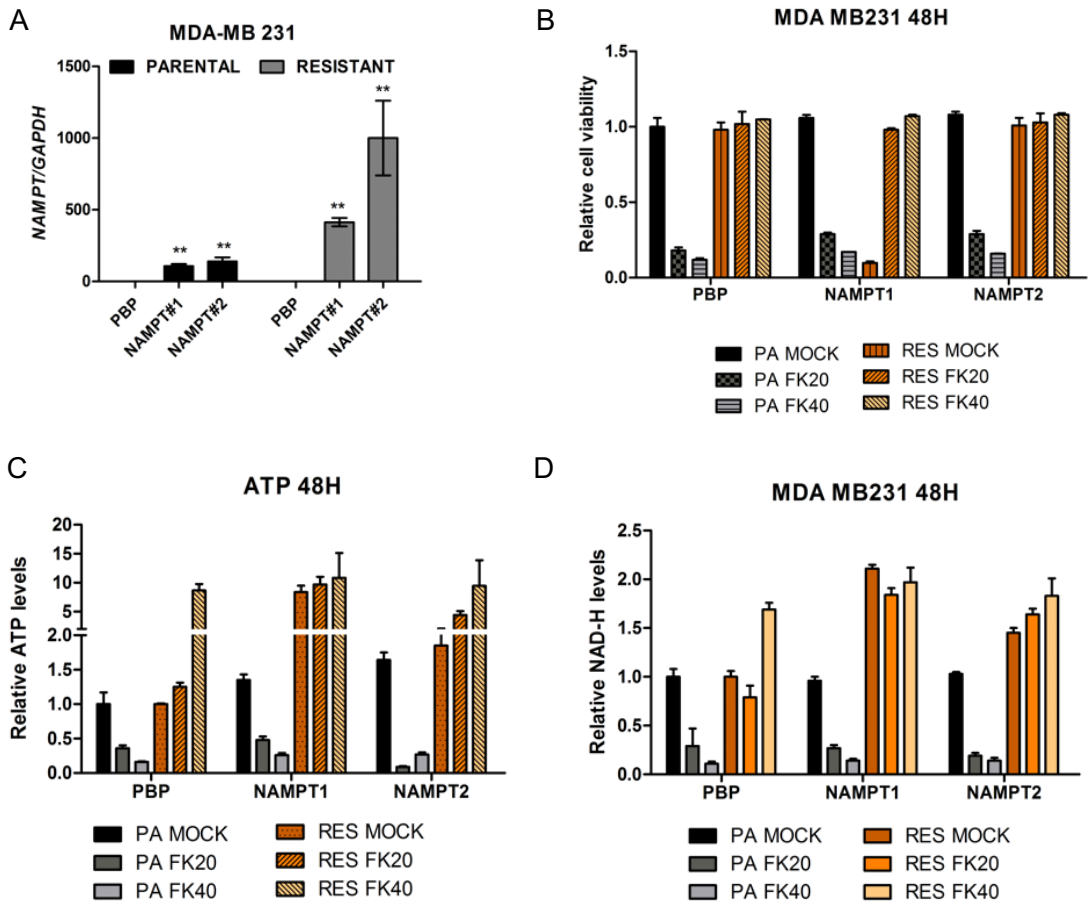

Figure 43 Overexpressed NAMPT in MDA cells
MDA PA and MDA RES cells were transiently transfected with empty vector control (MDA RES/PBP) and NAMPT overexpressed-plasmids (MDA RES/NAMPT). **A**. *NAMPT* mRNA level was analyzed by RT-PCR, *GAPDH* was used as a housekeeping gene. Twenty-four hours after transfection, cells were treated with indicated concentrations of FK866 for 48h. **B**, Cell viability was measured using ozblue cell viability kit. **C**, ATP levels was determined by luciferin-luciferin based assay. **D**, NAD levels was determined. Data was represented as relative of Mean with SD conducted from two biological experiments with technical triplicates.

It has been reported that depletion of *NAMPT* directly induced cell death [161]. We further examined the expression level of *NAMPT* by RT-PCR and cellular NAD activity detecting by a biochemical assay in numerous cancer cell lines. Differential expression of *NAMPT* mRNA levels and NAD enzymatic activity across a panel of nine cancer cell lines were illustrated in **Figure 44A** and **44B**, respectively. Among those lines, MDA cell line expressed the highest level of *NAMPT* and correlated with NAD activity. Furthermore, we attempted to understand the correlation of *NAMPT* expression or cellular NAD levels in respond to FK866 sensitivity. Thus, FK866 drug screening was performed in all

those cell lines. Depletion of NAD by FK866 induced cell death in most of indicated cell lines except CEM RES and MDA RES cells (**Figure 44C**). FK866 potentiated B-ALL (NALM and 697) cell mortality. Unfortunately, it was difficult to draw a correlation between *NAMPT* mRNA expression and NAD level with cell susceptibility to FK866 in those panel of cell lines. However, we could appreciate the significant effect of FK866 strongly induced cell death suggesting a crucial role of NAMPT in various types of cancer cells.

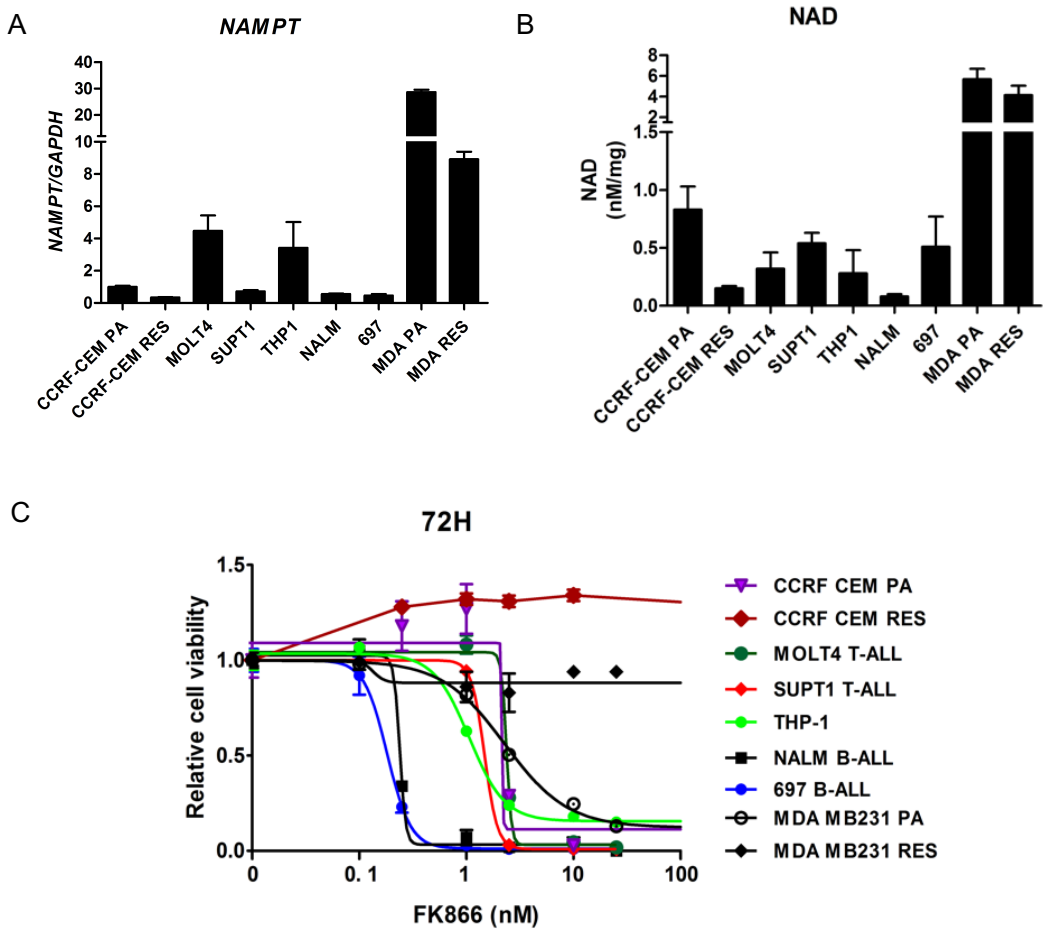

Figure 44 Differential expression of NAMPT levels and NAD activity in a panel of cancer cell lines

A, *NAMPT* mRNA levels of indicated cell lines was analyzed by quantitative RT-PCR, *GAPDH* was served as a housekeeping gene. **B**, Cellular NAD activity was measured by NAD biochemical assay. **C**, Cytotoxicity of FK866 in a panel of nine human cell lines, cells were exposed in various concentration of FK866 for 72h. Cell viability was measured by ozblue cell viability kit. Curve fitting and parameter estimation were performed with a standard sigmoidal concentration-response model with variable slope using Graph Prism software. The value was represented as relative of Mean with SD conducted from three biological experiments with technical triplicates for **A** and **C** and two biological experiments with technical triplicates for **B**.

Lactate dehydrogenase (LDH)

MDA RES cells revealed differently from leukemia cells (CEM) in metabolic control, the latter cells find alternative metabolic solution to the production of NAD from tryptophan. Among of those key glycolysis enzymes, dose dependent enhanced LDH activity in CEM RES sub-clones mounting an evidence to intensively explore functional effect of LDH. We speculated whether a key glycolytic enzyme LDH possibly contributes to the acquisition of resistance of both CEM and MDA cells. To assess the role of putative LDH in tumor, the effect of a small potent molecule inhibitor of LDH, GSK2837808A (GSK) [111] was initially determined in both CEM and MDA cell lines. We observed that the resistant cells were more susceptible to LDH inhibition in respect to the parental one as evidence by lower in EC50 of GSK (**Figure 45A** and **B**) as well as the number of viable cells (**Figure 45C** and **D**) both in CEM and MDA resistant cells. EC50 at 48h of GSK was 19.2μM (R^2=0.994) in CEM PA and 12.1μM (R^2=0.95) in CEM RES cells. We evaluated if downregulation of LDH enzyme levels upon GSK treatment resulted in depletion of cellular energy production. ATP and NAD levels were analyzed in CEM and MDA cells. Results showed marked reduction in ATP and NAD levels toward GSK treatment in CEM cells. Interestingly, we could appreciate a greater impact of GSK in the depletion of ATP and NAD levels in CEM RES than CEM PA (**Figure 46A** and **B**) suggesting that LDH might play a significant role in promoting glycolysis facilitated resistant phenomenon in leukemia. GSK significantly decreased ATP levels in MDA cells (**Figure 45C**). In contrast, no significant different in NAD level was observed in MDA cells (**Figure 45D**). In addition, the effect of GSK on cell cycle distribution of CEM PA and CEM RES cells were determined by flow cytometry and showed alteration in G0/G1, S, and G2/M phase of cell cycle under the different treatment conditions. Treatment with GSK slightly increase G2/M phase accumulation in CEM PA cells (**Figure 47 B-D**). In comparison to parental cells, a dramatic increase in S and G2/M phase arrest was observed in the resistant population (**Figure 47** and **Table 1**). Importantly, GSK induced apoptosis was obviously detectable only in the CEM resistant not in the CEM parental one (**Figure 47G** and **H**). These results mounting an evidence to an important role of LDH in cell cycle progression

in CEM RES cells. CEM RES cells displayed a tendency to be more sensitive to the inhibition of LDH than MDA RES cells.

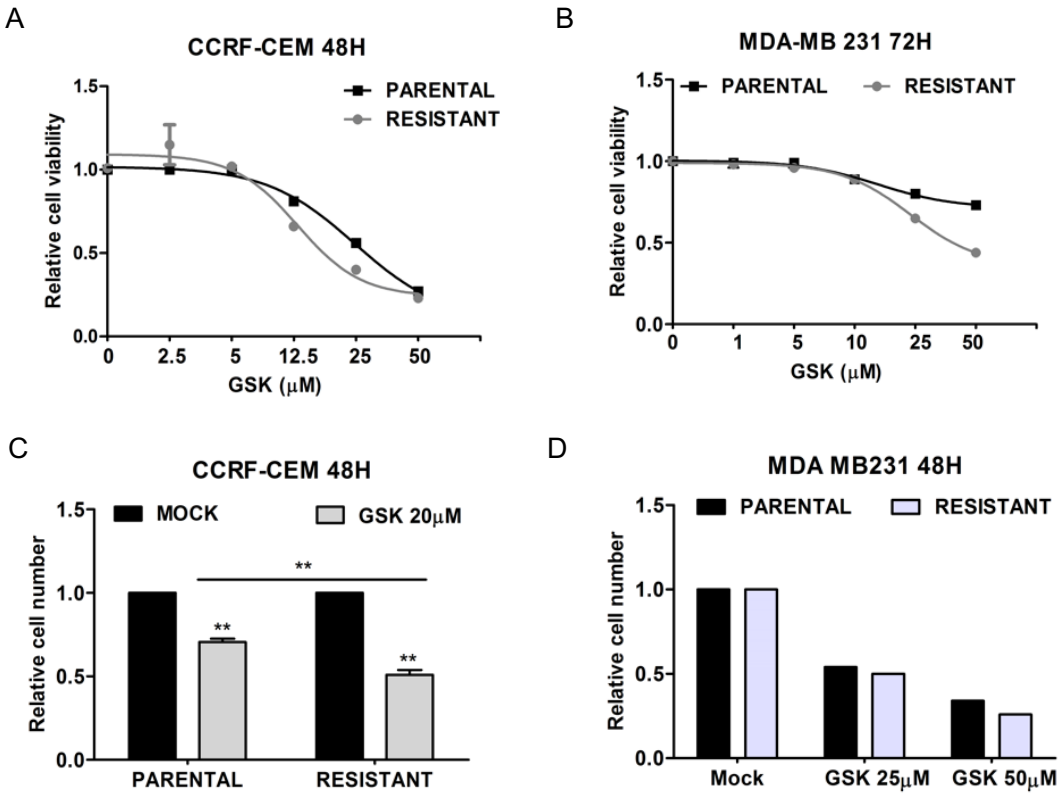

Figure 45 Resistant cells are susceptible to a LDH inhibitor.
A, CEM PA and CEM RES cells were exposed to various concentrations of GSK a potent LDH inhibitor. **B**, MDA PA and MDA RES cells were exposed to various concentrations of GSK. Cell viability was determined after 48h of treatment using ozblue cell viability kit. **C**, CEM cells were treated to GSK as an indicated concentration for 48h. **D**, MDA cells were treated to GSK as an indicated concentration for 48h. Relative of cell number was conducted from automate counting device (Invitrogen). Data was represented as relative of Mean with SD from three biological experiments (A, B, C) and a preliminary experiment for figure 45D.

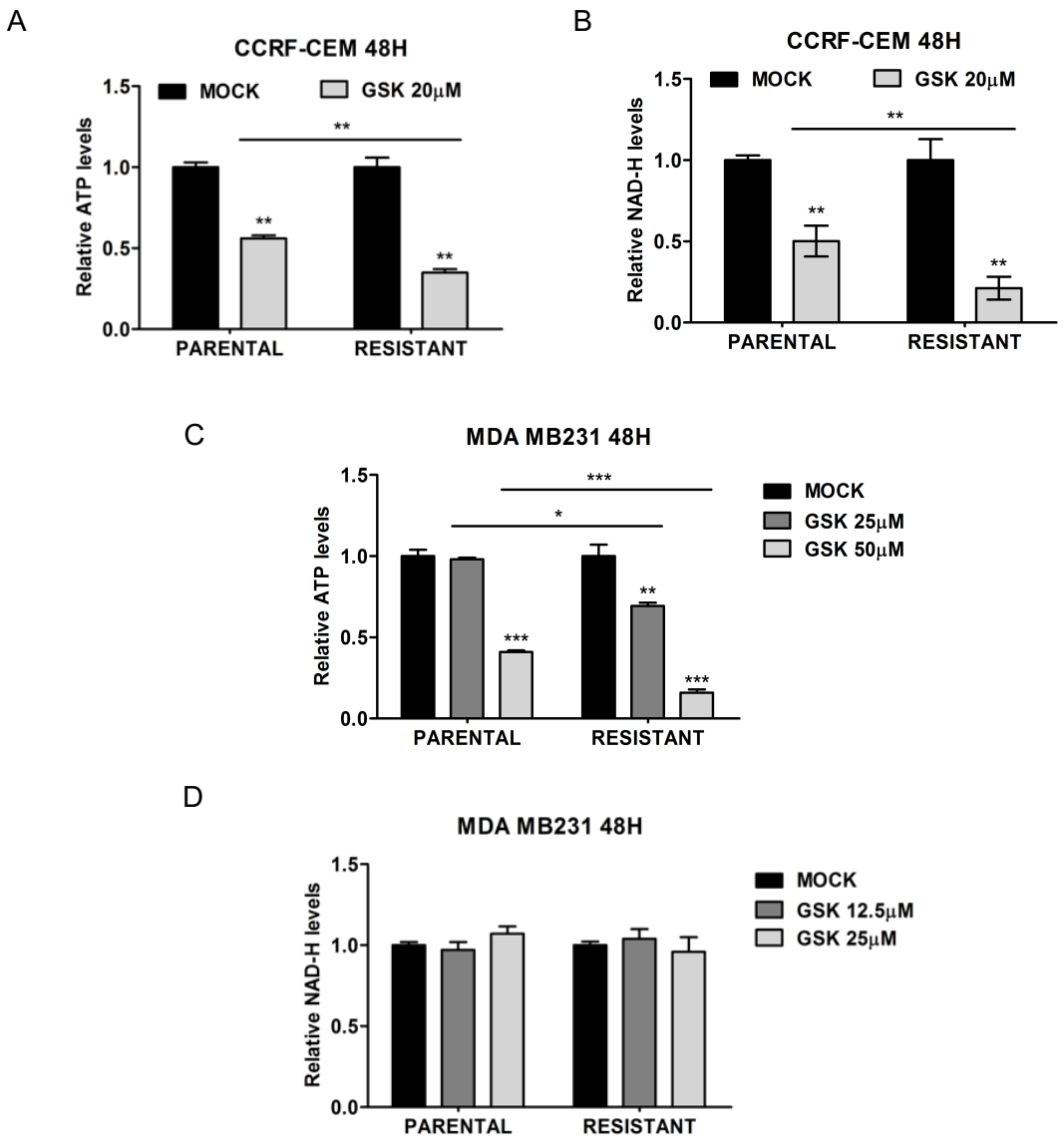

Figure 46 Inhibition of LDH impacts ATP and NAD production in CEM RES cells. **A**, CEM cells were exposed to DMSO (Mock) and 20μM GSK. ATP levels was measured 48h after treatment. **B**, NAD levels was measured 48h after treatment DMSO (Mock) and 20μM GSK in CEM cells. **C**, MDA cells were exposed to indicated concentrations of GSK. ATP levels was measured 48h after treatment. **D**, NAD levels was measured 48h after treatment with DMSO (Mock) and indicated concentrations of GSK in MDA cells. Data was represented as Mean with SD conducted from four biological experiments with technical quadruplicates (**A, B**) and three biological experiments with technical quadruplicates (**C, D**). (***p<0.01)

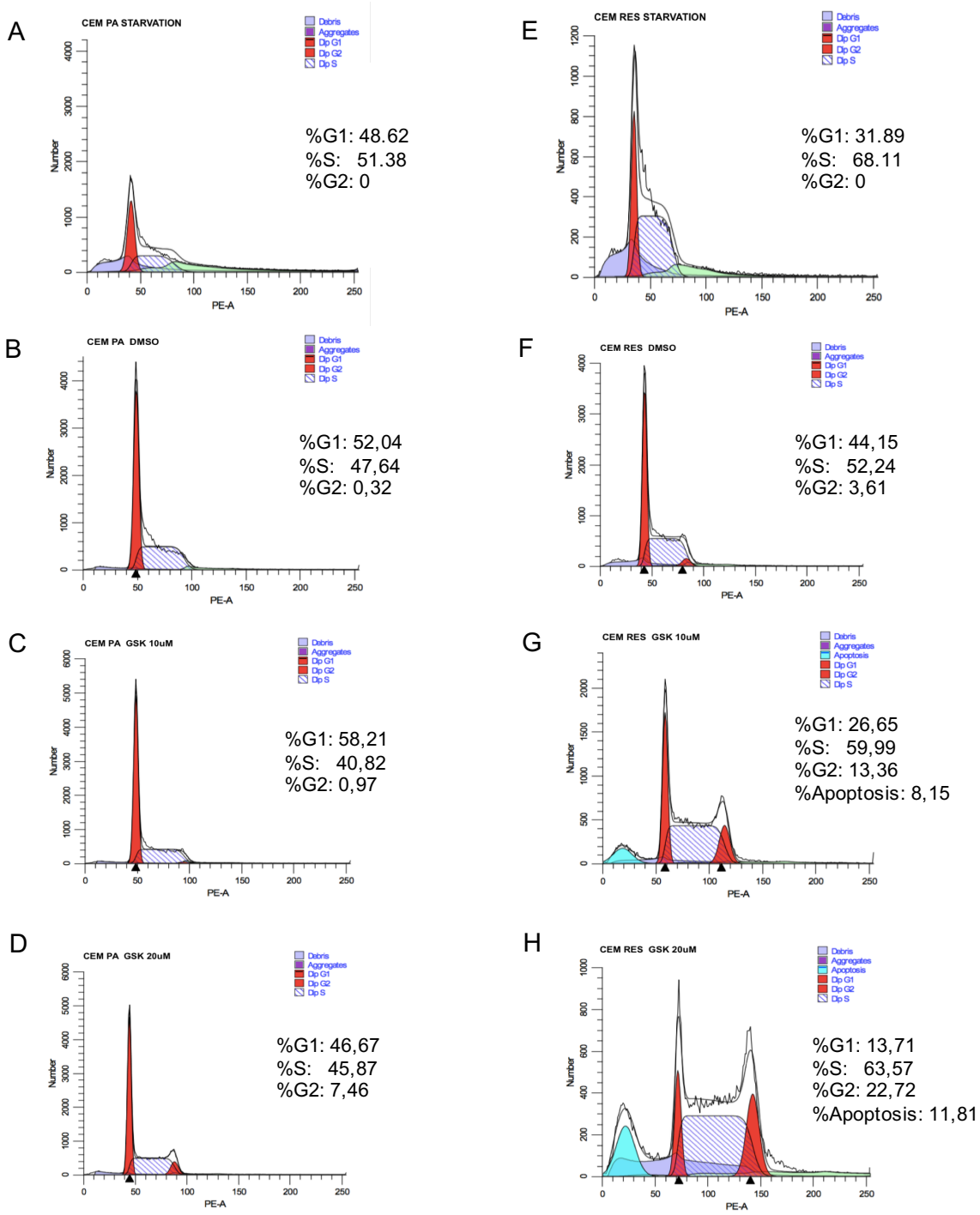

Figure 47 GSK induces apoptosis in CEM RES cells

FACS-mediated cell-cycle analysis by propidium iodide (PI) staining of CEM PA and CEM RES cells. CEM cells were treated with following conditions; serum free starvation, DMSO (Mock), GSK 10μM, and GSK 20μM in CEM PA cells (**A, B, C** and **D**) and in CEM RES cells (**E, F, G** and **H**), respectively. Forty-eight hours after treatment cell were lyzed with 0.5% Triton X, then incubated with the PI and thereby cell cycle analysis was performed using flow cytometry. A representative data of FACS from two biological experiments was shown.

Table 1 Cell cycle analysis by PI staining in CEM PA and CEM RES cells

Cells	Treatments	%G1	%S	%G2	G2/G1	%CV	%Apoptosis
CEM PA	Starvation	48.62	51,38	0	2.00	8.41	-
	Colchicine 100ng/ml	51.91	47.91	0.18	1.94	4.93	-
	DMSO	52.04	47.69	0.32	1.91	4.92	-
	GSK 10uM	58.21	40.82	0.97	1.97	4.41	-
	GSK 20uM	46.67	45.87	7.46	2.00	4.06	-
CEM RES	Starvation	31.89	68.11	0	2.00	6.80	
	DMSO	44.15	52.24	3.61	1.95	4.88	-
	GSK 10uM	26.65	59.99	13.36	1.96	4.22	8.15
	GSK 20uM	13.71	63.57	22.72	1.97	4.33	11.81

GSK administration significantly down-regulated *LDHA* mRNA expression in the parental cells of both CEM and MDA cells (**Figure 48A** and **48D**). We found that GSK significantly activated of *CHOP/ATF4* in both CEM PA and CEM RES cells (**Figure 48B** and **48C**). In contrast, GSK slightly activated *ATF4* mRNA expression in MDA cells (**Figure 48F**) but no activation of *CHOP* activation was in MDA resistant (**Figure 48E**). This highlights a difference in the pharmacological response to the LDH inhibition between CEM and MDA cell lines, in which GSK is more potent in CEM cells than MDA cells.

Drug combination has been applied as a potential therapeutic platform for cancer therapy. It usually gives better and more reliable therapeutic outcomes than single anti-cancer treatment. To evaluate if GSK restore FK866 sensitivity and improve the toxicity outcome. We performed drug combination experiment between NAMPT inhibitor (FK866) and a metabolic drug targeted lactate dehydrogenase enzyme (GSK). Although MDA cells was not strongly susceptible to GSK single treatment but we observed the synergistic effect in the combined treatment of GSK and FK866 (**Figure 49B and 49C**). EC50 of GSK single treatment and GSK+20nM FK866 were 29.1 nM (R^2=0.97) and 17.7 nM (R^2=0.96) in MDA 48h, respectively (**Figure 49B**). However, we did not observe a clear enhanced toxicity of GSK+FK866 co-treatment in CEM cells (**Figure 49A**). We observed the difference in drug sensitivity toward GSK treatment between CEM and MDA cells. Combination of FK866 and GSK was not improve the toxicity in CEM cells whereas the presence of GSK could resensitize the

FK866 susceptibility in MDA RES cells. Since, CEM cell displays as a low glycolytic cell and the metabolic enhanced glycolysis occurs once CEM cells became pharmacoresistant to FK866 whereas MDA-MB231 cell has been characterized as a high glycolytic cell. Therefore, initially difference between these two cell lines may cause the different mechanism in acquiring FK866 resistance. However, LDH plays a pivotal role in both cell line.

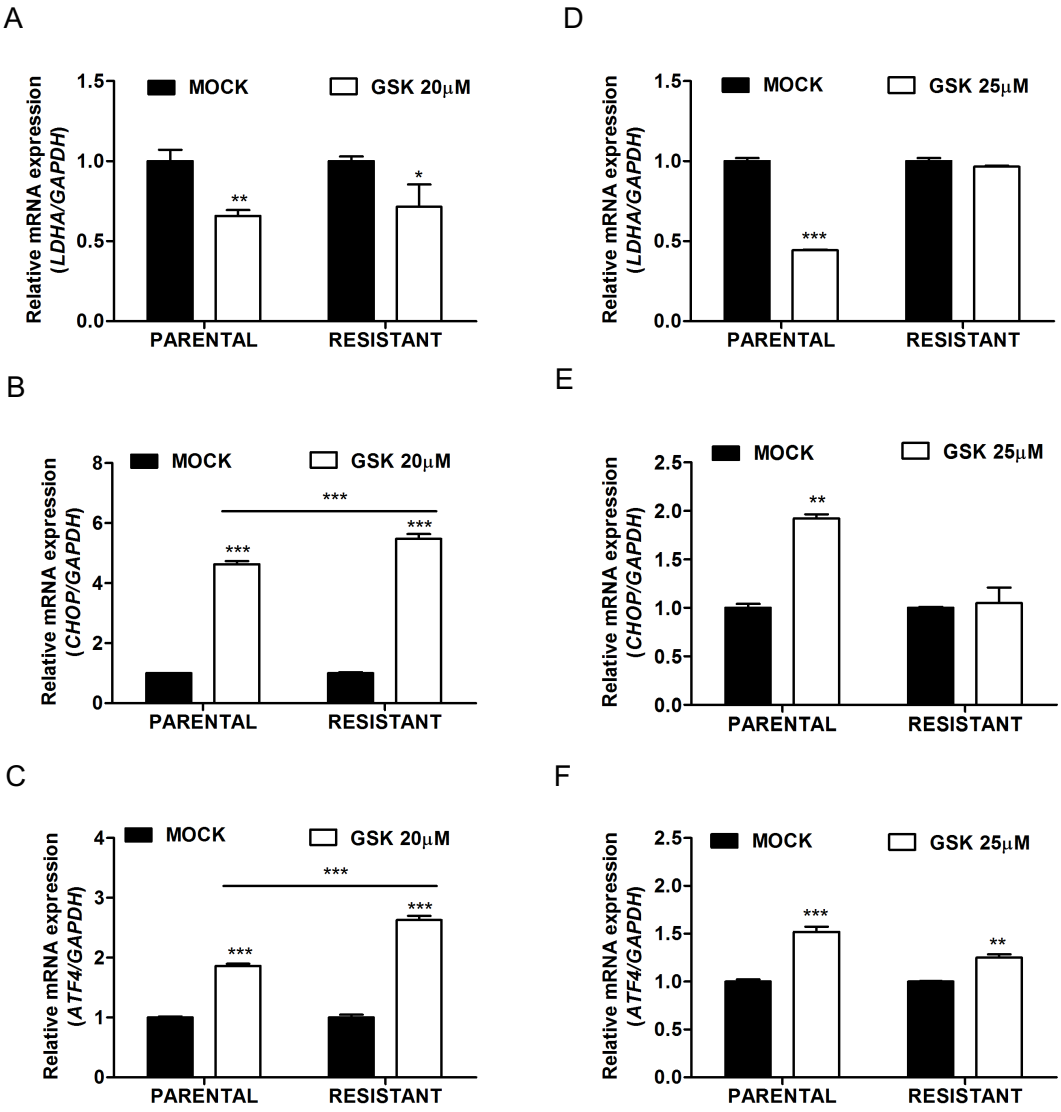

Figure 48 Inhibition of *LDHA* by GSK induces the CHOP/ATF4 activation.
CEM PA and CEM RES cells were treated with 20μM GSK for 48h. Expression levels of *LDHA* **(A)**, *CHOP* **(B)**, and *ATF4* **(C)** were measured using qRT-PCR. MDA PA and MDA RES cells were exposed to 25μM GSK for 48h. Expression levels of *LDHA* **(D)**, *CHOP* **(E)**, and *ATF4* **(F)** were measured by qRT-PCR. *GADPH* was served as a house keeping gene. Data is represented relative of Mean with SD compared to MOCK of each cell line of three biological experiments with technical triplicates.

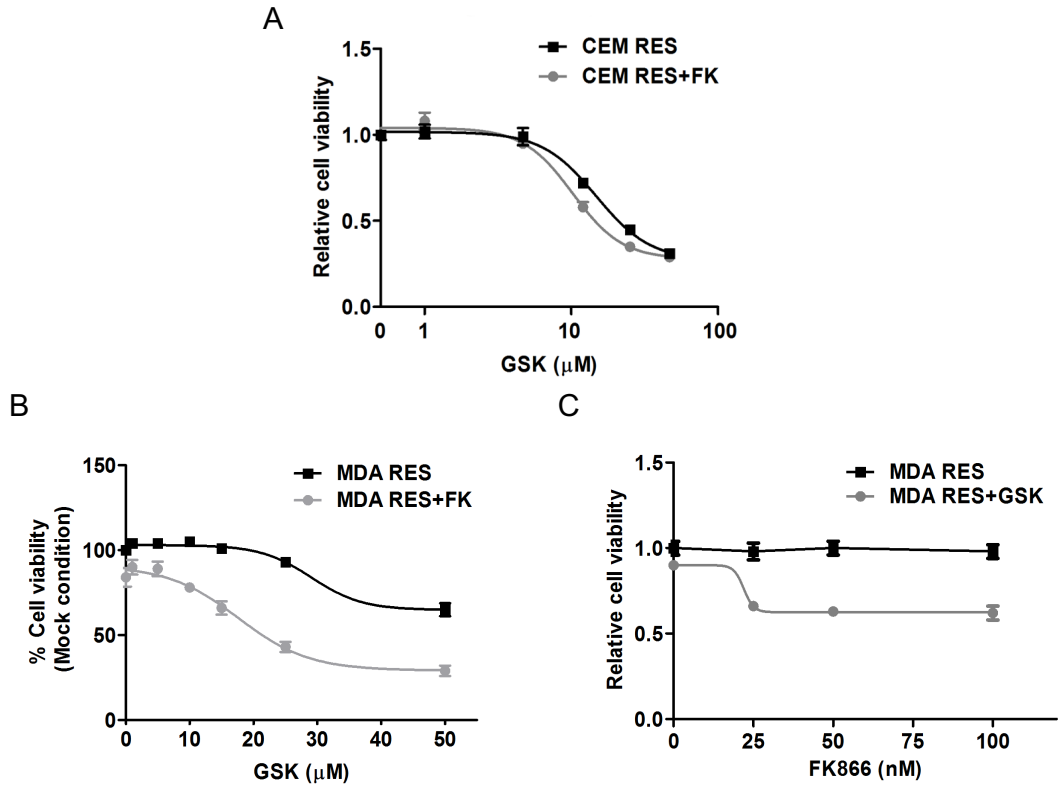

Figure 49 Drug combination between FK866 and GSK
A, CEM PA and CEM RES cells were treated with combination of 50nM FK866 and vary concentrations of GSK (0-50μM). **B**, MDA PA and MDA RES cells were co-treated with 20nM FK866 and vary concentrations of GSK (0-50μM). **C**, MDA PA and MDA RES cells were co-treated with various concentration of FK866 (0-100nM) and 25μM GSK. Cell viability was measured and analyzed 48h after treatment by ozblue cell viability kit. Data was plotted as relative Mean with SD of three biological experiments with technical triplicates.

Apoptosis contributes to cell death in the CEM RES cells treated with a LDH inhibitor GSK concurrently with a significant depletion of ATP and NAD levels, indicate critical roles of LDH contributing to metabolic regulation and gaining resistance to FK866. Therefore, we sought to investigate genetic data supporting of *LDHA* mediated metabolic adaptations that able to confer advantages to FK866 resistance. We performed a transiently knock-down the *LDHA* expression in MDA PA and MDA RES cells (**Figure 50A** and **50B**). To further evaluate if downregulation of *LDHA* by siRNA targeting human *LDHA* results in depletion of cellular energy production. Level of ATP and NAD were examined in scramble siRNA Control (MDA SCR) and *LDHA* silencing MDA (MDA si*LDHA*). A significant depletion of ATP but not NAD levels were obtained in MDA RES cells silenced *LDHA.* (**Figure 50C** and **50D**). We appreciate the synergy of GSK and

FK866 treatment in MDA RES displaying an enhanced in cancer cell growth inhibition in respect to the single treatment of GSK (**Figure 49C** and **49D)** revealing an imperative role of *LDHA* involved in establishing the resistance to FK866 of MDA RES cells. We thus speculated that the loss of *LDHA* may resensitize the drug sensitivity toward FK866 especially in the resistant cells. To address this hypothesis, we performed transiently knock-down of *LDHA* in MDA RES cells by siRNA targeting human *LDHA* to down-regulated LDHA expression both protein and mRNA levels (**Figure 50A** and **51A**). Loss function of *LDHA* mediated cancer cell death through the activation of *CHOP/ATF4* mRNA expression (**Figure 51B** and **51C)**. Interestingly, a genetic evidence showing that the ablation of *LDHA* by siRNA coordinated treatment of FK866 significantly improve toxicity by activation of CHOP/ATF4 (**Figure 51B** and **51C**) in consistent with pharmacological outcome of an LDH inhibitor (GSK) and FK866 combined treatment in MDA resistant cells.

Taken together, a potent NAMPT inhibitor FK866 targets the most active pathway of NAD biosynthesis in several cancers. However, lack of tumor-selectivity for the use of FK866 as a single drug treated leukemia has been deteriorated its therapeutic potency. We revealed the significant function of LDH mediated metabolic adaptions or conferred advantage to FK866 acquiring resistance in cancer cells. Combination treatments targeting metabolic functions could open the potential therapeutic window for cancer therapy in particular T-lymphoblastic leukemia. However, deepen investigation regarding to cancer acquiring LDH inhibitor resistance could be considered for further investigation.

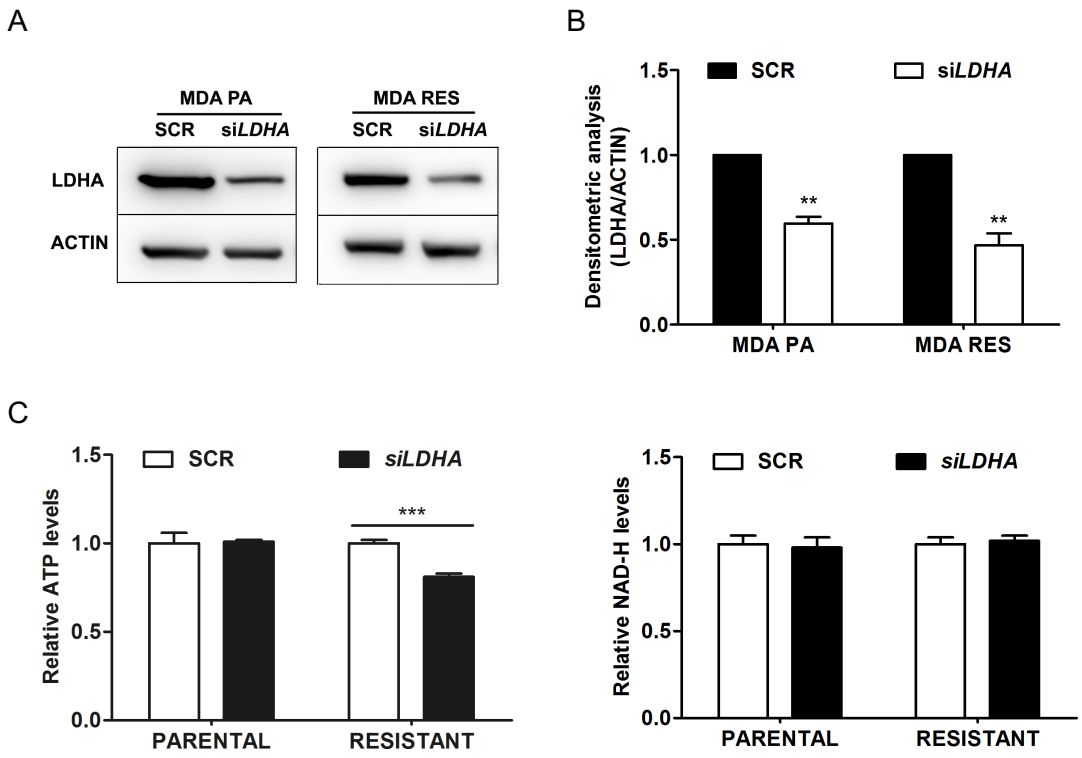

Figure 50 Ablation of *LDHA* by siRNA leads to a decrease in ATP production in MDA cells.

Down regulation of *LDHA*, siRNAs targeting human *LDHA* were transfected via interferin transfection reagent (Polyplus) to knock down the *LDHA* expression transiently in MDA PA and MDA RES cells. **A**, Immunoblotting was performed on whole cell lysates, probed with mouse-monoclonal anti-LDHA, and reprobed with anti-β-actin as a loading control. **B**, Densitometric analysis of *LDHA* silencing in MDA PA and MDA RES. **C**, ATP levels was determined after 48h of silencing with si*LDHA* in MDA cells. **D**, NAD levels was determined after 48h of silencing with si*LDHA* in MDA cells. Data is represented as Mean with SD of three biological experiments with technical triplicates. (***p<0.01)

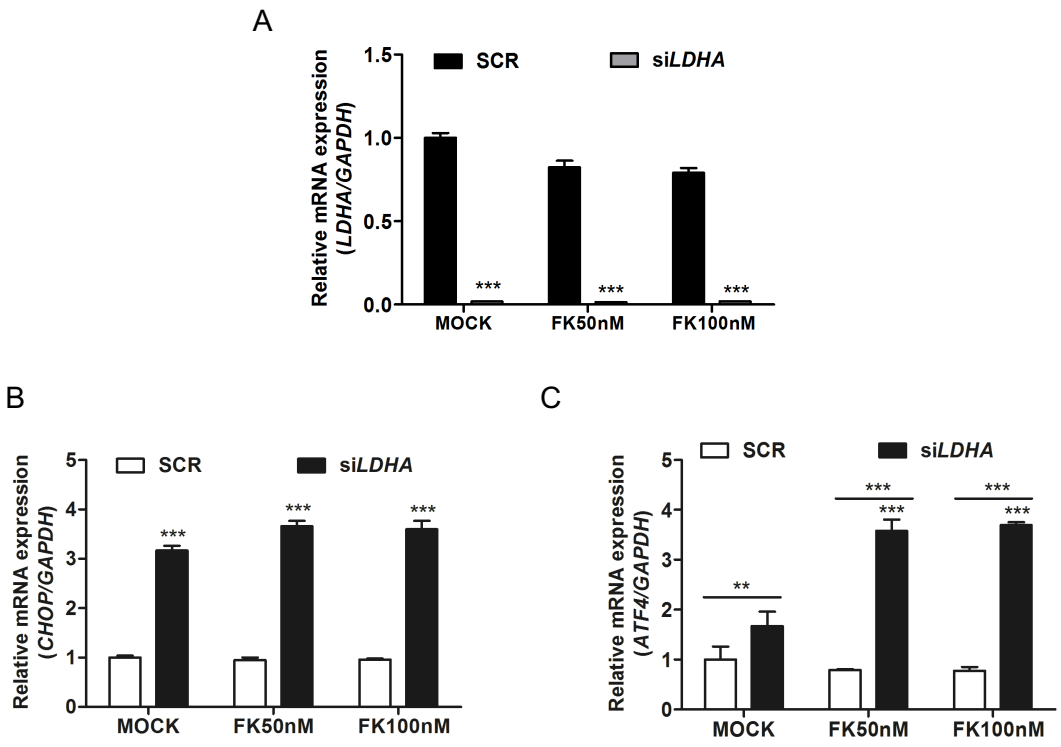

Figure 51 Treatment of FK866 coordinated with down-regulation of *LDHA* potentiates the activation of CHOP/ATF4 in the resistant cells.
siRNAs targeting human *LDHA* were transfected via interferin transfection reagent to knock down *LDHA* expression in MDA RES cells. Twenty-four hours after silencing, MDA RES cells were treated with 50nM and 100nM of FK866 for 48h. Expression levels of *LDHA* **(A)**, *CHOP* **(B)**, and *ATF4* **(C)** were determined by qRT-PCR. *GAPDH* expression was served as a housekeeping gene. Relative expression level of genes compared to MOCK condition was analyzed. Data was represented as relative of Mean with SD. from three biological experiments with technical triplicates.

FUTURE PERSPECTIVES

Pharmacological characterization and metabolic function were evaluated in the NAMPT inhibitor resistant cells. Expression of ABC transporters prevents drug accumulation in the resistant cell by improving drug efflux [153]. However, (i) investigation of mitochondria function, (ii) analysis metabolomic function, (iii) involvement of amino acid uptake of parental and resistant cells, as well as (vi) involvement of the existence of cancer stem-like cells which may represent a resistant subpopulation of cancer cells with high tumor or metastasis-forming ability and drug resistance to NAMPT or LDH inhibitors would be highly interested for further investigation.

DISCUSSION

In the current study, we provide evidence for understanding molecular mechanism of pharmacoresistance to NAMPT inhibitor in leukemia and breast cancer cell lines. This is based on 5 lines of evidence; (i) protein translation control was not inhibited in the resistant cells during FK866 treatment, (ii) the molecular mechanism by which FK866 resistant CCRF-CEM cells utilized L-tryptophan as an alternative source for NAMPT-independent NAD production to fuel cell metabolism, (iii) we highlighted metabolic reprogramming of the CEM resistance enhances toward glycolysis (Warburg effect), (iv) two remarkable evidences of amino acid interference impacted cell survival and synergistic effect of the NAMPT inhibitor with amino acid inhibitors in the resistance (v) We proposed LDH as a pivotal target having functional effects responsible for cell survival. Inhibition of LDHA expression in resistant cells are more vulnerable to deplete ATP, NAD synthesis than in parental cells rendering a synthetic lethality and drug susceptible towards FK866.

Development of drug resistance by cancer cells is one of the major causes of therapy failure limiting the effectiveness of chemotherapy. Growing evidences support the idea that deregulated cellular metabolism or metabolic alteration is linked to such resistance [162]. Indeed, both components of the glycolytic and mitochondrial pathways are involved in altered metabolism. Understanding metabolic alterations associated with drug resistance opens up unexplored opportunities for the development of new strategy for cancer therapy. During the past decade, FK866 has also been evaluated in a broad variety of tumor cells including leukemia and solid tumors namely in gastric cancer [48], T-ALL [71], small lung carcinoma [157], triple-negative breast cancer [37], murine tumor [163,164], neuroblastoma [165], hepatocarcinoma [76] and prostate cancer [166]. Interestingly, FK866 is much less toxic in non-tumor cell cultures and animal model [74]. Similarly, high sensitivity to the drug is displayed by leukemia and lymphoma cells, but not by normal hematopoietic progenitors [14,74]. However, the link between tumor metabolism and drug resistance to FK866 has not been deeply investigated. Therefore, we applied a selection strategy to obtain a cancerous CCRF-CEM ALL cell designated CEM RES that was capable of tolerating exposure to a NAMPT inhibitor FK866. MDA-MB231 resistant cells (MDA RES)

were also generated as a comparative model for intensive understanding the generality of molecular mechanism of pharmacoresistance to FK866 in other cancers. However, the precise pattern of the acquisition of *bona fide* drug resistance heterogeneity is unknown. It has been proposed that the drug-tolerant cancer could be expanded from a pre-existing cells, which may even provide a latent reservoir of cells for the emergence of heterogeneous drug resistance mechanism [167]. Dramatically decrease of NAD level and thereby drop of ATP levels are the distinctive drug signature of FK866 (**Figure 18A** and **18B**). In agreement with several studies highlighted a crucial role of a NAMPT inhibition FK866 which led to depletion of NAD, secondarily displaying a decrease in ATP subsequent cell death in many cell lines [69,149].

AMPK actively restrained aerobic glycolysis in T-ALL cells through inhibition of mTORC1 while promoting oxidative metabolism and mitochondrial Complex I activity [168]. Here in, we observed no activation of AMPK/mTOR mediated protein translation during reactivation with FK866 treatment in the resistant cells of both CEM and MDA resistant models (**Figure 20** and **39**). An inhibition of mTOR subset (FKBP12) led to an impaired functions of mitochondria and increased lactate production, concurrent enhanced aerobic glycolysis in Jurkat cells [169]. Interestingly, decrease in AMPK activity can be rescued by leucine and glucose supplementation [170]. Accordingly, we postulated that dysfunction of AMPK/mTOR signaling pathway might be one of explanation contributing to an increase in aerobic glycolysis and suppressed mitochondria function in the resistance.

In this study, we revealed different metabolic adaptation of CEM RES and MDA RES cells in which CEM RES cells displayed an enhanced glycolysis dependency to confer metabolic advantage to FK866. Although 2DG inhibits cancer cell growth through an oxidative stress mechanism in multiple cancer cell lines including MDA-MB231cells [171], but we did not observe metabolic alteration in MDA RES cells in respect to the parental one. This glycolysis dependency feature in CEM RES cells was confirmed by upregulation of key glycolytic enzyme activity, coupled with increased in lactate production, and higher level of glucose consumption. In contrary, switch of bioenergetics back from aerobic glycolysis to mitochondrial oxidative phosphorylation has also been known to

increase tumor resistance [162]. Reverse Warburg effect in which metabolic shifts from Warburg (aerobic glycolysis) to OXPHOS has been reported in docetaxel prostate cancer resistant cells [162]. Under radiation, MCF-7 cells can be quickly adapted to genotoxic condition via mTOR-mediated reprogramming of bioenergetics from predominantly glycolysis to OXPHOS [172]. Recently, Wu Hao and colleagues revealed that lactic acidosis has been found to be a factor responsible for metabolic switch from aerobic glycolysis to dominant OXPHOS [173]. Interestingly, glycolysis rate can dramatically be reduced by the 0.4 unit decrease of pH due to alteration of glycolytic enzymes including HK and PFK1 and also glucose transporters were sensitive to proton inhibition[173]. Although lactic acidosis could alter glucose metabolism in most cancer cells and has a capacity to feedback to glucose utilization/metabolism but this issue has not been addressed in CEM RES. Increased mRNA levels of *Hk2, Pfkfb2, Slc2a1*, and *Slca4* were observed in cardiomyocytes treated with FK866 [174]. Inhibition of glycolysis, by the use of synthetic compound 2DG concealed the clue of glycolysis dependency that resistant cells compensated the decrease of OXPHOS activity, due to a limited availability of NAD/NADH at its turned due to the decrease of NAMPT enzyme. Similar event has been shown earlier in leukemia cells, in which the increased glycolysis rate is due to an up-regulation of several genes involved in glycolysis or glucose uptake and consequent an excessive production of lactate in ALL cell lines [175] and most of ALL cell lines are sensitive to 2DG [176].

Susceptible to JPH203 a selective LAT-1 inhibitor of CEM RES lighted up the possibility that LAT1 involvement and tryptophan utilization served as an alternative source for NAMPT-independent NAD production. JPH203 inhibitor has been documented both *in vitro* and *in vivo* against HT-29 tumors transplanted in nude mice [177,178], and apoptosis induction in YD-38 human oral cancer cells [179]. *In vivo* assay, a dietary flavonoids (Proanthocyanidins) up-regulated hepatic *SIRT* mRNA and other specific genes involved in *de novo* NAD synthesis (*Qprt* and *Nadsyn1*) but not *Tdo2* or any genes involved in salvage NAD+ biosynthesis pathway [180]. Even though, intracellular NAD+ concentration and NAMPT levels was increased in LTKO mice (a triply null; *FoxO1*, *FoxO3*, and *FoxO4*) but there was no significant alteration of genes associated NAD synthesis pathway (*Qprt,*

Nadsyn1, Nmnat1-3) in LTKO mice [181] implying the dynamic mRNA regulation that might differ among different organs and tissues. We observed the stable in *QPRT* mRNA level upon FK866 re-exposure in CEM RES cells. But evidences of cell sensitivity to JPH203 and a synergistic effect of combined FK866 and JPH203 weightily indicated the involvement of LAT1 transporters responsible for amino acid translocation into the cells in particular tryptophan. *IDO* downregulation induces sensitivity to FK866 and others metabolic drugs such as gemcitabine and pemetrexed in human cancer cells [182]. We detected a very low expression level of *IDO* in CCRF-CEM cells in compared to MDA MB231 cell line. Multi-drug resistance is not only solely achieved by enhanced efflux capacity but also by suppresses intake of the drug in leukemia [183,184]. Even though, there was no significantly different in LAT1 expression between parental and resistant cells (**Figure 30**). But essential amino acid (AAE) was preferentially required to maintain cell survival in the resistance as well as tryptophan potentially rescued cell death during energetic stress from JPH203 and combined of FK866 and JPH203 (**Figure 31** and **32**). Consistent work was reported in Hela cells supporting that the *CHOP* gene is transcriptionally induced by amino acid starvation in particular leucine deprivation. Moreover, ATF4 and ATF2 were found to be involved in amino acid control of *CHOP* expression [86,185].

MDA resistant model, a comparative model was developed to investigate the degree of generality of pharmacoresistance in cancer. Numerous common phenotypes were comparable to CEM RES cells including no alteration of ATP, restoration of NAD levels (**Figure 19** and **38**), dysfunction of translation control (**Figure 20** and **39**), and similarly down-regulation in *NAMPT* mRNA levels to escape from FK866 toxicity and likely potentiate an alternative biochemical mechanism of NAD production. Although two resistant models shared many common characteristics but they displayed distinct metabolic reprogramming acquiring energy source to fuel cell metabolism. Certainly, LAT1 was involved in CEM RES but not in MDA RES cells due to tryptophan served as a source to supply cell metabolism by sustained the production of NAD only in CEM RES cells. In a review of Chung and Gadupudi showed that tryptophan metabolites play a complementary role in promoting carcinogenesis in bladder tumor [186,187]. Likewise, these metabolites from the IDO could also be involved in leukemia,

skin, breast, or lung cancer [186]. However, here we revealed the dissimilar metabolic requirement between CEM RES and MDA RES cells by displaying an enhanced glycolysis dependency in CEM RES but not in MDA RES cells. In addition, phenomena in which cancer cells exhibit a cross-resistant phenotype which is known as multidrug resistance features such as enhanced drug efflux by overexpression of ABC transporters, decreased cellular uptake by changes in lipid membrane composition or drug detoxification by increases in drug metabolizing enzymes might be involved as causes for cell acquiring resistance as well as they could also be strategies to overcome drug resistance [153].

Development of drug resistance commonly confers by gene mutation. Six mutations in the *NAMPT* gene have been reported in GNE-618 resistant cells derived from RD (rhabdosarcoma), MiaPaCa-2 (pancreatic cancer) and NCIH460 (non-small cell lung cancer) cell lines. Particularly, mutation at Ser 165 residue of NAMPT in NCI-H460 cells turned cells to become resistant at high concentration of GNE-618 due to the unwinding of an α-helix that binds the NAMPT substrate PRPP [150]. Additionally, we did not observe any mutations in *NAMPT* coding region neither in our CEM resistant nor parental cells. Down-regulation of NAMPT level was observed in both CEM and MDA cells once cells gaining resistance to FK866 which was controversy to a report from Olesen and coworkers showing that over-expression of *NAMPT* associated with FK866 resistance in HEK293T cells [69] denoting that high expressed NAMPT cancers display less sensitive to pharmacological events by NAMPT inhibitors. Genetic ablation of *NAMPT* might not be directly responsible for acquiring resistance to FK866. Most cancer cell lines were sensitive to FK866 treatment but diverse levels of *NAMPT* mRNA or NAD activity was not correlated with cells susceptibility to FK866 treatment. We unsuccessfully sought out the correlation between *NAMPT* or NAD levels to FK866 cell sensitivity (**Figure 44**). In this regard, the contribution of the different NAD+ biosynthetic pathway and the relevance of the utilization of extracellular NAD+ precursors to generate NAD may differ among different organs and tissues [188]. Transiently overexpression of *NAMPT* failed to reestablish sensitivity of MDA RES toward FK866 in our system (**Figure 43**). This is probably due to cellular NAD level supplied from tryptophan, an alternative source of NAD synthesis was more dominant and sufficient to

sustain cell metabolism subsequent cell survival in the resistance, than those partial declined NAD level through inhibition of NAMPT by FK866 which exposed less impact to cell survival, as depicted in *NAMPT* overexpressed cells.

Current strategies seek to address inevitable resistance mechanism such as the use of ganetespib (Hsp90 inhibitor) to overcome resistance of PARP inhibitors in breast cancer by targeting core protein in DNA repair machinery[98]. Recently, it has been demonstrated that treatment of cerdulatinib (dual SYK/JAK inhibitor) overcomes ibrutinib resistance in CLL by induced apoptosis [95] and targeting AMPK-ULK-mediated autophagy to combat BET inhibitor resistance has been explored in acute myeloid leukemia stemcells [97]. The resistance to a standard chemotherapy of T-ALL, L-asparaginase has been found to link to *ASNS* expression which can be silenced through methylation [100]. Most cancers express multiple genetic alterations or abnormalities, it is seldom very useful by only using one anticancer drug. Therefore, combination treatment displays promising results than single treatment. Combination of BRAF and MEK inhibitors has been reported to surpass outcomes compared with single therapy with either BRAF or MEK inhibitors alone in melanoma [189]. Recently, costunolide and dehyrocostuslactone combination treatment has been shown to inhibit breast cancer by inducing apoptosis [190] as well as the use of Hsp90 inhibitor combined treatment with doxorubicin enhanced the cytotoxicity, apoptosis in non small cell lung cancer (NSCLC) [191]. Similar report was shown by Bertaina and colleages that combination treatment of bortezomib with other chemotherapeutic agents including doxorubicin, vincristine and pegylated asparaginase provided therapeutic advance in childhood relapsed/refractory acute leukemia and lymphoma (ALL) [192]. In addition, drug combination of NAMPT inhibitors with GMX1777(8) [193], PARP inhibitor [37], and CD73 inhibitor [188] have been found to improve the therapeutic levels in cancer. Indeed, here we documented that the great combination of FK866 with drugs associated amino acid metabolism including a LAT1 inhibitor (**Figure 29**) and L-asparaginase (**Figure 34**) effectively profound synergism in CEM RES cells, and in MDA RES cells (**Figure 45E**). Likewise, combined treatment of LDH inhibitors with phenformin or PFKPB3 causes additive inhibition of bladder cancer cells [194]. Furthermore, combined inhibition of glycolysis and pentose cycle selectively increases cytotoxicity in

breast and prostate cancer [171]. High *LDHA* levels have been linked to poor prognosis in many cancers such as bone metastases, liver and lung cancer [195] and with the concomitant of down regulation of *LDHA* levels in cancer cells by siRNA or shRNA stimulates mitochondrial respiration and reduces cellular proliferative and tumorigenic potential *in vitro* and in xenograft models [103,110,111]. Suppression of LDHA by oxamate decreased the lactate production and inhibited tumor invasion in human gastric cancer cells [196], suppressed cell proliferation through induction of G2/M or G0/G1 in nasopharyngeal cells [197] as well as down-regulated Warburg effect in glioblastoma [198]. Oxamate is a pyruvate analogue which directly inhibits LDH and tissue lactate production in diabetes mice [199]. Here in, we demonstrated that inhibition of *LDHA* was sufficient to induce significant cancer cell death promoted apoptosis in CEM RES cells (**Figure 47**). Consistently, treatment with quinolone 3-sulfonamids (a NADH-competitive LDHA inhibitor) promoted apoptosis in Snu398 cells [110]. CEM RES could be more vulnerable to LDH blockade due to the overall lower capacity of their mitochondria function in cancer stem cells which has also been consistent to a recent report in CSCs isolated from glioblastoma [200]. Ablation of *LDHA* in MDA-RES cells by siRNA significantly increased the sensitivity of FK866-MDA RES cell towards FK866 treatment as evident by CHOP/ATF4 activation (**Figure 51B, C**). Interestingly, our current observations were consistent to the studies in human breast cancer where down-regulating *LDHA* by siRNA resensitized the sensitivity of Taxol-resistant cells to taxol treatment [104]. Thus, by exploiting the altered metabolism of cancer resistance as reported here by targeting LDH, this may offer novel opportunities for selective therapeutic targeting of cancer cells particularly the cancer addicted to aerobic glycolysis for survival as part of combinatorial approach to other metabolic drugs.

CONCLUSION

Loss of protein translation inhibition and down-regulation of NAMPT level were evidently observed in both CEM and MDA resistant models. Here in, we revealed the distinct in molecular of pharmacoresistance between two cell lines as summarized in **Table 2**. We highlighted that FK866 CEM RES cells utilized L-tryptophan as an alternative source for NAMPT-independent NAD synthesis pathway and metabolic alterations once cells acquired resistance led to profound an enhanced glycolysis dependency consistent with the Warburg phenotypes which could be tracked by increase in glycolysis enzymatic activity and lactate production concomitant the reduction of mitochondria ATP production and low oxygen consumption. Eventhough, initial distinction in glycolytic status among CEM and MDA may cause the difference mechanism in FK866 resistance but LDH hypothetically plays pivotal roles in metabolic regulation and acquiring resistance to FK866. More importantly, our finding suggests the used of FK866 in combination with other drugs targeting metabolism may improve the clinical strategy to overcome cancer resistance in particular of those rely on aerobic glycolysis for survival.

Table 2 Summary of the characterization in parental and FK866 resistant models

Treatments or categories	Cell lines			
	CEM PA	CEM RES	MDA PA	MDA RES
FK866 (NAMPT inhibitor)	Highly sensitive	Resistant	sensitive	Resistant
CHS-828 (NAMPT inhibitor)	Highly sensitive	Resistant	sensitive	Resistant
NAMPT levels		*down regulated		*down regulated
Protein translation control	arrested	No inhibition	arrested	No inhibition
ATP with FK866 treatment	Highly sensitive	no response	Highly sensitive	no response
NAD with FK866 treatment	Highly sensitive	Partially sensitive	Highly sensitive	Partially sensitive
JPH203 (LAT1 inhibitor)	Partially sensitive	Highly sensitive	-	-
L-Asparaginase	Partially sensitive	Highly sensitive	Partially sensitive	Partially sensitive
2DG (inhibitor of glucose metabolism)	Partially sensitive	Highly sensitive	-	-
Oligomycin (inhibitor of mitochodria ATP syntase)	-	-	sensitive	sensitive
Metabolic alteration		*Enhanced glycolysis	no alter	no alter
GSK (LDH inhibitor)	sensitive	Highly sensitive (Apoptosis)	Partially sensitive	Sensitive

* Pair comparison was evaluated between parental vs resistance of each cell line.

SECOND PROJECT

CHARACTERIZATION OF SMALL MOLECULE OF PKC INHIBITORS THAT SPECIFICALLY MODULATE YAP FUNCTIONALITY IN PDAC CELLS

BRIEF SUMMARY

In 2016, we published a research article ***"The GSK3β inhibitor BIS I reverts YAP-dependent EMT signature in PDAC cell lines by decreasing SMADs expression level"*** *in Oncotarget Journal* [201]*. This publication reflects my personal contribution to the work as the first-coauthor. For clarify, I myself performed and had fully involved in most experiments except initial drug screening, two-dimension western blotting analysis and ChIP assay which were conducted by Ilaria Castiglioni (Laboratory of Gene Expression and Muscular Dystrophy, San Raffaele Scientific Institute, Milan, Italy). I decided to describe this work in this session as the second project due to all results were published in Oncotarget Journal (2016) and I could not represent them all again as result figures in my thesis body. Full article is enclosed in Appendix (****page 142****). Research background, finding results represented as Figures following* [201]*, and discussion were briefly summarized in this session.*

Background

Pancreatic ductal adenocarcinoma (PDAC) is a type of exocrine pancreas which is the most common malignancy of pancreas [202]. PDAC is generally thought to arise from pancreatic ductal cells [203]. Molecular and pathological analysis of PDAC has discovered a characteristic pattern of genetic lesions. Mutations of *KRAS, CDKN2A, TP53, BRCA2* and *SMAD4/DPC4* have been shown to drive pancreatic neoplasia (**Figure 52**) [204]. In particular mutation of *KRAS* has been reported to increase in frequency with disease progression, and frequently found in PDAC [202].

The Hippo pathway is an evolutionarily conserved regulators for cell growth, apoptosis, development and migration in many cancers [205,206]. It is also crucial for stem cell self-renewal and the maintenance of genomic stability [206]. YAP functions have been found to be regulated by the multiple post-translational modifications (PTMs) [207]. The Hippo signaling pathway, initially well-described as an organ size regulator in *Drosophila* [202]*.* This kinase cascade is able to negatively regulate YAP localization and activity, by phosphorylating YAP at Ser127 [201,205]. Phosphorylation of YAP by the Hippo pathway leads to its accumulation in the cytoplasm and, by interaction with 14–3–3 proteins. YAP is degraded by a ubiquitination-dependent proteasomal process [205,206] as illustrated in **Figure 53**. Therefore, the Hippo pathway negatively regulates YAP

functionality and presence in the nucleus by modulating its cell distribution and its protein expression levels[201]. The Hippo pathway-induced phosphorylation of YAP is regulated according to cell density [205]. Importantly, at low density, YAP is predominantly localized in the nucleus while YAP translocates to the cytoplasm at high cell density as depicted in PDAC cell lines [201]. Nuclear localization of YAP protein is associated with TAZ which is its co-transcriptional activity [205,208]. In addition, the core of the Wnt signaling pathway has been involved the regulation of β-catenin which is its nuclear transducer. Wnt cytoplasmic destruction complex consists of Axin that interacts with other factors, including adenomatous polyposis coli (APC), CK1, and glycogen synthase kinase-3 (GSK3) [209]. In absence of Wnt signaling, the destruction complex targets β-catenin to degradation through β-catenin phosphorylation by GSK3 and its ubiquitination by β-TrCP. The presence of Wnt ligand results in functional inactivation of the destruction complex, leading to the accumulation of free β-catenin. Translocation of β-catenin to the nuclear where it forms complex to DNA-binding partners TCF/Lef triggering the downstream target of wnt signaling [205]. Interestingly, some Wnt target genes are under joined control of both YAP/TAZ and β-catenin, in a sort of "double-assurance" mechanism [209,210]. For example, both YAP/TEAD and β-catenin/TCF bind cooperatively to cognate promoter elements in the *Sox2* and *Snai2* genes in cardiomyocytes [210]; and in colorectal cancer cells, YAP and β-catenin seem to share a common DNA-binding platform of *TBX5* the transcription factor regulation the transcription of *Birc5* and *Bcl2/2* pro-survival genes [209].

However, YAP has been shown the crosstalk to many signaling pathways. YAP function is mediated by the the upstream stimuli or the binding to its down-stream targets. TEAD family was found to be critical partners of YAP in the regulation of gene expression such as *CTGF* which has been identified as a direct target gene of YAP-TEAD in mammalian cells [201,211]. CTGF is crucial in mediating the growth-stimulating and oncogenic function of YAP-TEAD complex [212] but its transcriptional expression depends on the contribution from other YAP interacting transcription factors such as SMADs [208]. *Smad2/3*, are direct targets of the TGFβ. The phosphorylation of Smad2 and Smad3 induces complex formations with Smad4 in the nucleus where triggering activators or repressors

orchestrate transcription (**Figure 54**) [207,213]. In PDAC mouse models, YAP is a vital promoter of mutant *KRAS* oncogenic program, specifically inducing the expression of *CTGF* and *CYR61* which are direct downstream target of YAP [204] Moreover, YAP associated with FOS involved to Epithelial to Mesenchymal Transition (EMT) by regulating the expression of genes such as *E-cadherin, SLUG, SNAIL* and *Vimentin* [214]. In pancreatic cancer development, YAP potentially plays an important role in EMT [201]. Therefore, the identification of inhibitors of YAP activity could be suitable as a new therapeutic option for PDAC treatment.

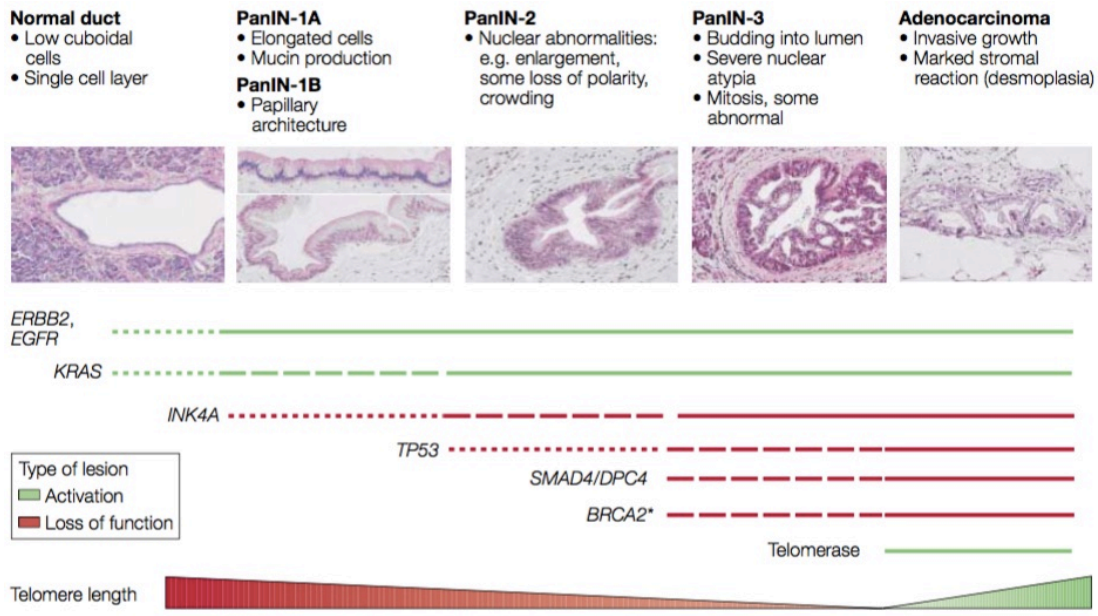

Figure 52 Genetic progression model of pancreatic adenocarcinoma.
Pancreatic intraepithelial neoplasias (PanINs) seem to represent progressive stages of neoplastic growth that are precursors to pancreatic adenocarcinomas. Activating *KRAS* mutations are the first genetic changes that show the earliest stages of histological disturbance in pancreatic. The stage of onset of these lesions is depicted. The thickness of the line corresponds to the frequency of a lesion [203].

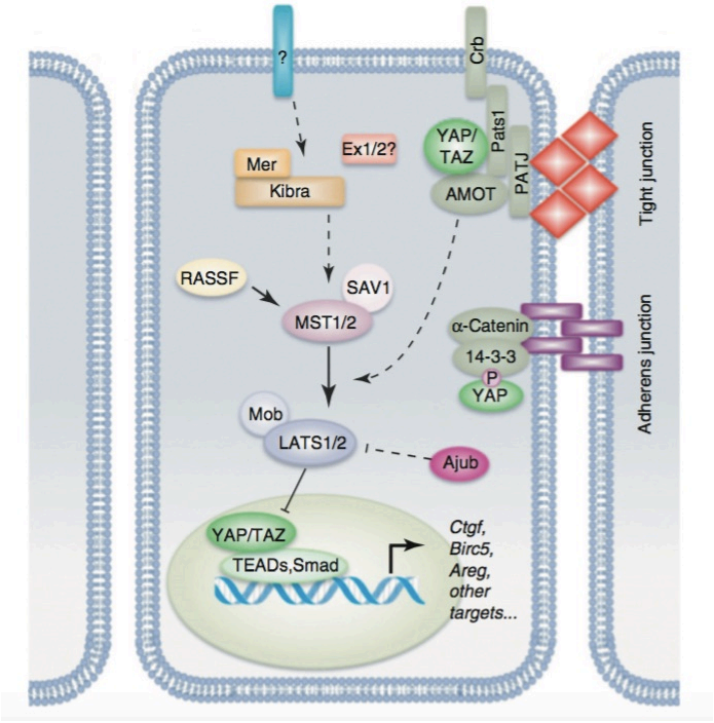

Figure 53 Schematic model of the Hippo signaling cascade in mammals [206].

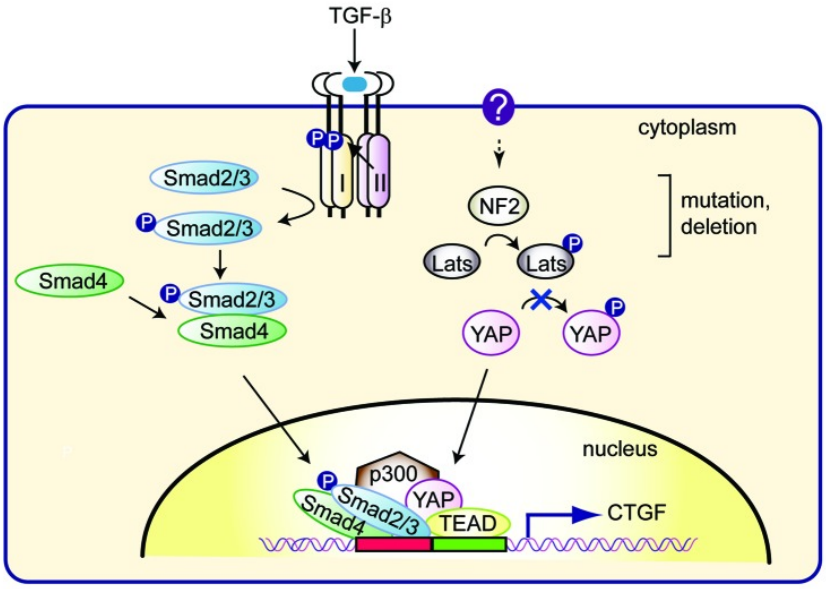

Figure 54 Schematic model of CTGF promoter activation through TGF-β/Smad signaling and Hippo pathway

Genetic disturbance in NF2 and/or Lats2, Yap was dephosphorylated and constitutively translocated to the nucleus. On the other hand, upon TGF-β stimulation, Smad2/3 and Smad4 associate, move to the nucleus, make a complex with YAP/TEAD, and recruit p300 to the promoter to activate *CTGF* expression [207].

Results and discussion

Refer to the publication of Thongon, et al. 2016 ***"The GSK3β inhibitor BIS I reverts YAP-dependent EMT signature in PDAC cell lines by decreasing SMADs expression level"*** *in Oncotarget Journal* [201]*. (**page 141**)*

We aimed to to identify compounds that can specifically modulate YAP functionality in PDAC cell lines. We initially performed a small-scale high-content screening for the identification of PKC inhibitors which able to interfere with YAP localization and functionality. The screening part was conducted by Ilaria Castiglioni. This approach allowed us to assign to the widely used Receptor Tyrosine Kinase (RTK) Inhibitor, erlotinib, the ability to sequester YAP into the cytoplasm blocking its co-transcriptional function (as shown in **Table 1**, *Thongon, et al.* 2016). Importantly, we found a small molecule, GF 109203X (BIS I), induces YAP nuclear accumulation and activation. In this study, we showed that BIS I, an inhibitor of the PKCδ/GSK3β pathway, reverts the EMT transcriptional program in PDAC cell lines inhibiting the TGF-β pathway and de-potentiating YAP contribution to EMT via down-regulation of *SMAD2/3*.

YAP regulates anchorage-independent growth in PDAC cell lines.

Figure 1, figure title "Importance of YAP in PDAC cell lines".

I have contributed to all experiment in this figure.

Expression level of YAP in a panel of four PDAC cell lines were determined using western blotting and qRT-PC. PANC1 and PK9 exhibited moderate to high YAP protein levels, respectively, in comparison to BXPC3 and MIAPACA2 cells (**Figure 1A**) indicating diverse expression levels of YAP among different cell lines. Cell density regulates phosphorylation and localization of YAP via the Hippo signaling pathway [206]. At high density of cell, YAP predominantly localized in cytoplasm while YAP appears mainly in the nucleus in sparse cell condition which has been reported in breast cancer cells [205,215]. We observed that sub-cellular distribution of YAP protein was equivalent in both cases with PANC1 cells, but YAP significantly shuttled from nucleus to the cytoplasm at high cell density in PK9 cells, as determined by high content imaging analysis (**Figure 1B**). To understand the YAP functionality, we down-regulation *YAP* by using shRNA then evaluated *CTGF* and *CYR61* mRNA levels, known targets of YAP.

they were significantly reduced in shYAP-PANC1 and shYAP-PK9 (**Figure 1C**). On the other hand, *CTGF* expression was found to be increased in *YAP* overexpression (O/E) both in PK9 and in PANC1 (**Figure 1D**). Interestingly, ablation of YAP inhibited anchorage-independent growth in PANC1 cells in soft agar (**Figure 1E**). Therefore, in PDAC cell lines cultured at high-density, YAP is partially redistributed in the cytoplasm, it has a transcriptional effect controlling the expression of known target genes, it regulates proliferation and the ability of PDAC cells to grow in anchorage-independent conditions.

BIS I changes YAP co-transcriptional activity and inhibits anchorage independent growth.

Figure 2, figure title "Identification of modulators of YAP localization"

*I have contributed in **Figure 2B-D**. **Figure 2A** and **2F** were performed by Ilaria Castiglioni.*

From the screening, we found a small molecule BIS I that induces YAP nuclear accumulation and activation in PK9 cells (**Figure 2A** and **Table 1**). BIS I is a cell-permeable and reversible inhibitor of protein kinases C (PKCs) both conventional and atypical, but also of GSK3β [216]. We observed that BIS I activated TEA-reporter and down-regulated *CTGF* and *CYR61* mRNA expression (**Figure 2B-C**), and induced YAP nuclear localization in PDAC cell lines, confirming the indication coming from the screening experiment (**Figure 2D**). Hippo signaling pathway was not directly involved in the observed PTMs because we did not observed a change at the phosphorylation state of YAP-S127 and LATS-S909 (**Figure 2F**).

Figure 3, figure title "BIS I treatment phenocopies YAP functional ablation"

*I have contributed in **Figure 3A-B**. **Figure 3C** was performed by Ilaria Castiglioni.*

BIS I amplified TEA reporter signaling in the basal conditions in PANC1 cells and during *YAP* overexpression both in PK9 and PANC1 cells (**Figure 3A**). Unexpectedly, BIS I significantly suppressed *CTGF* and *CYR61* mRNA expression but slightly increased *AREG* and *BIRC5* mRNA expression in PK9 and PANC1 cells at 24 hours of treatment, indicating that functional roles of BIS I mimicking *YAP* ablation (**Figure 3B**). To evaluate if BIS I displaces YAP from

CTGF promoter, even though YAP is located in the nucleus but we performed chromatin immunoprecipitation of YAP and evaluated the amplification of the CTGF promoter [31]. Indeed, YAP was no more associated with the CTGF promoter during BIS I treatment, but TEAD1 was still present (**Figure 3C**).

Figure 4, figure title "The CTGF expression level was modulated by the TGF-β and Hippo pathways in PDAC"

I have contributed to all experiment in this figure.

Interestingly, we observed that BIS I inhibited TGF-β induced *CTGF* expression in a YAP independent manner (**Figure 4A**) and it down-regulated SMAD2/3 protein levels in PK9 cells (**Figure 4B**). Most importantly, BIS I was readily effective in reducing the anchorage-independent growth of PDAC cell lines. BIS I reduced the total number of colonies of PANC1, MIAPACA2, and PK9 and reduced the colony dimensions of PANC1 and PK9 but increasing MIAPACA2 ones (**Figure 4C**). Taken together, BIS I induced YAP into the nucleus and triggered TEAD response. However, BIS I inhibited anchorage-independent cancer cell growth and proliferation, phenocopying YAP ablation and inhibiting TGFβ-dependent cell response by decreasing the expression of *SMADs* and SMAD/YAP co-regulated genes.

Given the relative specificity of BIS I for PKCδ/GSK3β, while Go9676 is more specific for PKCα, we hypothesized that PKCδ/GSK3β ablation could mimic BIS I treatment. Transient silencing of *PKCδ* and *GSK3β* were performed in PK9 cells. The results showed that *CTGF* decreased during *PKCδ* and *GSK3β* down-regulation indicating the link of the activity of these two kinases in *CTGF* expression regulation (**Figure 4D**). Silencing of *GSK3β* activated TEA reporter only in the presence of *YAP* overexpression, similarly to BIS I treatment and reduced the expression of *SMAD3* mRNA (**Figure 4E**) as BIS I treatment.

CD133 gene expression is regulated by YAP and inhibited by BIS I.

Figure 5, figure title "BIS I activates β-catenin and downregulates the expression level of cancer staminality genes"

I have contributed to all experiment in this figure.

Since the association of YAP to the WNT/β-catenin destruction complex has been reported [209], we evaluated the activation of the WNT/β-catenin signaling in PDAC cell lines during BIS I treatment. We performed a reporter assay with a construct expressing luciferase under TCF binding site (TOPFlash) or a mutated one (FOPFlash). BIS I significantly induced WNT/β-catenin reporter activity in all of the PDAC cell lines and also in HEK293T cells (**Figure 5A**) as well as induced the accumulation of β-catenin in the nucleus (**Figure 5B**). Coherently, Go9676 did not activate TCF/LEF reporter nor induced β-Catenin into the nucleus (**Figure 5A, 5B**). Since, YAP and β-Catenin play role in regulating differentiation, we further investigated if BIS I could affect the expression levels of stemness markers of PDAC. Among of those checked markers, *CD133* was up-regulated upon β-Catenin over-expression (**Figure 5C**) but it was suppressed during BIS I treatment (**Figure 5D**). Interestingly, only *CD133* was affected by *YAP* and *GSK3β* silencing (**Figure 5E** and **5F**). Moreover, *YAP* overexpression induced the up-regulation of *CD133* that was blocked by BIS I (**Figure 5G**). Therefore, these results identified *CD133* as a new gene regulated by YAP and GSK3β.

YAP-dependent EMT transcriptional program is inhibited by BIS I.

Figure 6, figure title "BIS I reverts YAP-induced EMT in PDAC cell lines"

I have contributed to all experiment in this figure.

BIS I induced YAP and β-Catenin nuclear accumulation by inhibiting the PKCδ/GSK3β pathway. *CD133* is a new critical regulator of EMT in PDAC. We revealed the different expression levels of E-cadherin in PDAC (**Figure 6A, 6B**) in which PK9 and BxPC3 cell lines showed high E-cadherin protein expression whereas PANC1 and MIAPACA2 expressed very low to undetectable E-cadherin protein levels (**Figure 6A**). This expression profile of E-cadherin in PDAC is consistent with its mRNA levels (**Figure 6B**). Our results show that endogenous levels of E-cadherin are inversely correlated with the anchorage-independent growth ability of these PDAC cell lines (**Figure 4C**). Importantly, EMT signature was dependent on YAP as, in shYAP-PK9 and shYAP-PANC1, *E-cadherin* and *CD133* expression was reverted.

Figure 7, figure title "Genetic ablation of YAP and BIS I treatment regulate cell migration"

I have contributed to all experiment in this figure.

During BIS I treatment, the clonogenic and migration abilities of PDAC, markers of EMT, were completely inhibited (**Figure 4C, 7A**). Migration of PANC1 cells decreased by administration of BIS I in shYAP PANC1 cells at 48 hours (**Figure 7A**). More notably, BIS I was able to revert the EMT signature by restoring *E-Cadherin* expression, as well as by regulating other EMT markers as *Vimentin*, *ZEB1* and *CD133* also in the presence of TGF-β (**Figure 5G, 7B, 7C, 7D**).

Conclusion

In this study, we revealed that BIS I, an inhibitor of the PKCδ/GSK3β pathway by inducing displacement of YAP from CTGF promoter, displaying a loss of function of nuclear YAP on specific genes, likely driven by the loss of SMADs partner and de-potentiating YAP contribution to EMT via down-regulation of *SMAD2/3*. BIS I induced the downregulation of many cancer stem genes, *CD133* included. We found that this new marker of EMT is highly regulated as YAP, GSK3β, and β-catenin modulated *CD133* expression, addressing this gene as a co-regulated gene by these three factors which may establish critical roles in maintaining pancreatic cancer.

CONTRIBUTION PROJECTS

During my PhD I have also been involved into 2 other side projects as following; **1st project** is mainly focus on the RNA binding protein HuR/ELAVL1, a widely characterized eukaryotic post-transcriptional regulator. HuR mediates cellular response to different kinds of stimuli, namely proliferation, survival and apoptosis, helping to determine cell fate by binding to many target mRNAs and influencing their splicing, shuttling, stability and translation efficiency. An impaired localization and activity of HuR have been associated with many forms of cancer and the protein has generated interest as a potent drug target.

This project led to two publications, I have contributed as a co-author.

"Targeting the Multifaceted HuR Protein, Benefits and Caveats"

Zucal C et al., Curr Drug Targets 2015.

"Dihydrotanshinone-I interferes with the RNA-binding activity of HuR affecting its posttranscriptional function"

D'Agostino VG et al., Sci Rep 2015.

2nd project is mainly focus on the effect of Dexamethasone and understanding the pharmacological features of NAMPT inhibitor and Dexamethasone cross resistance modulated by glucocorticoid receptor (GR) regulation in leukemia and glioblastoma. To date, it is an ongoing project in collaboration with Michele Cea (MD. PhD), and Alessio Nencioni (PhD) from Department of Internal Medicine, University of Genoa, Genoa, Italy.

LIST OF PUBLICATIONS

No	Publication Type	Title
1	Research article	*"The GSK3β inhibitor BIS I reverts YAP-dependent EMT signature in PDAC cell lines by decreasing SMADs expression level."* **N. Thongon**, I. Castiglioni, C. Zucal, E. Latorre, V. D'Agostino, I. Bauer, M. Pancher, A. Ballestrero, G. Feldmann, A. Nencioni, and A. Provenzani, Oncotarget, vol. 7, no. 18, 2016 (IF:5.008).
2	Patent	*"Nuovi derivati aza-tanshinonici, procedimento per la loro preparazione e loro uso in terapia"* Alla domanda è stato assegnato il seguente numero:102016000061247 (14/06/2016)
3	Research article	*"EIF2a-dependent translational arrest protects leukemia cells from the energetic stress induced by NAMPT inhibition."* C. Zucal, V. G. D'Agostino, A. Casini, B. Mantelli, **N. Thongon**, D. Soncini, I. Caffa, M. Cea, A. Ballestrero, A. Quattrone, S. Indraccolo, A. Nencioni, and A. Provenzani, BMC Cancer, vol. 15, no. 1, p. 855, Jan. 2015. (IF:3.265).
4	Research article	*"Dihydrotanshinone-I interferes with the RNA-binding activity of HuR affecting its post-transcriptional function."* V. G. D'Agostino, P. Lal, B. Mantelli, C. Tiedje, C. Zucal, **N. Thongon**, M. Gaestel, E. Latorre, L. Marinelli, P. Seneci, M. Amadio, and A. Provenzani, Sci. Rep., vol. 5, no. October, p. 16478, 2015. (IF: 5.228).
5	Review article	*"Targeting the Multifaceted HuR Protein, Benefits and Caveats."* C. Zucal, V. D'Agostino, R. Loffredo, B. Mantelli, **N. Thongon**, P. Lal, E. Latorre, and A. Provenzani, Curr. Drug Targets, vol. 16, no. FEBRUARY, pp. 1–17, 2015. (IF:3.029).
	Research article	My thesis project, Molecular mechanism of phamacoresistance to NAMPT inhibitor in cancers *(Manuscript preparation).*

REFERENCES

1. Hanahan, D. & Weinberg, R. a. The Hallmarks of Cancer Review University of California at San Francisco. *Cell Press* **100,** 57–70 (2000).

2. Hanahan, D. & Weinberg, R. A. Hallmarks of cancer: The next generation. *Cell* **144,** 646–674 (2011).

3. Phan, L. M., Yeung, S.-C. J. & Lee, M.-H. Cancer metabolic reprogramming: importance, main features, and potentials for precise targeted anti-cancer therapies. *Cancer Biol. Med.* **11,** 1–19 (2014).

4. Chang, C.-H. *et al.* Posttranscriptional control of T cell effector function by aerobic glycolysis. *Cell* **153,** 1239–51 (2013).

5. Mamane, Y., Petroulakis, E., LeBacquer, O. & Sonenberg, N. mTOR, translation initiation and cancer. *Oncogene* **25,** 6416–6422 (2006).

6. DeBerardinis, R. J. & Chandel, N. S. Fundamentals of cancer metabolism. *Sci. Adv.* **2,** e1600200 (2016).

7. Faivre, S., Kroemer, G. & Raymond, E. Current development of mTOR inhibitors as anticancer agents. *Nat. Rev. Drug Discov.* **5,** 671–688 (2006).

8. Yin, C., Qie, S. & Sang, N. Carbon source metabolism and its regulation in cancer cells. *Crit. Rev. Eukaryot. Gene Expr.* **22,** 17–35 (2012).

9. Lu, J., Tan, M. & Cai, Q. The Warburg effect in tumor progression: Mitochondrial oxidative metabolism as an anti-metastasis mechanism. *Cancer Lett.* **356,** 156–164 (2015).

10. WARBURG, O. On respiratory impairment in cancer cells. *Science* **124,** 269–70 (1956).

11. Koppenol, W. H., Bounds, P. L. & Dang, C. V. Otto Warburg's contributions to current concepts of cancer metabolism. *Nat. Rev. Cancer* **11,** 325–37 (2011).

12. Pelicano, H., Martin, D. S., Xu, R.-H. & Huang, P. Glycolysis inhibition for anticancer treatment. *Oncogene* **25,** 4633–4646 (2006).

13. Porporato, P. E., Dhup, S., Dadhich, R. K., Copetti, T. & Sonveaux, P. Anticancer targets in the glycolytic metabolism of tumors: A comprehensive review. *Front. Pharmacol.* **AUG,** 1–18 (2011).

14. Chiarugi, A., Dölle, C., Felici, R. & Ziegler, M. The NAD metabolome — a key determinant of cancer cell biology. *Nat. Rev. Cancer* **12,** 741–752 (2012).

15. Carew, J. S. *et al.* Mitochondrial DNA mutations in primary leukemia cells after chemotherapy: clinical significance and therapeutic implications. *Leukemia* **17,** 1437–47 (2003).

16. Xu, R.-H. *et al.* Inhibition of glycolysis in cancer cells: a novel strategy to overcome drug resistance associated with mitochondrial respiratory defect and hypoxia. *Cancer Res.* **65,** 613–21 (2005).

17. Chen, J. Z. & Kadlubar, F. F. Mitochondrial mutagenesis and oxidative stress in human prostate cancer. *J. Environ. Sci. Health. C. Environ. Carcinog. Ecotoxicol. Rev.* **22,** 1–12 (2004).

18. Zapico, S. C. & Ubelaker, D. H. mtDNA Mutations and Their Role in Aging, Diseases and Forensic Sciences. *Aging Dis.* **4,** 364–80 (2013).

19. Giatromanolaki, A. & Harris, A. L. Tumour hypoxia, hypoxia signaling pathways and hypoxia inducible factor expression in human cancer. *Anticancer Res.* **21,** 4317–24

20. Brown, J. M. in *Methods in enzymology* **435,** 295–321 (2007).

21. Solaini, G., Baracca, A., Lenaz, G. & Sgarbi, G. Hypoxia and mitochondrial oxidative metabolism. *Biochim. Biophys. Acta - Bioenerg.* **1797,** 1171–1177 (2010).

22. Liu, L. *et al.* Hypoxia-induced energy stress regulates mRNA translation and cell growth. *Mol. Cell* **21,** 521–31 (2006).

23. Le, A. *et al.* Inhibition of lactate dehydrogenase A induces oxidative stress and inhibits tumor progression. *Proc. Natl. Acad. Sci. U. S. A.* **107,** 2037–2042 (2010).

24. Stine, Z. E., Walton, Z. E., Altman, B. J., Hsieh, A. L. & Dang, C. V. MYC, Metabolism, and Cancer. *Cancer Discov.* **5,** (2015).

25. Kondoh, H. *et al.* Glycolytic enzymes can modulate cellular life span. *Cancer Res.* **65,** 177–85 (2005).

26. Puzio-Kuter, A. M. The Role of p53 in Metabolic Regulation. *Genes Cancer* **2,** 385–91 (2011).

27. Schwartzenberg-Bar-Yoseph, F., Armoni, M. & Karnieli, E. The tumor suppressor p53 down-regulates glucose transporters GLUT1 and GLUT4 gene expression. *Cancer Res.* **64,** 2627–33 (2004).

28. Blum, R., Jacob-Hirsch, J., Amariglio, N., Rechavi, G. & Kloog, Y. Ras inhibition in glioblastoma down-regulates hypoxia-inducible factor-1alpha, causing glycolysis shutdown and cell death. *Cancer Res.* **65,** 999–1006 (2005).

29. Zhu, Y. *et al.* Cardiac PI3K-Akt impairs insulin-stimulated glucose uptake independent of mTORC1 and GLUT4 translocation. *Mol. Endocrinol.* **27,** 172–84 (2013).

30. Yu, Z. *et al.* Proviral insertion in murine lymphomas 2 (PIM2) oncogene phosphorylates pyruvate kinase M2 (PKM2) and promotes glycolysis in cancer cells. *J. Biol. Chem.* **288,** 35406–16 (2013).

31. Bensinger, S. J. & Christofk, H. R. New aspects of the Warburg effect in cancer cell biology. *Semin. Cell Dev. Biol.* **23,** 352–361 (2012).

32. Chen, Z., Zhang, H., Lu, W. & Huang, P. Role of mitochondria-associated hexokinase II in cancer cell death induced by 3-bromopyruvate. *Biochim. Biophys. Acta* **1787,** 553–60 (2009).

33. Rutter, J., Winge, D. R. & Schiffman, J. D. Succinate dehydrogenase - Assembly, regulation and role in human disease. *Mitochondrion* **10,** 393–401 (2010).

34. Xu, X. *et al.* Tumor suppressor NDRG2 inhibits glycolysis and glutaminolysis in colorectal cancer cells by repressing c-Myc expression. *Oncotarget* **6,** 26161–76 (2015).

35. Garten, A., Petzold, S., Körner, A., Imai, S.-I. & Kiess, W. Nampt: linking NAD biology, metabolism and cancer. *Trends Endocrinol. Metab.* **20,** 130–8 (2009).

36. Imai, S., Kitano, H., Basu, R. & et al. The NAD World 2.0: the importance of the inter-tissue communication mediated by NAMPT/NAD+/SIRT1 in mammalian aging and longevity control. *npj Syst. Biol. Appl.* **2,** 16018 (2016).

37. Bajrami, I. *et al.* Synthetic lethality of PARP and NAMPT inhibition in triple-negative breast cancer cells. *EMBO Mol. Med.* **4,** 1087–1096 (2012).

38. Garten, A. *et al.* Physiological and pathophysiological roles of NAMPT and NAD metabolism. *Nat. Rev. Endocrinol.* **11,** 535–46 (2015).

39. Ratajczak, J. *et al.* NRK1 controls nicotinamide mononucleotide and nicotinamide riboside metabolism in mammalian cells. *Nat. Commun.* **7,** 13103 (2016).

40. Sahar, S. & Sassone-Corsi, P. Metabolism and cancer: the circadian clock connection. *Nat. Rev. Cancer* **9,** 886–896 (2009).

41. Wang, B. *et al.* NAMPT overexpression in prostate cancer and its contribution to tumor cell survival and stress response. *Oncogene* **30,** 907–921 (2011).

42. PREISS, J. & HANDLER, P. Enzymatic synthesis of nicotinamide mononucleotide. *J. Biol. Chem.* **225,** 759–70 (1957).

43. Imai, S. Nicotinamide Phosphoribosyltransferase (Nampt): A Link Between NAD Biology, Metabolism, and Diseases. *Curr. Pharm. Des.* **15,** 20–28 (2009).

44. Körner, A. *et al.* Molecular characteristics of serum visfatin and differential detection by immunoassays. *J. Clin. Endocrinol. Metab.* **92,** 4783–91 (2007).

45. Revollo, J. R. *et al.* Nampt/PBEF/Visfatin regulates insulin secretion in beta cells as a systemic NAD biosynthetic enzyme. *Cell Metab.* **6,** 363–75 (2007).

46. Shackelford, R. E., Mayhall, K., Maxwell, N. M., Kandil, E. & Coppola, D. Nicotinamide Phosphoribosyltransferase in Malignancy: A Review. *Genes Cancer* **4,** 447–456 (2013).

47. Van Beijnum, J. R. *et al.* Target validation for genomics using peptide-specific phage antibodies: a study of five gene products overexpressed in colorectal cancer. *Int. J. cancer* **101,** 118–27 (2002).

48. Bi, T.-Q. *et al.* Overexpression of Nampt in gastric cancer and chemopotentiating effects of the Nampt inhibitor FK866 in combination with fluorouracil. *Oncol. Rep.* **26,** 1251–7 (2011).

49. Olesen, U. H., Hastrup, N. & Sehested, M. Expression patterns of nicotinamide phosphoribosyltransferase and nicotinic acid phosphoribosyltransferase in human malignant lymphomas. *APMIS* **119,** 296–303 (2011).

50. Tian, W. *et al.* Visfatin, a potential biomarker and prognostic factor for endometrial cancer. *Gynecol. Oncol.* **129,** 505–12 (2013).

51. Folgueira, M. A. A. K. *et al.* Gene expression profile associated with response to doxorubicin-based therapy in breast cancer. *Clin. Cancer Res.* **11,** 7434–43 (2005).

52. Li, Y. *et al.* Extracellular Nampt promotes macrophage survival via a nonenzymatic interleukin-6/STAT3 signaling mechanism. *J. Biol. Chem.* **283,** 34833–43 (2008).

53. Pillai, V. B. *et al.* Nampt secreted from cardiomyocytes promotes development of cardiac hypertrophy and adverse ventricular remodeling. *Am. J. Physiol. Heart Circ. Physiol.* **304,** H415–26 (2013).

54. Ninomiya, S. *et al.* Possible role of visfatin in hepatoma progression and the effects of branched-chain amino acids on visfatin-induced proliferation in human hepatoma cells. *Cancer Prev. Res. (Phila).* **4,** 2092–100 (2011).

55. Preyat, N. & Leo, O. Complex role of nicotinamide adenine dinucleotide in the regulation of programmed cell death pathways. *Biochem. Pharmacol.* **101,** 13–26 (2016).

56. Ramsey, K. M. *et al.* Circadian clock feedback cycle through NAMPT-mediated NAD+ biosynthesis. *Science* **324,** 651–4 (2009).

57. Satoh, A., Stein, L. & Imai, S. The role of mammalian sirtuins in the regulation of metabolism, aging, and longevity. *Handb. Exp. Pharmacol.* **206,** 125–62 (2011).

58. Hau, C. S. *et al.* Visfatin Enhances the Production of Cathelicidin Antimicrobial Peptide, Human β-Defensin-2, Human β-Defensin-3, and S100A7 in Human Keratinocytes and Their Orthologs in Murine Imiquimod-Induced Psoriatic Skin. *Am. J. Pathol.* **182,** 1705–1717 (2013).

59. Wu, W. *et al.* Expression of tryptophan 2,3-dioxygenase and production of kynurenine pathway metabolites in triple transgenic mice and human Alzheimer's disease brain. *PLoS One* **8,** e59749 (2013).

60. Zhai, L. *et al.* Molecular Pathways: Targeting IDO1 and Other Tryptophan Dioxygenases for Cancer Immunotherapy. *Clin. Cancer Res.* **21,** 5427–5433

(2015).

61. O'Farrell, K. & Harkin, A. Stress-related regulation of the kynurenine pathway: Relevance to neuropsychiatric and degenerative disorders. *Neuropharmacology* (2015). doi:10.1016/j.neuropharm.2015.12.004

62. Metz, R. *et al.* IDO inhibits a tryptophan sufficiency signal that stimulates mTOR: A novel IDO effector pathway targeted by D-1-methyl-tryptophan. *Oncoimmunology* **1,** 1460–1468 (2012).

63. Liu, K.-T. *et al.* Neutrophils are Essential in Short Hairpin RNA of Indoleamine 2,3-Dioxygenase Mediated-antitumor Efficiency. *Mol. Ther. Nucleic Acids* **5,** e397 (2016).

64. Munn, D. H. *et al.* Inhibition of T cell proliferation by macrophage tryptophan catabolism. *J. Exp. Med.* **189,** 1363–72 (1999).

65. Munn, D. H. *et al.* GCN2 kinase in T cells mediates proliferative arrest and anergy induction in response to indoleamine 2,3-dioxygenase. *Immunity* **22,** 633–42 (2005).

66. Fallarino, F. *et al.* T cell apoptosis by tryptophan catabolism. *Cell Death Differ.* **9,** 1069–77 (2002).

67. Foster, A. C. & Schwarcz, R. Characterization of quinolinic acid phosphoribosyltransferase in human blood and observations in Huntington's disease. *J. Neurochem.* **45,** 199–205 (1985).

68. Sahm, F. *et al.* The endogenous tryptophan metabolite and NAD+ precursor quinolinic acid confers resistance of gliomas to oxidative stress. *Cancer Res.* **73,** 3225–34 (2013).

69. Olesen, U. H. *et al.* Target enzyme mutations are the molecular basis for resistance towards pharmacological inhibition of nicotinamide phosphoribosyltransferase. *BMC Cancer* **10,** 677 (2010).

70. Kim, M.-K. *et al.* Crystal structure of visfatin/pre-B cell colony-enhancing factor 1/nicotinamide phosphoribosyltransferase, free and in complex with the anti-cancer agent FK-866. *J. Mol. Biol.* **362,** 66–77 (2006).

71. Zucal, C. *et al.* EIF2A-dependent translational arrest protects leukemia cells from the energetic stress induced by NAMPT inhibition. *BMC Cancer* **15,** 855 (2015).

72. Hasmann, M. & Schemainda, I. FK866, a highly specific noncompetitive inhibitor of nicotinamide phosphoribosyltransferase, represents a novel mechanism for induction of tumor cell apoptosis. *Cancer Res.* **63,** 7436–42 (2003).

73. Holen, K., Saltz, L. B., Hollywood, E., Burk, K. & Hanauske, A.-R. The pharmacokinetics, toxicities, and biologic effects of FK866, a nicotinamide adenine dinucleotide biosynthesis inhibitor. *Invest. New Drugs* **26,** 45–51 (2008).

74. Nahimana, A. *et al.* The NAD biosynthesis inhibitor APO866 has potent antitumor

activity against hematologic malignancies. *Blood* **113,** 3276–86 (2009).

75. Nencioni, A. *et al.* Nicotinamide phosphoribosyltransferase inhibition reduces intraplaque CXCL1 production and associated neutrophil infiltration in atherosclerotic mice. *Thromb. Haemost.* **111,** 308–322 (2013).

76. Schuster, S. *et al.* FK866-induced NAMPT inhibition activates AMPK and downregulates mTOR signaling in hepatocarcinoma cells. *Biochem. Biophys. Res. Commun.* **458,** 334–40 (2015).

77. Chakrabarti, G., Boothman, D. & Gerber, D. Expanding antitumor therapeutic windows by targeting cancer-specific nicotinamide adenine dinucleotide phosphate-biogenesis pathways. *Clin. Pharmacol. Adv. Appl.* **Volume 7,** 57 (2015).

78. Vig Hjarnaa, P.-J. *et al.* CHS 828, a Novel Pyridyl Cyanoguanidine with Potent Antitumor Activity in Vitro and in Vivo. *Cancer Res.* **59,** (1999).

79. Ravaud, A. *et al.* Phase I study and pharmacokinetic of CHS-828, a guanidino-containing compound, administered orally as a single dose every 3 weeks in solid tumours: an ECSG/EORTC study. *Eur. J. Cancer* **41,** 702–7 (2005).

80. Ye, J. *et al.* The GCN2-ATF4 pathway is critical for tumour cell survival and proliferation in response to nutrient deprivation. *EMBO J.* **29,** 2082–96 (2010).

81. Nguyen, H. A., Su, Y. & Lavie, A. Design and Characterization of Erwinia Chrysanthemi l-Asparaginase Variants with Diminished l-Glutaminase Activity. *J. Biol. Chem.* **291,** 17664–76 (2016).

82. Hasawi, N. Al, Alkandari, M. F. & Luqmani, Y. A. Phosphofructokinase: A mediator of glycolytic flux in cancer progression. *Crit. Rev. Oncol. Hematol.* **92,** 312–321 (2014).

83. Altman, B. J., Stine, Z. E. & Dang, C. V. From Krebs to clinic: glutamine metabolism to cancer therapy. *Nat. Rev. Cancer* (2016). doi:10.1038/nrc.2016.71

84. Nicklin, P. *et al.* Bidirectional transport of amino acids regulates mTOR and autophagy. *Cell* **136,** 521–34 (2009).

85. Lorin, S. *et al.* Glutamate dehydrogenase contributes to leucine sensing in the regulation of autophagy. *Autophagy* **9,** 850–60 (2013).

86. Jiang, H.-Y. *et al.* Activating Transcription Factor 3 Is Integral to the Eukaryotic Initiation Factor 2 Kinase Stress Response. *Mol. Cell. Biol.* **24,** 1365–1377 (2004).

87. Balasubramanian, M. N., Butterworth, E. a & Kilberg, M. S. Asparagine synthetase: regulation by cell stress and involvement in tumor biology. *Am. J. Physiol. Endocrinol. Metab.* **304,** E789–99 (2013).

88. Liu, H. *et al.* GCN2-Dependent Metabolic Stress Is Essential for Endotoxemic Cytokine Induction and Pathology. *Mol. Cell. Biol.* **34,** 428–438 (2014).

89. Cedar, H. & Schwartz, J. H. Production of L-Asparaginase II by Escherichia coli. *J. Bacteriol.* **96,** 2043–2048 (1968).

90. Asselin, B. & Rizzari, C. Asparaginase pharmacokinetics and implications of therapeutic drug monitoring. *Leuk. Lymphoma* **56,** 2273–80 (2015).

91. Chien, W.-W. *et al.* Differential mechanisms of asparaginase resistance in B-type acute lymphoblastic leukemia and malignant natural killer cell lines. *Sci. Rep.* **5,** 8068 (2015).

92. Fujiwara, T. & Ozaki, T. Overcoming Therapeutic Resistance of Bone Sarcomas: Overview of the Molecular Mechanisms and Therapeutic Targets for Bone Sarcoma Stem Cells. *Stem Cells Int.* **2016,** 1–13 (2016).

93. Wang, H. *et al.* Multiple mechanisms underlying acquired resistance to taxanes in selected docetaxel-resistant MCF-7 breast cancer cells. *BMC Cancer* **14,** 37 (2014).

94. Lal, S. *et al.* Pharmacogenetics of Target Genes Across Doxorubicin Disposition Pathway: A Review. *Curr. Drug Metab.* **11,** 115–128 (2010).

95. Guo, A. *et al.* Dual SYK/JAK inhibition overcomes ibrutinib resistance in chronic lymphocytic leukemia: Cerdulatinib, but not ibrutinib, induces apoptosis of tumor cells protected by the microenvironment. *Oncotarget* (2015). doi:10.18632/oncotarget.14588

96. Milojkovic, D. & Apperley, J. F. Mechanisms of resistance to imatinib and second-generation tyrosine inhibitors in chronic myeloid leukemia. *Clin. Cancer Res.* **15,** 7519–7527 (2009).

97. Jang, J. E. *et al.* Targeting AMPK-ULK1-mediated autophagy for combating BET inhibitor resistance in acute myeloid leukemia stem cells. *Autophagy* 00–00 (2017). doi:10.1080/15548627.2016.1278328

98. Jiang, J. *et al.* Ganetespib overcomes resistance to PARP inhibitors in breast cancer by targeting core proteins in the DNA repair machinery. *Invest. New Drugs* (2017). doi:10.1007/s10637-016-0424-x

99. Pogorzala, M., Kubicka, M., Rafinska, B., Wysocki, M. & Styczynski, J. Drug-resistance Profile in Multiple-relapsed Childhood Acute Lymphoblastic Leukemia. *Anticancer Res.* **35,** 5667–70 (2015).

100. Serravalle, S., Bertuccio, S. N., Astolfi, A., Melchionda, F. & Pession, A. Synergistic Cytotoxic Effect of L-Asparaginase Combined with Decitabine as a Demethylating Agent in Pediatric T-ALL, with Specific Epigenetic Signature. *Biomed Res. Int.* **2016,** 1–6 (2016).

101. Gujar, A. D. *et al.* An NAD^+-dependent transcriptional program governs self-renewal and radiation resistance in glioblastoma. *Proc. Natl. Acad. Sci.* **113,** E8247–E8256 (2016).

102. Zhang, Y. *et al.* Prognostic Role of Lactate Dehydrogenase Expression in Urologic

Cancers: A Systematic Review and Meta-Analysis. *Oncol. Res. Treat.* **39,** 592–604 (2016).

103. Wang, Z. Y. *et al.* LDH-A silencing suppresses breast cancer tumorigenicity through induction of oxidative stress mediated mitochondrial pathway apoptosis. *Breast Cancer Res. Treat.* **131,** 791–800 (2012).

104. Zhou, M. *et al.* Warburg effect in chemosensitivity: targeting lactate dehydrogenase-A re-sensitizes taxol-resistant cancer cells to taxol. *Mol. Cancer* **9,** 33 (2010).

105. DAWSON, D. M., GOODFRIEND, T. L., KAPLAN, N. O. & Kaplan, N. O. Lactic dehydrogenases: functions of the two types rates of synthesis of the two major forms can be correlated with metabolic differentiation. *Science* **143,** 929–33 (1964).

106. Fantin, V. R., St-Pierre, J. & Leder, P. Attenuation of LDH-A expression uncovers a link between glycolysis, mitochondrial physiology, and tumor maintenance. *Cancer Cell* **9,** 425–34 (2006).

107. Rani, R. & Kumar, V. Recent Update on Human Lactate Dehydrogenase Enzyme 5 (h LDH5) Inhibitors: A Promising Approach for Cancer Chemotherapy. **5,** (2016).

108. Cui, J. *et al.* FOXM1 promotes the warburg effect and pancreatic cancer progression via transactivation of LDHA expression. *Clin. Cancer Res.* **20,** 2595–606 (2014).

109. Neri, D. & Supuran, C. T. Interfering with pH regulation in tumours as a therapeutic strategy. *Nat. Rev. Drug Discov.* **10,** 767–77 (2011).

110. Billiard, J. *et al.* Quinoline 3-sulfonamides inhibit lactate dehydrogenase A and reverse aerobic glycolysis in cancer cells. *Cancer Metab.* **1,** 19 (2013).

111. Xie, H. *et al.* Targeting lactate dehydrogenase--a inhibits tumorigenesis and tumor progression in mouse models of lung cancer and impacts tumor-initiating cells. *Cell Metab.* **19,** 795–809 (2014).

112. HAN, R. L., WANG, F. P., ZHANG, P. A., ZHOU, X. Y. & LI, Y. miR-383 inhibits ovarian cancer cell proliferation, invasion and aerobic glycolysis by targeting LDHA. *Neoplasma* **64,** (2016).

113. Wang, J. *et al.* Lactate dehydrogenase A negatively regulated by miRNAs promotes aerobic glycolysis and is increased in colorectal cancer. *Oncotarget* **6,** 19456–19468 (2015).

114. Smeitink, J., Heuvel, L. Van Den & Dimauro, S. the Genetics and Pathology of Oxidative Phosphorylation. **2,** 342–352 (2001).

115. Kim, J., Gao, P., Liu, Y.-C., Semenza, G. L. & Dang, C. V. Hypoxia-inducible factor 1 and dysregulated c-Myc cooperatively induce vascular endothelial growth factor and metabolic switches hexokinase 2 and pyruvate dehydrogenase kinase 1. *Mol.*

Cell. Biol. **27,** 7381–93 (2007).

116. Gottlob, K. *et al.* Inhibition of early apoptotic events by Akt/PKB is dependent on the first committed step of glycolysis and mitochondrial hexokinase. *Genes Dev.* **15,** 1406–18 (2001).

117. Mendoza, E. E. *et al.* Control of Glycolytic Flux by AMP-Activated Protein Kinase in Tumor Cells Adapted to Low pH. *Transl. Oncol.* **5,** 208–16 (2012).

118. Sola-Penna, M., Da Silva, D., Coelho, W. S., Marinho-Carvalho, M. M. & Zancan, P. Regulation of mammalian muscle type 6-phosphofructo-1-kinase and its implication for the control of the metabolism. *IUBMB Life* **62,** 791–796 (2010).

119. Chung-Faye, G. *et al.* Fecal M2-pyruvate kinase (M2-PK): a novel marker of intestinal inflammation. *Inflamm. Bowel Dis.* **13,** 1374–8 (2007).

120. Luo, W. *et al.* Pyruvate kinase M2 is a PHD3-stimulated coactivator for hypoxia-inducible factor 1. *Cell* **145,** 732–44 (2011).

121. Vermeersch, K. A. & Styczynski, M. P. Applications of metabolomics in cancer research. *J. Carcinog.* **12,** 9 (2013).

122. Cheong, H., Lu, C., Lindsten, T. & Thompson, C. B. Therapeutic targets in cancer cell metabolism and autophagy. *Nat. Biotechnol.* **30,** 671–678 (2012).

123. Larue, L. & Bellacosa, A. Epithelial-mesenchymal transition in development and cancer: role of phosphatidylinositol 3' kinase/AKT pathways. *Oncogene* **24,** 7443–54 (2005).

124. Vignot, S., Faivre, S., Aguirre, D. & Raymond, E. mTOR-targeted therapy of cancer with rapamycin derivatives. *Ann. Oncol.* **16,** 525–37 (2005).

125. Tchevkina, E. & Komelkov, A. in *Protein Phosphorylation in Human Health* (InTech, 2012). doi:10.5772/48274

126. Avruch, J. *et al.* Protein kinases of the Hippo pathway: Regulation and substrates. *Semin. Cell Dev. Biol.* **23,** 770–784 (2012).

127. Fang, J. Y. & Richardson, B. C. The MAPK signalling pathways and colorectal cancer. *Lancet. Oncol.* **6,** 322–7 (2005).

128. Basu, A. & Haldar, S. The relationship between Bcl2, Bax and p53: consequences for cell cycle progression and cell death. *Mol. Hum. Reprod.* **4,** 1099–1109 (1998).

129. Mendoza, M. C., Er, E. E. & Blenis, J. The Ras-ERK and PI3K-mTOR pathways: cross-talk and compensation. *Trends Biochem. Sci.* **36,** 320–8 (2011).

130. Slomovitz, B. M. & Coleman, R. L. The PI3K/AKT/mTOR Pathway as a Therapeutic Target in Endometrial Cancer. *Clin. Cancer Res.* **18,** (2012).

131. Carracedo, A. & Pandolfi, P. P. The PTEN–PI3K pathway: of feedbacks and

cross-talks. *Oncogene* **27,** 5527–5541 (2008).

132. Gwinn, D. M. *et al.* AMPK phosphorylation of raptor mediates a metabolic checkpoint. *Mol. Cell* **30,** 214–26 (2008).

133. Zadra, G. *et al.* A novel direct activator of AMPK inhibits prostate cancer growth by blocking lipogenesis. *EMBO Mol. Med.* **6,** 519–38 (2014).

134. Kishton, R. J. *et al.* AMPK Is Essential to Balance Glycolysis and Mitochondrial Metabolism to Control T-ALL Cell Stress and Survival. *Cell Metab.* **23,** 649–662 (2016).

135. Nguyen, H. B., Babcock, J. T., Wells, C. D. & Quilliam, L. A. LKB1 tumor suppressor regulates AMP kinase/mTOR-independent cell growth and proliferation via the phosphorylation of Yap. *Oncogene* **32,** 4100–9 (2013).

136. Shackelford, D. B. Unravelling the connection between metabolism and tumorigenesis through studies of the liver kinase B1 tumour suppressor. *J. Carcinog.* **12,** 16 (2013).

137. Ros, S. & Schulze, A. Balancing glycolytic flux: the role of 6-phosphofructo-2-kinase/fructose 2,6-bisphosphatases in cancer metabolism. *Cancer Metab.* **1,** 8 (2013).

138. Hinnebusch, A. G. Translational Homeostasis via eIF4E and 4E-BP1. *Mol. Cell* **46,** 717–719 (2012).

139. Hsieh, A. C. & Ruggero, D. Targeting eukaryotic translation initiation factor 4E (eIF4E) in cancer. *Clin. Cancer Res.* **16,** 4914–4920 (2010).

140. Gingras, A. C. *et al.* Hierarchical phosphorylation of the translation inhibitor 4E-BP1. *Genes Dev.* **15,** 2852–64 (2001).

141. Inagi, R., Ishimoto, Y. & Nangaku, M. Proteostasis in endoplasmic reticulum--new mechanisms in kidney disease. *Nat. Rev. Nephrol.* **10,** 369–78 (2014).

142. Tsai, Y. C. & Weissman, A. M. The Unfolded Protein Response, Degradation from Endoplasmic Reticulum and Cancer. *Genes Cancer* **1,** 764–778 (2010).

143. Ron, D. & Walter, P. Signal integration in the endoplasmic reticulum unfolded protein response. *Nat Rev Mol Cell Biol* **8,** 519–529 (2007).

144. Rosilio, C. *et al.* L-type amino-acid transporter 1 (LAT1): a therapeutic target supporting growth and survival of T-cell lymphoblastic lymphoma/T-cell acute lymphoblastic leukemia. *Leukemia* (2014). doi:10.1038/leu.2014.338

145. Chou, T.-C. Drug combination studies and their synergy quantification using the Chou-Talalay method. *Cancer Res.* **70,** 440–6 (2010).

146. Zamporlini, F. *et al.* Novel assay for simultaneous measurement of pyridine mononucleotides synthesizing activities allows dissection of the NAD + biosynthetic machinery in mammalian cells. **281,** 5104–5119 (2014).

147. Marini, C. *et al.* Discovery of a novel glucose metabolism in cancer: The role of endoplasmic reticulum beyond glycolysis and pentose phosphate shunt. *Sci. Rep.* **6,** 25092 (2016).

148. Moschoi, R. *et al.* Protective mitochondrial transfer from bone marrow stromal cells to acute myeloid leukemic cells during chemotherapy. *Blood* **128,** 253–64 (2016).

149. Zucal, C. Molecular effects of the NAMPT inhibitor FK866 on leukemia cells. (University of Trento, 2016).

150. Wang, W. *et al.* Structural basis for resistance to diverse classes of NAMPT inhibitors. *PLoS One* **9,** e109366 (2014).

151. Bender, D. A. & Olufunwa, R. Utilization of tryptophan, nicotinamide and nicotinic acid as precursors for nicotinamide nucleotide synthesis in isolated rat liver cells. *Br. J. Nutr.* **59,** 279–87 (1988).

152. Moffett, J. R. & Namboodiri, M. A. Tryptophan and the immune response. *Immunol. Cell Biol.* **81,** 247–265 (2003).

153. Saraswathy, M. & Gong, S. Different strategies to overcome multidrug resistance in cancer. *Biotechnol. Adv.* **31,** 1397–1407 (2013).

154. Napolitano, L. *et al.* LAT1 is the transport competent unit of the LAT1/CD98 heterodimeric amino acid transporter. *Int. J. Biochem. Cell Biol.* **67,** 25–33 (2015).

155. Bhutia, Y. D., Babu, E., Prasad, P. D. & Ganapathy, V. The amino acid transporter SLC6A14 in cancer and its potential use in chemotherapy. *Asian J. Pharm. Sci.* **9,** 293–303 (2014).

156. Richard, D. M. *et al.* L-Tryptophan: Basic Metabolic Functions, Behavioral Research and Therapeutic Indications. *Int. J. Tryptophan Res.* **2,** 45–60 (2009).

157. Olesen, U. H. *et al.* Anticancer agent CHS-828 inhibits cellular synthesis of NAD. *Biochem. Biophys. Res. Commun.* **367,** 799–804 (2008).

158. Willems, L. *et al.* Inhibiting glutamine uptake represents an attractive new strategy for treating acute myeloid leukemia. *Blood* **122,** 3521–32 (2013).

159. Samudio, I. & Konopleva, M. Asparaginase unveils glutamine-addicted AML. *Blood* **122,** 3398–400 (2013).

160. Chan, W. K. *et al.* The Glutaminase Activity Of L-Asparaginase Is Not Required For Anticancer Activity Against Asns-Negative Cell Lines. *Blood* **122,** 1 (2013).

161. Del Nagro, C., Xiao, Y., Rangell, L., Reichelt, M. & O'Brien, T. Depletion of the central metabolite NAD leads to oncosis-mediated cell death. *J. Biol. Chem.* **289,** 35182–92 (2014).

162. Ippolito, L. *et al.* Metabolic shift toward oxidative phosphorylation in docetaxel resistant prostate cancer cells. *Oncotarget* (2016). doi:10.18632/oncotarget.11301

163. Galluzzi, L., Kepp, O., Vander Heiden, M. G. & Kroemer, G. Metabolic targets for cancer therapy. *Nat. Publ. Gr.* **12,** (2013).

164. Drevs, J., Löser, R., Rattel, B. & Esser, N. Antiangiogenic potency of FK866/K22.175, a new inhibitor of intracellular NAD biosynthesis, in murine renal cell carcinoma. *Anticancer Res.* **23,** 4853–8 (2003).

165. Travelli, C. *et al.* Reciprocal potentiation of the antitumoral activities of FK866, an inhibitor of nicotinamide phosphoribosyltransferase, and etoposide or cisplatin in neuroblastoma cells. *J. Pharmacol. Exp. Ther.* **338,** 829–40 (2011).

166. Bowlby, S. C., Thomas, M. J., D'Agostino, R. B. & Kridel, S. J. Nicotinamide phosphoribosyl transferase (Nampt) is required for de novo lipogenesis in tumor cells. *PLoS One* **7,** (2012).

167. Ramirez, M. *et al.* Diverse drug-resistance mechanisms can emerge from drug-tolerant cancer persister cells. *Nat. Commun.* 1–8 (2016). doi:10.1038/ncomms10690

168. Kishton, R. J. *et al.* AMPK Is Essential to Balance Glycolysis and Mitochondrial Metabolism to Control T-ALL Cell Stress and Survival. *Cell Metab.* **23,** 649–62 (2016).

169. Ramanathan, A. & Schreiber, S. L. Direct control of mitochondrial function by mTOR. *Proc. Natl. Acad. Sci. U. S. A.* **106,** 22229–32 (2009).

170. Saha, A. K. *et al.* Downregulation of AMPK Accompanies Leucine- and Glucose-Induced Increases in Protein Synthesis and Insulin Resistance in Rat Skeletal Muscle. *Diabetes* **59,** (2010).

171. Li, L., Fath, M. A., Scarbrough, P. M., Watson, W. H. & Spitz, D. R. Combined inhibition of glycolysis, the pentose cycle, and thioredoxin metabolism selectively increases cytotoxicity and oxidative stress in human breast and prostate cancer. *Redox Biol.* **4,** 127–135 (2015).

172. Lu, C.-L. *et al.* Tumor Cells Switch to Mitochondrial Oxidative Phosphorylation under Radiation via mTOR-Mediated Hexokinase II Inhibition - A Warburg-Reversing Effect. (2015). doi:10.1371/journal.pone.0121046

173. Wu, H., Ying, M. & Hu, X. Lactic acidosis switches cancer cells from aerobic glycolysis back to dominant oxidative phosphorylation. **7,** 36–38 (2016).

174. Oyarzún, A. P. *et al.* FK866 compromises mitochondrial metabolism and adaptive stress responses in cultured cardiomyocytes. *Biochem. Pharmacol.* **98,** 92–101 (2015).

175. Hulleman, E. *et al.* Inhibition of glycolysis modulates prednisolone resistance in acute lymphoblastic leukemia cells. *Blood* **113,** 2014–2021 (2009).

176. Boag, J. M. *et al.* Altered glucose metabolism in childhood pre-B acute lymphoblastic leukaemia. *Leukemia* **20,** 1731–7 (2006).

177. Oda, K. *et al.* L-type amino acid transporter 1 inhibitors inhibit tumor cell growth. *Cancer Sci.* **101,** 173–9 (2010).

178. Wempe, M. F. *et al.* Metabolism and Pharmacokinetic Studies of JPH203, an L-Amino Acid Transporter 1 (LAT1) Selective Compound. *Drug Metab. Pharmacokinet.* **27,** 155–161 (2012).

179. Yun, D.-W. *et al.* JPH203, an L-type amino acid transporter 1-selective compound, induces apoptosis of YD-38 human oral cancer cells. *J. Pharmacol. Sci.* **124,** 208–17 (2014).

180. Aragonès, G. *et al.* Dietary proanthocyanidins boost hepatic NAD(+) metabolism and SIRT1 expression and activity in a dose-dependent manner in healthy rats. *Sci. Rep.* **6,** 24977 (2016).

181. Tao, R. *et al.* Hepatic FoxOs regulate lipid metabolism via modulation of expression of the nicotinamide phosphoribosyltransferase gene. *J. Biol. Chem.* **286,** 14681–90 (2011).

182. Maleki Vareki, S. *et al.* IDO Downregulation Induces Sensitivity to Pemetrexed, Gemcitabine, FK866, and Methoxyamine in Human Cancer Cells. *PLoS One* **10,** e0143435 (2015).

183. Pisco, A. O., Jackson, D. A. & Huang, S. Reduced Intracellular Drug Accumulation in Drug-Resistant Leukemia Cells is Not Only Solely Due to MDR-Mediated Efflux but also to Decreased Uptake. *Front. Oncol.* **4,** 1–9 (2014).

184. Malayeri, R. *et al.* Multidrug resistance in leukemias and its reversal. *Leuk. Lymphoma* **23,** 451–8 (1996).

185. Averous, J. *et al.* Induction of CHOP expression by amino acid limitation requires both ATF4 expression and ATF2 phosphorylation. *J. Biol. Chem.* **279,** 5288–97 (2004).

186. Chung, K.-T. & Gadupudi, G. S. Possible roles of excess tryptophan metabolites in cancer. *Environ. Mol. Mutagen.* **52,** 81–104 (2011).

187. Yoshida, O., Brown, R. R. & Bryan, G. T. Relationship between tryptophan metabolism and heterotopic recurrences of human urinary bladder tumors. *Cancer* **25,** 773–80 (1970).

188. Sociali, G. *et al.* Antitumor effect of combined NAMPT and CD73 inhibition in an ovarian cancer model. *Oncotarget* **7,** 2968–84 (2016).

189. Iams, W. T., Sosman, J. A. & Chandra, S. Novel Targeted Therapies for Metastatic Melanoma. *Cancer J.* **23,** 54–58 (2017).

190. Peng, Z. *et al.* Costunolide and dehydrocostuslactone combination treatment

inhibit breast cancer by inducing cell cycle arrest and apoptosis through c-Myc/p53 and AKT/14-3-3 pathway. *Sci. Rep.* **7,** 41254 (2017).

191. Sulthana, S. *et al.* Combination Therapy of NSCLC Using Hsp90 Inhibitor and Doxorubicin Carrying Functional Nanoceria. *Mol. Pharm.* acs.molpharmaceut.6b01076 (2017). doi:10.1021/acs.molpharmaceut.6b01076

192. Bertaina, A. *et al.* The combination of bortezomib with chemotherapy to treat relapsed/refractory acute lymphoblastic leukaemia of childhood. *Br. J. Haematol.* (2017). doi:10.1111/bjh.14505

193. Chan, M. *et al.* Synergy between the NAMPT inhibitor GMX1777(8) and pemetrexed in non-small cell lung cancer cells is mediated by PARP activation and enhanced NAD consumption. *Cancer Res.* **74,** 5948–5954 (2014).

194. Lea, M. A., Guzman, Y. & Desbordes, C. Inhibition of Growth by Combined Treatment with Inhibitors of Lactate Dehydrogenase and either Phenformin or Inhibitors of 6-Phosphofructo-2-kinase/Fructose-2,6-bisphosphatase 3. *Anticancer Res.* **36,** 1479–88 (2016).

195. Hermes, A., Gatzemeier, U., Waschki, B. & Reck, M. Lactate dehydrogenase as prognostic factor in limited and extensive disease stage small cell lung cancer – A retrospective single institution analysis. *Respir. Med.* **104,** 1937–1942 (2010).

196. Liu, X. *et al.* Effects of the suppression of lactate dehydrogenase A on the growth and invasion of human gastric cancer cells. *Oncol. Rep.* **33,** 157–162 (2015).

197. Wu, Y., Yang, Y., Wan, J., Zhu, R. & Wu, Y. Inhibition of LDH-A by oxamate induces G2/M arrest, apoptosis and increases radiosensitivity in nasopharyngeal carcinoma cells. *Oncol. Rep.* **30,** 2983–91 (2013).

198. Li, J. *et al.* Suppression of lactate dehydrogenase A compromises tumor progression by downregulation of the Warburg effect in glioblastoma. *Neuroreport* **27,** 110–5 (2016).

199. Ye, W. *et al.* Oxamate improves glycemic control and insulin sensitivity via inhibition of tissue lactate production in db/db mice. *PLoS One* **11,** 1–19 (2016).

200. Daniele, S. *et al.* Lactate dehydrogenase-A inhibition induces human glioblastoma multiforme stem cell differentiation and death. *Nat. Publ. Gr.* 1–17 (2015). doi:10.1038/srep15556

201. Thongon, N. *et al.* The GSK3b inhibitor BIS I reverts YAP-dependent EMT signature in PDAC cell lines by decreasing SMADs expression level. *Oncotarget* **7,** (2016).

202. Eser, S., Schnieke, A., Schneider, G. & Saur, D. Oncogenic KRAS signalling in pancreatic cancer. *Br. J. Cancer* **111,** 817–822 (2014).

203. Bardeesy, N. & DePinho, R. A. Pancreatic cancer biology and genetics. *Nat. Rev. Cancer* **2,** 897–909 (2002).

204. di Magliano, M. P. & Logsdon, C. D. Roles for KRAS in Pancreatic Tumor Development and Progression. *Gastroenterology* **144,** 1220–1229 (2013).

205. Piccolo, S., Dupont, S. & Cordenonsi, M. The biology of YAP/TAZ: hippo signaling and beyond. *Physiol. Rev.* **94,** 1287–312 (2014).

206. Ramos, A. & Camargo, F. D. The Hippo signaling pathway and stem cell biology. *Trends Cell Biol.* **22,** 339–346 (2012).

207. Fujii, M. *et al.* Convergent signaling in the regulation of connective tissue growth factor in malignant mesothelioma: TGFbeta signaling and defects in the Hippo signaling cascade. *Cell Cycle* **11,** 3373–3379 (2012).

208. Grannas, K. *et al.* Crosstalk between Hippo and TGFβ: Subcellular Localization of YAP/TAZ/Smad Complexes. *J. Mol. Biol.* **427,** 3407–15 (2015).

209. Rosenbluh, J., Nijhawan, D., Cox, A. G. & et al. β-Catenin-driven cancers require a YAP1 transcriptional complex for survival and tumorigenesis. *Cell* **151,** 1457–73 (2012).

210. Heallen, T. *et al.* Hippo Pathway Inhibits Wnt Signaling to Restrain Cardiomyocyte Proliferation and Heart Size. *Science (80-.).* **332,** 458–461 (2011).

211. Dornhöfer, N. *et al.* Connective tissue growth factor-specific monoclonal antibody therapy inhibits pancreatic tumor growth and metastasis. *Cancer Res.* **66,** 5816–27 (2006).

212. Zhao, B. *et al.* TEAD mediates YAP-dependent gene induction and growth control. *Genes Dev.* **22,** 1962–1971 (2008).

213. Sundqvist, A. *et al.* Specific interactions between Smad proteins and AP-1 components determine TGFβ-induced breast cancer cell invasion. *Oncogene* **32,** 3606–3615 (2013).

214. Shao, D. D. *et al.* KRAS and YAP1 Converge to Regulate EMT and Tumor Survival. *Cell* **158,** 171–184 (2014).

215. Kim, N.-G., Koh, E., Chen, X. & Gumbiner, B. M. E-cadherin mediates contact inhibition of proliferation through Hippo signaling-pathway components. *Proc. Natl. Acad. Sci.* **108,** 11930–11935 (2011).

216. Hers, I., Tavaré, J. M. & Denton, R. M. The protein kinase C inhibitors bisindolylmaleimide I (GF 109203x) and IX (Ro 31-8220) are potent inhibitors of glycogen synthase kinase-3 activity. *FEBS Lett.* **460,** 433–6 (1999).

APPENDIX

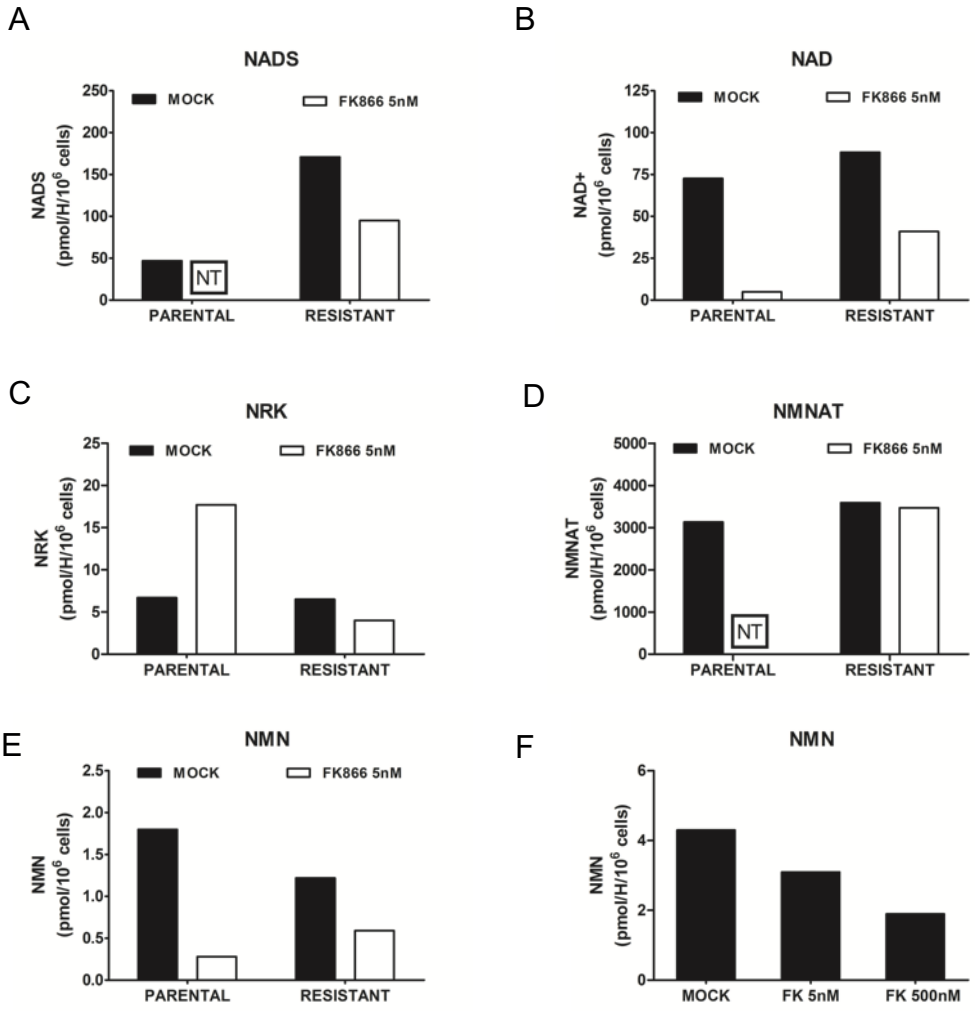

Supplementary Figure 1 Evaluation the activity of enzymes involved NAD biosynthesis pathway.

CEM PA and CEM RES cells were treated with FK866 for 48h, they were then subjected for enzymatic assay evaluating for (**A**) NADS, (**B**) NAD, (**C**) NRK, (**D**) NMNAT, and (**E**, **F**) NMN as described in [146].

Table 3 Sequences of primers

Name	Primer sequence 5' ⇒ 3'
NAMPT	NC_000007.14 (sigma)
LDHA	NM_001135239 (sigma)
HK2	NM_000189 (sigma)
ND1	FW ATGGCCAACCTCCTACTCCT RV TAGATGTGGCGGGTTTTAGG
ND2	FW CCGGACAATGAACCATAACC RV TCAGAAGTGAAAGGGGGCTA
ND3	FW CCCTCCTTTTACCCCTACCA RV GGCCAGACTTAGGGCTAGGA
ND5	FW ACCTGCCCCTACTCCTCCTA RV TATGCCTTTTTGGGTTGAGG
NDL4	FW TAACCCTCAACACCCACTCC RV GGCCATATGTGTTGGAGATTG
COX3	FW TCCACTCCATAACGCTCCTC RV GTGGCCTTGGTATGTGCTTT
ATP8	FW ATGGCCCACCATAATTACCC RV TTTTATGGGCTTTGGTGAGG
CHOP	FW AGAACCAGGAAACGGAAACAGA RV TCTCCTTCATGCGCTGCTTT
ATF4	FW GTTCTCCAGCGACAAGGCTA RV ATCCTGCTTGCTGTTGTTGG
ASNS1	FW GCACGCCCTCTATGACAATG RV TTCAACAGAGTGGCAGCAAC
KYNU	FW ATTCCTGCCATCACAAAAGC RV TTTCATGAATGAAGGCACCA
QPRT	FW1 CCCTCTGGGTCACACATCTT RV1 GTGCTCATTATCACCGCAGA

Zucal *et al. BMC Cancer* (2015) 15:855
DOI 10.1186/s12885-015-1845-1

BMC Cancer

RESEARCH ARTICLE Open Access

EIF2A-dependent translational arrest protects leukemia cells from the energetic stress induced by NAMPT inhibition

Chiara Zucal[1†], Vito G. D'Agostino[1†], Antonio Casini[2], Barbara Mantelli[1], Natthakan Thongon[1], Debora Soncini[4], Irene Caffa[3], Michele Cea[3], Alberto Ballestrero[3], Alessandro Quattrone[4], Stefano Indraccolo[5], Alessio Nencioni[3*] and Alessandro Provenzani[1*]

Abstract

Background: Nicotinamide phosphoribosyltransferase (NAMPT), the rate-limiting enzyme in NAD^+ biosynthesis from nicotinamide, is one of the major factors regulating cancer cells metabolism and is considered a promising target for treating cancer. The prototypical NAMPT inhibitor FK866 effectively lowers NAD^+ levels in cancer cells, reducing the activity of NAD^+-dependent enzymes, lowering intracellular ATP, and promoting cell death.

Results: We show that FK866 induces a translational arrest in leukemia cells through inhibition of MTOR/4EBP1 signaling and of the initiation factors EIF4E and EIF2A. Specifically, treatment with FK866 is shown to induce 5′AMP-activated protein kinase (AMPK) activation, which, together with EIF2A phosphorylation, is responsible for the inhibition of protein synthesis. Notably, such an effect was also observed in patients' derived primary leukemia cells including T-cell Acute Lymphoblastic Leukemia. Jurkat cells in which AMPK or LKB1 expression was silenced or in which a non-phosphorylatable EIF2A mutant was ectopically expressed showed enhanced sensitivity to the NAMPT inhibitor, confirming a key role for the LKB1-AMPK-EIF2A axis in cell fate determination in response to energetic stress *via* NAD^+ depletion.

Conclusions: We identified EIF2A phosphorylation as a novel early molecular event occurring in response to NAMPT inhibition and mediating protein synthesis arrest. In addition, our data suggest that tumors exhibiting an impaired LBK1- AMPK- EIF2A response may be especially susceptible to NAMPT inhibitors and thus become an elective indication for this type of agents.

Keywords: NAMPT, EIF2A, AMPK, Energetic stress, Translation arrest, UPR

Background

Aberrant activation of metabolic pathways has emerged as an hallmark of proliferating cancer cells and pharmaceutical approaches targeting cell metabolism hold potential for treating cancer [1]. Nicotinamide adenine dinucleotide (NAD^+) plays a key role in different biochemical processes, acting as a coenzyme in redox reactions or as a substrate for NAD^+ degrading enzymes, such as poly(ADP-ribose) polymerases (PARPs), cluster of differentiation 38 (CD38), and sirtuins. Intracellular NAD^+ is continuously replenished utilizing either tryptophan, nicotinamide, nicotinic acid or nicotinamide riboside as a substrate [2], and nicotinamide phosphoribosyltransferase, NAMPT, is the rate-limiting enzyme for NAD^+ biosynthesis from nicotinamide in mammalian cells [3]. High NAMPT levels, whose activity appears to be also important in the differentiation of myeloid cells [4], were shown to be required to support cancer cell growth, survival and epithelial-mesenchymal transition (EMT) transition [5, 6], and have been reported in different types of tumors [7, 8]. In line with these notions, several studies have highlighted a strong activity of NAMPT inhibitors in preclinical models of inflammatory and malignant disorders, including leukemia [2, 9–11]. FK866, a prototypical NAMPT inhibitor, was found to

* Correspondence: alessio.nencioni@unige.it; alessandro.provenzani@unitn.it
†Equal contributors
[3]Department of Internal Medicine, University of Genoa, Genoa, Italy
[1]Laboratory of Genomic Screening, CIBIO, University of Trento, Trento, Italy
Full list of author information is available at the end of the article

promote cell death in both lymphoid- and myeloid-derived hematological malignancies and its activity clearly resulted from intracellular NAD^+ depletion [12–14]. Notably, opposite to cancer cells, activated immune cells [10], along with many other types of healthy cells, such as hematopoietic stem cells [12], appear unaffected by NAMPT inhibitors, and consistently, agents such as FK866 or CHS-828 are well tolerated in patients [15, 16].

The molecular consequences upon NAMPT inhibition are only partially understood. The induced NAD^+ depletion clearly affects intracellular ATP levels resulting in mitochondrial dysfunction and activation of cell death pathways: reactive oxygen species generation and activation of the apoptotic cascade have both been involved in cell demise in response to NAMPT inhibitors [17]. ATP depletion has been related to the loss of plasma membrane homeostasis invariably leading to oncosis cell death [18]. Different groups have suggested a role for autophagic cell death in the cytotoxic activity of these drugs [10, 12, 13, 19]. In particular, Cea and colleagues proposed that FK866 would induce autophagy *via* activation of transcription factor EB (TFEB), a master regulator of the lysosomal-autophagic pathway [20], and through MTORC1/AKT and ERK1/2 pathway inhibition [21]. There is also evidence that AMP-activated protein kinase (AMPK), an important coordinator of metabolic pathways in response to energetic fluctuations [22], is activated by FK866 in prostate cancer cells affecting lipogenesis [23] and in hepatocarcinoma cells with impact on MTOR/4EBP1 signaling [24]. Moreover, NAMPT-dependent AMPK activation associated with deacetylation of liver kinase B1 (LKB1), an upstream kinase of AMPK, has been linked with modulation of NAD levels and with significant impact on neuron cell survival [25]. Translation inhibition is often observed during cell stress [26] and this event often involves a re-programming of translation leading to differential regulation of mRNAs, occurring also *via* alternative mechanisms, aimed at reorganizing cell physiology to respond to the insult.

In this study, we focused on the pre-toxic molecular events induced by FK866 in acute lymphoblastic leukemia cells, known to be sensitive to the drug [10], in order to define the molecular mechanism favoring cell death or cell survival. A marked global protein synthesis inhibition represented an early cellular response associated with the FK866-induced energetic stress and here we show that AMPK-EIF2A is a central hub in mediating this effect and is responsible for cell fate decisions.

Methods

Cell lines, primary B-CLL cell and T-ALL PDX isolation

Human Jurkat T-cell acute lymphoblastic leukemia (T-ALL) cells were purchased from the InterLab Cell Line Collection bank (ICLC HTL01002). SUP-T1 cells were purchased from ATCC (CRL-1942) and Molt-4 Clone 8 from NIH AIDS Reagent Program (Catalog #: 175). Human lung carcinoma A594 (CCL-185) and H460 (HTB-177) cells were purchased from ATCC. These cells were transduced with retroviral vectors encoding either LKB1 cDNA (pBABE-LKB1) or the pBABE control vector. Cell lines were grown in complete RPMI 1640 (Gibco Life Technologies) supplemented with 10 % fetal bovine serum (FBS, Lonza), 2 mM L-glutamine, 100 U/ml penicillin-streptomycin (Lonza). All cell lines were grown at 37 °C under 5 % CO_2 and regularly tested for mycoplasma contamination. For primary B-CLL cell isolation, a 5 ml blood sample was obtained from patients presenting with marked lymphocytosis (>20000/μl) according to a protocol that was approved by the Ethics Committee of the Hospital IRCCS AOU San Martino IST in Genoa (#840, February 18th 2011). Patients' written informed consent was collected. B-CLL cells were isolated by density gradient centrifugation on Ficoll-Hypaque (Biotest). The phenotype of the obtained cell preparations was confirmed by immunostaining with anti-CD19, anti-CD5, and anti-CD23 (Immunotech), and subsequent flow cytometric analysis. T-ALL xenografts (PD T-ALL) were established from BM (bone marrow) of newly diagnosed ALL pediatric patients, according to a protocol approved by the ethics committee of the University of Padova (Project number 16B/2013). The PD T-ALL cells used in this study have been published elsewhere [27]. At time of PD T-ALL establishment, written informed consent was obtained from the parents of the children. *In vitro* studies were performed with T-ALL cultures established from the spleen of the xenografts. Purity of the cultures (in terms of percentage of human CD5+ cells) was checked by flow cytometry and was always >85 %. Research carried out on human material was in compliance with the Helsinki Declaration.

Chemicals

FK866 (sc-205325) was bought from Santa Cruz, Compound C (P5499), Nicotinic acid (N0761), Actinomycin D (A9415), (S)-(+)-Camptothecin (C9911), Cycloheximide (C1988), MG-132 (M7449), Doxorubicin hydrochloride (D1515) and Dexamethasone (D4902) were bought from Sigma-Aldrich, CHS-828 (200484-11-3) from Cayman chemical, Torin 1 (S2827) and Rapamycin (S1039) from Selleck Chemicals, Cisplatin (ALX-400-040) from Enzo Life Sciences and Propidium Iodide Staining Solution from BD Pharmingen. Jurkat cells were treated with drugs dissolved in DMSO at the same cell density ($5X10^5$ cells/ml).

Viability assays

Cell viability was assessed with the Annexin V-FITC Apoptosis Detection Kit I and 7-Aminoactinomycin D

(7-AAD) Staining Solution (BD Pharmingen) according to manufacturer's instruction. EC_{50} values of FK866 were determined by nonlinear regression analysis (GraphPad Prism software v5.01,) *vs* viable cells in mock conditions (DMSO).

Jurkat, A549 and H460 cell lines were grown and treated in 96 well-plate for 48 h. Cells were then assayed for viability using Thiazolyl blue tetrazolium bromide (MTT) M5655 (Sigma). In brief, MTT (5 mg/ml) at 10 % volume of culture media was added to each well and cells were further incubated for 2 h at 37 °C. Then 100 μl of DMSO was used to dissolve formazan. Absorbance was then determined at 565 nm by microplate reader. Cell survival was calculated and EC_{50} values were determined.

Determination of NAD^+-NADH and ATP levels and caspase/protease activity

Intracellular NAD^+-NADH content was assessed with a NAD^+-NADH Quantification Kit (BioVision) according to the manufacturer's protocol. Intracellular ATP content was determined using Cell titer Glo Luminescent Cell Viability Assay (Promega). NAD^+-NADH and ATP values were normalized to the number of viable cells as determined using Trypan Blue (Lonza). EnzChek Protease Assay Kit, containing a casein derivative labeled with green-fluorescent BODIPY FL (Life Technologies), was used to determine protease activity after treatment of $2x10^6$ cells. Cells were washed once with PBS and lysed in 500 μl of 1X digestion buffer, sonicated and centrifuged for 5 min at maximum speed. One μl of the BODIPY casein 100X was added to 100 μl of the supernatant and incubated for 1 h protected from light. Fluorescence was measured and normalized to protein concentration in the cell lysates (Bradford Reagent, Sigma). Caspase-Glo 3/7 Assay (Promega) was used to quantify caspase activity.

RNA and protein click-iT labeling kits

Click-iT RNA Alexa Fluor 488 Imaging Kit (Life Technologies) was used to quantify the level of global RNA synthesis by flow-cytometry. Jurkat cells ($3x10^6$/sample) were treated for 45 h with FK866 (or DMSO) and then incubated for 3 h with 1X EU working solution without removing the drug-containing media. EU detection was performed following the manufacturer's protocol after cell fixation and permeabilization. Click-iT AHA Alexa Fluor 488 Protein Synthesis Assay (Life Technologies) was used to measure the rate of translation. Cells ($3x10^6$/sample) were treated for 45 h with FK866, centrifuged and incubated for 3 h with 50 μM AHA in L-methionine-free medium (RPMI Medium 1640, Sigma-Aldrich) containing the drug (or DMSO). After fixation and permeabilization, AHA incorporation was assessed by flow cytometry. 7-AAD Staining Solution (0.25 μg/sample) allowed the exclusion of non-viable cells.

Western blotting, antibody list and plasmids

Cells were lysed for 5 min on ice in RIPA lysis buffer supplemented with Protease Inhibitor Cocktail (Sigma-Aldrich). After sonication and clarification, equal amounts of proteins were separated by SDS–PAGE and blotted onto PVDF membranes (Immobilon-P, Millipore), as in [28]. The antibodies used were: 4EBP1 (sc-6936), p-4EBP1 (Ser 65/Thr 70; sc-12884), EIF4E (sc-9976), p-EIF4E (Ser 209; sc-12885), AKT1/2/3 (sc-8312), p-AKT1/2/3 (Ser 473; sc-7985), MTOR (sc-8319), BCL-2 (sc-509), NAMPT (sc-130058) from Santa Cruz; EIF2S1 (ab26197), p-EIF2S1 (Ser 51; ab32157), and p-MTOR (Ser 2448; ab1093) from Abcam; AMPKα (2603), p-AMPKα (Thr 172; 2531), ACC (3676) and p-ACC (Ser 79; 3661) and MCL1 (4572) from Cell Signaling. A mouse anti-β-actin antibody (3700, Cell Signaling) was used as a protein loading control. eIF2a 1 (Addgene plasmid # 21807), eIF2a 2 (Addgene plasmid # 21808) and eIF2a 3 (Addgene plasmid # 21809) were a gift from David Ron. A549 cells were transfected using Lipofectamine 3000 Reagent from Life Technologies. Cells were plated in 6 well and transfected at 70 % confluence for 24 h with 1 μg of DNA. Jurkat cells were transfected for 48 h with 1 μg of DNA in 24- well plate.

Real-time PCR

Total RNA was extracted with Quick-RNA MiniPrep kit (Zymo Research) and treated with DNAse. cDNA was synthesized using RevertAid First Strand cDNA Synthesis Kit (Fermentas) following the manufacturer's recommendation. Real-time PCR reactions were performed using the KAPA SYBR FAST Universal qPCR Kit on a CFX96 Real-Time PCR Detection System (BioRad). Relative mRNA quantification was obtained with the ΔCq method using β-actin (*ACTB*) as housekeeping gene. Primers' sequences are reported as follows: *BiP/Grp78* (Fw: TGTTCAACCAATTATCAGCAAACTC Rev: TTC TGCTGTATCCTCTTCACCAGT) *ACTB* (Fw: CTGGA ACGGTGAAGGTGACA Rev: AGGGACTTCCTGTAA CAATGCA) *STK11*/*LKB1* (Fw: GAGCTGATGTCGGT GGGTATG Rev: CACCTTGCCGTAAGAGCCT).

Lentiviral particles production and luciferase assay

Lentiviral particles were produced using the pHR-SIN-*R*-Myc-F, pHR-SIN-F-HCV-*R* and pHR-SIN-F-CrPV-*R* transfer vectors [29], coding for reporter genes controlled by a cMyc-5′UTR, HCV or CrPV IRESes regulated translation, by co-transfection of 293 T cells with the packaging plasmid pCMV-deltaR8.91 and the VSV envelope-coding plasmid pMD2.G. Five thousand Jurkat cells/sample were transduced. After treatment with FK866, luciferase activity

was measured using the Dual-Glo Luciferase Assay System (Promega) and normalized for protein concentration.

Silencing with shRNAs

The pLKO.1-based lentiviral plasmids containing AMPKa1 shRNA (TRCN0000000859), AMPKa2 shRNA (TRCN0000002169) or NAMPT shRNA expression cassette (TRCN0000116180) and (TRCN0000116181) were purchased from Sigma-Aldrich. Scramble shRNA (Addgene plasmid #1864 [30]) was used as a control. Vectors were produced in 293 T cells by cotransfection of the different transfer vectors with the packaging plasmid pCMV-deltaR8.91 and the VSV envelope-coding plasmid pMD2.G. 1 million of Jurkat cells were transduced with lentiviral particles expressing the control (shSCR) or NAMPT-silencing short hairpin RNA (shNAMPT) by spinning them down with vector-containing supernatants for 2 h at 1600xg at room temperature and leaving them incubate overnight at 37 °C without replacing the transduction supernatant. After changing the medium, the cells were further incubated for 72 h before collection for WB.

For AMPK silencing experiments, Jurkat cells were first transduced with the shRNA vector targeting the α1 subunit (shAMPKα1) as reported before. After 24 h from the first transduction the cells were then transduced again, following the same protocol, with the lentiviral vector coding for the shRNA targeting the AMPK α2 subunit (shAMPKα2). After changing the medium the next morning, the cells were further incubated for 48 h and then treated for additional 48 h with or without (DMSO) 5 nM of FK866.

To obtain LKB1 silencing, pLKO.1 transfer vectors were prepared by cloning annealed oligos coding for shRNAs (clone TRCN0000000408 for LKB1-A and clone TRCN0000000409 for LKB1-B) into the TRC cloning vector (Addgene plasmid #10878 [31] according to the TRC standard protocol. Cells were transduced by spinning them down with vector-containing supernatants and leaving them incubate overnight. After changing the medium, the cells were incubated for 72 h and then treated for additional 48 h with or without FK866.

Statistical analysis

Experiments were performed in biological triplicates. *T*-test was used to calculate final *p*-values, without assuming variances to be equal (Welch's *t*-test). *P*-value <0.05 was considered statistically significant.

Results

Sensitivity of leukemia cells to the NAMPT inhibitor FK866

FK866 was previously shown to have cytotoxic activity at nanomolar concentrations against different types of hematological malignancies, including myeloid and lymphoid leukemias and multiple myeloma [12, 21]. We monitored FK866-induced cell death in Jurkat cells by quantifying early and late apoptosis with 7AAD and Annexin V staining. In line with previous reports, FK866 cytotoxic activity started to become evident between 48 and 72 h of exposure with approximately 74 and 47 % of viable cells left at these time points when cells are treated with FK866 100 nM (Fig. 1a), respectively. This suggests the existence of a lag phase through which cells can cope with the energetic shortage. Starting from a concentration of 10 nM, FK866 cytotoxic activity reached a plateau and an EC_{50} of 5.3 nM could be estimated after 48 h of exposure (Fig. 1a). Indeed, at 120 h we measured an effective IC_{50} of 10 nM, highlighting the inability of these cells to compensate for the energetic stress induced by FK866 in long term treatment (Fig. 1a). Cell cycle analysis of FK866-treated cells, at 48 h, showed a non-significant accumulation of cells in G2/M phase, while, as predicted, serum starvation resulted in accumulation of cells in G0/G1 phase (Fig. 1b and Additional file 1A). Forty-eight hours treatment with FK866 led to approximately 25 % of cell death, but did not lead to massive protease or caspase activation (Fig. 1c and d). However, 5 nM FK866 was sufficient to effectively reduce NAD^+(H) and ATP levels in Jurkat cells, representing a pre-toxic experimental condition to apply for further experiments (Fig. 1e).

FK866 and NAMPT ablation blocks cap-dependent translation, but not gene transcription, through MTOR/4EBP1, EIF4E, and EIF2A inhibition in cancer cells

We assessed the impact of FK866 on global transcriptional and translational efficiencies in Jurkat cells. Global RNA transcription and translation were monitored using the *Click-it* chemistry and flow-cytometry by the incorporation of the nucleoside analog 5-ethynyl uridine (EU) and of an aminoacid analog (AHA), respectively. In the viable Jurkat cell population, FK866 caused a reduction in the incorporation of EU in a dose–dependent manner, with 70 and 55 % of transcriptionally active cells in the presence of 5 and 100 nM FK866, respectively. Thus, despite NAD^+ and ATP depletion, cells treated with FK866 for 48 h essentially retained their ability to perform RNA transcription. By contrast, even 5 nM FK866 determined a striking reduction (up to 30 %) of the fraction of viable cells showing active protein synthesis (Fig. 2a and Additional file 1B). The utilization of bicistronic reporter assays to test the efficacy of cap or IRES (Internal Ribosome Entry Site) dependent translation confirmed that FK866 induced a strong translation arrest with a major impact on cap-dependent translation in Jurkat cells (Additional file 2).

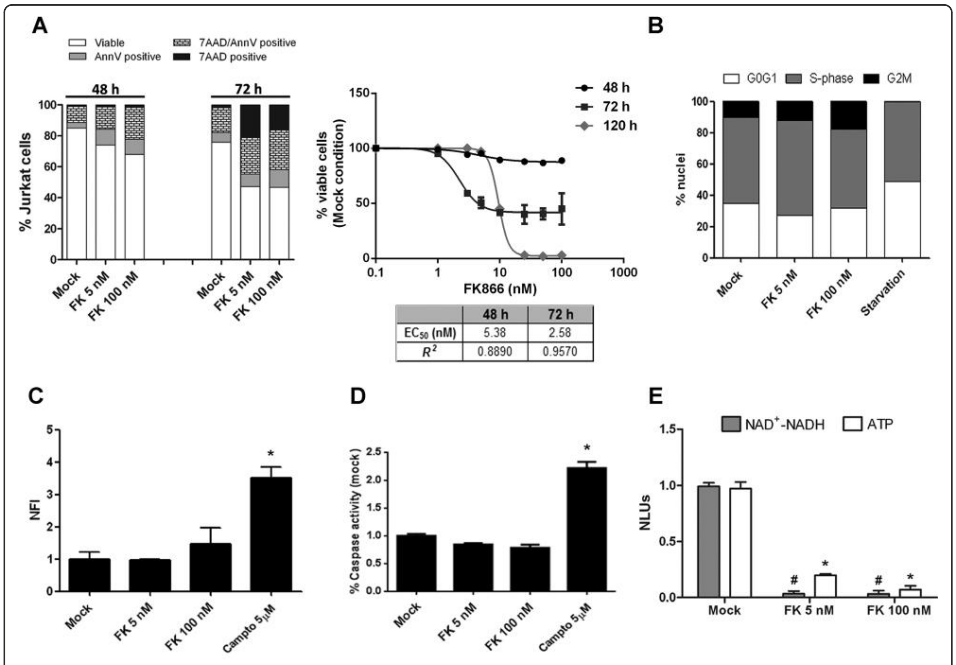

	48 h	72 h
EC_{50} (nM)	5.38	2.58
R^2	0.8890	0.9570

Fig. 1 FK866 affects NAD^+(H) and ATP levels in Jurkat cells leading to cell death. **a** Flow-cytometric quantification of cell viability with AnnexinV (FITC) and 7AAD (PerCP-Cy5-5-A) staining. Jurkat cells were treated with FK866 for 48,72 and 120 h. Mock, 5 nM FK866 and 100 nM FK866 (at 48 and 72 h) are shown as representative samples. Flow-cytometry experiments were carried out on two biological replicates and statistics were based on the acquisition of 10000 events/sample. **b** Cell-cycle analysis with PI staining of the nuclei after 48 h of treatment. Overnight serum starvation is shown as positive control of induced cell cycle synchronization in G0/G1 phase. Histograms quantify the cell cycle phase distribution. Flow-cytometry experiments were carried out on two biological replicates and statistics were based on acquisition of 30000 events/sample. Cell cycle phase analysis was done using ModFit LT 3.2 software and the Sync Wizard model. **c** Jurkat cells were treated with FK866 for 48 h. Alternatively, cells were exposed to 5 μM of Camptothecin for 4 h as a positive control. Protease activity in cell extracts was assessed with a commercially available kit and values were normalized to the protein concentration in the same extracts. **d** Caspase 3/7 activity was measured in Jurkat cells treated as in **c**. **e** Jurkat cells were treated with FK866 for 48 h. Thereafter, intracellular NAD^+(H) and ATP levels were evaluated in comparison with control Jurkat cells. RLUs were normalized to number of viable cells. In **c**-**e** the means with SD of at least three independent experiments are shown. Statistical significance was calculated with *t*-test (* and # indicates *p*-value <0.05)

Since the initiation phase is considered the limiting step of translation [32], we evaluated the activation of three signaling pathways regulating the canonical cap-dependent translation process. The Mammalian Target of Rapamycin (MTOR) kinase regulates the p70 ribosomal S6 kinase (p70-S6K) and the eukaryotic translation initiation factor 4E-binding protein 4EBP1, whose phosphorylation determines EIF4E availability for its interacting partner EIF4G, which is involved in mRNA recruitment to the ribosomes for protein translation [32]. It has been recently shown that FK866 induces MTOR de-phosphorylation [24], thereby inducing autophagic cell death in multiple myeloma cells [21, 33]. As shown in Fig. 2b, Jurkat cells treated with FK866 indeed showed a marked de-phosphorylation of MTOR and 4EBP1. Enhanced AKT phosphorylation at Ser-473 was also observed (Fig. 2b), which is in line with the paradoxical activation of AKT by MTORC2 complex following inhibition of MTOR as reported with different MTOR inhibitors in multiple myeloma cells [34]. Notably, treatment with FK866 led to a previously unappreciated de-phosphorylation of EIF4E on serine 209, suggesting that the MAP Kinase Interacting Serine/Threonine Kinase (MNK)-dependent pathway is also affected [35] (Fig. 2c), and to an increased phosphorylation on Ser-51 of EIF2A, an initiation factor that transfers methionyl-initiator tRNA (Met) to the small ribosomal subunit. When phosphorylated (Fig. 2c), EIF2A loses its

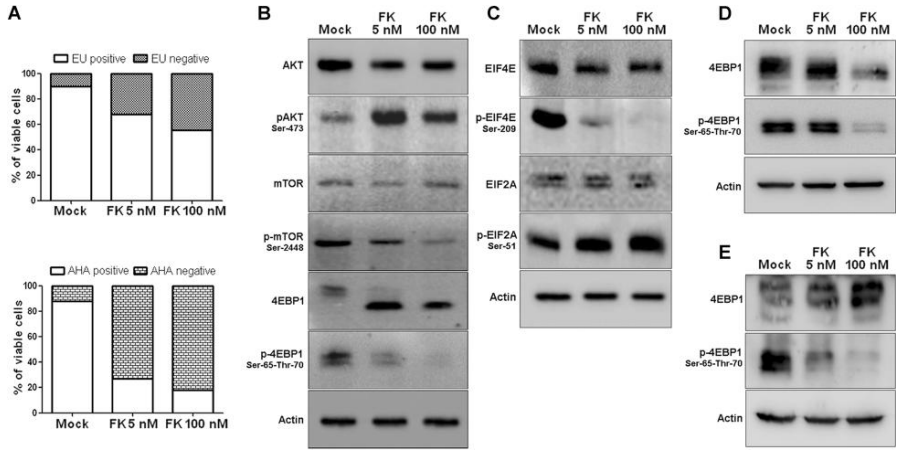

Fig. 2 FK866 inhibits the signaling cascades controlling protein synthesis in T-ALL cell lines. **a** RNA synthesis was determined by monitoring EU incorporation with *Click-it* chemistry. Jurkat cells were treated for 48 h with or without (Mock) the indicated concentration of FK866 or for 3 h with 5 μM Actinomycin D, an RNA synthesis blocking agent. The histogram quantifies the dose-dependent transcription inhibition induced by FK866 in the viable cell population. In the lower part, *Click-it* chemistry based on the incorporation of an aminoacid analog (AHA) was used to monitor protein synthesis. Jurkat cells were treated for 48 h with or without (Mock) the indicated concentration of FK866 or for 3 h with 350 μM Cycloheximide, as a positive control for protein synthesis inhibition. The histogram quantifies FK866-induced protein synthesis arrest in the viable cell population. Flow-cytometry experiments were carried out on two biological replicates and statistics were based on acquisition of 50000 events/sample. **b** Jurkat cells were treated for 48 h with or without (Mock) the indicated concentration of FK866. Thereafter, cells were lysed and the levels of total and p-Akt (Ser-473), total and p-MTOR (Ser-2448), total and p-4EBP1 (Ser-65 and Thr-70), **c**) total and p-EIF4E (Ser-209), total and p-EIF2A (Ser-51) were detected by immunoblotting. **d** Molt-4 cells were treated with FK866 for 48 h and the levels of total 4EBP1 and p-4EBP1 were evaluated. **e** Western blot analysis as in **d** in SupT1 cells. **b**-**e**, one representative experiment out of at least three biological replicates is presented and β-actin was used as loading control

ability to exchange GDP and GTP, impairing the formation of a complex with the EIF2B subunit and thus preventing translation initiation [36]. Analogously, SUP-T1 and Molt-4 Clone 8 T-ALL cell lines presented the same FK866-induced inhibition of the activation of 4EBP1, supporting the existence of a general mechanism underlying the FK866-induced translational arrest in leukemia cells (Fig. 2d, e). These effects were also observed using another inhibitor of NAMPT enzymatic activity, CHS-828 (Additional file 3A), but not with other commonly used chemotherapeutics as cisplatin, doxorubicin, dexamethasone and rapamycin, at equivalent pre-toxic doses. Indeed, FK866 induced a stronger protein synthesis arrest than the MTOR inhibitor rapamycin suggesting that this event is a molecular hallmark of FK866. Additionally, FK886 concomitantly induced EIF2A phosphorylation and 4EBP1 de-phosphorylation, uniquely among all the other drugs, thus mechanistically supporting the strong protein synthesis arrest. The other drugs tested were ineffective (Additional file 3B, C, D). In conclusion, these experiments show the modulation of several hubs of the signaling apparatus controlling translation initiation in response to FK866, providing a robust explanation for the marked protein synthesis inhibition observed after drug treatment.

FK866 induces AMPK and EIF2A phosphorylation in Jurkat and primary leukemia cells

In view of the strong translation inhibition and considering its energy-sensing activity in controlling translation [37], we investigated in Jurkat cells the impact of FK866 and CHS-828 on the phosphorylation status of AMPK, whose activation has been previously shown to be induced by FK866 in prostate and hepatic cancer cells [23, 24]. FK866 caused a partial reduction in total AMPK levels at the highest dose used, but, at a same time, a parallel dose-dependent increase of the phosphorylation of its Thr-172 and of its *bona fide* target ACC (Acetyl-CoA Carboxylase) (Fig. 3a), indicating a significant activation of AMPK. We evaluated the effect of FK866 on two important antiapoptotic factors, MCL1 (Myeloid Cell Leukemia 1) and BCL-2 (B-Cell Lymphoma 2). BCL-2 protein levels were essentially not affected by FK866 treatment as compared to the strong down-regulation of MCL1 (Fig. 3a). Notably, nicotinic acid (NA) supplementation, which blocks FK866 cytotoxic activity by allowing NAD^+ biosynthesis through

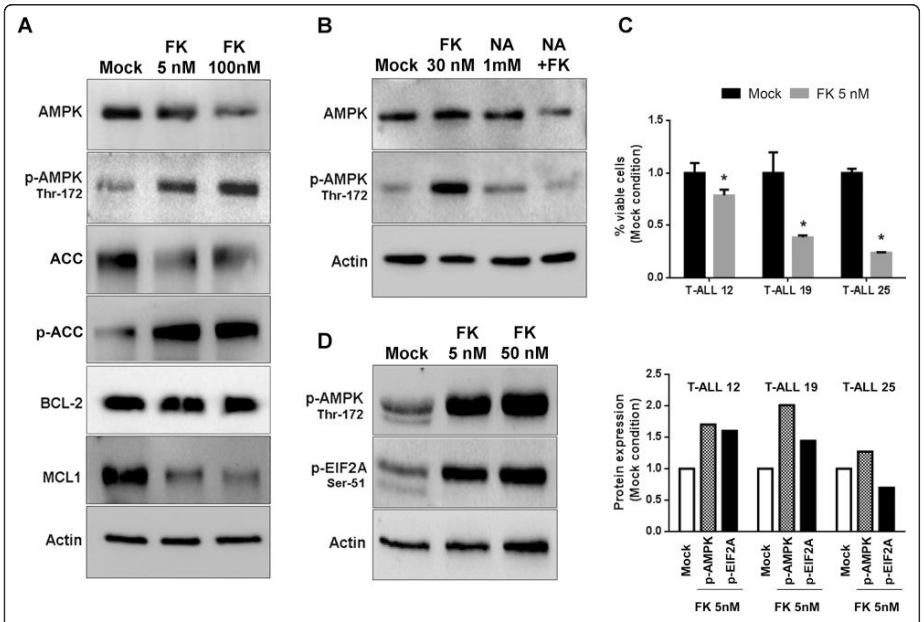

Fig. 3 FK866 induces AMPK and EIF2A phosphorylation in primary leukemia cells. **a** Jurkat cells were treated for 48 h with or without (Mock) the indicated concentration of FK866. Thereafter, cells were lysed and the levels of total and p-AMPK (Thr-172), ACC and p-ACC, BCL-2, MCL1 and β-actin as loading control were detected by immunoblotting. One representative experiment out of three biological replicates. **b** primary B-CLL cells (source: peripheral blood; RAI stage III, 86 years, CD38-pos) were treated for 48 h with or without FK866 in the presence or absence of 1 mM NA. Thereafter, protein lysates were immunoblotted for AMPK and p-AMPK. **c** Cell viability with respect to Mock condition, measured by CellTiter Glo, of three different T-ALL xenografts (PD T-ALL 12, 19 and 25) after treatment with FK866 5nM for 48 h. **d** WB of PD T-ALL 12 as representative of T-ALL xenografts samples. Cells were treated with 5 and 50 nM FK866 for 48 h. Histogram shows the densitometric analysis of p-AMPK and p-EIF2A in the three T-ALL xenografts (PD T-ALL 12, 19 and 25)

an alternative pathway (*via* nicotinic acid phosphoribosyltransferase, NAPRT1), completely prevented AMPK phosphorylation in primary B-CLL (Fig. 3b, Additional file 3E), confirming that NAD^+ depletion is responsible for AMPK activation. In patient-derived T-ALL xenografts (PD T-ALL) the drug induced cell death and activated AMPK as well as EIF2A phosphorylation (Fig. 3c and d), demonstrating that this molecular event is not limited to cell line models but is also present in primary leukemia cells.

EIF2A phosphorylation precedes 4EBP1 de-phosphorylation in Jurkat cells

NAMPT expression level during FK866 treatment remained unchanged as expected (Fig. 4a). Genetic ablation of NAMPT by lentiviral transduction in Jurkat cells (Fig. 4b) lowered NAD^+(H) level to 75 % of the control while ATP level was not significantly decreased thus inducing an intermediate condition of energetic stress compared to the one obtained with 5 nM FK866 administration (Fig. 4c). In these conditions of mild stress, AMPK was marginally activated but, nevertheless, we observed a significant phosphorylation of EIF2A but not the de-phosphorylation of 4EBP1, suggesting that the first event precedes the second one (Fig. 4d). Importantly, we observed a clear down-regulation of MCL1, as observed with FK866 treatment (Fig. 3a), suggesting that EIF2A activation is an early response to NAD^+(H) shortage.

FK866-induced AMPK activation regulates EIF2A phosphorylation

To formally assess the role of AMPK in FK866-induced translational arrest, we pharmacologically blocked AMPK with Compound C, a small molecule inhibitor of this enzyme, although not selective [38]. In addition, we down-regulated AMPK using lentiviral transduction of shRNAs. Compound C administration to Jurkat cells treated with FK866 abrogated AMPK phosphorylation,

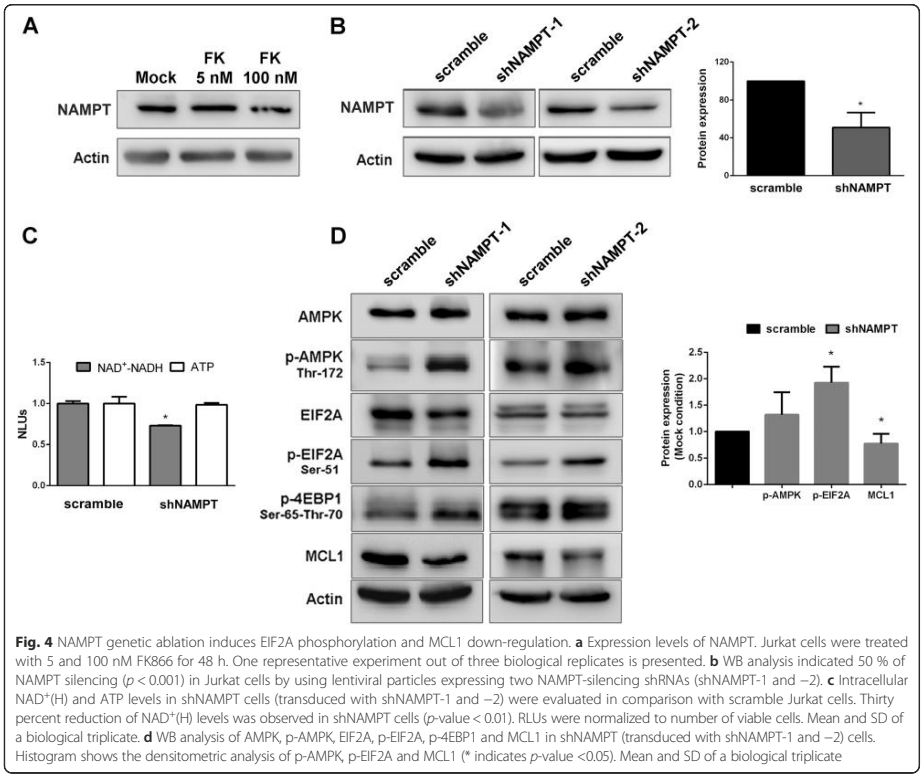

Fig. 4 NAMPT genetic ablation induces EIF2A phosphorylation and MCL1 down-regulation. **a** Expression levels of NAMPT. Jurkat cells were treated with 5 and 100 nM FK866 for 48 h. One representative experiment out of three biological replicates is presented. **b** WB analysis indicated 50 % of NAMPT silencing ($p < 0.001$) in Jurkat cells by using lentiviral particles expressing two NAMPT-silencing shRNAs (shNAMPT-1 and −2). **c** Intracellular NAD^+(H) and ATP levels in shNAMPT cells (transduced with shNAMPT-1 and −2) were evaluated in comparison with scramble Jurkat cells. Thirty percent reduction of NAD^+(H) levels was observed in shNAMPT cells (p-value < 0.01). RLUs were normalized to number of viable cells. Mean and SD of a biological triplicate. **d** WB analysis of AMPK, p-AMPK, EIF2A, p-EIF2A, p-4EBP1 and MCL1 in shNAMPT (transduced with shNAMPT-1 and −2) cells. Histogram shows the densitometric analysis of p-AMPK, p-EIF2A and MCL1 (* indicates p-value <0.05). Mean and SD of a biological triplicate

reactivated the MTOR/4EBP1 pathway and restored EIF2A in its un-phosphorylated state (Fig. 5a). Rescue experiments with Compound C did not show any down-regulation of MCL1 protein level with no change in BCL2 expression (Fig. 5a). Co-treatment with Compound C partially reverted FK866-induced ATP loss but activated the apoptotic response (Fig. 5b). Down-regulation of AMPK was achieved by targeting both AMPKα1 and AMPKα2 isoforms (shAMPK cells). We then exposed silenced and control (scramble) cells to 5 nM of FK866 for 48 h (Fig. 5c). In shAMPK cells we observed a significant decrease of EIF2A phosphorylation but not of 4EBP1 de-phosphorylation. This supports the notion that FK866-induced AMPK activation is primarily involved in the regulation of EIF2A phosphorylation and subsequently in 4EBP1 de-phosphorylation (Fig. 5c). Importantly, shAMPK Jurkat cells showed an increased sensitivity to FK866 with respect to control cells, as revealed by PI staining and flow-cytometry (Fig. 5d), pointing out the protective effect of AMPK in FK866-induced stress conditions.

EIF2A mediates the AMPK pro-survival effect during FK866 treatment

Given the protective role of AMPK in a context of FK866-sensitive cancer cell, we hypothesized that the liver kinase B1 (LKB1), a well-established AMPK regulator, can also exert the same protective effect. Indeed, genetic ablation of LKB1 in Jurkat cells led to an increase toxicity of FK866 treatment (Fig. 6a). Accordingly, we used two lung adenocarcinoma cell lines (H460 and A549), bearing genetic inactivation of LKB1 to prove the dependency of FK866 efficacy on the activation of the LKB1/AMPK pathway. These results provide a rationale for the utilization of NAMPT inhibitors in cancers with this type of genetic background. The cells were stably transduced with retroviral vectors encoding parental LKB1 cDNA (LKB1 WT) or with a control vector

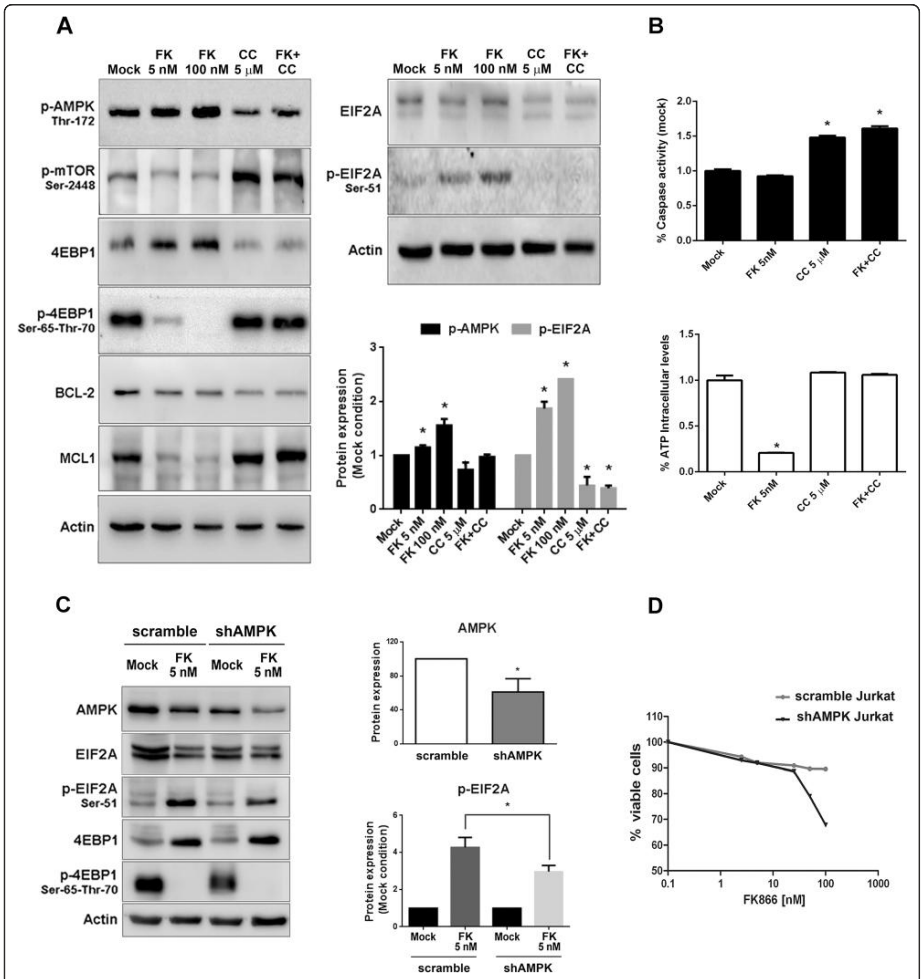

Fig. 5 AMPK regulates EIF2A phosphorylation and is a pro-survival factor in Jurkat cells. **a** Jurkat cells were treated with or without FK866 at the indicated concentrations in the presence or absence of Compound C 5 μM for 48 h. Thereafter, cells were lysed and the levels of p-AMPK (Thr-172), p-MTOR, 4EBP1, p-4EBP1, BCL-2, MCL1, EIF2A and p-EIF2A were revealed by immunoblotting. Histogram shows the densitometric analysis of p-AMPK and p-EIF2A. **b** In the same samples, caspase 3/7 activity was quantified and relative ATP levels were determined and then normalized to the number of viable cells (* indicates *p*-value <0.05). **a** and **b** are representative of a biological triplicate (mean and SD). **c** Jurkat cells were transduced with lentiviral particles containing scramble or shAMPK (targeting the α1 and the α2 subunit), then treated for 48 h with or without 5 nM FK866. Cell lysates were used for total AMPK, EIF2A, p-EIF2A, 4EBP1, p-4EBP1 and β-actin immunoblotting. WB analysis indicated 40 % of AMPK silencing (*p*-value < 0.05) and densitometric analysis shows the significant decrease of p-EIF2A in shAMPK Jurkat cells (*p*-value < 0.03). Mean and SD of a biological triplicate. **d** Jurkat scramble and shAMPK cells were treated for 48 h with the indicated doses of FK866. Cell viability was determined by PI staining and flow-cytometry (two biological replicates and statistics based on the acquisition of 10000 events/sample)

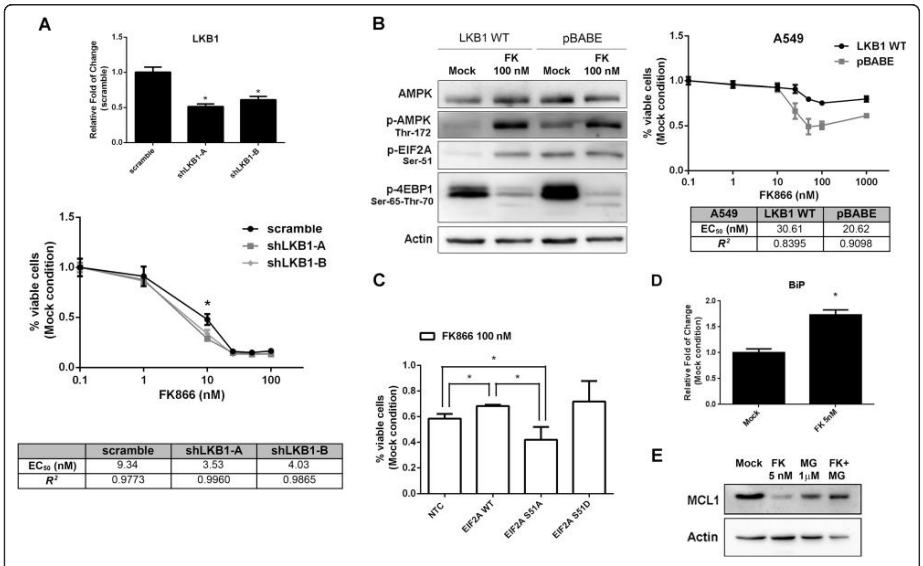

	scramble	shLKB1-A	shLKB1-B
EC_{50} (nM)	9.34	3.53	4.03
R^2	0.9773	0.9960	0.9865

A549	LKB1 WT	pBABE
EC_{50} (nM)	30.61	20.62
R^2	0.8395	0.9098

Fig. 6 Protective role of EIF2A and FK866 induced UPR. **a** Expression level of LKB1 mRNA, evaluated in Jurkat cells after 120 h of lentiviral transduction with shRNAs expressing the control sequence (scramble) or two LKB1-silencing shRNAs (shLKB1-**a** and –**b**), in the upper panel. Cells were transduced for 72 h and then treated with FK866 for 48 h. Viability was measured by MTT assay in comparison with Mock (DMSO) condition, in the lower panel. Mean and SD of a biological triplicate (*, *p*-value < 0.05). **b** WB analysis indicated the levels of AMPK, p-AMPK, p-EIF2A, p-4EBP1 in A594 cells expressing LKB1 (LKB1 WT) or transduced with an empty vector (pBABE) treated or not (Mock) with 100 nM FK866 for 48 h, left panel. A549 cells were treated with indicated concentration of FK866 for 48 h and cell viability as shown in dose–response curve was evaluated by MTT assay, right panel. Mean and SD of three biological replicates. **c** A549 viability after 48 h of treatment with FK866 100 nM in un-transfected (NTC) cells and transfected with EIF2A wild type, EIF2A-S51A, EIF2A-S51D (mean and SD of three experiments,*, *p*-value < 0.05). **d** Expression level of BiP mRNA, evaluated in Jurkat cells after 48 h of treatment with FK866 5nM (*, *p*-value < 0.0005). Mean and SD of a biological triplicate. **e** WB analysis of MCL1 in Jurkat cells treated with FK866 for 48 h and with the proteasome inhibitor MG132 1 μM for 24 h. MG132 was added after 24 h of FK866 treatment. One representative experiment out of three biological replicates

(pBABE). FK866 treatment induced AMPK and EIF2A phosphorylation in addition to 4EBP1 de-phosphorylation only when LKB1 was active. On the other hand, albeit to a different extent among the two cell lines, FK866 was not able to activate AMPK or EIF2A but was still effective in de-phosphorylating 4EBP1 when LKB1 was inactive. Viability assays indicated an increased sensitivity of LKB1 negative, EIF2A un-phosphorylated cells to FK866 compared to LKB1 expressing cells (Fig. 6b and Additional file 4A). Finally, in order to assess the relevance of EIF2A in mediating the AMPK induced protection from FK866, we treated with the drug A549 and Jurkat cells transfected with EIF2A, its phosphomimetic mutant S51D or with the non-phosphorylatable mutant S51A. In the context of inactive LKB1, the overexpression of EIF2A and the EIF2A-S51D isoform led to a protective effect, while the alanine mutant induced an increase of cell toxicity (Fig. 6c). The same trend was observed also in Jurkat cells (Additional file 4B). Therefore, these data indicate that the translation arrest induced by EIF2A mediates the protective effect of AMPK from FK866 induced stress.

EIF2A balances pro-survival and pro-death pathways

EIF2A is a key factor regulating the translation machinery in response to a myriad of factors including nutrient depletion, presence of exogenous mRNA and the Unfolded Protein Response (UPR) following the induction of Endoplasmic Reticulum (ER) stress [39]. Indeed, FK866 induced the overexpression of BiP/Grp78 mRNA, coding for a chaperone involved in the folding of ER proteins (Fig. 6d), thus indicating UPR activation in Jurkat cells after 48 h treatment. Moreover, FK866 induced MCL1 down-regulation was dependent on proteasome activation as demonstrated by the rescue of its expression level by MG132 treatment in Jurkat cells (Fig. 6e) [40]. In conclusion, FK866 induces an AMPK-

EIF2A mediated translational arrest, which is responsible for MCL1 down-regulation and the activation of the UPR response, that is a strategic pausing step necessary to protect cells from FK866-induced energetic stress.

Discussion

We investigated the link between NAD^+(H) depletion and cell death using a T-ALL cell model after induction of the primary effects of NAMPT inhibition, namely NAD^+(H) and ATP depletion, while nearly preserving total cell viability. The functional consequences of NAD^+(H) depletion upon FK866 treatment resulted in a marked inhibition of the three major pathways regulating the translation process and in a striking arrest of protein synthesis. Interestingly, FK866 efficacy in blocking protein synthesis was higher than all the other chemotherapeutics tested and even higher than the MTOR inhibitor rapamycin, suggesting that this is a crucial event in the cell response to FK866. This phenomenon is general because it was observed in primary leukemic samples, coming both from B-CLL and T-ALL patients, and in T-ALL derived cancer cell lines. Nicotinic acid rescue experiments, treatment with the FK866 analog CHS-828 and NAMPT genetic ablation showed that translation arrest was dependent on the shortage of ATP and NAD^+(H) induced by the inhibition of the NAMPT catalytic function and not by unspecific FK866 effects. FK866 has been shown to have contrasting effects on AMPK. In neuronal cells FK866 decreased AMPK activation and was detrimental for neuronal survival [25], however in cancer cells that have a dysregulated metabolic demand, it has been observed the opposite. In prostate cancer cells, FK866 treatment reduced fatty acid and phospholipid synthesis, partly *via* AMPK activation [23]. FK866 induced activation of AMPK and subsequent decreased phosphorylation of 4EBP1 by MTOR has been observed in hepatocarcinoma cells. Given the importance of MTOR in sustaining cancer cell growth, this event was proposed as an effective mechanism to target cancer cells [23]. By evaluating the early molecular effects of FK866 treatment on protein synthesis, we observed the involvement of the same pathway but, in addition, we showed a protective role for AMPK and EIF2A. In our experimental conditions, the inactivation of MTOR by AMPK and consequent protein synthesis arrest had a protective effect conferring temporary resistance to the FK866-induced energetic stress. Additionally, we determined that AMPK-induced hyper-phosphorylation of EIF2A is regulated by the fluctuations of NAD availability at the intracellular level. This molecular mechanism, leading to inhibition of translation initiation, followed AMPK activation. In fact, genetic AMPK down-regulation of both isoforms of the α catalytic subunit rescued the FK866 induced hyper-phosphorylation of EIF2A. As a further confirmation, the same results were obtained by AMPK functional ablation using the inhibitor Compound C or by inactivation of its upstream regulator LKB1. Indeed, rescue of 4EBP1 phosphorylation levels was observed only after Compound C administration, suggesting that EIF2A is a preferential target of the AMPK signaling cascade, at least in the initial phase of cell response to FK866. Interestingly, in our cell model and at the doses we used, we did not observe Compound C-induced phosphorylation of EIF2A as recently reported in different cancer cells [41]. Our cell model resembles the AICAR-induced AMPK activation that leads to EIF2A phosphorylation in adipocytes, an event shown to be crucial for AMPK-induced apoptosis [42], and supports the idea that FK866 induced activation of the AMPK-EIF2A axis can be a novel pathway to be investigated to elucidate the pharmacology of FK866.

Many types of cancer, as sporadic lung, cervical, and endometrial cancers, carry LKB1 deficiency that can be exploited with metabolic drugs since these cells are unable to appropriately respond to metabolic stress [43]. Given the protective role of LKB1/AMPK pathway against FK866, our study suggests the utilization of FK866 as a metabolism-based cancer therapeutic to selectively target LKB1-deficient tumors. Indeed in cells lacking a functional LKB1 pathway, metabolic stress has been demonstrated to result in rapid apoptosis as the cells are unable to sense energetic stresses and activate mechanisms to restore energy homeostasis [44].

Previous studies have shown that inhibition of the MTOR/4EBP1 pathway in leukemia cells leads to a reduction in the levels of the anti-apoptotic protein MCL1, with important implications for chemosensitivity [45]. Down-regulation of MCL1 through inhibition of translation has been clearly associated with enhanced lethality in Jurkat cells [46]. Importantly, FK866 administration led to smooth death [40] *via* EIF2A-dependent MCL1 down-regulation consequent to translation arrest and simultaneous proteasome activation. Indeed, MCL1 intracellular levels were shown to be strictly dependent on the activation of EIF2A [47] and AMPK [48], and to the subsequent translation arrest. This could provide a molecular explanation for the anti-leukemic activity of NAMPT inhibitors. Notably, the ectopic expression of the non-phosphorylatable mutant EIF2A-S51A increased FK866 toxicity. Therefore the activation of the AMPK-EIF2A axis is essential for the tumor cell to adapt to the shortage of NAD^+(H). For example, the increased expression level of BiP mRNA is a specific adaptive response observed in the integrated stress response (ISR) and translational repression [49]. The exacerbation of proteasome inhibition with bortezomib has been shown to potentiate FK866 efficacy through the activation of

the caspases' cascade [40]. Here we show the relevance of EIF2A activation in this mechanism. Additionally, the synergistic effect of FK866 with cyclosporine in leukemia cells has been ascribed to the activation of the UPR [50]. This suggests that the exacerbation of the UPR, which is dependent on EIF2A, can be thought as a relevant strategy to potentiate the effect of FK866 in conditions in which activation of the EIF2A-dependent UPR is desirable, i.e., diabetes, atherosclerosis, or neurodegenerative disorders [51]. Indeed, FK866 effects on translation resemble the ones induced by metformin, a well-known AMPK activator with antidiabetic and antitumoral properties [52, 53]. Finally, de-phosphorylation of EIF4E, never linked to NAMPT inhibitors or AMPK activation before, completes the general picture of a global inhibition of the translation process, even though the mechanism leading to upstream MNK activation has not been investigated yet.

Conclusions

In conclusion, this work describes the activation of a complex signaling network in which the AMPK-EIF2A axis is responsible for the early cellular response to the metabolic stress produced by FK866. In an experimental condition in which catastrophic proteolytic cascades are not yet started but the energetic demand is high, EIF2A acts as an early master regulator of cell fate, blocking anabolic processes and, at the same time, modulating cell death and adaptive pathways. Therefore EIF2A-dependent processes, such as protein synthesis and UPR, acquire fundamental relevance in explaining the mechanism of action of NAMPT inhibitors.

Additional files

Additional file 1: Cell-cycle analysis and *Click-iT* detection of RNA and Protein synthesis. A) Cell-cycle analysis with PI staining of the nuclei after 48 h of treatment. Overnight serum starvation is shown as a positive control of induced cell cycle synchronization in G0/G1 phase. Cell phase analysis was done with ModFit LT 3.2 software by using the Sync Wizard model (30000 cells/sample in biological duplicate). B) Jurkat cells were treated for 48 h with or without (Mock) the indicated concentration of FK866 or for 3 h with 5 μM Actinomycin D, an RNA synthesis blocking agent, then subjected to *Click-it* biochemistry and flow-cytometry analyses including 7-AAD to identify living cells. C) Jurkat cells were treated for 48 h with or without (Mock) the indicated concentration of FK866 or for 3 h with 350 μM Cycloheximide, as a positive control for protein synthesis inhibition, then stained as in B. In B and C. Experiments were carried out on two biological replicates (50000 events/sample). (PDF 1562 kb)

Additional file 2: Luciferase assays. A) Light units, normalized to protein concentration, of RLuc-cMyc 5'UTR IRES-FLuc reporter vector transduced in Jurkat cells with lentiviral particles after 48 h of treatment with or without (Mock) the indicated concentration of FK866. Two hour treatment with 250 nM of Torin 1 served as a positive control for IRES-dependent protein translation (p-value <0.05). B) Light units, normalized to protein concentration, of FLuc-HCV-RLuc and FLuc-CrPV-RLuc reporter vectors transduced in Jurkat cells with lentiviral particles. Cap-dependent translation (FLuc) was strongly reduced with 5 nM and 100 nM FK866 (48 h) in comparison to Mock condition (p-value <0.0001). RLuc signal is not shown because of its low level and its variability between technical and biological replicates. Cells transduced with the pHR-SIN-F-HCV-R were serum starved for 5 h as a positive control of IRES activation, as shown in the graph (p-value <0.05). In A and B data are represented as mean and SD of three independent experiments. (PDF 584 kb)

Additional file 3: Effects of CHS-828 and chemotherapeutics on protein translation. A) Jurkat cells were treated for 48 h with or without (Mock) the indicated concentration of CHS-828. Caspase 3/7 activity was quantified (using 5 μM of Camptothecin for 4 h as a positive control of apoptosis) and relative ATP levels were determined and then normalized to the number of viable cells. The levels of total AMPK, p-AMPK, total EIF2A and p-EIF2A, total 4EBP1, p-4EBP1 were evaluated by WB. Histogram shows the densitometric analysis of p-AMPK and p-EIF2A (* indicates p-value <0.05). Mean and SD of a biological triplicate. B) Jurkat cells were treated with the indicated concentration of drugs for 48 h and cell viability was measured by Cell Titer Glo. Data are represented as mean and SD of three independent experiments. C) *Click-it* chemistry based on the incorporation of an aminoacid analog (AHA) was used to monitor protein synthesis. Jurkat cells were treated for 48 h with or without (Mock) the indicated concentration of FK866, Rapamycin (RAPA), Doxorubicin (DOXO), Cisplatin (CIS) and Dexamethasone (DEXA). The histogram quantifies the % of AHA positive cells (active protein-synthesizing cells) in the viable cell population. Flow-cytometry experiments were carried out on two biological replicates and statistics were based on acquisition of 20000 events/sample. D) Jurkat cells were treated as in C and the level of p-EIF2A and p-4EBP1 was evaluated. Histogram shows the densitometric analysis of p-EIF2A (* indicates p-value <0.05). Mean and SD of a biological triplicate. E) Primary B-CLL cells were treated for 48 h with or without 30 nM FK866 in the presence or absence of 1 mM NA. Histogram shows the densitometric analysis of p-AMPK/AMPK. (PDF 691 kb)

Additional file 4: Protective role of EIF2A. A) WB analysis indicated the levels of AMPK, p-AMPK, p-EIF2A, p-4EBP1 in H460 cells expressing LKB1 (LKB1 WT) or transduced with an empty vector (pBABE) treated or not (Mock) with 100 nM FK866 for 48 h, left panel. H460 cells were treated with indicated concentration of FK866 for 48 h and cell viability as shown in dose–response curve was evaluated by MTT assay, right panel. Mean and SD of three biological replicates. B) Jurkat viability after 48 h of treatment with FK866 5nM in un-transfected (NTC) cells and transfected with EIF2A wild type, EIF2A-S51A, EIF2A-S51D (mean and SD of three experiments,§, p-value < 0.1). (PDF 274 kb)

Abbreviations

4EBP1: Eukaryotic translation initiation factor 4E-binding protein 1; ACC: Acetyl-CoA carboxylase; AKT: v-akt murine thymoma viral oncogene homolog 1; AMPK: AMP-activated protein kinase; BCL-2: B-Cell lymphoma 2; B-CLL: B-cell chronic lymphocytic Leukemia; BiP: Glucose-regulated protein 78 kDa; EIF2A: Eukaryotic translation initiation factor 2A; EIF4E: Eukaryotic translation initiation factor 4E; EMT: Epithelial-mesenchymal transition; ERK: Mitogen-activated protein kinase; LKB1: Liver kinase B1; MCL1: Myeloid cell leukemia 1; MNK: MAP Kinase Interacting Serine/Threonine Kinase; MTOR: Mammalian target of rapamycin; NA: Nicotinic acid; NAD: Nicotinamide adenine dinucleotide; NAMPT: Nicotinamide phosphoribosyltransferase; T-ALL: T-cell acute lymphoblastic Leukemia; UPR: Unfolded protein response.

Competing interests

Authors declare no competing interests.

Authors' contributions

CZ and VGD carried out most of the experiments, participated in the study design and drafted the manuscript, AC cloned and produced viral vectors, BM, NT, DS, MC and IC helped with immunoassays and genetic experiments, AB, SI, AQ provided clinical samples and participated in the study design, AN and AP conceived the study, participated in its design and coordination and wrote the manuscript. All authors drafted, read and approved the final manuscript.

Acknowledgements

We thank Dr V. Adami, High Throughput Screening Facility, and I. Pesce, Cell Analysis and Separation Facility, University of Trento, Italy, for helpful support;

Dr Sabatini DM for shscramble pLKO based vector provided through Addgene and Dr Root DE for pLKO.1 - TRC cloning vector. The pBABE-LKB1 vector was received from Dr. Lewis Cantley through Addgene.

Financial support
AP and AN thank the Italian Ministry of Health grant GR-2008-1135635 and FP7 project PANACREAS #256986. AN thanks AIRC Start-Up grant #6108, Compagnia di San Paolo, Fondazione Umberto Veronesi, Fondazione CARIGE, Università di Genova. AP thanks the CIBIO start-up grant, University of Trento.

Author details
[1]Laboratory of Genomic Screening, CIBIO, University of Trento, Trento, Italy. [2]Laboratory of Molecular Virology, CIBIO, University of Trento, Trento, Italy. [3]Department of Internal Medicine, University of Genoa, Genoa, Italy. [4]Laboratory of Translational Networks, CIBIO, University of Trento, Trento, Italy. [5]Istituto Oncologico Veneto IOV-IRCCS, Padova, Italy.

Received: 15 April 2015 Accepted: 23 October 2015
Published online: 05 November 2015

References

1. Kroemer G, Pouyssegur J. Tumor cell metabolism: cancer's Achilles' heel. Cancer Cell. 2008;13(6):472–82.
2. Tan B, Young DA, Lu Z-H, Wang T, Meier TI, Shepard RL, et al. Pharmacological inhibition of nicotinamide phosphoribosyltransferase (NAMPT), an enzyme essential for NAD+ biosynthesis, in human cancer cells: metabolic basis and potential clinical implications. J Biol Chem. 2013;288(5):3500–11.
3. Revollo JR, Grimm AA, Imai S. The NAD biosynthesis pathway mediated by nicotinamide phosphoribosyltransferase regulates Sir2 activity in mammalian cells. J Biol Chem. 2004;279(49):50754–63.
4. Skokowa J, Lan D, Thakur BK, Wang F, Gupta K, Cario G, et al. NAMPT is essential for the G-CSF-induced myeloid differentiation via a NAD(+)-sirtuin-1-dependent pathway. Nat Med. 2009;15(2):151–8.
5. Xiao Y, Elkins K, Durieux JK, Lee L, Oeh J, Yang LX, et al. Dependence of Tumor Cell Lines and Patient-Derived Tumors on the NAD Salvage Pathway Renders Them Sensitive to NAMPT Inhibition with GNE-618. Neoplasia. 2013;15(10):1151–60.
6. Soncini D, Caffa I, Zoppoli G, Cea M, Cagnetta A, Passalacqua M, et al. Nicotinamide phosphoribosyltransferase promotes epithelial-to-mesenchymal transition as a soluble factor independent of its enzymatic activity. J Biol Chem. 2014;289(49):34189–204.
7. Wang B, Hasan MK, Alvarado E, Yuan H, Wu H, Chen WY. NAMPT overexpression in prostate cancer and its contribution to tumor cell survival and stress response. Oncogene. 2011;30(8):907–21.
8. Nakajima TE, Yamada Y, Hamano T, Furuta K, Gotoda T, Katai H, et al. Adipocytokine levels in gastric cancer patients: resistin and visfatin as biomarkers of gastric cancer. J Gastroenterol. 2009;44(7):685–90.
9. Montecucco F, Cea M, Cagnetta A, Damonte P, Nahimana A, Ballestrero A, et al. Nicotinamide phosphoribosyltransferase as a target in inflammation-related disorders. Curr Top Med Chem. 2013;13(23):2930–8.
10. Bruzzone S, Fruscione F, Morando S, Ferrando T, Poggi A, Garuti A, et al. Catastrophic NAD+ depletion in activated T lymphocytes through Nampt inhibition reduces demyelination and disability in EAE. PLoS One. 2009;4(11):e7897.
11. Zoppoli G, Cea M, Soncini D, Fruscione F, Rudner J, Moran E, et al. Potent synergistic interaction between the Nampt inhibitor APO866 and the apoptosis activator TRAIL in human leukemia cells. Exp Hematol. 2010;38(11):979–88.
12. Nahimana A, Attinger A, Aubry D, Greaney P, Ireson C, Thougaard AV, et al. The NAD biosynthesis inhibitor APO866 has potent antitumor activity against hematologic malignancies. Blood. 2009;113(14):3276–86.
13. Nencioni A, Cea M, Montecucco F, Longo VD, Patrone F, Carella AM, et al. Autophagy in blood cancers: biological role and therapeutic implications. Haematologica. 2013;98(9):1335–43.
14. Wosikowski K, Mattern K, Schemainda I, Hasmann M, Rattel B, Löser R. WK175, a novel antitumor agent, decreases the intracellular nicotinamide adenine dinucleotide concentration and induces the apoptotic cascade in human leukemia cells. Cancer Res. 2002;62(4):1057–62.
15. Christensen MK, Erichsen KD, Olesen UH, Tjørnelund J, Fristrup P, Thougaard A, et al. Nicotinamide phosphoribosyltransferase inhibitors, design, preparation, and structure-activity relationship. J Med Chem. 2013;56(22):9071–88.
16. Montecucco F, Cea M, Bauer I, Soncini D, Caffa I, Lasigliè D, et al. Nicotinamide phosphoribosyltransferase (NAMPT) inhibitors as therapeutics: rationales, controversies, clinical experience. Curr Drug Targets. 2013;14(6):637–43.
17. Cerna D, Li H, Flaherty S, Takebe N, Coleman CN, Yoo SS. Inhibition of nicotinamide phosphoribosyltransferase (NAMPT) activity by small molecule GMX1778 regulates reactive oxygen species (ROS)-mediated cytotoxicity in a p53- and nicotinic acid phosphoribosyltransferase1 (NAPRT1)-dependent manner. J Biol Chem. 2012;287(26):22408–17.
18. Del Nagro C, Xiao Y, Rangell L, Reichelt M, O'Brien T. Depletion of the Central Metabolite NAD Leads to Oncosis-mediated Cell Death. J Biol Chem. 2014;289(51):35182–92.
19. Ginet V, Puyal J, Rummel C, Aubry D, Breton C, Cloux A-J, et al. A critical role of autophagy in antileukemia/lymphoma effects of APO866, an inhibitor of NAD biosynthesis. Autophagy. 2014;10(4):603–17.
20. Settembre C, De Cegli R, Mansueto G, Saha PK, Vetrini F, Visvikis O, et al. TFEB controls cellular lipid metabolism through a starvation-induced autoregulatory loop. Nat Cell Biol. 2013;15(6):647–58.
21. Cea M, Cagnetta A, Fulciniti M, Tai Y-T, Hideshima T, Chauhan D, et al. Targeting NAD+ salvage pathway induces autophagy in multiple myeloma cells via mTORC1 and extracellular signal-regulated kinase (ERK1/2) inhibition. Blood. 2012;120(17):3519–29.
22. Hardie DG. The AMP-activated protein kinase pathway–new players upstream and downstream. J Cell Sci. 2004;117(Pt 23):5479–87.
23. Bowlby SC, Thomas MJ, D'Agostino RB, Kridel SJ. Nicotinamide phosphoribosyl transferase (Nampt) is required for de novo lipogenesis in tumor cells. PLoS One. 2012;7(6):e40195.
24. Schuster S, Penke M, Gorski T, Gebhardt R, Weiss TS, Kiess W, et al. FK866-induced NAMPT inhibition activates AMPK and downregulates mTOR signaling in hepatocarcinoma cells. Biochem Biophys Res Commun. 2015;458(2):334–40.
25. Wang P, Xu T-Y, Guan Y-F, Tian W-W, Viollet B, Rui Y-C, et al. Nicotinamide phosphoribosyltransferase protects against ischemic stroke through SIRT1-dependent adenosine monophosphate-activated kinase pathway. Ann Neurol. 2011;69(2):360–74.
26. Spriggs KA, Stoneley M, Bushell M, Willis AE. Re-programming of translation following cell stress allows IRES-mediated translation to predominate. Biol Cell. 2008;100(1):27–38.
27. Agnusdei V, Minuzzo S, Frasson C, Grassi A, Axelrod F, Satyal S, et al. Therapeutic antibody targeting of Notch1 in T-acute lymphoblastic leukemia xenografts. Leukemia. 2013;28(2):278–88.
28. D'Agostino VG, Adami V, Provenzani A. A novel high throughput biochemical assay to evaluate the HuR protein-RNA complex formation. PLoS One. 2013;8(8):e72426.
29. Zufferey R, Nagy D, Mandel RJ, Naldini L, Trono D. Multiply attenuated lentiviral vector achieves efficient gene delivery in vivo. Nat Biotechnol. 1997;15(9):871–5.
30. Sarbassov DD, Guertin DA, Ali SM, Sabatini DM. Phosphorylation and regulation of Akt/PKB by the rictor-mTOR complex. Science. 2005;307(5712):1098–101.
31. Moffat J, Grueneberg DA, Yang X, Kim SY, Kloepfer AM, Hinkle G, et al. A lentiviral RNAi library for human and mouse genes applied to an arrayed viral high-content screen. Cell. 2006;124(6):1283–98.
32. Sonenberg N, Hinnebusch AG. Regulation of translation initiation in eukaryotes: mechanisms and biological targets. Cell Elsevier Inc. 2009;136(4):731–45.
33. Cea M, Cagnetta A, Patrone F, Nencioni A, Golbbi M, Anderson KC. Intracellular NAD(+) depletion induces autophagic death in multiple myeloma cells. Autophagy. 2013;9(3):410–2.
34. Shi Y, Yan H, Frost P, Gera J, Lichtenstein A. Mammalian target of rapamycin inhibitors activate the AKT kinase in multiple myeloma cells by up-regulating the insulin-like growth factor receptor/insulin receptor substrate-1/phosphatidylinositol 3-kinase cascade. Mol Cancer Ther. 2005;4(10):1533–40.
35. Waskiewicz AJ, Flynn A, Proud CG, Cooper JA. Mitogen-activated protein kinases activate the serine/threonine kinases Mnk1 and Mnk2. EMBO J. 1997;16(8):1909–20.
36. Krishnamoorthy T, Pavitt GD, Zhang F, Dever TE, Hinnebusch AG. Tight binding of the phosphorylated alpha subunit of initiation factor 2 (eIF2alpha) to the regulatory subunits of guanine nucleotide exchange

factor eIF2B is required for inhibition of translation initiation. Mol Cell Biol. 2001;21(15):5018–30.
37. Zhang C-S, Jiang B, Li M, Zhu M, Peng Y, Zhang Y-L, et al. The Lysosomal v-ATPase-Ragulator Complex Is a Common Activator for AMPK and mTORC1, Acting as a Switch between Catabolism and Anabolism. Cell Metab. 2014;20(3):526–40.
38. Liu X, Chhipa RR, Nakano I, Dasgupta B. The AMPK inhibitor compound C is a potent AMPK-independent antiglioma agent. Mol Cancer Ther. 2014;13(3):596–605.
39. Wang S, Kaufman RJ. The impact of the unfolded protein response on human disease. J Cell Biol. 2012;197(7):857–67.
40. Cagnetta A, Cea M, Calimeri T, Acharya C, Fulciniti M, Tai Y-T, et al. Intracellular NAD$^+$ depletion enhances bortezomib-induced anti-myeloma activity. Blood. 2013;122(7):1243–55.
41. Dai RY, Zhao XF, Li JJ, Chen R, Luo ZL, Yu LX, et al. Implication of transcriptional repression in compound C-induced apoptosis in cancer cells. Cell Death Dis. 2013;4:e883.
42. Dagon Y, Avraham Y, Berry EM. AMPK activation regulates apoptosis, adipogenesis, and lipolysis by eIF2alpha in adipocytes. Biochem Biophys Res Commun. 2006;340(1):43–7.
43. Shackelford DB, Abt E, Gerken L, Vasquez DS, Seki A, Leblanc M, et al. LKB1 inactivation dictates therapeutic response of non-small cell lung cancer to the metabolism drug phenformin. Cancer Cell. 2013;23(2):143–58.
44. Shaw RJ, Kosmatka M, Bardeesy N, Hurley RL, Witters LA, DePinho RA, et al. The tumor suppressor LKB1 kinase directly activates AMP-activated kinase and regulates apoptosis in response to energy stress. Proc Natl Acad Sci U S A. 2004;101(10):3329–35.
45. Mills JR, Hippo Y, Robert F, Chen SMH, Malina A, Lin C-J, et al. mTORC1 promotes survival through translational control of Mcl-1. Proc Natl Acad Sci U S A. 2008;105(31):10853–8.
46. Zhou T, Li G, Cao B, Liu L, Cheng Q, Kong H, et al. Downregulation of Mcl-1 through inhibition of translation contributes to benzyl isothiocyanate-induced cell cycle arrest and apoptosis in human leukemia cells. Cell Death Dis. 2013;4:e515.
47. Fritsch RM, Schneider G, Saur D, Scheibel M, Schmid RM. Translational repression of MCL-1 couples stress-induced eIF2 alpha phosphorylation to mitochondrial apoptosis initiation. J Biol Chem. 2007;282(31):22551–62.
48. Pradelli LA, Bénéteau M, Chauvin C, Jacquin MA, Marchetti S, Muñoz-Pinedo C, et al. Glycolysis inhibition sensitizes tumor cells to death receptors-induced apoptosis by AMP kinase activation leading to Mcl-1 block in translation. Oncogene. 2010;29(11):1641–52.
49. Palam LR, Baird TD, Wek RC. Phosphorylation of eIF2 facilitates ribosomal bypass of an inhibitory upstream ORF to enhance CHOP translation. J Biol Chem. 2011;286(13):10939–49.
50. Cagnetta A, Caffa I, Acharya C, Soncini D, Acharya P, Adamia S, et al. APO866 Increases Antitumor Activity of Cyclosporin-A by Inducing Mitochondrial and Endoplasmic Reticulum Stress in Leukemia Cells. Clin Cancer Res. 2015;21(17):3934–45.
51. Fullwood MJ, Zhou W, Shenolikar S. Targeting phosphorylation of eukaryotic initiation factor-2α to treat human disease. Prog Mol Biol Transl Sci. 2012;106:75–106.
52. Dowling RJO, Zakikhani M, Fantus IG, Pollak M, Sonenberg N. Metformin inhibits mammalian target of rapamycin-dependent translation initiation in breast cancer cells. Cancer Res. 2007;67(22):10804–12.
53. Larsson O, Morita M, Topisirovic I, Alain T, Blouin M-J, Pollak M, et al. Distinct perturbation of the translatome by the antidiabetic drug metformin. Proc Natl Acad Sci U S A. 2012;109(23):8977–82.

www.impactjournals.com/oncotarget/ Oncotarget, Advance Publications 2016

The GSK3β inhibitor BIS I reverts YAP-dependent EMT signature in PDAC cell lines by decreasing SMADs expression level

Natthakan Thongon[1,*], Ilaria Castiglioni[2,*], Chiara Zucal[1], Elisa Latorre[1], Vito D'Agostino[1], Inga Bauer[3], Michael Pancher[4], Alberto Ballestrero[3], Georg Feldmann[5], Alessio Nencioni[3], Alessandro Provenzani[1]

[1]Laboratory of Genomic Screening, Centre for Integrative Biology, University of Trento, Trento, Italy

[2]Laboratory of Gene Expression and Muscular Dystrophy, San Raffaele Scientific Institute, Milan, Italy

[3]Department of Internal Medicine, University of Genoa, Genoa, Italy

[4]High Throughput Screening Facility, Centre for Integrative Biology, University of Trento, Trento, Italy

[5]Laboratory of Pancreatic Cancer Translational Research, Clinic University of Bonn, Bonn, Germany

[*]These authors have contributed equally to this work

Correspondence to: *Alessandro Provenzani,* ***e-mail:*** *alessandro.provenzani@unitn.it*

Keywords: *YAP, EMT, CTGF, PDAC, bisindolylmaleimides*

Received: *August 28, 2015* ***Accepted:*** *March 06, 2016* ***Published:*** *March 28, 2016*

ABSTRACT

The Yes-associated protein, YAP, is a transcriptional co-activator, mediating the Epithelial to Mesenchymal Transition program in pancreatic ductal adenocarcinoma (PDAC). With the aim to identify compounds that can specifically modulate YAP functionality in PDAC cell lines, we performed a small scale, drug-based screening experiment using YAP cell localization as the read-out. We identified erlotinib as an inducer of YAP cytoplasmic localization, an inhibitor of the TEA luciferase reporter system and the expression of the *bona fide* YAP target gene, Connective Tissue Growth Factor CTGF. On the other hand, BIS I, an inhibitor of PKCδ and GSK3β, caused YAP accumulation into the nucleus. Activation of β-catenin reporter and interfering experiments show that inhibition of the PKCδ/GSK3β pathway triggers YAP nuclear accumulation inducing YAP/TEAD transcriptional response. Inhibition of GSK3β by BIS I reduced the expression levels of SMADs protein and reduced YAP contribution to EMT. Notably, BIS I reduced proliferation, migration and clonogenicity of PDAC cells *in vitro*, phenocopying YAP genetic down-regulation. As shown by chromatin immunoprecipitation experiments and YAP over-expressing rescue experiments, BIS I reverted YAP-dependent EMT program by modulating the expression of the YAP target genes *E-cadherin*, *vimentin*, *CTGF* and of the newly identified target, *CD133*. In conclusion, we identified two different molecules, erlotinib and BIS I, modulating YAP functionality although *via* different mechanisms of action, with the second one specifically inhibiting the YAP-dependent EMT program in PDAC cell lines.

INTRODUCTION

The Yes-associated protein, YAP, is a transcriptional co-activator containing a proline-rich region responsible for the interaction with SH3 domains of c-Yes and many other proteins [1]. Multiple post-translational modifications (PTMs) regulate the functions of YAP. The Hippo signaling pathway, initially defined as a tissue growth and organ size regulator in *Drosophila*, is a kinase cascade able to negatively regulate YAP localization and activity, by phosphorylating YAP at Serine127. Phosphorylation of YAP by the Hippo pathway leads to its accumulation in the cytoplasm and, by interaction with 14–3–3 proteins, YAP is degraded by a ubiquitination-dependent proteasomal process. Therefore, the Hippo pathway negatively regulates YAP functionality and presence in the nucleus by modulating its cell distribution and its protein expression levels too. Importantly, the Hippo pathway-induced phosphorylation of YAP rules its functionality according to cell density. At low density,

YAP is predominantly localized in the nucleus while YAP translocates to the cytoplasm at high cell density [2]. Cytoplasmic YAP has been found associated with numerous protein complexes that mainly mediate its sequestration and consequent functional inactivation. As an example, Angiomotins recruit YAP to Tight Junctions or the actin cytoskeleton, in a Hippo pathway-independent manner, resulting in reduced YAP nuclear localization [3,4]. On the same line, when the WNT pathway is off, the association of YAP with beta-catenin leads to reciprocal inhibition of both proteins [5–7]. GSK3β inhibition by 6-bromoindirubin-30-oxime (BIO) promotes the activation of YAP *via* de-activation of the Hippo pathway [6]. Nuclear localization of YAP protein is associated with its co-transcriptional activity. However, YAP is at the crossroad of many signaling pathways, where it plays a role depending on the upstream stimuli and the binding to its multiple targets. Among the transcription factors bound to YAP, members of the TEAD family were found to be critical partners of YAP in the regulation of gene expression. CTGF has been identified as a direct target gene of YAP-TEAD in mammalian cells, and is crucial in mediating the growth-stimulating and oncogenic function of YAP-TEAD complex [8], but its transcriptional expression depends on the contribution from other YAP interacting transcription factors such as SMADs [9]. Additionally, many other transcription factors have been found associated with YAP such as p73 [10], showing that YAP can mediate oncosuppressive gene expression program according to the cell context. Several pieces of evidence support an important role of YAP in different types of cancer [11,12], pancreatic ductal adenocarcinoma (PDAC) included [13,14]. Indeed, YAP expression, *via* immunohistochemistry studies in pancreatic tumor tissues, was reported as moderate to strong in the nucleus and cytoplasm of the tumor cells compared to adjacent normal tissues. In cell lines, YAP localization was modulated by cell density and its genetic ablation led to a decrease of growth in soft agar of pancreatic cancer cells [12,13]. In PDAC mouse models, YAP has been shown to be an essential promoter of mutant KRAS oncogenic program, specifically inducing the expression of secreted factors as CTGF and CYR61 [15] and associating with FOS to regulate the expression of Epithelial to Mesenchymal Transition genes as *E-cadherin*, *SLUG*, *SNAIL* and *Vimentin* [16]. These pieces of evidence suggest a role of YAP in pancreatic cancer development, potentially playing an important role in the Epithelial to Mesenchymal Transition (EMT) of pancreatic cancer cells. Therefore, the identification of inhibitors of YAP activity could be suitable as a new therapeutic option for PDAC treatment.

However, an intricate network of signaling pathways contributes to EMT in PDAC. TGFβ signaling pathway is frequently genetically altered in PDAC [17], and the "late TGFβ signature" [18] actively promotes late EMT also cooperating with YAP [9] and activating the RAS-ERK pathway promoting the expression of EMT transcription factors such as SNAIL and ZEB1 [19]. CD133 is a well-known cancer stem marker [20] which has been included to the plethora of genes responsible for EMT promotion by activating SRC pathway [21–23].

We performed a small-scale high-content screening for the identification of compounds able to interfere with YAP localization and functionality. This approach allowed us to assign to the widely used Receptor Tyrosine Kinase (RTK) Inhibitor, erlotinib, the ability to sequester YAP into the cytoplasm blocking its co-transcriptional function. Additionally, we found that a small molecule, GF 109203X (BIS I), induces YAP nuclear accumulation and activation, however, modulating its co-transcriptional activity by blocking the YAP-dependent EMT program downregulating SMAD2/3.

RESULTS

YAP regulates anchorage-independent growth in PDAC cell lines

We measured the expression level of YAP in a panel of four PDAC cell lines using western blotting and qRT-PCR: PANC1 and PK9 exhibited moderate to high YAP protein levels, respectively, in comparison to BXPC3 and MIAPACA2 cells (Figure 1A). Cell density regulates phosphorylation and localization of YAP *via* the Hippo signaling pathway. High cell density predicts a cytoplasmic YAP localization while YAP appears mainly localized in the nucleus in sparse cell culture of breast cancer cells [24]. We investigated whether cell density regulates YAP localization in pancreatic cancer cells. We assessed the expression level and localization of YAP at different cell densities using immunofluorescence in PK9 and PANC1 cells. Sub-cellular distribution of YAP protein was equivalent in both cases with PANC1 cells, but YAP significantly shuttled from nucleus to the cytoplasm at high cell density in PK9 cells, as determined by high content imaging analysis (Figure 1B). To investigate the functional role of YAP, we interfered YAP expression in PK9 and PANC1 cells using lentiviral transduction of specific shRNA (Supplementary Figure S1A). shYAP-PANC1 and shYAP-PK9 cells showed a decrease of 90% and 40% of YAP mRNA compared to (SCR) control cells, respectively (Figure 1C). *CTGF* and *Cyr61* mRNA expression, *bona fide* YAP targets, were significantly reduced in shYAP-PANC1 and shYAP-PK9 (Figure 1C), whereas other targets like *AREG* and *BIRC5* were distinctly up-regulated in silenced cells, indicating a transcriptional impact due to YAP modulation. On the other hand, *CTGF* expression was found increased in the case of YAP overexpression (O/E) both in PK9 and in PANC1. *CYR61* expression was increased in PK9 O/E YAP. (Figure 1D). Phenotypically, both YAP stable silencing (shYAP) and its transient functional ablation inhibited anchorage-independent

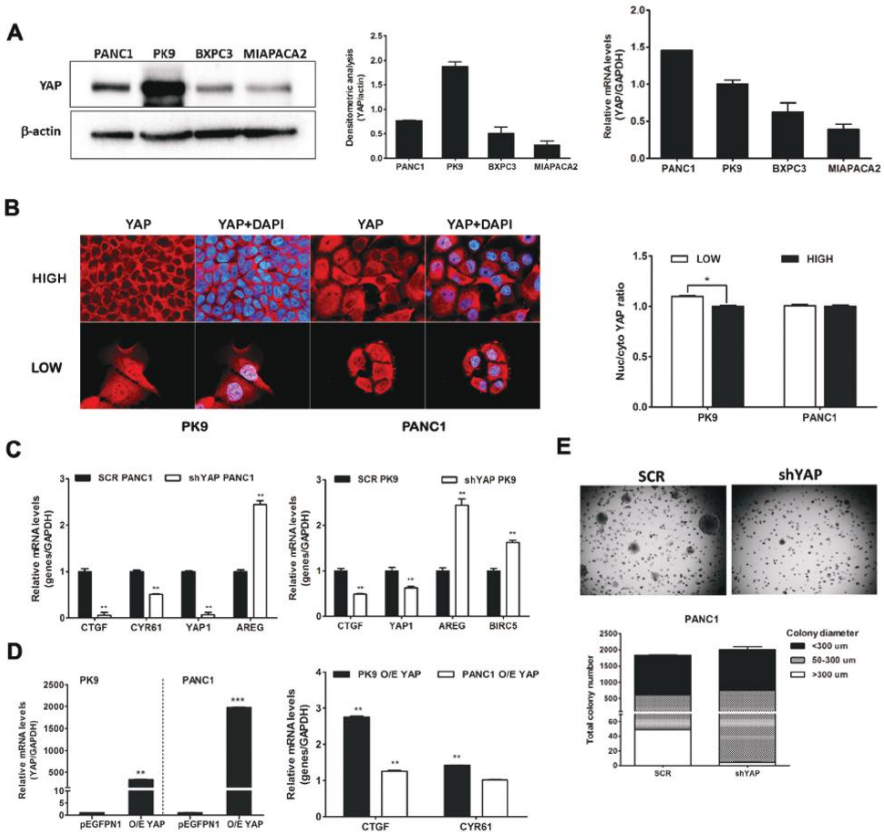

Figure 1: Importance of YAP in PDAC cell lines. A. YAP is expressed in PDAC lines at different levels. Western blot analysis of endogenous level of YAP in PDAC cell lines and qRT-PCR analysis of YAP mRNA expression. The relative intensity of the bands (left) and YAP mRNA level (right) are shown. **B. Localization of YAP is regulated by cell density in PK9.** PK9 and PANC1 cells were cultured sparsely (LOW) and densely (HIGH) onto glass cover slides (Left panel) and in 96 well-plate (right panel) for 48H. Cells were fixed and nuclei were counterstained with DAPI. The localization of YAP was visualized using a Zeiss Observer Z1 microscope equipped with Apotome module, with a Plan Apochromatic (63X, NA 1.4) objective. Images were acquired using Zen 1.1 (blue edition) imaging software (Zeiss) and assembled with Adobe Photoshop CS3 (Left panel). Quantitative analysis of sub-cellular localization of YAP was quantified using Operetta instrument and Harmony 3.5.2 software. Ratio of YAP Nuc/Cyto is shown. (*p<0.05). **C. YAP functional ablation down-regulates *CTFG* and *CYR61* but not *AREG* and *BIRC5* mRNA levels.** PANC1 (left) and PK9 cells (right) were stably transduced with a lentiviral vector encoding shRNA targeting YAP or a non-targeting control shRNA (SCR). After stable selection with puromycin, the relative levels of endogenous *YAP* and its target genes, *CTGF*, *CYR61*, *AREG* and *BIRC5* mRNA were measured by qRT-PCR (mean±SD). (**P<0.0, **P<0.01 versus SCR). **D. Overexpression of YAP increases *CTGF* and *CYR61* levels in PK9 cells.** PK9 and PANC1 cells were transiently transfected with pEGFP-YAP or empty vector (pEGFPN1) for 24H. Overexpression of YAP was confirmed by qRT-PCR analyses. The expression levels of *CTGF* and *CYR61* were then evaluated. **E. YAP functional ablation attenuates anchorage-independent growth in soft agar.** PANC1 cells were stably transduced with a lentiviral vector encoding shRNA targeting YAP or a non-targeting control shRNA (SCR). These clones ($1.5x10^4$ cells) were seeded in 0.35% agar (top agar) medium in 6 well-plates coated with 0.7% agar (based agar) for 2 weeks. Total colony number and colony diameter were measured using Operetta and Harmony 3.5.2 software (below).

growth of PANC1 cells in soft agar (Figure 1E) and slowed their proliferation rate (Supplementary Figure S1B), in good agreement with previous data [14, 25]. Therefore, in PDAC cell lines cultured at high-density, YAP is partially redistributed in the cytoplasm, it has a transcriptional effect controlling the expression of known target genes, it regulates proliferation and the ability of PDAC cells to grow in anchorage-independent conditions.

Identification of modulators of YAP localization

To gain further insight into the molecular players regulating YAP localization, we performed a small-scale nucleo-cytoplasmic high content assay to quantify YAP protein subcellular localization in PDAC cells. As a cell model, we used PK9 cells as YAP was re-localizing into the cytoplasm at high cell density (Figure 1B). We used a library of 80 characterized kinase inhibitors (see methods) with the aim to find molecules that could modulate accumulation of YAP in the cytoplasm or the nucleus, to identify the signaling cascade responsible for these subcellular re-localizations and the biological effects caused by its sub-cellular re-distribution. Most of the molecules did not affect YAP localization being the Z-score values of the nuclear/cytoplasmic intensity close to controls (Figure 2A, Table 1, Supplementary Table S1). Few compounds were further increasing cytoplasmic YAP compared to control, and only two compounds led to significant YAP accumulation into the nucleus. Interestingly, first hits among YAP cytoplasmic accumulators were inhibitors of tyrosine kinase receptors (RTKIs) such as Genistein and Tyrphostins and one inhibitor of the RAS pathway as ZM336372. On the other hand, inducers of YAP nuclear shuttling were BIS I and Ro 31-8220, two representatives of the bisindolylmaleimide family of Ser/Thr kinase inhibitors, as PKCs (Table 1).

Cytoplasmic inducers marginally modulate YAP co-transcriptional activity

As the receptor tyrosine kinase inhibitors identified belong to the family of tyrphostin [26], precursors of the more potent and clinically used inhibitors of RTKIs, such as erlotinib and lapatinib, we decided to use these two drugs for further investigation. Moreover, given the importance of the constitutive activation of the RAS pathway in PDAC [27], we also evaluated the efficacy of ZM336372 in inhibiting YAP-dependent transcriptional effects by using TEA luciferase reporter system as a readout. Only erlotinib inhibited modestly, but significantly, TEA reporter and reduced the expression level of *CTGF* but with no efficacy on *Cyr61* (Figure 2B, 2C). On the contrary, lapatinib and ZM336372 increased *CTGF* and *Cyr61* expression levels (Figure 2C). Summing up, only erlotinib showed a minimal, although significant, negative modulation of YAP co-transcriptional activity.

BIS I changes YAP co-transcriptional activity and inhibits anchorage independent growth

Bisindolylmaleimide chemical family of compounds are strong inhibitors of several kinases in the nanomolar range and, therefore, it is difficult to associate a molecular target directly to its efficacy. BIS I is a cell-permeable and reversible inhibitor of protein kinases C (PKCs) both conventional and atypical, but also of GSK3β [28]. Moreover, compounds of the same class show differential selectivity towards the same serine/threonine kinases. For example, Go9676 was reported to be more specific for PKCα than for PKCδ [29], while BIS I behaves oppositely [30]. Since bisindolylmaleimides are fluorescent compounds and could have interfered with the immunofluorescence-based screening, we performed nuclear/cytoplasmic separation and Western blots analyzes of YAP levels upon drug treatments. We observed that BIS I induced YAP nuclear localization in PDAC cell lines, confirming the indication coming from the HCS experiment (Figure 2D). Then we evaluated the stability of YAP protein during BIS I treatment, and, in the time frame of 48 hours, YAP protein was stable, suggesting that we observed a pure subcellular re-localization not affected by changes in protein expression level (Supplementary Figure S1C). During re-localization, the YAP post-translation status was deeply changed, as many phosphorylation spots were present in the two-dimensional western blots (Figure 2E). Hippo signaling pathway was not directly involved in the observed PTMs because the phosphorylation state of YAP-S127 and LATS-S909 did not change (Figure 2F). Additionally, we observed a decrease in the expression level of LATS protein, an effect that is likely independent of the activation of the Hippo signaling but might contribute to the translocation of YAP into the nucleus. BIS I amplified TEA reporter signal in the basal conditions in PANC1 cells and during YAP overexpression both in PK9 and PANC1 cells (Figure 3A) and induced TEA reporter signal reduction during functional ablation of YAP. Therefore, the effect of BIS I on TEA reporter depends on the presence of YAP (Figure 2B, 3A). Unexpectedly, BIS I significantly suppressed *CTGF* and *Cyr61* mRNA expression and slightly increased *AREG* and *BIRC5* mRNA expression in PK9 and PANC1 cells at 24 hours of treatment, mimicking YAP ablation (Figure 3B). To evaluate if BIS I displaces YAP from *CTGF* promoter, despite YAP presence in the nucleus, we performed chromatin immunoprecipitation of YAP and evaluated the amplification of the *CTGF* promoter [31]. Indeed, YAP was no more associated with the *CTGF* promoter during BIS I treatment, but TEAD1 was still present (Figure 3C). Additionally, we observed that BIS I inhibited TGF-β induced *CTGF* expression in a YAP independent manner but activated TEA reporter in a TGF-β independent manner (Figure 4A and Supplementary Figure S1D). BIS I treatment reduced

the expression level of *SMAD2/3* mRNAs and proteins in a YAP independent manner (Figure 4A, Figure 4B, Supplementary Figure S1E). BIS I phenocopied the effects of YAP functional ablation: it slowed down cell proliferation and induced an accumulation in the S-phase (Supplementary Figure S1B, S1F). Most importantly, BIS I was readily effective in reducing the anchorage-independent growth of PDAC cell lines. Among the four cell lines tested, PANC1 and MIAPACA2 formed colonies within two weeks, while PK9 took longer and we could not detect BXPC3 colony formation. BIS I reduced the total number of colonies of PANC1, MIAPACA2, and PK9 and reduced the colony dimensions of PANC1 and PK9 but increasing MIAPACA2 ones (Figure 4C). Summing up,

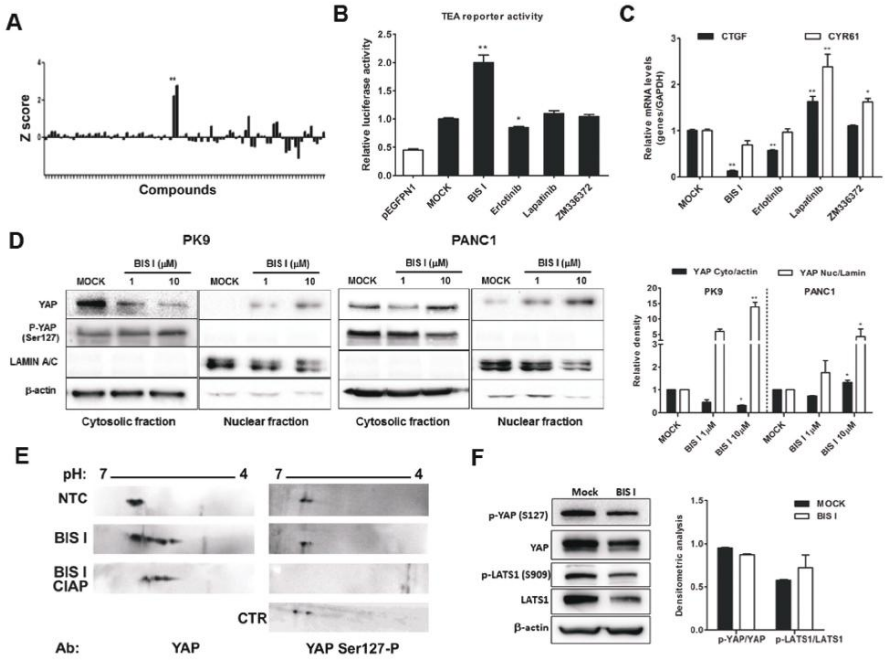

Figure 2: Identification of modulators of YAP localization. A. High-content screening evaluating YAP localization. A kinase inhibitor's library was administrated to PK9 cells using a high-throughput approach (1μM, 24H). The ratio between nuclear and cytoplasmic regions was calculated and normalized to untreated controls. The Z-score was reported in a graph, positive and negative values indicate nuclear accumulation and cytoplasmic localization, respectively. Fixed cells were incubated with antibody against YAP and DAPI staining. Sub-cellular localization of endogenous YAP protein was detected by Operetta and analyzed with Harmony 3.5.2 software. **B. Modulation of TEA reporter by hit compounds.** PK9 cells were transiently co-transfected with pEGFPN1 or YAP, TEA reporter (8xGTIIC-Luc reporter), and *Renilla* luciferase to record YAP/TAZ-dependent transcriptional activity. Cells were then treated with different compounds for 24 H and the firefly luciferase signals were normalized to the ones of *Renilla* luciferase. Data are globally normalized to MOCK and are presented as mean±SD. **C. Modulation of *CTGF* and *CYR61* by hit compounds.** The panel represent qRT-PCR for YAP/TAZ target genes *CTGF* and *Cyr61*, relative to *GAPDH* expression. PK9 cells were treated with 5μM of different compounds and data, normalized to MOCK, are presented as mean±SD. (*p<0.05 and **p<0.01). **D. BIS I induces YAP nuclear accumulation.** Western blot analysis of nuclear fraction and cytosolic fraction of YAP in PK9 and PANC1 cell lines after treatment with 1μM and 10μM of BIS I for 24H. The relative intensities of the bands are also shown (right). Data are normalized to MOCK and presented as mean±SD. (*p<0.05 and **p<0.01). **E. BIS I induces YAP post-translational modifications.** Filters were blotted with antibodies against YAP and YAP Ser127-P. As negative control for phosphorylation the treated sample was incubated with calf intestinal alkaline phosphatase (CIAP). As positive control for phosphorylation at Ser127, cell lysates from high density culture was used. **F. BIS I does not affect the Hippo pathway.** Western blot analysis of an upstream regulator of YAP, LATS1 and its phosphorylated form (Ser909). PK9 cells were treated with BIS I 10μM for 24 H. Phosphorylation of YAP and LATS1 was measured by western blot. The relative intensities of the bands were normalized to β-actin levels (right).

Table 1: Hits from High-Content Screening

Z-score	Molecule	Molecular Target
YAP Nuclear Accumulators		
0.915	GF 109203X	PKC
0.971	Ro 31-8220	PKC
YAP Cytoplasmic Accumulators		
1.382	Tyrphostin AG 1295	Tyrosine kinases
1.355	ZM 336372	cRAF
1.238	Genistein	Tyrosine Kinases
1.182	N9-Isopropyl-olomoucine	CDK
1.18	SP 600125	JNK
1.171	AG-1296	PDGFRK
1.169	Kenpaullone	GSK3β
1.132	AG-494	EGFRK, PDGFRK

Lower values indicate higher nuclear accumulation, higher values indicate higher cytoplasmic accumulation

BIS I induced YAP into the nucleus and triggered TEAD response; however, it inhibited anchorage-independent cancer cell growth and proliferation, phenocopying YAP ablation and inhibiting TGFβ-dependent cell response by decreasing the expression of SMADs and SMAD/YAP co-regulated genes.

CD133 gene expression is regulated by YAP and inhibited by BIS I

To further investigate the molecular mechanism of bisindolylmaleimides leading to YAP nuclear accumulation, we evaluated four of them for their ability to modulate *CTGF* expression levels. BIS I and BIS II reduced *CTGF* expression in PK9 and PANC1 cells, although to a different extent, while Go9676 increased *CTGF* expression. BIS IV showed an increase of *CTGF* expression only in PK9 cells with no activity in the other cell lines (Supplementary Figure S2A). None of the bisindolylmaleimides tested showed toxic effects (Supplementary Figure S2B). Given the relative specificity of BIS I for PKCδ/GSK3β, while Go9676 is more specific for PKCα, we hypothesized that PKCδ/GSK3β ablation could phenocopy BIS I treatment. Transient silencing of PKCδ and GSK3β showed that *CTGF* decreased in both cases linking the activity of these two kinases in *CTGF* expression regulation (Figure 4D, Supplementary Figure S2C). Short-term treatment with the GSK3β inhibitor LiCl induced the expression of *CTGF* mRNA, but long-term treatment decreased *CTGF* expression [32]. Interestingly, the downregulation of *SMAD2* mRNA occurred only at a late time point whereas *SMAD3* was already down-regulated at 6 hours (Supplementary Figure S2D). BIS I induced the downregulation of both *SMADs* already at 6 hours. Silencing of GSK3β activated TEA reporter only in the presence of YAP overexpression, similarly to BIS I treatment (Supplementary Figure S2E) and reduced the expression of *SMAD3* mRNA (Figure 4E) as BIS I treatment. Since the association of YAP to the destruction complex has been reported [5], we evaluated the activation of the WNT/β-catenin signaling in PDAC cell lines during BIS I treatment. We performed a reporter assay with a construct expressing luciferase under the control of tandem repeats of TCF binding site (TOPFlash) or a mutated one (FOPFlash). BIS I strongly activated WNT/β-catenin reporter activity in all of the PDAC cell lines used and in HEK293T cells (Figure 5A, Supplementary Figure S2F) as well as induced the accumulation of β-catenin in the nucleus (Figure 5B). Coherently, Go9676 did not activate TCF/LCF reporter nor induced β-Catenin into the nucleus (Figure 5A, 5B).

Given the importance of YAP and β-Catenin in regulating differentiation, we investigated if BIS I could affect the expression levels of stemness markers of PDAC. In our case, pancreatic stemness gene *CD133* was up-regulated upon β-Catenin over-expression (Figure 5C). These stemness genes were down-regulated during BIS I treatment (Figure 5D), but, interestingly, only *CD133* was affected by YAP and GSK3β ablation (Figure 5E and 5F). Moreover, YAP overexpression induced the up-regulation of *CD133* that was blocked by BIS I (Figure 5G), therefore identifying *CD133* as a new gene regulated by YAP and GSK3β. To sum up, BIS I induced YAP and β-Catenin nuclear accumulation by inhibiting the PKCδ/GSK3β pathway. Moreover, BIS I treatment decreased the level of cancer stem cell markers, but only the effect on *CD133* could be ascribed to a loss of YAP functionality. Notably, this gene is a new critical regulator of EMT in PDAC [21,23].

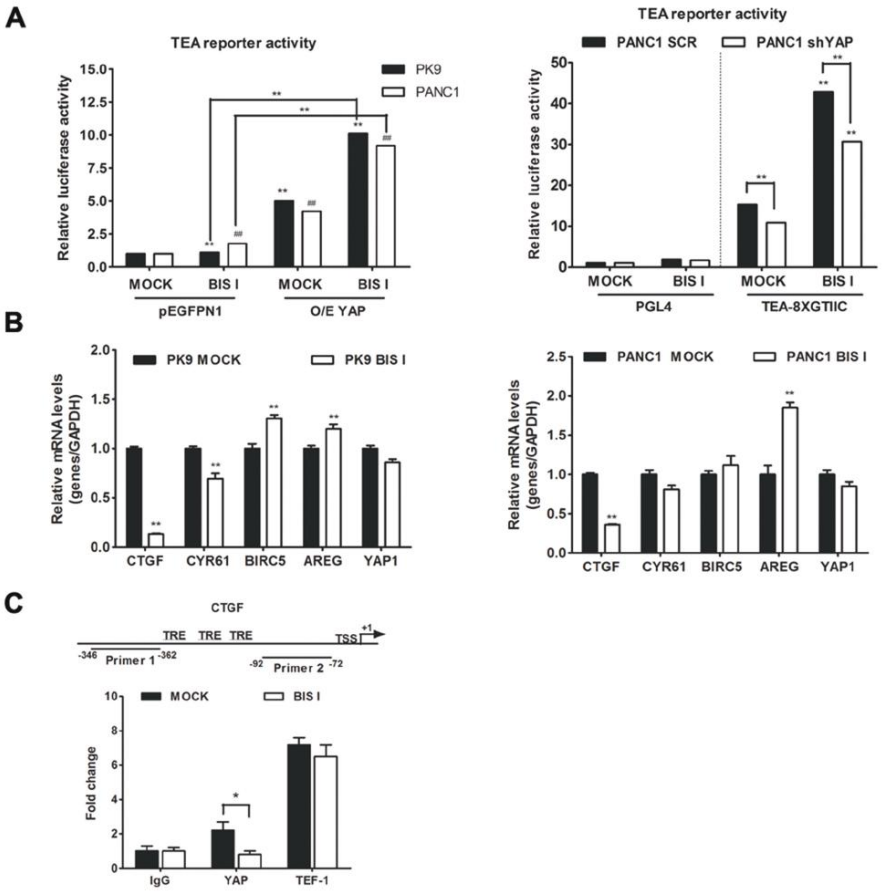

Figure 3: BIS I treatment phenocopies YAP functional ablation. A. BIS I modulates TEA reporter in YAP-dependent manner. Left panel: BIS I activates TEA reporter activity. PK9 and PANC1 cells were transiently co-transfected with YAP (O/E YAP) or without YAP (pEGFPN1) and TEA reporter (8xGTIIC-Luc reporter), then treated with BIS I 5μM for 24H. Right panel: YAP is required for TEA reporter activation. Stably YAP silenced PANC1 cells were co-transfected with TEA reporter (8xGTIIC-Luc reporter) or its empty vector (pGL4), and *Renilla*. The firefly luciferase signals were normalized to the ones of *Renilla.* (mean±SD from biological triplicates) (*p<0.05 and **p<0.01 versus MOCK of PK9 and #p<0.05 and ##p<0.01 versus MOCK of PANC1). **B. BIS I modulates YAP target genes.** PK9 (left panel) and PANC1 (right panel) cells were treated with 5μM BIS I for 24H. Quantitative RT-PCRs of *CTGF*, *Cyr61*, *BIRC5*, *AREG*, YAP/TAZ target genes and *YAP* relative to *GAPDH* expression with respect to MOCK are presented as mean±SD. (*p<0.05 and **p<0.01 versus MOCK). **C. BIS I displaces YAP from CTGF promoter.** Map of CTGF promoter region with positions of the two primers used for ChIP analysis. TSS indicates the transcription start site, while TRE indicate the previously identified TEAD responsive elements. Chromatin immunoprecipitation (ChIP) at CTGF promoter was performed using antibodies against YAP, TEF-1 and IgG as negative control. After DNA extraction and qRT-PCR, results were normalized to non immunoprecipitated sample (INPUT) and compared to IgG for statistical significance. BIS I was able to reduce the DNA enrichment observed for YAP, whereas it was ineffective against TEF-1 DNA-binding protein.

YAP-dependent EMT transcriptional program is inhibited by BIS I

EMT signature, in PDAC, in mainly driven by the activation of the RAS pathway in association with the transcriptional program induced by FOS, SMADs, and YAP [16] and the loss of E-cadherin is a major event during EMT [22]. Our cell lines exhibit different expression levels of E-cadherin (Figure 6A, 6B). PK9 and BxPC3 cell lines showed high protein level of E-cadherin whereas PANC1 and MIAPACA2 had low to undetectable E-cadherin protein levels (Figure 6A). This expression profile of E-cadherin in PDAC is consistent with its mRNA levels (Figure 6B). Our results show that endogenous levels of E-cadherin are inversely correlated with the anchorage-independent growth ability of these PDAC cell lines (Figure 4C). Importantly, EMT signature was dependent on YAP as, in shYAP-PK9 and shYAP-PANC1, E-cadherin and CD133 expression was reverted (Figure 6C, Figure 5E, 5G). During BIS I treatment, the clonogenic and migration abilities of

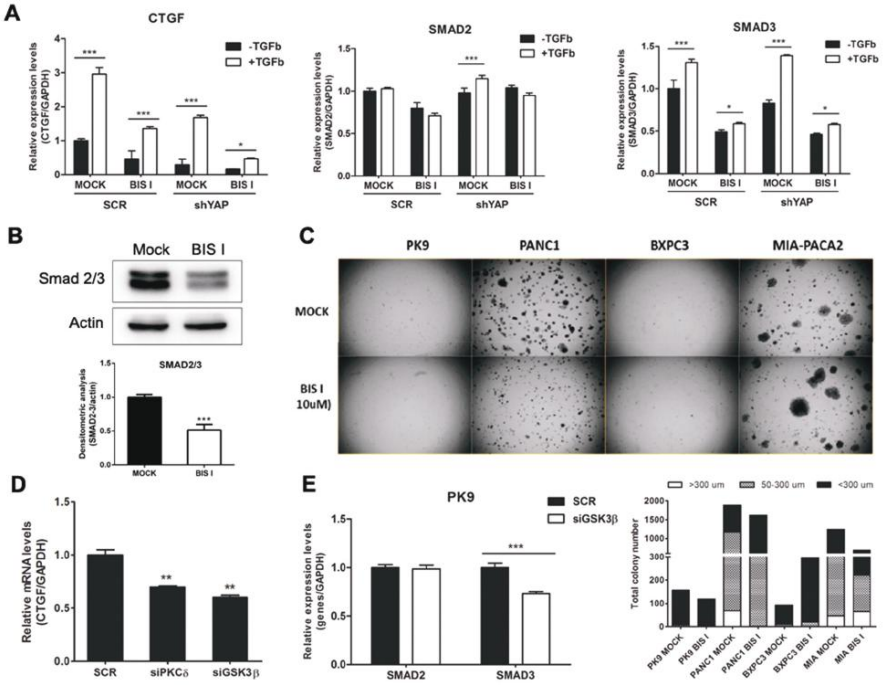

Figure 4: The CTGF expression level was modulated by the TGF-β and Hippo pathways in PDAC. A. BIS I inhibits TGF-β induced *CTGF* expression and reduces *SMAD2/3* gene expression levels. PK9 cells were stably transduced with a lentiviral vector encoding shRNA targeting YAP (shYAP) or a non-targeting control shRNA (SCR). They were then treated with BIS I 5μM in the presence and absence of TGF-β 50ng/ml for 24H. The expression levels of *CTGF, SMAD2* and *SMAD3* were then evaluated. (*p<0.05 and ***p<0.001 versus MOCK). **B. BIS I down-regulated Smad2/3 protein levels.** PK9 cells were seeded and treated with BIS I 10μM for 24H. The endogenous protein level of Smad2/3 was evaluated by western blotting against Smad2/3 antibody. The relative intensities of the bands normalized by β-actin are shown below. (***p<0.001 versus MOCK). **C. BIS I inhibits anchorage-independent growth of PDAC.** PDAC ($1.5x10^4$ cells) were seeded on 0.35% agar (top agar) culture medium in 6 well-plated coated with 0.7% agar (based agar). Cells were treated with BIS I 10μM for 2 weeks. Total colony number and colony diameter were measured using Operetta instrument. **D. The CTGF expression level was modulated by PKCδ and GSK3β in PK9 cells.** PK9 cells were incubated with siRNA targeting PKCδ, GSK3β, and non-targeting control (SCR) for 72H. Quantitative RT-PCRs of *CTGF* relative to *GAPDH* expression with respect to SCR are presented as mean+SD. (*p<0.05 and **p<0.01 versus SCR). **E. Genetic ablation of GSK3β suppresses SMAD expression levels in PK9.** PK9 cells were incubated with siRNA targeting GSK3β, and non-targeting control (SCR) for 72H. Quantitative RT-PCRs of *CTGF* relative to *GAPDH* expression with respect to SCR are presented as mean+SD. (***p<0.01 versus SCR).

PDAC, markers of EMT, were completely inhibited (Figure 4C, 7A). BIS I was able to revert the EMT signature by restoring E-Cadherin expression, as well as by regulating other EMT markers as *vimentin*, *ZEB1* and *CD133* also in the presence of TGFβ (Figure 5G, 7B, 7C, 7D). Migration of PANC1 cells decreased by administration of BIS I in sh-YAP PANC1 cells at 48 hours (Figure 7A). More notably, the effect of BIS I on the modulation of *CTGF, E-cadherin, vimentin,* and *CD133* was rescued by YAP overexpression showing that BIS I mechanism of action

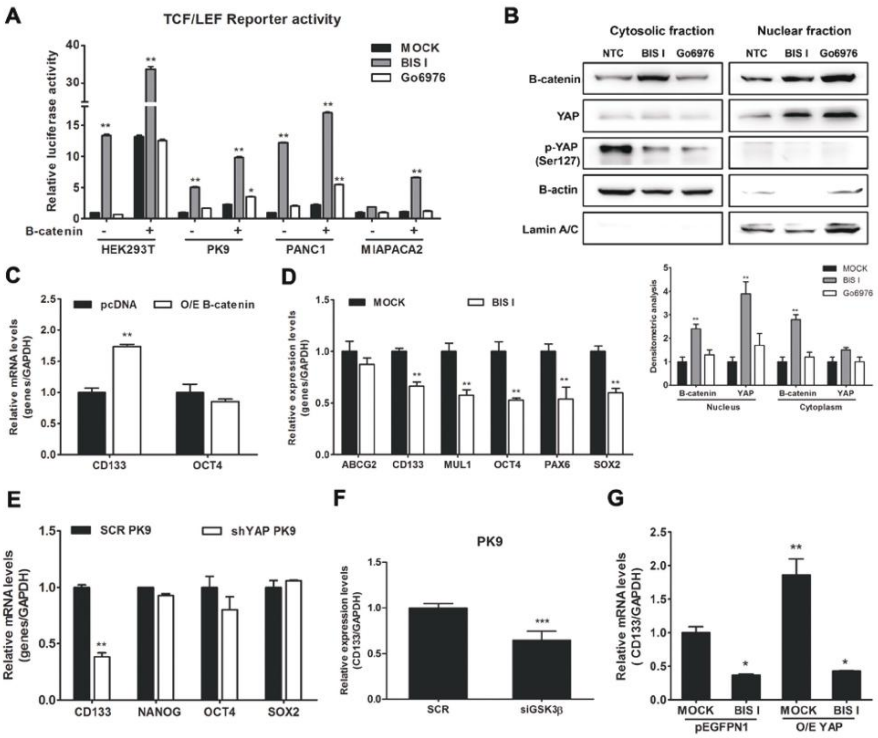

Figure 5: BIS I activates β-catenin and downregulates the expression level of cancer staminality genes. A. BIS I activates β-catenin signaling pathway. β-catenin induced activation of TOP-flash (TCF/LEF) luciferase reporter was performed in HEK293T and PDAC cells lines. Cells were co-transfected with TOP-flash luciferase reporter and in the presence and absence of β-catenin. BIS I and Go6976 5μM were used for 24H treatment after transfection. Data are presented as average fold induction relative to MOCK. (*p<0.05 and **p<0.01). **B. BIS I modulates β-catenin nuclear localization.** Western blot analysis of nuclear fraction and cytosolic fraction of β-catenin in PK9 cells after treatment with BIS-I and Go6976 10μM for 24H. The relative intensities of the bands are shown below. The relative intensities of the bands was normalized by β-actin and lamin A/C for cytosolic and nuclear protein levels, respectively. **C. β-catenin regulates CD133 expression.** PK9 cells were transiently transfected with indicated β-catenin plasmid for 24H. Quantitative RT-PCRs of *CD133* and *OCT4* relative to *GAPDH* expression with respect to MOCK are presented as mean±SD. (*p<0.05 and **p<0.01). **D. BIS I inhibits expression of staminality markers in PK9.** PK9 cells were treated with BIS I 5μM for 24H and expression levels of *ABCG2*, *CD133*, *MUL1*, *OCT4*, *PAX6*, and *SOX2* were analyzed by qRT-PCR relative to *GAPDH* expression. Data are presented as mean±SD. (**p<0.01 versus MOCK). **E. Genetic ablation of YAP down-regulates CD133 expression.** Stemness markers were measured by qRT-PCR in stably YAP silenced PK9 cells. Data are presented as mean±SD. (**p<0.01 versus SCR). **F. Genetic ablation of GSK3β down-regulates CD133 expression.** PK9 cells were incubated with siRNA targeting GSK3β, and non-targeting control (SCR) for 72H. Quantitative RT-PCRs of *CD133* relative to *GAPDH* expression with respect to SCR are presented as mean±SD. (***p<0.01 versus SCR). **G. BIS-I treatment reverts the CD133 up-regulation induced by YAP overexpression.** PK9 cells were transiently co-transfected with indicated plasmids (YAP and pEGFPN1) and in the presence and absence of BIS I treatment for 24H. *CD133* expression was measured by qRT-PCR. Data are presented as mean±SD. (*p<0.05 and **p<0.01 versus MOCK).

relies on the inhibition of the EMT-related, YAP-dependent transcriptional program (Figure 5G, 7D). In sum, we show that BIS I inhibits EMT in PDAC cell lines triggering the expression of epithelium markers by down-regulating SMAD2/3 and blunting YAP co-transcriptional activity.

DISCUSSION

In this study, we show that BIS I, an inhibitor of the PKCδ/GSK3β pathway, reverts the EMT transcriptional program in PDAC cell lines inhibiting the TGFβ pathway and de-potentiating YAP contribution to EMT *via* down-regulation of SMAD2/3.

In agreement with previous reports [14,33,34], we observed that, in PDAC cell lines, YAP mainly regulates anchorage-independent growth, migration, and proliferation. However, YAP governs the expression of only some of the *bona fide* YAP target genes in these cell lines as only *CTGF* and *CYR61*, but not *AREG* or *BIRC5*, decreased during YAP functional ablation. Indeed, in a KRAS mutant context, YAP, being post-translationally modulated by KRAS/MAPK signaling cascade, promotes

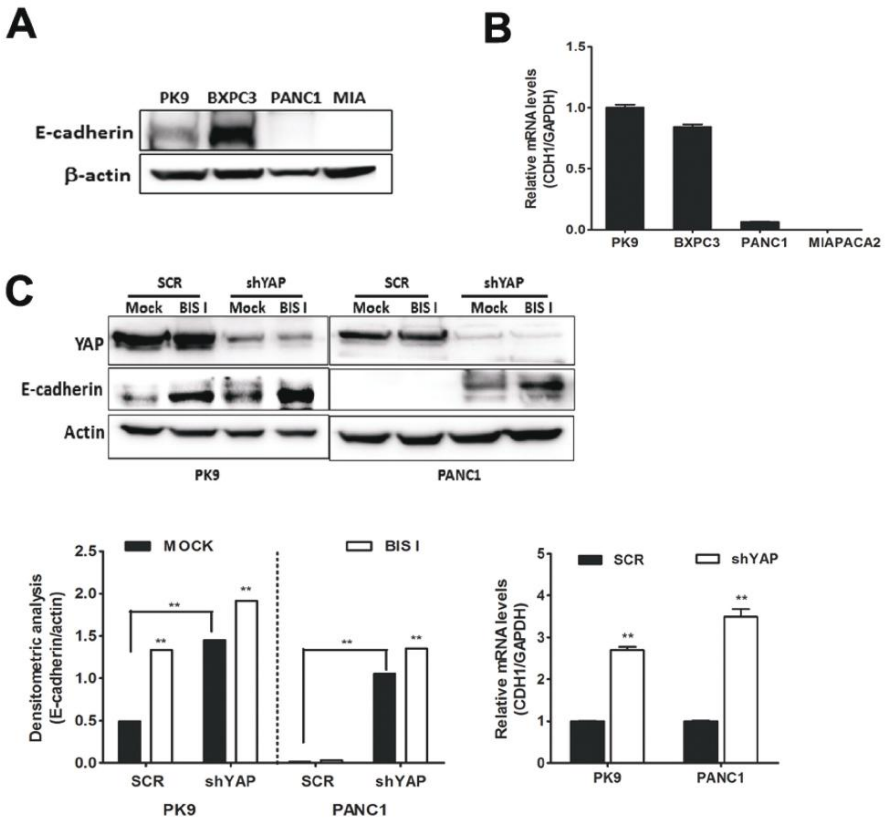

Figure 6: BIS I reverts YAP-induced EMT in PDAC cell lines. A. Endogenous protein level of E-cadherin in PDAC cell lines. Western blot analysis of endogenous level of E-cadherin in PDAC cell lines. **B. Expression level of E-cadherin mRNA in PDAC cell lines.** qRT-PCR analysis of *CDH1* mRNA expression was performed in PDAC cell lines. **C. Both genetic ablation of YAP and BIS I treatment induce E-cadherin expression levels.** SCR or stably YAP-silenced PK9 and PANC1 cells were treated with BIS I 5μM for 24H. Western blot analysis of endogenous level of YAP and E-cadherin was performed. The relative levels of endogenous E-cadherin protein (left) and mRNA levels from these lysates (right) were evaluated by immunoblot and qRT-PCR, as shown below.

the expression of pro-proliferative secretory factors as *CTGF* and *CYR61*, preferentially [15]. From our small-scale screening of kinase inhibitors, using as reporter system the localization of the endogenous YAP protein, we found out that general inhibitors of RTKs and one RAS inhibitor induced YAP accumulation into the cytoplasm. This finding suggests a functional link between the EGFR and RAS pathway and YAP activity as observed in *Drosophila* [35], liver carcinoma [36], NSCLC cells [37] and pancreas itself [16]. Unfortunately, none of these inhibitors was potent enough to inhibit TEA reporter system and decrease *CTGF* expression, suggesting that the residual amount of nuclear YAP was still active. Only erlotinib showed a small but significant trend towards inhibition of YAP co-transcriptional activity. Indeed, erlotinib arrests NRG1-ERBB4-YAP signaling in breast cancer cell lines [38], and suggests a further rationale for the utilization of erlotinib in PDAC [39]. Additionally, we found of interest the behavior of YAP nuclear accumulators, i.e. bisindolylmaleimides. The mechanistic explanation can be linked to the pleiotropic effect of BIS I. One possibility is that BIS I induced arrest of the proteasome leading to accumulation of β-catenin [40, 41] and YAP, being both proteins targeted for degradation. Alternatively, the BIS I induced inhibition of PKCδ/GSK3β activity can lead to the degradation of the destruction complex as proved by β-catenin and YAP nuclear accumulation. Inhibition of the GSK3β by BIS I led to osteogenic differentiation and suppression of adipocyte differentiation by β-catenin stabilization [42, 43]. More importantly, these data are in agreement with the inhibition of the GSK3β by BIO that led to the activation of YAP/TEAD response [6]. We did not observe a clear inactivation of the Hippo pathway but a down-regulation

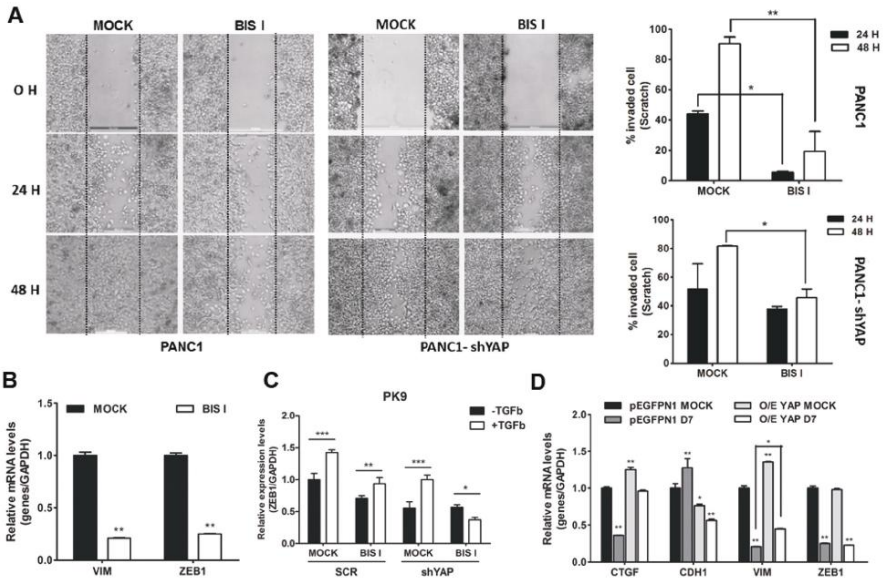

Figure 7: Genetic ablation of YAP and BIS I treatment regulate cell migration. A. BIS I reduces cell migration synergizing with YAP silencing. Scratch assay was performed in SCR or stably YAP-silenced PANC1 cells. Images of invaded cells at 0, 24, and 48 H after scratching and treatment with BIS I were taken from a time-lapse sequence of PANC1 cell migration; wounds with consistent shape within each well were generated using 200 µl tip. Percentage of invaded cells at different time point is indicated (right panels) as calculated by ImageJ softwre. (*p<0.05 and **p<0.01). **B. BIS I down-regulates *VIM* and *ZEB1* mRNAs.** PK9 cells were treated with BIS I for 24H. Expression level of *VIM* and *ZEB1* were measured by qRT-PCR. Data are presented as mean±SD. (**p<0.01 versus MOCK). **C. BIS I inhibits TFG-β induced ZEB1 expression.** PK9 cells were stably transduced with a lentiviral vector encoding shRNA targeting YAP (shYAP) or a non-targeting control shRNA (SCR). They were then treated with BIS I 5µM in the presence and absence of TGF-β 50ng/ml for 24H. The expression levels of *ZEB1* was evaluated. (*p<0.05, **p<0.01 and ***p<0.001). **D. Overexpression of YAP reverts the effect of BIS-I on the expression of *CTGF*, *CDH1* and *VIM*.** PK9 cells were transiently co-transfected with YAP and pEGFPN1 plasmids and treated with BIS I for 24H. *CTGF*, *CDH1*, *VIM*, and *ZEB1* expression levels were measured by qRT-PCR. Data are presented as mean±SD. (*p<0.05 and **p<0.01).

of LATS that explains the nuclear translocation of YAP, also in an independent manner from the association to the destruction complex [6]. Indeed, we observed the activation of the TEA reporter system during BIS I treatment, but, at the same time, a clear, YAP-dependent, decrease of *CTGF* and *CYR61* mRNAs. *CTGF* promoter region is highly regulated, and several transcription factors contribute to the activation of this locus. In mesangial and gingival cells, BIS I blockage of basal and TGFβ-induced regulation of *CTGF* [44,45] was explained by inhibition of GSK3β. Moreover, in hepatocarcinoma cells, PKCδ-mediated TGFβ signaling led to *CTGF* expression by inhibiting the phosphatase PPM1A, which is responsible for the SMAD2/3 inactivation [46]. Downregulation of *CTGF* upon functional ablation of PKCδ and GSK3β highlights that the similar mechanisms occur in PDAC cell lines (Figure 4D) and can be explained by *SMAD3* mRNA downregulation (Figure 4E). GSK3β inhibition by LiCl induces a biphasic *CTGF* expression regulation: an initial burst of expression, coherent with YAP nuclear accumulation, is followed by a long-term downregulation of the gene. This secondary response is likely due to the parallel downregulation of *SMAD2/3* (Supplementary Figure S2D, S2E). BIS I down-regulated *CTGF* and *SMAD2/3* already at 6 hours, therefore showing a strong potency in blocking TGFβ in a *SMAD4* deficient context, a frequent lesion in PDAC [47] and our cell lines. The same mechanism applies to YAP/SMADs co-regulated genes and, given the importance of this association in promoting EMT [48], it explains the specific reversion of EMT markers. Therefore, the down-regulation of SMADs dampens the YAP co-transcriptional activity of EMT genes. Indeed, YAP overexpression rescued phenotypically the ability to migrate and grow in anchorage-independent condition, and, molecularly, it inhibited the re-expression of E-cadherin and blunted the downregulation of *CTGF*, *CD133,* and *Vimentin*. Additionally, we showed that BIS I induced displacement of YAP from *CTGF* promoter, showing a loss of function of nuclear YAP on specific genes, likely driven by the loss of SMADs partner. Finally, we observed that BIS I induced the downregulation of many cancer stem genes, CD133 included, and we found that this new marker of EMT is highly regulated as YAP, GSK3β, and β-catenin modulated CD133 expression, addressing this gene as a co-regulated gene by these three factors. Further experiments are necessary to clarify this point. However, it suggests that inhibition of the SRC pathway *via* dasatinib [23,49] may influence EMT in PDAC by modulating YAP activity.

MATERIALS AND METHODS

Antibodies, plasmids and reagents

The following antibodies were used: Anti-YAP (sc-101199), anti TEF-1 (sc-376113), Anti-GSK3β (sc-9166), Anti phospho GSK3β Ser9 (sc-11757), Anti β-catenin (sc-7199) (Santa Cruz Biotechnology). Anti-Lats1 (3477), Anti-phospho Lats1 Ser909 (9157), Anti-Smad2/3 (8685) and Anti-phospho-YAP (S127) (4911), Anti β-actin (3700) (Cell Signaling). Alexa Fluor 488-conjugated secondary antibodies (Invitrogen). The chemicals were used in this study: GF 109203X (B6292), Go6976 (G1171), phorbol 12-myristate 13-acetate (PMA) (Sigma, P1585) were purchased from sigma. Lapatinib (S1028), Erlotinib (S1023) were purchased from Selleckchem. Recombinant human transforming growth factor 1 (TGF-β) (PHG9204) was purchased from Life technologies. The plasmids were used: 8xGTIIC-luciferase (#34615), YAP-GFP (12), pEGFP-N1 (Clontech), pGL4 (Promega), human B-catenin pcDNA3 (#16828), c-Flag pcDNA3 (#20011), TOP flash and FOP flash were gifted from Dr. Arthit [50].

Cell culture and transfections

Human pancreatic carcinoma cell lines (PK9, MIAPACA2, PANC1, BxPC3) were kindly provided by G. Feldmann [12] and HEK293T were cultured at 37°C in high glucose Dulbecco's modified Eagle's medium (DMEM) supplemented with 10% Fetal bovine serum (FBS) (Invitrogen), 1X vitamin solution (Sigma), 1X non-essential amino-acid solution (NEAA, Biosource), 1X Sodiumpyruvate (Gibco) and 1X Penicillin-Streptomycin (LONZA) in a humidified incubator with 5% CO2. Transfections were carried out in 6 or 24 well-plates using Lipofectamine 3000 kit (Life Techonologies) as described by the manufacturer. siRNAs for knockdown of PKCδ (sc-36253) and GSK3β (sc-35527) and control siRNA (sc-37007) were transfected using INTERFERIN siRNA transfection reagent (Polyplus transfection) according to manufacturer's protocol. After 72 h of incubation, proteins were extracted for analysis by western blot analysis as describe below.

Lentriviral particles production and stable clones selection

To generate shYAP expressing stable PK9 and PANC1 cells, The pLKO.1-based lentiviral plasmid containing YAP shRNA (NM006106) expression cassettes were purchased from Sigma-Aldrich. Scramble shRNA (Addgene plasmid 1864) was used as a control. Vectors were produced in HEK293T cells by co-transfection of the different transfer vectors with the packaging plasmid pCMV-deltaR8.91 and the VSV envelope-coding plasmid pMD2.G. After transfection (48h), lentiviral supernatant was filtered through a 0.45 μm syringe filter and used to infect YAP into PK9 and PANC1 cells by spinning them down with vector containing supernatants for 90 min at 1500xg at room temperature and leaving them incubate overnight at 37°C, then the fresh medium were replaced the transduction supernatant. Cells were then further

incubated for 72H before collection for WB. Stable silent cells were selected using 3 μg/ml puromycin (Sigma) in the culture medium.

Immunofluorescence staining and drug screening

PK9 and PANC1 cells were cultured sparsely (LOW) and densely (HIGH) onto glass cover slides and in 96 well-plate for 48 H. Cells were fixed and localization of YAP was visualized and nuclei were counterstained with DAPI. Immunofluorescence analysis was performed using a Zeiss Observer Z1 microscope equipped with Apotome module, with a Plan Apochromatic (63X, NA 1.4) objective. Images were acquired using Zen 1.1 (blue edition) imaging software (Zeiss) and assembled with Adobe Photoshop CS3. Drug screening, PK9 cells were seeded on OptiPlate-96 Black, Black Opaque 96-well Microplate (PerkinElmer) at a density of 5000 cells/well, to obtain a 70% confluence at the end of the assay. The library of known kinase inhibitors was re-suspended in DMSO and diluted in PBS 1X. The compounds were administrated at the final concentration of 1μM for 24H. Cells were fixed as previously described [52], primary antibody against YAP (1:500) and secondary fluorophore conjugated (Alexa 488) antibody (1:10000) were diluted in PBS + BSA 0.2%. DAPI (1.5 μg/ml) in PBS + BSA 0.2% was used to detect nuclei. PerkinElmer image plate reader Operetta was used for imaging and evaluation. The ratio between nuclear and cytoplasmic signal represents the mean of single cells for every well and it were normalized to untreated control. The Z score was calculated to evaluate the significance of results from the screening. Z score was calculated as follow: Z = (X–mean)/standard deviation. X = normalized sample ratio [51].

Soft-agar and cell migration assay

Each 6-well plate was coated with 1 ml of bottom agar (DMEM containing 10% FBS with and 0.7% agar). PDAC cell lines, shYAP expressing stable PANC-1 (1.5x104 cells) were resuspended in 1ml of top agar (DMEM containing 10% FBS with and 0.35% agar) into each well. Cells were treated with 1ml of BIS I and incubated for 2-3 weeks. They were replaced with fresh medium with/without treatment every 3 days. PerkinElmer image plate reader Operetta was used for imaging and colony evaluation.

Cell migration assay. Confluent cells were seeded in 6-well plate and wounded by a 200μl pipette tip. Media were replaced with BIS I treatment. Images of the same field were acquired immediately (0h), after 24 and 48 hours using a Leica DM IL Led microscope (5X magnification). Wounded-open areas were photographed and measured at the time of scratch and 2 days. Relative invaded area was measured using Image-J software.

Western blot and sub-cellular fractionation

Cells were treated for 24H then they were lysed in cold modified cytosolic lysis buffer (10mM HEPES pH 7.0, 10mM KCl, 1mM EDTA, 0.5% NP-40, 1mM DTT, and Protease inhibitor cocktail). The supernatant containing cytosolic fraction was collected by centrifugation at 3000xg for 5 minutes at 4°C. Nuclear pellets were then re-suspended in cold modified nuclear lysis buffer (10mM HEPES pH 7.0, 400mM NaCl, 1mM EDTA, 25% Glycerol, 1mM DTT, and Protease inhibitor cocktail). The nuclear extract was harvested by centrifugation at 12000xg for 15 minutes at 4°C. Equal quantities of proteins were separated by electrophoresis on a 12% SDS-page gels. The blots were incubated with YAP1, Phospho-YAP-1 (Ser127), β-catenin antibodies overnight at 4°C. β-actin and Lamin A/C served as the loading controls for the cytosolic and nuclear fraction, respectively.

Luciferase reporter assay. HEK293T, PK9 and PANC1 were seeded in 24 well-plates then indicated plasmids were co-transfected using Lipofectamine 3000 (Invitrogen) or TransIT-LT1 Transfection Reagent (Mirus). After transfection (24H), cells were treated with BIS family compounds including GF 109203X or BIS I (5μM), Go6976 (5μM), Erlotinib (5μM), Lapatinib (5 μM), and PMA (1 μM) for 24H. Cells were lysed and luciferase activity was assayed using the enhanced luciferase assay kit (Promega) following the manufacturer's instructions. The firefly luciferase activity levels were measure and normalized to Renilla luciferase activity.

RNA isolation, real-time PCR and ChIP assay

Total RNA was extracted using RNA isolation Mini Kit (Agilent Technologies and successively treated with RNA-free DNase. RNA was subjected for reverse transcription (RT) with iScript reverse transcriptase (Bio-rad). cDNA was then diluted and 50ng total of cDNA was used for qRT-PCR with gene-specific primers using KAPA SYBR FAST qPCR master mix (Kapa biosystem) or HOT FIREPol EvaGreen qPCR Mix (Solis BioDyne). Relative abundance of mRNA was calculated by normalization to GAPDH mRNA. The reactions were carried out on a CFX96TM real-time system (BIO-RAD). For ChIP assay, DNA was extracted by phenol/chloroform/isoamyl alcohol, ethanol precipitated and re-suspended in water. In mRNA expression experiments, Ct values of every gene were normalized to the housekeeping GAPDH, while in ChIP assays, the normalization were calculated by the following formula: (X–IgG)/INPUT, where X is the Ct of the sequence of interest derived from the immunoprecipitated DNA bound to the protein of interest; IgG is the Ct of the same sequence derived from the DNA immunoprecipitated with an irrelevant antibody and INPUT is the Ct derived from the total DNA

before immunoprecipitation. Primers for quantitative real time PCR (for ChIP assay) were obtained from MWG/Operon, with the following sequences: Forward: 5′ TTGGTGCTGGAAATACTGCG 3′, Reverse: 5′ CTCA GCGGGGAAGAGTTGTT 3′. Other primers used in this work are listed in Supplementary Table S2.

Cell cycle and real-time cell proliferation assay

Cells were incubated in a 96-well plate (200 ul of medium/well) with the tested compounds for 24H and cell viability was quantitatively determined by a colorimetric MTT assay. In brief, MTT (5mg/ml) at 10% volume of culture media was added to each well and cells were further incubated for 2H at 37°C. Then supernatant containing MTT was replaced by 100µl of DMSO to dissolve formazan. Absorbance was then determined at 565nM by microplate reader. Cell survival was calculated and EC50 values were determined. Cell cycle was measured by FACS analysis at 24H after treatment using propidium iodide (PI) staining. Real time cell proliferation assay: PK9 were seeded 5000 cells/well in E-plates (Roche), in triplicates. The cell growth curves were automatically recorded on the xCELLigence System (Roche) in real time. The cell attachment was monitored every 15 minutes by a cell electronic system. The doubling times were calculated according with cell index. The cell index is an arbitrary unit for displaying inpedence. SCR or siRNAs transfection PK9 cells were performed by replacing cell medium, including untreated control to operate at the same working conditions.

Two-dimensional electrophoresis

The experiment was performed according to previous protocols [52]. Proteins were extracted using a lysis buffer (8M urea, 4% CHAPS, 50mM dithioerythritol and 0,0002% Bromophenol blue) and rehydrated with 8M urea, 2% CHAPS, 20mM dithioerythritol, 0.8% IPG buffer, carrier ampholytes pH 6-11 linear. The first dimension isoelectric focusing (IEF) was performed in immobiline dry strips (GE) with a pH range from 7 to 4. IEF was performed on IPGphor (GE) according to the manufacturer recommendations. The gels were then equilibrated in 6M urea, 3% SDS, 375mM Tris pH 8.6, 30% glycerol, 2% DTE and then incubated with 3% iodoacetamide (IAA) and traces of bromophenol blue (BBP). The second dimension was performed using an 8% SDS-PAGE gel. Transfer and detection were carried out as previously described.

Statistical analysis

The Data are presented as mean±SD and the standard deviation of the mean (SD) in this study were calculated for 3 replicates in each of the 3 independent experiments. Statistical comparisons were assessed with analysis of Student's test and One-way ANOVA calculated with GraphPad Prism version 5.0 for Windows (GraphPad Software). $P<0.05$ was considered statistically significant difference and $P<0.01$, and $P<0.001$ were considered as highly significant difference.

ACKNOWLEDGMENTS

We thank Dr Arthit Chairoungdua for providing us the plasmids for β-catenin experiments.

CONFLICTS OF INTEREST

The authors disclose no conflicts of interest.

GRANT SUPPORT

The research leading to these results has received funding from the European Community's Seventh Framework Programme [FP7-2007-2013] under grant agreement n° HEALTH-F2-2011-256986–project acronym PANACREAS to AP, AN and GF, and from Ministero della Salute (GR-2008-1135635) to AN, AP.

REFERENCES

1. Sudol M. Yes-associated protein (YAP65) is a proline-rich phosphoprotein that binds to the SH3 domain of the Yes proto-oncogene product. Oncogene. 1994;9:2145–52.
2. Zhao B, Wei X, Li W, Udan RS, Yang Q, Kim J, et al. Inactivation of YAP oncoprotein by the Hippo pathway is involved in cell contact inhibition and tissue growth control. Genes Dev. 2007;21:2747–61.
3. Zhao B, Li L, Lu Q, Wang LH, Liu C-Y, Lei Q, et al. Angiomotin is a novel Hippo pathway component that inhibits YAP oncoprotein. Genes Dev. 2011;25:51–63.
4. Chan SW, Lim CJ, Chong YF, Pobbati A V, Huang C, Hong W. Hippo pathway-independent restriction of TAZ and YAP by angiomotin. J Biol Chem. 2011;286:7018–26.
5. Azzolin L, Panciera T, Soligo S, Enzo E, Bicciato S, Dupont S, et al. YAP/TAZ incorporation in the β-catenin destruction complex orchestrates the Wnt response. Cell. 2014;158:157–70.
6. Cai J, Maitra A, Anders RA, Taketo MM, Pan D. β-Catenin destruction complex-independent regulation of Hippo-YAP signaling by APC in intestinal tumorigenesis. Genes Dev. 2015;29:1493–506.
7. Park J, Jeong S. Wnt activated β-catenin and YAP proteins enhance the expression of non-coding RNA component of RNase MRP in colon cancer cells. Oncotarget. 2015;6:34658–68. doi: 10.18632/oncotarget.5778.
8. Zhao B, Ye X, Yu J, Li L, Li W, Li S, et al. TEAD mediates YAP-dependent gene induction and growth control. Genes Dev. 2008;1962–71.

9. Fujii M, Toyoda T, Nakanishi H, Yatabe Y, Sato A, Matsudaira Y, et al. TGF-β synergizes with defects in the Hippo pathway to stimulate human malignant mesothelioma growth. J Exp Med. 2012;209:479-94.
10. Strano S, Monti O, Pediconi N, Baccarini A, Fontemaggi G, Lapi E, et al. The transcriptional coactivator Yes-associated protein drives p73 gene-target specificity in response to DNA Damage. Mol Cell. 2005;18:447–59.
11. Camargo FD, Gokhale S, Johnnidis JB, Fu D, Bell GW, Jaenisch R, et al. YAP1 increases organ size and expands undifferentiated progenitor cells. Curr Biol. 2007;17:2054–60.
12. Dong J, Feldmann G, Huang J, Wu S, Zhang N, Comerford SA, et al. Elucidation of a universal size-control mechanism in Drosophila and mammals. Cell. 2007;130:1120–33.
13. Guo J, Kleeff J, Zhao Y, Li J, Giese T, Esposito I, et al. Yes-associated protein (YAP65) in relation to Smad7 expression in human pancreatic ductal adenocarcinoma. Int J Mol Med. 2006;17:761–7.
14. Diep CH, Zucker KM, Hostetter G, Watanabe A, Hu C, Munoz RM, et al. Down-regulation of Yes Associated Protein 1 expression reduces cell proliferation and clonogenicity of pancreatic cancer cells. PLoS One. 2012;7:e32783.
15. Zhang W, Nandakumar N, Shi Y, Manzano M, Smith A, Graham G, et al. Downstream of mutant KRAS, the transcription regulator YAP is essential for neoplastic progression to pancreatic ductal adenocarcinoma. Sci Signal. 2014;7:ra42.
16. Shao DD, Xue W, Krall EB, Bhutkar A, Piccioni F, Wang X, et al. KRAS and YAP1 converge to regulate EMT and tumor survival. Cell. 2014;158:171–84.
17. Jones S, Zhang X, Parsons DW, Lin JC-H, Leary RJ, Angenendt P, et al. Core signaling pathways in human pancreatic cancers revealed by global genomic analyses. Science. 2008;321:1801–6.
18. Coulouarn C, Factor VM, Thorgeirsson SS. Transforming growth factor-beta gene expression signature in mouse hepatocytes predicts clinical outcome in human cancer. Hepatology. 2008;47:2059–67.
19. Neuzillet C, de Gramont A, Tijeras-Raballand A, de Mestier L, Cros J, Faivre S, et al. Perspectives of TGF-β inhibition in pancreatic and hepatocellular carcinomas. Oncotarget. 2014;5:78–94. doi: 10.18632/oncotarget.1569.
20. Grosse-Gehling P, Fargeas CA, Dittfeld C, Garbe Y, Alison MR, Corbeil D, et al. CD133 as a biomarker for putative cancer stem cells in solid tumours: limitations, problems and challenges. J Pathol. 2013;229:355–78.
21. Nomura A, Banerjee S, Chugh R, Dudeja V, Yamamoto M, Vickers SM, et al. CD133 initiates tumors, induces epithelial-mesenchymal transition and increases metastasis in pancreatic cancer. Oncotarget. 2015;6:8313–22.doi: 10.18632/oncotarget.3228.
22. Nagathihalli NS, Merchant NB. Src-mediated regulation of E-cadherin and EMT in pancreatic cancer. Front Biosci (Landmark Ed). 2012;17:2059–69.
23. Ding Q, Miyazaki Y, Tsukasa K, Matsubara S, Yoshimitsu M, Takao S. CD133 facilitates epithelial-mesenchymal transition through interaction with the ERK pathway in pancreatic cancer metastasis. Mol Cancer. 2014;13:15.
24. Kim N, Koh E, Chen X, Gumbiner BM. E-cadherin mediates contact inhibition of proliferation through Hippo signaling-pathway components. Proc Natl Acad Sci U S A. 2011;108:11930-5.
25. Shen Z, Stanger BZ. YAP regulates S-phase entry in endothelial cells. PLoS One. 2015;10:e0117522.
26. Levitzki A, Mishani E. Tyrphostins and other tyrosine kinase inhibitors. Annu Rev Biochem. 2006;75:93–109.
27. Almoguera C, Shibata D, Forrester K, Martin J, Arnheim N, Perucho M. Most human carcinomas of the exocrine pancreas contain mutant c-K-ras genes. Cell. 1988;53:549–54.
28. Hers I, Tavaré JM, Denton RM. The protein kinase C inhibitors bisindolylmaleimide I (GF 109203x) and IX (Ro 31-8220) are potent inhibitors of glycogen synthase kinase-3 activity. FEBS Lett. 1999;460:433–6.
29. Kinehara M, Kawamura S, Tateyama D, Suga M, Matsumura H, Mimura S, et al. Protein kinase C regulates human pluripotent stem cell self-renewal. PLoS One. 2013;8:e54122.
30. Brehmer D, Godl K, Zech B, Wissing J, Daub H. Proteome-wide identification of cellular targets affected by bisindolylmaleimide-type protein kinase C inhibitors. Mol Cell Proteomics. 2004;3:490–500.
31. Zhang H, Liu C-Y, Zha Z-Y, Zhao B, Yao J, Zhao S, et al. TEAD transcription factors mediate the function of TAZ in cell growth and epithelial-mesenchymal transition. J Biol Chem. 2009;284:13355–62.
32. Deng Y-Z, Chen P-P, Wang Y, Yin D, Koeffler HP, Li B, et al. Connective tissue growth factor is overexpressed in esophageal squamous cell carcinoma and promotes tumorigenicity through beta-catenin-T-cell factor/Lef signaling. J Biol Chem. 2007;282:36571–81.
33. Overholtzer M, Zhang J, Smolen G a, Muir B, Li W, Sgroi DC, et al. Transforming properties of YAP, a candidate oncogene on the chromosome 11q22 amplicon. Proc Natl Acad Sci U S A. 2006;103:12405–10.
34. Hall CA, Wang R, Miao J, Oliva E, Shen X, Wheeler T, et al. Hippo pathway effector Yap is an ovarian cancer oncogene. Cancer Res. 2010;70:8517–25.
35. Reddy BVVG, Irvine KD. Regulation of Hippo signaling by EGFR-MAPK signaling through Ajuba family proteins. Dev Cell. 2013;24:459–71.
36. Urtasun R, Latasa MU, Demartis MI, Balzani S, Goñi S, Garcia-Irigoyen O, et al. Connective tissue growth factor autocriny in human hepatocellular carcinoma: oncogenic role and regulation by epidermal growth factor receptor/yes-associated protein-mediated activation. Hepatology. 2011;54:2149–58.

37. You B, Yang Y-L, Xu Z, Dai Y, Liu S, Mao J-H, et al. Inhibition of ERK1/2 down-regulates the Hippo/YAP signaling pathway in human NSCLC cells. Oncotarget. 2015;6:4357–68. doi: 10.18632/oncotarget.2974.

38. Haskins JW, Nguyen DX, Stern DF. Neuregulin 1-activated ERBB4 interacts with YAP to induce Hippo pathway target genes and promote cell migration. Sci Signal. 2014;7:ra116.

39. Wang JP, Wu C-Y, Yeh Y-C, Shyr Y-M, Wu Y-Y, Kuo C-Y, et al. Erlotinib is effective in pancreatic cancer with epidermal growth factor receptor mutations: a randomized, open-label, prospective trial. Oncotarget. 2015;6:18162–73. doi: 10.18632/oncotarget.4216.

40. Orford K, Crockett C, Jensen JP, Weissman AM, Byers SW. Serine phosphorylation-regulated ubiquitination and degradation of beta-catenin. J Biol Chem. 1997;272:24735–8.

41. Easwaran V, Song V, Polakis P, Byers S. The ubiquitin-proteasome pathway and serine kinase activity modulate adenomatous polyposis coli protein-mediated regulation of beta-catenin-lymphocyte enhancer-binding factor signaling. J Biol Chem. 1999;274:16641–5.

42. Cho M, Park S, Gwak J, Kim D-E, Yea SS, Shin J-G, et al. Bisindoylmaleimide I suppresses adipocyte differentiation through stabilization of intracellular beta-catenin protein. Biochem Biophys Res Commun. 2008;367:195–200.

43. Zhou F, Huang H, Zhang L. Bisindoylmaleimide I enhances osteogenic differentiation. Protein Cell. 2012;3:311–20.

44. Chen Y, Blom IE, Sa S, Goldschmeding R, Abraham DJ, Leask A. CTGF expression in mesangial cells: involvement of SMADs, MAP kinase, and PKC. Kidney Int. 2002;62:1149–59.

45. Bahammam M, Black SA, Sume SS, Assaggaf MA, Faibish M, Trackman PC. Requirement for active glycogen synthase kinase-3β in TGF-β1 upregulation of connective tissue growth factor (CCN2/CTGF) levels in human gingival fibroblasts. Am J Physiol Cell Physiol. 2013;305:C581–90.

46. Lee SJ, Kang JH, Choi SY, Kwon OS. PKCδ as a regulator for TGF-β-stimulated connective tissue growth factor production in human hepatocarcinoma (HepG2) cells. Biochem J. 2013;456:109–18.

47. Jones S, Zhang X, Parsons DW, Lin JC-H, Leary RJ, Angenendt P, et al. Core signaling pathways in human pancreatic cancers revealed by global genomic analyses. Science. 2008;321:1801–6.

48. Zhang H, von Gise A, Liu Q, Hu T, Tian X, He L, et al. Yap1 is required for endothelial to mesenchymal transition of the atrioventricular cushion. J Biol Chem. 2014;289:18681–92.

49. Taccioli C, Sorrentino G, Zannini A, Caroli J, Beneventano D, Anderlucci L, et al. MDP, a database linking drug response data to genomic information, identifies dasatinib and statins as a combinatorial strategy to inhibit YAP/TAZ in cancer cells. Oncotarget. 2015;6:38854–65. doi: 10.18632/oncotarget.5749.

50. Bhukhai K, Suksen K, Bhummaphan N, Janjorn K, Thongon N, Tantikanlayaporn D, et al. A phytoestrogen diarylheptanoid mediates estrogen receptor/Akt/glycogen synthase kinase 3β protein-dependent activation of the Wnt/β-catenin signaling pathway. J Biol Chem. 2012;287:36168–78.

51. D'Agostino VG, Adami V, Provenzani A. A Novel High Throughput Biochemical Assay to Evaluate the HuR Protein-RNA Complex Formation. PLoS One. 2013;8:e72426.

52. Latorre E, Tebaldi T, Viero G, Spartà AM, Quattrone A, Provenzani A. Downregulation of HuR as a new mechanism of doxorubicin resistance in breast cancer cells. Mol Cancer. 2012;11:13.

GRANT SUPPORT

The research leading to the result part of this thesis has been supported by Bando Giovani Ricercatori 2008, Italian Ministry of Health: “Preclinical evaluation of the NAMPT inhibitor FK866 for the treatment of autoimmunity and lymphoblastic leukemia” and from the European Community’s Seventh Framework Programme [FP7-2007-2013] under agreement number HEALTH-F2-2011-256986-project acronym PANACREAS.

ACKNOWLEDGMENT

Immeasurable appreciation and deepest gratitude for fully support and help are extended to the following person who in one way or another have contributed in making my PhD study possible.

First and most of all, I would like to express my sincere gratitude and appreciation to **Dr. Alessandro Provenzani**, my amazing PI, for providing me one of the great opportunity in my life doing PhD here in his Laboratory. Thanks for his expertise, guidance, encouragement, and patience throughout the process of work, writing this thesis and throughout my PhD. He is one of the kindest PI I have even had and I really like to thank you for being so understandable and believed in me. I am very lucky to work with you.

I would like to thank all members and students in Laboratory of genomic screening. Special thanks to **Chiara**, for her support, help and for everything. She is one of my best friend, colleague, and best translator ever. We have had a very good time working together. Thanks **Vito** my advisor, for his help, support, guidance, and many of his genius ideas. I have learned a lot from his research expertise. Thanks to **Rosa, Ilaria, Preet, Barbara, Isabelle,** and **Nausicaa,** my lovely colleagues, **Alice, Simone, and Diego** my students for the numerous ways they have helped, motivated, and supported me during my time here.

I thank profusely all our collaboration, **Dr. Jean-Francois and** everyone from team4 C3M**,** Nice. I had amazing time and good experience working there**. Prof. Nadia Raffaelli, Dr. Silvia Ravera, Dr. Michele Cea** and **Dr. Alessio Nencioni** for their support and provided us necessary materials and complete some critical experiment to accomplish my project. I would like to thank all my thesis referees and committee members for their valuable comments and suggestions.
I would like to thanks all my BFF **Toan, Steve, Vasu** and **Bird** (distance does not dilute your support). They have each made my wonderful time here since the first time we met, thanks for keeping me company on long walks, you guys make me happy, thanks for an amazing encouragement and inspiration. Thanks for being here with me no matter what.

I would like to thank all my dear friends, all cibio people. Thanks to **Betty, Dr. Paolo Macchi** and PhD school for their support, and help throughout my study.

I take this opportunity to acknowledge all the staffs in cibio facility including **Valentina, Pamela, Michael,** and **Isabella** for their professional help and collaboration throughout my research period.

It is my privilege to thank my parents, my brother, my family, and my previous advisors in Thailand for their unconditional love, understanding, fully support, and remarkable encouragement. Without you none of this would indeed be possible.